Interreg CENTRAL EUROPE

Co-funded by the European Union

TRANSGEO

Engineering workflows for retrofitting abandoned wells

TRANSGEO Deliverable 1.1.6

Version 1

12 2024

D1.1.6: ENGINEERING WORKFLOWS FOR RETROFITTING ABANDONED WELLS

Corresponding author		
Hannes Hofmann hannes.hofmann@gfz.de	Helmholtz-Centre Potsdam German Research Centre for Geosciences (GFZ)	Germany
Contributors		
Monika Hölzel Stefan Hoyer Philipp Werkl Jacques Brives	GeoSphere Austria (GSA)	Austria
Lingkan Finna Christi Yuxuan Liu Guido Blöcher Elena Petrova	Helmholtz-Centre Potsdam German Research Centre for Geosciences (GFZ)	Germany
Tomislav Kurevija Luka Perković Marija Macenić Daria Karasalihović Sedlar Ivan Smajla	University of Zagreb - Faculty of Mining, Geology and Petroleum Engineering (UNIZG - RGNF)	Croatia
Matej Prkič	Local Energy Agency Pomurje (LEAP)	Slovenia
Katrin Sieron	State Office for Mining, Geology and Raw Material of Brandenburg (LBGR)	Germany
Ferenc Fedor Catarina C. Castro János Szanyi János Kovács	University of Pécs (PTE)	Hungary
Max Svetina	ONEO Austria	Austria

Table of Contents

Executive Summary

This report was prepared by the consortium of the project TRANSGEO and represents deliverable D1.1.6, "Engineering workflows for retrofitting abandoned wells." It aims to inform experts, including well owners and municipalities, agriculture, and industry about the technological options, requirements, and possible workflows for well reuse. The goal is to make these experts and other interested stakeholders aware of the opportunities of well reuse and to increase their knowledge about the potential reuse technologies with the proof-of-concept studies.

This work is based on literature reviews and numerical modelling studies which demonstrate the technical feasibility of five different well reuse options (described individually below) applied to five different reference well locations, and which demonstrate the required well, reservoir, and heat consumer requirements for successful well reuse. The well repurpose procedures include all technical measures to be performed to reuse wells with different specifications for a variety of purposes. This deliverable serves as input for TRANSGEO Activity 1.3, a criteria catalogue for well repurpose potential assessment. The report reflects the views of the authors.

Overall, the most suitable wells for any geothermal reuse are 1) still open and not yet abandoned, 2) not too old or have recently proven well integrity, and 3) have a large enough well diameter. Additionally, these wells need to be 4) located close to the heat demand/source. From a geological point of view, depending on the application, 5) a certain reservoir/bottomhole temperature is required, and open geothermal reuse technologies also require 6) a geothermal reservoir with high transmissivity (permeability times pay zone thickness).

The general well reuse workflow includes 1) a feasibility assessment including evaluation of the technical, geological, legal, economical, heat demand, and environmental aspects for different reuse options, 2) well rehabilitation and evaluation including a detailed technical plan, well site access, well site preparation, removing obstructions in the well, evaluating wellbore integrity and reservoir, performing necessary repairs, making changes to the well such as side-tracks, perforations, and installation of pipes and downhole pumps, 3) construction of surface infrastructure to extract the heat/produce electricity and for grid connection, 4) operating the system in the long-term including monitoring, and 5) engaging with local communities and stakeholders throughout the project.

Different aspects need to be considered for the application of different technologies:

Deep Borehole Heat Exchangers (DBHEs) are boreholes with a closed-loop system of pipes inside for circulation of a working fluid (usually water). The working fluid is pumped (or flows naturally) through the borehole, where it absorbs heat from the surrounding rock and groundwater. Often heat pumps are used to reach the required target temperature of the produced fluid. These systems are particularly valuable in areas where conventional geothermal reservoirs do not exist. Since it is only required to install a pipe in the existing well it is an easy-to-implement technology. Using PE piping instead of steel pipes can make the technology significantly cheaper as no drilling rig is required for the installation. However, PE pipes have relatively low temperature limits, making them impossible to use in very deep and hot wells. Therefore, there is a need for the development of different pipe materials that do not require expensive equipment for installation and that can withstand high temperatures. Since the heat transfer mechanism in such a system is heat conduction from the rock/groundwater to the working fluid DBHEs deliver only limited thermal power in the range between a few tens of kilowatts to a few hundreds of kilowatts depending on depth, geothermal gradient and thermal properties of the rock mass and the well. Therefore, DBHEs are a typical well reuse technology and usually no new dedicated DBHE wells are drilled for economic reasons. For the same economic reason also no abandoned wells can be used as redrilling the well and plugging it after the DBHE use is too expensive; the well condition should be known

and good since costs for logging/testing, well intervention and site preparation are too high; and the heat customer needs to be nearby as long heat transfer lines are too expensive. In the TRANSGEO partner countries 11 DBHE reuse projects were realised out of which 4 are still operating.

Borehole Thermal Energy Storage (BTES) are typically shallow storage systems consisting of hundreds of wells drilled very close to each other. No deep BTES exists in the TRANSGEO partner countries, likely because single deep wells are less efficient than shallow well arrays and BTES requires many years of charging before heat can be stored efficiently. BTES is the only heat storage option in deep wells when no permeable aquifer is present and the techno-economic considerations are similar to DBHEs since the amount of heat that can be stored in such a system is limited. When a heat source is nearby and available at low cost, storing heat in a DBHE with a co-axial design is the most viable option for the BTES reuse of deep wells.

Hydrothermal Energy (HE) is the conventional deep geothermal energy production option with many examples of conventional use and well reuse in Central Europe. In the low enthalpy hydrothermal systems in central Europe hot water is produced from a permeable hot water reservoir through at least one production well and after heat extraction at the surface cold water is often reinjected through at least one injection well. These open systems yield significantly larger thermal power in the range of a few megawatts to a few tens of megawatts. Electricity generation is also possible, but the electric power output of such a system is only about 1/10th of the thermal power output. Different hydrothermal reuse options exist. 1) Hot water can be co-produced together with hydrocarbons when water-cut is high towards the end of hydrocarbon production. This would just require a change in the surface facilities (installation of a heat exchanger and connection to the customer). However, the water production rates are typically <10 L/s and thermal power output of co-production is thus typically in the range of only a few megawatt. 2) Water can be produced from the hydrocarbon reservoir after hydrocarbon production has been finished. However, low reservoir pressure after decades of production and low relative permeability of water due to residual oil/gas limit the water flow rates and possible thermal power output. On the other hand, low reservoir pressure may make a well a good candidate for reinjection of produced water. 3) The existing well can be deepened into the geothermal reservoir. The drawback here is that this reduces the well diameter, which could result in high frictional pressure losses, especially when the new well section is very long, the new well diameter is small and the water production/injection rates are high. 4) Also shallower geothermal reservoirs can be accessed from an existing well through perforations or a sidetrack. The challenge here is to achieve sufficient reservoir access through possibly multiple layers of casing and cement and that the diameter of the sidetrack is also restricted by the size of the main well. 5) The best option is to reuse a hydrocarbon exploration well that found hot water instead of oil or gas, because least workover is needed and the well has not been produced for many years.

Aquifer Thermal Energy Storage (ATES) systems are systems where hot or cold water is stored in a porous and permeable rock formation. ATES wells serve both as injector and producer. Since ATES systems are typically developed in shallow depth the costs of drilling new wells are not as high as for deeper systems and the focus of reusing hydrocarbon wells is to deploy deeper wells (~1-2 km) for high-temperature ATES. ATES allows to store very large amounts of energy over long times. However, only few ATES exist in Central Europe and none of them reuses old wells.

Enhanced Geothermal Systems (EGSs) are open geothermal systems where new fractures are developed and/or existing fractures are improved by well stimulation treatments. These fractures form the fluid pathways and heat exchangers in an otherwise low permeability rock mass from which the heat is extracted by the fluid (typically water) that is circulated in between at least one production and one injection well which are hydraulically connected by these fractures. While EGSs are currently the only option for large-scale heat production (tens of megawatts of thermal power) and power generation (about 1/10th of thermal power) in Central Europe in areas where no permeable aquifer exists, these

systems are currently still in the research and development phase. Multiple EGS demonstration projects have utilized existing hydrocarbon wells including locations in Central Europe. Three reuse options exist: 1) Massive stimulation of an existing well (above, within or below the hydrocarbon reservoir) to improve the injectivity or productivity of that well either by overcoming near wellbore damage to access a permeable reservoir or to improve the flow towards the well from an intermediately permeable reservoir. 2) Long horizontal (depending on the stress field) wells with multiple parallel stimulation stages seem to be the most suitable EGS development option. This typically would require a side-track from a relatively shallow section from an existing well to end up with the required well diameter of at least 7" of the horizontal section. 3) Since induced seismicity is a risk to EGS development and since induced seismic events are used to track the fracture development it is vital to have a seismic monitoring well close to the EGS wells. The most suitable reuse option for EGS developments is therefore to use an existing well as monitoring well.

In this TRANSGEO project report we summarise the overall requirements for well reuse (Chapter A), describe the overall workflow for well reuse (Chapter B), and discuss five different well reuse technologies:

- Deep Borehole Heat Exchangers (DBHEs, Chapter C)
- Borehole Thermal Energy Storage (BTES, Chapter D)
- Hydrothermal Energy production (HE, Chapter E)
- Aquifer Thermal Energy Storage (ATES, Chapter F)
- Enhanced Geothermal Systems (EGS, Chapter G)

The TRANSGEO project (https://www.interreg-central.eu/projects/transgeo/) is co-funded by the European Regional Development Fund through the Interreg Central Europe program. The overall objective of TRANSGEO is to investigate the potential to transform abandoned hydrocarbon wells into new sources of green geothermal energy. To reach this goal, we will provide new tools and knowledge to support communities and industries in the energy transition and to break down economic and technical barriers to well reuse.

A. Overall Well Reuse Requirements

A.1. Author

Hannes Hofmann	GFZ	hannes.hofmann@gfz-potsdam.de	Germany

A.2. Well parameters

A.2.1. Well status

Shut-in wells, active wells, and wells that are to be developed in the future are the optimal targets for reuse. However, the time plan for stopping operations of active and new wells must fit with the schedule for the reuse and the associated energy demand. Permanently abandoned wells require a higher investment as they must be discovered, recovered, and reopened, including redrilling cement plugs and testing well integrity. Accordingly, the technologies DBHE and BTES are generally not suitable for abandoned wells, as they do not produce sufficient income to justify these costs due to the relatively low amount of energy that can be stored or produced.

A.2.2. Well integrity and age

For reuse, the well should be in a good condition and well integrity must be proven before reuse. Wells with a record of well integrity problems should in general not be considered for reuse. Younger wells typically have fewer well integrity problems and are therefore preferred for reuse. Since hydrocarbon wells are typically designed for a lifetime of at least 20-30 years, we suggest that wells that are younger than 30 years may be considered for reuse. The integrity of wells that are between 30 and 60 years old should be carefully assessed and wells older than 60 years can typically not be considered for reuse.

A.2.3. Casing size

Typical geothermal reuse cases require a casing size of at least 7 inches, to accommodate a downhole pump or a co-axial pipe and to allow sufficiently high flow rates with low frictional pressure losses. Therefore, we suggest that wells with a minimum casing size of 7 inches or larger are in principle suitable for reuse, and wells with smaller minimum casing sizes should be assessed in detail.

A.3. Reservoir parameters

A.3.1. Temperature

The required temperature depends on the foreseen geothermal use (or on the required heat storage temperature for thermal underground storage applications). Typically, higher temperatures and higher thermal gradients improve the economic feasibility of a reuse project. For underground thermal energy storage applications, there is not a minimum temperature limit. For geothermal energy production, certain minimum temperatures are required for economic feasibility. These limits may be as low as 20°C for Deep Borehole Heat Exchangers (DBHE), 35°C for Hydrothermal Energy (HE) applications (mostly combined with heat pumps), and 60°C for Enhanced Geothermal Systems (EGS). We consider that the more costly and

technically demanding solutions require higher temperatures for economic feasibility. For the closed borehole systems, the bottomhole temperature is relevant, and for open systems, the reservoir temperature is considered. However, high temperatures can also reduce the reuse options because some materials, such as inexpensive polyethylene pipes in borehole heat exchangers, may not withstand higher temperatures.

A.3.2. Permeability

Open systems require a certain minimum reservoir transmissivity (which is the product of permeability and effective reservoir thickness) or well productivity/injectivity (which is the flow rate divided by the bottomhole pressure change) to be able to produce economic rates of geothermal fluids. If the permeability is below ~10 mD, only closed systems or EGS may be used. Above 100 mD, open systems can be considered (if the reservoir is thick enough). In between these two values, the well/reservoir should be evaluated in detail to determine its best use. In terms of transmissivity, we consider these boundaries roughly at 1 Dm and 10 Dm. In terms of productivity or injectivity index, we see these boundaries at 5 L/s/MPa and 10 L/s/MPa, and the corresponding flow rates are roughly 10 L/s and 50 L/s. However, depending on the application and the cost for well workover and operational cost, these numbers may vary and only provide a rough estimation by the authors of this document.

A.3.3. Reservoir Thickness

The effective reservoir thickness (“pay zone” thickness) is equally important as the reservoir permeability for open systems. We consider a reservoir thickness of <10 m as insufficient and a thickness of >20 m as potentially sufficient for HE or Aquifer Thermal Energy System (ATES) use. A detailed study is required between 10 and 20 m.

A.3.4. Groundwater flow

Groundwater flow reduces the efficiency of underground thermal energy storage systems (ATES and Borehole Thermal Energy Sytems, BTES) since the heat that is to be stored in the vicinity of the well may be flushed away by the moving groundwater. Therefore, no or only insignificant groundwater flow should be present in potential reuse cases.

A.3.5. Cap rock

Since warm water rises upwards due to a lower density than cold water, ATES reservoirs additionally need a sealing cap rock to avoid excessive vertical heat loss.

A.3.6. Fluid chemistry

Highly saline fluids may potentially lead to scaling and corrosion in the future geothermal well. Therefore, lower salinity fluids are preferable over highly saline fluids for geothermal well reuse. However, geothermal brines may also contain critical raw materials, which may be (co-)produced. Therefore, knowledge on fluid chemistry is beneficial to decide whether a site is suitable for well reuse.

A.4. Market parameters

A.4.1. Well location

The key factor of geothermal reuse of hydrocarbon wells in Central Europe is that, given the temperature range of the geothermal resources, direct use of the geothermal energy is the most suitable option.

Therefore, the wells must be near potential heat consumers (e.g., district heating networks) or heat sources (for storage). In closed loop systems the heat transport pipelines at the surface would be too costly if the heat consumer/source is not in the immediate vicinity of the well. The maximum possible distance to the consumer/source depends on the reuse technology and the application, but should in general not be more than roughly 10 km.

A.4.2. Heat demand vs. supply

Finally, the heat demand must be matched with the geothermal heat supply. The open systems can typically provide thermal power in the order of tens of megawatts while the closed loop systems can provide typically only a few hundred kilowatts.

B. Overall Well Reuse Workflow

B.1. Author

Hannes Hofmann GFZ hannes.hofmann@gfz-potsdam.de Germany

B.2. Steps to conduct a Feasibility Assessment (e.g., using the TRANSGEO well assessment tool)

2.1. Determine the availability and accessibility of existing wells and well data in the desired area including ownership information. This can be accomplished via use of the TRANSGEO database (Deliverables D2.1.1-D2.1.4) and the TRANSGEO well assessment tool, which provides an assessment of potential well redevelopment targets in the hydrocarbon basins of Austria, Croatia, Germany, Hungary, and Slovenia (Deliverable D1.4.3).[1]

2.2. Evaluate the technical suitability of the wells for the different reuse options, based on available data, including but not limited to:

- *Well configuration:* Information about the well assembly helps determine the constraints of the wellbore, e.g., if the well can accommodate the production tubing, pumps, and flow rates and if it can withstand the temperatures and pressures associated with geothermal operations. This information includes details of the casing material and diameter, and the depth of each casing string and cemented section, the cement type, and plugged sections. Additionally, completion details are required for assessing the suitability of the existing completion for the anticipated geothermal operation. Completion details include type and depth interval of perforations, gravel pack, perforated liner, open hole section, and other. Additionally, information of any equipment lost-in-hole is required.
- *Well integrity:* Well integrity is crucial for safe geothermal operations and must be assessed for the planned operations and operational timeline. Any sign of corrosion, scale buildup, or mechanical damage reduces well integrity. Well integrity can be determined based on caliper logs, image logs, cement bond logs, electromagnetic casing inspection tools, borehole cameras, and buildup tests. A record of well maintenance and workover operations helps understand past problems and the current condition of the well. Besides well integrity, this includes, for example, reservoir compatibility, material compatibility, and environmental impact.

2.3. Evaluate the geological potential of the technically-suitable wells for the different reuse options, based on available data, including but not limited to:

- *Potential geothermal reservoirs:* Analyse lithology, depth, (effective) thickness, permeability, porosity, formation fluid properties, water saturation, and residual oil and gas saturations, which are essential for determining the hydrothermal and storage potential. Parameterization of the reservoir is essential for evaluating the potential of open geothermal systems (Hydrothermal Energy and Aquifer Thermal Energy Storage).

[1] The TRANSGEO well assessment tool, which uses the databases, is expected to be made available to the public in late 2025-early 2026.

- *Well logs, core samples and hydraulic tests:* Analyse well logs, including gamma ray, resistivity, porosity and temperature logs as well as laboratory measurements on cores to assess the properties of relevant geological formations.
- *Surface geophysical measurements:* The availability of surface geophysical measurements, such as 2D and 3D seismics helps identify the geological situation surrounding the well, which is essential to planning a geothermal well doublet.
- *Historic production data:* Review the production history of the well, including hydrocarbon production rates, reservoir pressure declines, and formation damage encountered during hydrocarbon extraction. This information can indicate the impact of previous activities on the well and reservoir and aid in assessing the feasibility of geothermal energy extraction or storage in the former hydrocarbon reservoir.
- *Parameterized static geological models and dynamic reservoir models:* These models integrate and interpret all available data and can be used to determine reservoir boundaries and locations of new injection or production wells in the vicinity of the investigated well.

2.4. Assess the potential for geothermal energy production or storage based on well configuration, local geology, estimated resource size, and analytical or numerical modelling studies (see Chapters C-G in this report). This includes assessment of whether a well is suitable for open systems (as production or injection well or both), for closed-loop systems, or as monitoring well (specifically for Enhanced Geothermal Systems).

2.5. Assess the economic viability by conducting a cost-benefit analysis of repurposing the well for geothermal energy production or storage including factors such as capital investment, operating costs, expected revenue, and anticipated lifespan of the project (see TRANSGEO socio-economic analyses, Deliverables D1.2.1-D1.2.3[2]).

2.6. Research and comply with local regulations and permits related to the conversion of the hydrocarbon well for the anticipated geothermal use (see TRANSGEO regional policy comparisons, Deliverable D3.1.1[3]).

2.7. Conduct an environmental impact assessment to ensure compliance with environmental standards and identify any potential risks and mitigations.

2.8. Perform a feasibility study and compare well reuse with drilling a new well to decide with which option to proceed (see TRANSGEO site-specific feasibility studies on 8 pilot sites, Deliverables D2.3.1-D2.3.8[4]).

B.3. Well rehabilitation and evaluation

3.1. Make a detailed technical plan for well rehabilitation.

3.2. Get the required permissions and comply with conditions for approval.

3.3. Prepare well access, drill pad, drill cellar, and well head for drilling and workover operations.

3.4. Remove any obstructions in the well, such as cement plugs, and clean the well.

3.5. Evaluate the well conditions, including structural integrity and overall suitability for geothermal operations (wellbore integrity).

[2] Available from the TRANSGEO website at https://www.interreg-central.eu/projects/transgeo/?tab=outputs
[3] Available from the TRANSGEO website at https://www.interreg-central.eu/projects/transgeo/?tab=outputs
[4] The TRANSGEO feasibility studies are expected to be made available to the public by the fall of 2025.

3.6. Perform necessary repairs.

3.7. Deepen the well, drill a side track, open shallower sections of the well by perforations, or close sections of the well according to the reuse technology to be applied.

3.8. Evaluate the reservoir, for example by determining temperature, permeability, and fluid composition through temperature logging, hydraulic testing, and fluid sampling.

3.9. Install the required subsurface equipment such as borehole heat exchanger pipes, electrical submersible pumps, injection or production tubing, and/or monitoring equipment in the well.

B.4. Construction of surface infrastructure

4.1. Based on the reservoir evaluation, design and construct or modify the surface infrastructure such as the heating and/or power plant system and heat transport lines and select appropriate technologies based on the resource temperature and other site-specific well and reservoir conditions as well as the site-specific geothermal energy use.

B.5. Operation

5.1. Establish long-term operation including maintenance protocols to ensure the long-term reliability and sustainability of the geothermal system.

5.2. Implement a comprehensive monitoring program for key parameters such as fluid injection and production rates as well as reservoir pressure and temperature to continuously assess geothermal reservoir performance and maintain reservoir sustainability.

5.3. Implement a comprehensive environmental monitoring programme to monitor and mitigate potential environmental risks, such as induced seismicity or groundwater contamination.

B.6. Community engagement

Engage with local communities and stakeholders to inform them about the project, address any concerns, and maintain open lines of communications. Provide regular updates about the project's progress, environmental performance, and socio-economic benefits throughout the planning, development, and operation stages to build trust and foster positive relationships.

C. Deep Borehole Heat Exchanger

C.1. Authors

Stefan Hoyer	GeoSphere Austria	stefan.hoyer@geosphere.at	Austria
Monika Hölzel	GeoSphere Austria	monika.hoelzel@geosphere.at	Austria
Philipp Werkl	GeoSphere Austria		Austria

With additional input from

Max Svetina	ONEO Austria	Austria
Ferenc Fedor	CROST	Hungary
Katrin Sieron	State Office for Mining, Geology and Raw Material of Brandenburg (LBGR)	Germany
Matej Prkič	Local Energy Agency Pomurje (LEAP)	Slovenia
Jacques Brives	GeoSphere Austria	Austria

C.2. Deep Borehole Heat Exchangers (DBHEs)

C.2.1. Description of technology

The technology of conventional, shallow Borehole Heat Exchangers (BHEs) has been studied extensively in the past and lays the foundation for the research of Deep Borehole Heat Exchangers (DBHEs). While shallow BHEs can be called state-of-the-art in the new building sector, DBHE is still an uncommon use of geothermal heat extraction as of today. The working principle of these systems is almost identical and uses a borehole in which a heat carrier fluid is pumped throughout a single well, in a closed-loop cycle without the need for an aquifer (Lund and Boyd, 2016; Raymond et al., 2015a). Thermal energy is passed on to the wellbore from the surrounding underground via conduction and the gained heat of the working fluid is then used by surface facilities depending on the site-specific needs, before the fluid is pumped down again (Gascuel et al., 2022). DBHEs have been studied as an alternative to enhanced geothermal systems by several authors, e.g. Doran et al. (2021), Falcone et al. (2018), Renaud et al. (2019). But while for shallow BHE systems U- or double U-tube designs had evolved as the standard technology, DBHE installations are typically completed in coaxial systems (Koltzer et al., 2024).

In literature, the terms of medium-deep and deep borehole heat exchangers are used interchangeably and there is no depth limit defined as of when a system is considered deep. Often, in China and Central Europe, boreholes reaching over 200 m are classified as deep, whereas in Northern Europe 400 m is considered the limit. Others regard 3000 m or 1000 m as an ideal boundary (Piipponen et al., 2022). Although the general operating principle of the shallow and deep application is the same, there are differences in their final power utilisation, advantages and disadvantages. While the primary focus of the deep technology lays on heating purposes and energy storage, shallow BHE can be utilised to extract heat and cold for e.g. space cooling in summer (Sliwa et al., 2015). From simulations to study

DBHE operation as well as from operational data several authors have clearly demonstrated that the heating performance increases significantly with depth (Holmberg et al., 2016; Lund et al., 2020; Wang et al., 2017). Another benefit is the higher return fluid temperatures (Piipponen et al., 2022).

Following this, DBHEs require less surface space than conventional shallow closed loop systems to cover the same heating requirements and are better suited for cases with higher heating than cooling demand (Cai et al., 2021; Deng et al., 2019a). This could be favourable especially in densely populated areas with spatial limitations. Nevertheless, high initial drilling cost and integrity issues are considered as strong counterarguments for utilising geothermal heat in closed-loop systems from deep underground (Kolo et al., 2023). One way to overcome the economic bottleneck of this technology is the repurposing of oil and gas wells that are no longer in use and to be abandoned. What the requirements of potential wells are and how the workflow to retrofit these should look like is presented in detail in Chapter C.8.
As mentioned above, the heat from the underground is gained via conduction and heavily depends on the well configuration of the system. Figure C 1 shows a vertical view of a borehole and indicates the temperature profile, as well as the heat flow mechanisms along the components of the wellbore. It is obvious that the properties of the components impact the temperature that can be achieved by a specific setup which calls for an optimisation before the construction work begins. The specific impact that each parameter has on the performance of the heat exchanger is investigated in Chapter C.6.5.

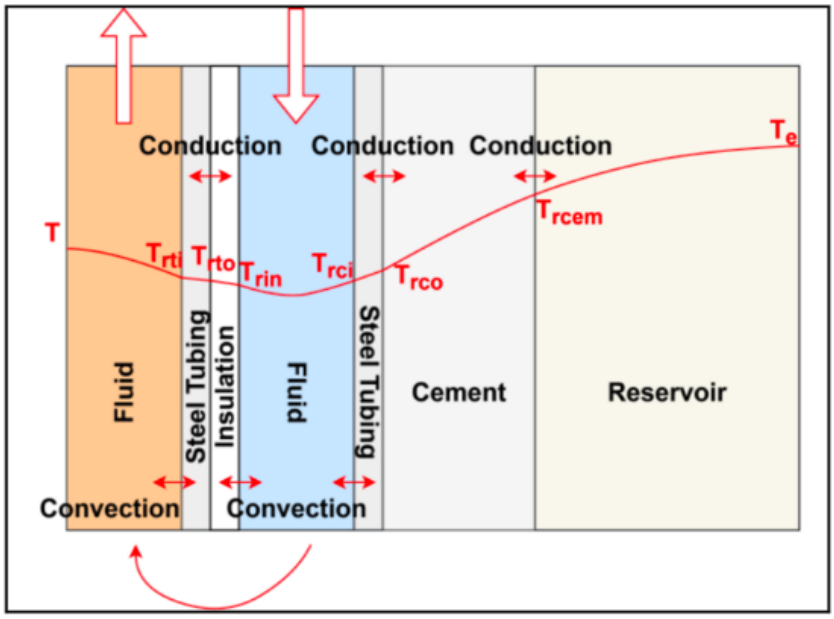

Figure C 1: Relevant heat flow mechanisms in the subsurface system.

The well type that is shown in Figure C 1 represents the coaxial DBHE with an annular inflow, where the wellbore itself consists of two concentric pipes of which the outer is closed at the bottom of the well (e.g., by cementation) and the inner is slightly shorter and open which induces a flow direction from the outer to the inner pipe. This specific configuration of in- and outlet pipes is considered to be most effective when comparing it to a coaxial configuration with a reversed flow direction (centred inlet) and U-tube designs. The better performance compared to U-tube configurations is due to a better thermal contact between the descending fluid and the surrounding rock, as well as less thermal contact between the ascending fluid in the formation which is particularly important for the upper

parts of the system, where the cold surrounding leads to a cooling of the fluid. Additionally, the flow rates can be higher for the same borehole diameter (Holmberg et al., 2016; Kalmar et al., 2020; Law et al., 2014; Wang et al., 2017). When comparing the two types of coaxial systems, the centred inflow flow direction is less effective for heating purposes (Law et al., 2014; Wang et al., 2017). In terms of the working fluid that is circulated in the borehole, water represents a promising trade-off between cost and performance. Depending on the temperatures that prevail in the system, an antifreeze might be added to prevent the circulation from freezing. Alternatives to water are currently under study: For instance the substitution of water by CO_2 for its more efficient heat carriage and less friction. The challenges that are known, however, are corrosion and the high pressure maintenance of the fluid (Gascuel et al., 2022). Another evaluation is ongoing, whether using additives like aluminum oxide yield a justified efficiency increase of the system (Alimonti et al., 2018).

As the technology description already makes it clear that there are various parameters in the system that affect the performance of the DBHE, thorough investigation, analysis, and design optimisation are mandatory segments of the project lifecycle that must be addressed prior to construction.

In the following chapter the influencing parameters and their respective effect are further analysed by literature review and are then further compared within a history-matched numerical simulation to determine their weight on the overall efficiency.

C.3. Literature review

Several papers, such as Gascuel et al. (2022) and Alimonti et al. (2016), focus on the **design aspects of DBHEs**, exploring how different configurations, materials, and operational parameters can be optimised for maximum efficiency in geothermal energy extraction.

The second focus of the screened literature is **numerical modelling, simulation and optimisation** of DBHE systems, for instance the works by Brown et al. (2022) and Duggal et al. (2022), are dedicated to the development and application of numerical models. Kolo et al. (2024) presents an extensive comparison of different methods based on a literature review. The authors group the available numerical methods in three basic types:

1. **Dual-continuum methods,** where the DBHE is discretised as 1D element within a 3D model. The 1D BHE is commonly solved through an analytical or semi-analytical approach, while the 3D surrounding can be a finite difference, finite element, or finite volume model.
2. **Cylindrical axisymmetric** methods**.**
3. **Full component**-discretisation methods.

Each of these methods have their limitations, pros and cons. Compared to full component-discretisation methods, the dual-continuum method seems to be the best trade-off between accuracy and computational efficiency, based on the screened literature. In comparison to cylindrical methods, these methods also allow implementation of BHE fields, groundwater flow and complex geological geometries.

Finally, there is also a share of papers, e.g. Sliwa et al. (2015) and Kolo et al. (2024) addressing the **economic viability and environmental impacts** of deploying BHE systems. These studies discuss the cost-benefit analysis of retrofitting existing wells, the long-term sustainability of geothermal energy, and the environmental benefits of using geothermal systems compared to traditional energy sources. **Error! Reference source not found.** presents an overview of the screened literature including the count of specific keywords as an attempt to define the focus of the papers.

Authors (short)	Title	Keyword count		
		Mod	Eco	Tec
Alimonti et al., 2016	Coupling of energy conversion systems and wellbore heat exchanger in a depleted oil well.	17	4	25
Alimonti et al., 2018	The wellbore heat exchangers: A technical review.	0	1	32
Blasi & Menichette 2012	Thermal conductivity distributed from a Thermal Response Test (TRT) in a borehole heat exchanger (BHE).	0	3	2
Bräuer, 2011	Energie aus Erde, Luft, Wasser-Wärmepumpen und Geothermie.	0	0	0
Bräuer, 2011	Geothermie aus bestehenden Sonden. Blue Globe Report.	0	0	0
Brown & Howell 2023	Unlocking deep geothermal energy in the UK using borehole heat exchangers.	0	0	0
Brown et al., 2023	Investigating scalability of deep borehole heat exchangers: Numerical modelling of arrays with varied modes of operation.	48	1	41
Bußmann, 2004	Geothermie-Energie für die Zukunft UMWELTPOLITIK.	0	0	0
Caulk & Tomac 2017	Reuse of abandoned oil and gas wells for geothermal energy production.	0	6	19
Chmielowska et al., 2020	The Utilization of Abandoned Petroleum Wells in Geothermal Energy Sector.	0	0	0
Dijkshoorn et al., 2013	Measurements and design calculations for a deep coaxial borehole heat exchanger in Aachen, Germany.	0	0	0
Doppelreiter, 2012	Geothermische Nachnutzung der Kohlenwasserstoffbohrung Mühlleiten 2 in Oberösterreich.	0	0	0
Doran et al., 2021	Modelling an unconventional closed-loop deep borehole heat exchanger (DBHE): sensitivity analysis on the Newberry volcanic setting.	60	1	42
Duggal et al., 2022	Analytical and Numerical Modelling of a Coaxial Borehole Heat Exchanger to Extract Geothermal Energy.	63	3	4
Dürnegger, 2009	Integration eines Bohrlochwärmetauschers in ein bestehendes Heizsystem.	0	0	0
Falcone et al., 2018	Assessment of deep geothermal energy exploitation methods: The need for novel single-well solutions.	0	0	0
Fritsche, 2012	Geologische und geothermische Ergebnisse aus dem Projekt Mitteltiefe Erdwärmesonde Heubach.	0	0	0
Gascuel et al., 2022	Design and optimization of deep coaxial borehole heat exchangers for cold sedimentary basins.	97	15	291
Gola et al., 2022	Geothermal deep closed-loop heat exchangers: A novel technical potential evaluation to answer the power and heat demands.	0	0	0

Kohl et al., 2000	Data analysis of the deep borehole heat exchanger plant Weissbad (Switzerland).	31	0	25
Kolm, 2012	Einzigartiges regionales Energie-Projekt aus einer Kombination von Erdwärme und Biomasse für Neukirchen a.d. Vöckla eröffnet.	0	0	0
Kolo et al., 2023	Repurposing a Geothermal Exploration Well as a Deep Borehole Heat Exchanger: Understanding Long-Term Effects of Lithological Layering, Flow Direction, and Circulation Flow Rate.	115	4	62
Kolo et al., 2024	A comprehensive review of deep borehole heat exchangers (DBHEs): subsurface modelling studies and applications.	221	19	50
Koltzer et al., 2024	Repurposing idle wells in the North German Basin as deep borehole heat exchangers	73	18	44
Ledet et al., 2023	Leveraging oil and gas infrastructure using closed-loop geothermal technologies	0	0	0
Macenić et al., 2020	Analytical and numerical modelling of heat extraction rates in the coaxial heat exchanger for a retrofitted deep oil and gas wells.	0	0	36
Geothermieforum Niedersachsen, 2021	Geothermische Nachnutzung von Bohrungen.	0	0	0
Piipponen et al., 2022	The Deeper the Better? A Thermogeological Analysis of Medium-deep Borehole Heat Exchanger Efficiency in Crystalline Rocks - not peer reviewed.	42	1	23
Rybach & Gorhan 2005	Country Update for Switzerland.	0	4	3
Sliwa et al., 2015	Applicability of Borehole R-1 as BHE for Heating of a Gas Well.	0	9	23

Table C 1: Overview of the screened literature including the count of specific keywords: **Mod**eling: "model, numerical, modelling"; **Eco**nomic: "economic, economics, economically"; **Tec**hnical: "technical, feasibility, casing, diameter, annular, grout(-ing)".

When undertaking numerical modelling of deep borehole heat exchangers, it is critical to begin with a clear definition of the primary objectives and scope of the model. This initial clarity helps to tailor the model to address specific questions, such as understanding the heat transfer dynamics within the DBHE, evaluating different operating modes, or assessing the scalability of DBHE arrays in different geological conditions, as highlighted by Brown et al. (2022). Determining the scope of the model is also critical, as it dictates the range of temporal and spatial scales that the model must accurately represent. Whether the focus is on short-term operational dynamics or long-term sustainability affects the level of detail and type of data required, as highlighted among others by Gascuel et al. (2022).

The choice of an appropriate model type is a fundamental decision in the modelling process. For scenarios requiring rapid, preliminary insights where high precision is not critical, analytical models are advantageous due to their simpler and faster computations. However, when dealing with complex geological settings or when detailed spatial analysis is required, numerical models are essential. Duggal et al. (2022) suggest that these models, although resource intensive, provide the flexibility needed to

simulate the complex interactions within DBHE systems. The choice of software is also critical, with tools such as OpenGeoSys offering advanced capabilities for simulating the thermo-hydro-mechanical processes in porous media that are essential for a comprehensive understanding of BHE behaviour. Kolo et al. (2024) present a thorough review of subsurface modelling studies and their various applications. The authors provide an overview about the different modelling approaches found in literature, including both numerical and analytical approaches, and evaluate their effectiveness in different contexts such as heat extraction, thermal energy storage, and cooling. While for single wells and heat one-directional usage with extraction only multiple methods and discretisation schemes are applied in literature, for thermal storage models finite element is the predominant discretisation scheme, especially when dealing with DBHE arrays.

Parameterisation involves the selection and definition of the variables that significantly affect the performance of the DBHE. Critical parameters often include geological properties such as rock thermal conductivity and porosity, borehole design parameters such as diameter and depth, and operational parameters such as flow rate and temperature of the heat transfer fluid. Alimonti et al. (2016) highlight the importance of conducting sensitivity analyses to identify which parameters have the strongest impact on the system efficiency. This step not only helps to optimise the model inputs, but also reduces computational overhead by focusing resources on the most influential variables.

The calibration and validation stages are where the model is refined and tested against reality. Calibration involves iteratively adjusting model parameters to match known outcomes, a process that can be based on benchmarking against experimental data or operational performance data from existing plants, as detailed by Kohl et al. (2000). Validation, on the other hand, is the process of verifying that the model accurately predicts new or independent data. This step is crucial in establishing the reliability of the model and ensuring that it can provide trustworthy predictions.

Running multiple simulations over a range of designed scenarios, as discussed by Brown et al. (2022), is essential to explore the potential behaviour of DBHE systems under different geological and operational conditions. These scenarios could include changes in the geological medium, variations in climate impacts on surface temperature, or different heat extraction technologies. Optimisation techniques, possibly involving genetic algorithms or machine learning approaches, are used to sift through these scenarios to find optimal solutions that balance efficiency, cost and environmental impact.

Documentation at all stages of the modelling process is essential to maintain the integrity and reproducibility of the model. Detailed records of assumptions made, parameters used and methodologies employed support the credibility of modelling efforts. Furthermore, as suggested by Gascuel et al. (2022), models should not be static, but should evolve through iterative improvement as new data become available or as further insight is gained into the behaviour of the system. This iterative approach ensures that the model remains relevant and accurate over time, providing valuable guidance for the design and operation of DBHE systems.

Overall, a comprehensive and methodical approach to numerical modelling of DBHEs involves an integration of technical, operational and contextual knowledge, ensuring that the models are not only technically sound, but also aligned with practical energy solutions and environmental sustainability goals.

Discretisation	Software	Depth (m)	Features	References
FVM	Inhouse MATLAB code	2500	2D model including fluid momentum balance equation, variable thermal properties, using water and CO_2 as circulation fluid	Bai et al. (2022)
FDM	Inhouse MATLAB code	2800	Nodal domain, 1D DBHE embedded in 3D subsurface	Brown et al. (2021)
FVM	Inhouse MATLAB code	4000 and 2600	Cylindrical axisymmetric domain, includes pressure loss in pipes, single DBHE	Bu et al. (2012, 2019)
FEM	OpenGeoSys	2000	3D subsurface element domain with 1D DBHE, multiple homogeneous DBHEs	Cai et al. (2021)
FVM	Inhouse MATLAB code	2000	2D model, single homogeneous DBHE	Liu et al. (2019), Cai et al. (2019)
FEM	COMSOL	1000-5000	2D model including Navier-Stokes for fluid flow, incompressible circulation fluid	Caulk and Tomac (2017)
FEM	OpenGeoSys	2600	3D subsurface element domain with 1D DBHE, locally thermal non-equilibrium	Chen et al. (2019)
FVM	Inhouse code	1000-3000	Cylindrical axisymmetric domain	Deng et al. (2020)
FDM	TOUGH2	2866	2D model including fluid mass and momentum balance equation, variable thermal properties, single heterogeneous DBHE	Doran et al. (2021)
FDM	Inhouse code	2600	2D model, single homogeneous DBHE	Fang et al. (2018), Zhang et al. (2021)
FDM	Inhouse MATLAB code	300-1000	Cylindrical axisymmetric domain, heat extraction and injection	Holmberg et al. (2016)
FDM	Inhouse Fortran90 code	500-800	Cylindrical axisymmetric domain, variable ground properties	Morchio and Fossa (2019)
FDM	SHEMAT	100-3600	Cylindrical axisymmetric domain, multiple heterogeneous DBHEs, heat extraction and injection	Mottaghy and Dijkshoorn (2012)
FVM	ANSYS Fluent	2070	2D CFD model, single heterogeneous DBHE	Renaud et al. (2019)
FDM	Inhouse code	5000	2D model, single heterogeneous DBHE	Song et al. (2018)
FEM	FEFLOW	400-1000	3D subsurface element domain with 1D DBHE, multiple homogeneous DBHEs, heat extraction and injection	Welsch et al. (2015)

Table C 2: Features of typical single coaxial DBHE numerical models, discretisation method and corresponding software (Table 1 in Kolo et al., 2024)

C.4. Deep Borehole Heat Exchanger projects

C.4.1. Deep Borehole Heat Exchanger projects in the TRANSGEO partner countries

For the North German Basin, the Molasse Basin in Germany and Austria, the Vienna Basin and the Pannonian Basin in Slovenia, Croatia and Hungary, the existence of Deep Borehole Heat Exchanger projects are evaluated. The projects are divided into planned or (numerically) simulated (but not realised) projects and realised projects. They include either new wells, reuse of depleted hydrocarbon wells, dry hydrocarbon or dry geothermal wells.

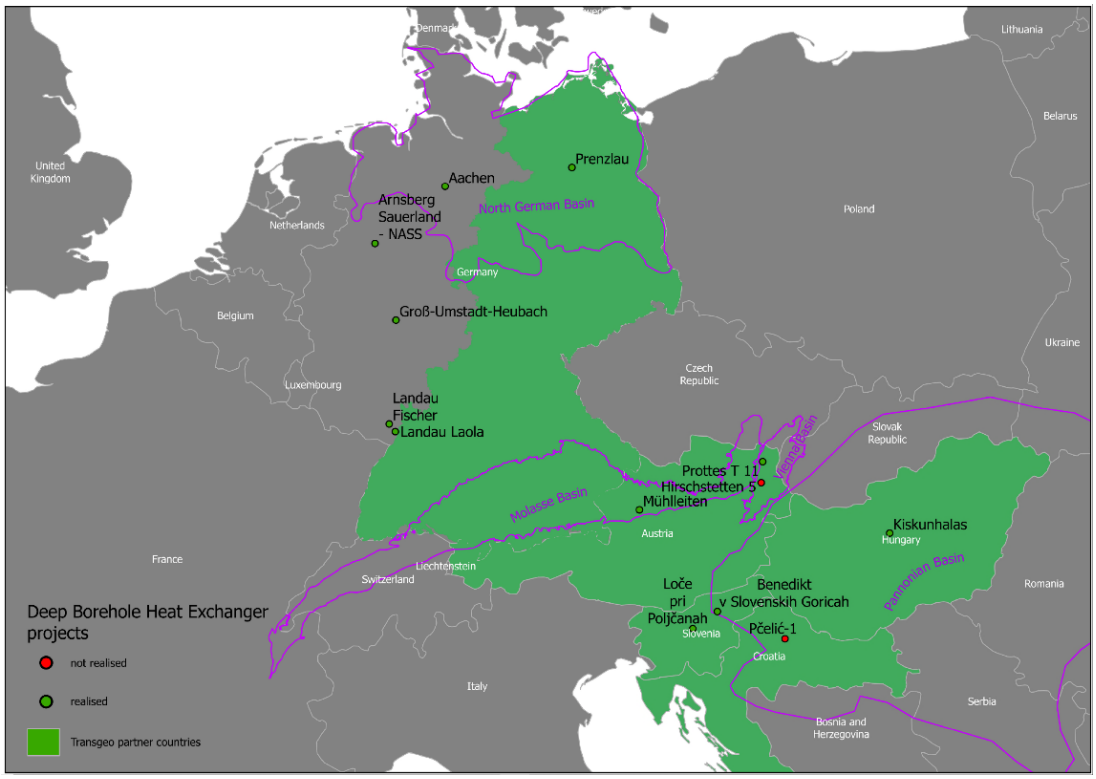

Figure C 2: Overview of realised and not realised Deep Borehole Heat Exchanger projects in the TRANSGEO partner countries in the central European region. The map includes either new drilled wells or well reuse.

In the TRANSGEO project region, 15 projects of deep borehole heat exchanger heat generation could be compiled. 11 of them were realised since the 1990ies. In Austria 2 projects (Mühlleiten 2, Prottes T11) were applied, in Germany there are 7 projects (Aachen, Arnsberg, Heubach, 2x Landau, Prenzlau), in Slovenia 2 (Benedikt v Slovenskih Goricah, Loče pri Poljčanahand) and in Hungary one project (Kiskunhalas).

At least 2 projects in Croatia and Austria were in the modelling phase with the focus on existing wells to reuse, but they did not come into operation. In Hungary one well is planned to be reused (Kiha-D-7), but the operators are still searching for a consumer.

Country	Site Name	Geological Unit	realised	Status	Date DBHE installed	Date abandoned	Well owner	Operator	Depth TD (TVD, m)	Depth used (TVD, m)
Austria	Hirschstetten 5	Vienna Basin	N	modelled	not realised	--	OMV	--	4007	2530 (cased section)
Austria	Mühlleiten (Neukirchen an der Vöckla)	Molasse Basin	Y	shut-in	2012	--	RAG	RAG	2875	N/A
Austria	Prottes T 11	Vienna Basin	Y	abandoned	2009	2012	OMV	OMV	2980	2230
Croatia	Pčelić-1	Pannonian Basin	N	modelled	not realised	--	N/A	--	5214	4500
Germany	Aachen (Super C)	North German Basin	Y	abandoned	2008	2014	N/A	N/A	2500	1965
Germany	Arnsberg im Sauerland (NASS)	North German Basin	Y	producing	2012	--	Stadtwerke Arnsberg	Stadtwerke Arnsberg	2835	2835
Germany	Groß-Umstadt-Heubach	Variscian Basement	Y	producing	2012	--	Entega	Entega	773	773
Germany	Landau Fischer (La-049)	Rhine Graben	Y	producing	2014	--	Wintershall, EnergieSüdwest	Energie Südwest	1430	794
Germany	Landau Laola (La-044)	Rhine Graben	Y	producing	2010	--	Wintershall, ONEO	ONEO, Energie Südwest	1094	800
Germany	Prenzlau	North German Basin	Y	abandoned	1994	N/A	former DDR well	Stadtwerke Prenzlau	--	2786
Hungary	Kiha-D-7 (Kiskunhalas)	Pannonian Basin	N	planned	--	--	BVH	WeHeat/MS Energy Solutions	N/A	N/A
Hungary	Kiha EK-14 (Kiskunhalas)	Pannonian Basin	Y	producing	2021	--	MOL	MS Energy Solutions + Municipality Kiskunhalas	1950	1820
Slovenia	Benedikt v Slovenskih Goricah	Pannonian Basin	Y	shut-in	2016	--	Municipality of Benedikt	Municipality of Benedikt	1858	1371
Slovenia	Loče pri Poljčanah	Pannonian Basin	Y	shut-in	2013	--	Private owner	Private owner	510	510

Table C 3: Overview of the 15 DBHE projects in the TRANSGEO partner countries. N/A means that there is no information about this parameter available; -- means that there should be no data (if in cell “Status”: abandoned, then in cell “Date abandoned”: --). The table is ordered alphabetically country wise and then per site names.

11 projects are based on reuse of wells drilled for another purpose than to serve as DBHE. This number includes the 2 modelled future projects from Croatia and Austria and one in Hungary, which are based on existing old wells too. At this time of reporting (2024) five projects are still operating.

The use for the produced geothermal energy is in all cases heat. Applications range from heating buildings and swimming pools to greenhouse heating. The end-temperature is in most cases reached by the support of heat pumps.

Country	Site Name	Geological Unit	realised	Well reuse	Original use of well	Purpose	Surface heating system
Austria	Hirschstetten 5	Vienna Basin	N	Y	HC well depleted	glass house heating	gas heat pumps/oil
Austria	Mühlleiten (Neukirchen an der Vöckla)	Molasse Basin	Y	Y	gas exploration	community heating	heat pump, CNG Combined heat and power plant (Blockheizkraftwerk)
Austria	Prottes T 11	Vienna Basin	Y	Y	HC well depleted	heating of a gym hall	gas heat pumps
Croatia	Pčelić-1	Pannonian Basin	N	Y	dry HC well, tool stuck	heating	plate heat exchanger (for direct energy supply; higher temperatures) heat pumps (for lower temperatures)
Germany	Aachen (Super C)	North German Basin	Y	N	--	heating new University building	heat pump
Germany	Arnsberg im Sauerland (NASS)	North German Basin	Y	N	--	heating of swimming pool, sports area, school	N/A
Germany	Groß-Umstadt-Heubach	Variscian Basement	Y	N	--	heating medium industrial building (6000 m²) and office building (1400 m²), test site	heat pump
Germany	Landau Fischer (La-049)	Rhine Graben	Y	Y	gas exploration	floor heating of a car seller's building	plate heat exchanger
Germany	Landau Laola (La-044)	Rhine Graben	Y	Y	HC well depleted	heating community swimming pool	heat pump
Germany	Prenzlau	North German Basin	Y	Y	deepend well	heating and warmwater for 550 living units	heat pump and gas/oil boiler (Güstrower Heat Exchanger Type Titan 26WW HTS)
Hungary	Kiha-D-7 (Kiskunhalas)	Pannonian Basin	N	Y	HC well depleted	test site	N/A
Hungary	Kiha EK-14 (Kiskunhalas)	Pannonian Basin	Y	Y	dry HC well (1981 tested for oil)	test site (for greenhouse)	N/A
Slovenia	Benedikt v Slovenskih Goricah	Pannonian Basin	Y	Y	dry HE well	community heating	N/A
Slovenia	Loče pri Poljčanah	Pannonian Basin	Y	Y	dry HE well	heating of few buildings	N/A

Table C 4: Overview of DBHE projects in the TRANSGEO partner countries focused on well reuse and purpose. N/A means that there is no information about this parameter available; -- means that there should be no data (if in cell "Status": abandoned, then in cell "Date abandoned": --). The table is ordered alphabetically country wise and then per site names.

C.4.1.1. Descriptions of well reuse for deep borehole heat exchanger energy production in the TRANSGEO region

In **Austria** one project in the Molasse Basin and one in the Vienna Basin were realised. Both of them were old hydrocarbon wells, repurposed after (test-) production.

In the Molasse Basin, RAG Austria, the owner of the well, used the well Mühlleiten 2 in the community Neukirchen at Vöckla to test a DBHE system. The hydrocarbon well Mühlleiten 2 was completed in 2009 and was not economically viable from an oil and gas production perspective. With a bottomhole temperature of 105°C, the 2850 metre deep borehole was suited for the extraction of geothermal energy. In 2011/2012, the Mühlleiten 2 borehole was upgraded to a deep borehole heat exchanger (German: Tiefe Erdwärmesonde – TEWS). The extracted heat was raised to a higher temperature level by means of a heat pump and supplied to Bioenergie Neukirchen, which operates a biomass heating plant and local heating network in the village of Neukirchen a. d. Vöckla, via a 1000 metre long underground connecting pipeline on the outskirts of Neukirchen (Doppelreiter, 2012). Due to not further known technical issues within the tubing, the well is currently shut-in.

Country	Site Name	Geological Unit	realised	Well reuse	Purpose	Pipeline distance to consumer (m)	System	Casing diameter (inch) at bottom DBHE	Tubing material and insulation	Temp bottomhole (°C)	Temp inlet (°C)	Temp outlet (°C)	Flow rate (l/s)	Total heating capacity (kWt)	Annual heat production (MWh/yr)
Austria	Hirschstetten 5	Vienna Basin	N	Y	glass house heating	40	co-axial	9 5/8	N/A	N/A	39 (best based on model)	58 (best based on model)	3,6 (best) (1 to 8 tested)	78 (at least needed)	--
Austria	Mühlleiten (Neukirchen an der Vöckla)	Molasse Basin	Y	Y	community heating	1000	co-axial	N/A	N/A	105	N/A	N/A	N/A	400-500 (after 2 yrs 200-250)	3500
Austria	Prottes T 11	Vienna Basin	Y	Y	heating of a gym hall	350	co-axial	7	N2 insulation	83 (at 2230 m initial) 60 (stable during production)	30	42	0.83 - 2.8	150 (max.)	N/A
Croatia	Pčelić-1	Pannonian Basin	N	Y	heating	N/A	co-axial	7	vacuum insulated tubing (VIT)	206.2 (at 4772 m)	N/A	70 50 10	10 20 30	500 1000 1250	N/A
Germany	Aachen (Super C)	North German Basin	Y	N	heating new University building	in the building	N/A	N/A	N/A	35	N/A	25	2.8	N/A	N/A
Germany	Arnsberg im Sauerland (NASS)	North German Basin	Y	N	heating of swimming pool, sports area, school	N/A	co-axial	N/A	steel-PP (long development phase to find right material)	90			20.0	350	N/A
Germany	Groß-Umstadt-Heubach	Variscian Basement	Y	N	heating medium industrial building (6000 m²) and office building (1400 m²), test site	N/A	co-axial	N/A	N/A	38	N/A	35	5.0	61	130.0
Germany	Landau Fischer (La-049)	Rhine Graben	Y	Y	floor heating of a car seller's building	~30	co-axial	7	Threelayer Material: PE-Xa und PE100 mit stainless steel armouring	112-83 (at 1050 m)	42	66-96	2.67-6.27	80	8.2
Germany	Landau Laola (La-044)	Rhine Graben	Y	Y	heating community swimming pool	500	co-axial	7	PE	63-80 (at 800 m)	37	63-80	2.67-6.27	88	0.5
Germany	Prenzlau	North German Basin	Y	Y	heating and warmwater for 550 living units	N/A	N/A	6 5/8	double steel insulated pipe	108	50	70	3.3	150	N/A
Hungary	Kiha-D-7 (Kiskunhalas)	Pannonian Basin	N	Y	test site	N/A	co-axial	N/A	N/A	N/A	N/A	N/A	N/A	N/A	N/A
Hungary	Kiha EK-14 (Kiskunhalas)	Pannonian Basin	Y	Y	test site (for greenhouse)	350	co-axial	7.0	N/A	N/A	N/A	N/A	N/A	520.0	N/A
Slovenia	Benedikt v Slovenskih Goricah	Pannonian Basin	Y	Y	community heating	N/A	co-axial	N/A	N/A	80 at 1000 - 1800 m	N/A	N/A	N/A	N/A	N/A
Slovenia	Loče pri Poljčanah	Pannonian Basin	Y	Y	heating of few buildings	N/A	u-type	N/A	N/A	N/A	N/A	N/A	N/A	N/A	N/A

Table C 5: Technical parameters of DBHE projects. N/A means that there is no information about this parameter available; -- means that there should be no data (if in cell "Status": abandoned, then in cell "Date abandoned": --). The table is ordered alphabetically country wise and then per site names.

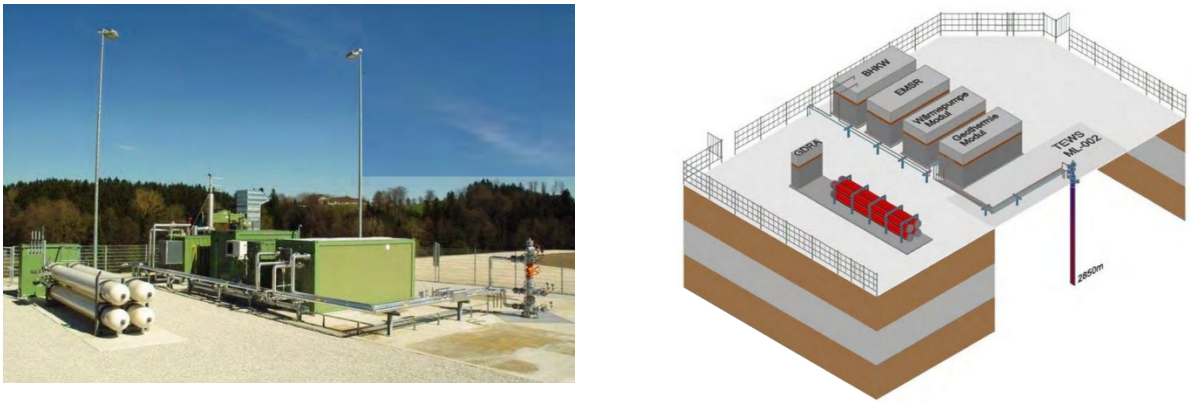

Figure C 3: Photo and construction sketch of surface facilities of reuse project Mühlleiten 2 (modified from Hinsch, 2012).

The DBHE project Prottes T 11 was situated in the central part of the Vienna Basin (Weinviertel) in Austria from 2009 until 2012. The well owner and operator was OMV. The site was developed as test site and the heat produced was used for heating a public gym hall.

The original depleted oil producer had a total depth (TD) of 2980 m, from which 2230 m (bottomhole temperature, BHT = 83°C) were used for the geothermal application. For the DBHE probe a coaxial tube was used. The tubing consists of the inner tube with the dimensions of 2 3/8' and the outer tube with 4 ½'. The casing has a diameter of 7'. The insulation chamber was filled with nitrogen.

With an adaptation of an eruptive cross, a new tubing and a geothermal container with the necessary sensors (EMSR equipment, which is a German automation term for “Elektro-, Mess-, Steuer- und Regelungstechnik”) the technical prerequisites for further applications were provided. The integration into an existing heating system took place in the form of the heating of the Prottes sports hall. For this purpose, a 350 m local heating pipe was laid. Three gas heat pumps were installed in parallel in the boiler room to raise the required temperature level.

Various temperatures and flow rates were tested, but above all, the inlet flow temperature, the inlet flow temperature, the BHT and the flow rate are of great importance. The inlet temperature is around 30°C, the outlet flow temperature is around 42°C and the flow rate of the heating medium is 1.4 l/s. This results in an extraction capacity of 65.5 kW.

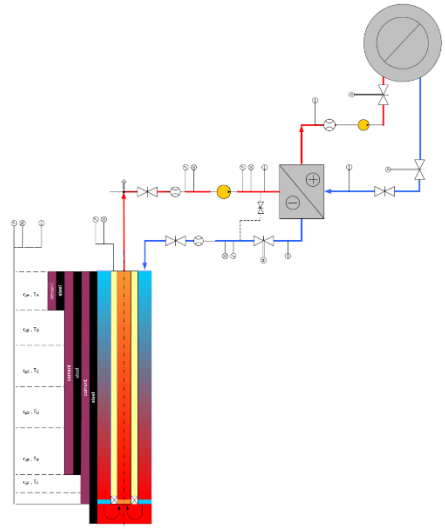

Figure C 4: Subsurface installation of the project Prottes T 11 (Bräuer, 2011).

Figure C 5: Pictures of the original hydrocarbon surface facilities before repurpose (Dürnegger, 2009).

Figure C 6: Surface installation of the project Prottes T 11 with the geothermal container, eruptive cross and recooler after repurposing (Bräuer, 2011).

In the Vienna Basin another depleted gas well, Hirschstetten 5, drilled in 1976, which is situated within the vicinity of Vienna, was modelled, but never realised (Dürnegger, 2009). The heat consumer should have been a greenhouse as a replacement for oil heating. The borehole was in the direct vicinity of the greenhouse.

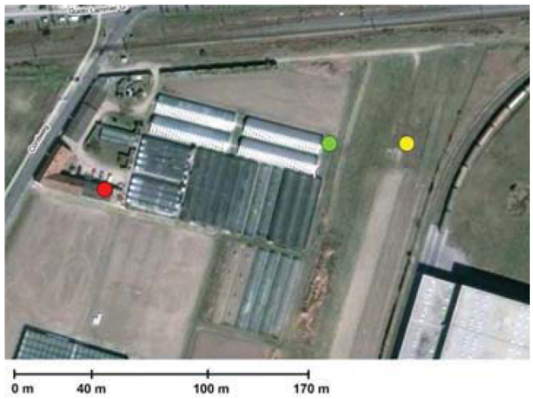

Figure C 7: Overview of distances of the greenhouses of “market garden Bach” and well location (Dürnegger, 2009). Yellow point: well Hirschstetten 5; green point: nearest greenhouse to well = 40 m; red point: oil heating system.

For Croatia, a future project of reuse was modelled by Macenić et al. (2020) for an existing well location, Pčelić-1, drilled and completed during 1989. The well has a total depth of 5214 m, from where 4500 should be used for heat extraction. The work focuses on determining maximum heating loads of the retrofitted well by means of installation of coaxial heat exchangers. With favourable geothermal gradient and heat flow, continental Croatia, settled mainly in the larger Pannonian Basin System (PBS), has good potential for using geothermal energy.

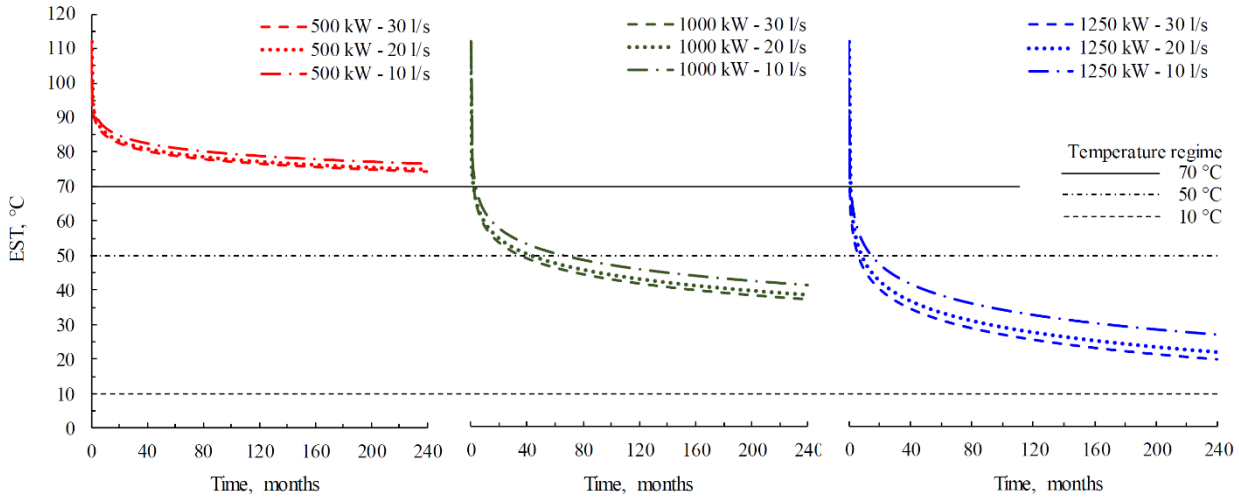

Figure C 8: Results of numerical modelling for different constant heat load values (500, 1000 and 1250 kWt) and different fluid flow (10, 20 and 30 l/s) for DBHE operation with an insulated tubing (Macencić et al., 2020)

In Germany, there are 3 DBHE projects which are using existing infrastructure of already drilled wells. They are situated in the North German Basin (project Prenzlau) and in the Rhine Graben (2 projects in the old oil and gas province Landau at Pfalz). The other 3 DBHE projects in Germany (Aachen, Arnsberg, Heubach) have newly drilled wells.

The DBHE Prenzlau was installed in 1994 in an old well which was deepened with a TD of 2786 m (Schneider et al., 1996). It provides heating and warm water for 550 living units. As tubing, a double steel insulated pipe is used. With a bottomhole temperature of 108 °C and flow rates from 0.083 – 1.083 l/s it reaches a heating capacity of 120 kWt without heat pumps. With heat pumps, the capacity reaches up to 550 kWt.

Figure C 9: Photos of the surface installation in Prenzlau (https://www.energie-experten.org/projekte/tiefen-erdwaermesonde-mit-waermepumpe-im-prenzlauer-waermenetz).

In the German part of the Rhine Graben, 2 sites of DBHEs in old hydrocarbon wells are realised and producing heat. They are both situated in Landau. A detailed description of the 2 sites in Landau can be found in Chapter C.6.2 as the sites are used for calibrating the numerical model of the TRANSGEO project (Activity 1.1.).

In Hungary, a hydrocarbon well was recompleted as DBHE in the vicinity of Kiskunhalas in the centre of the Pannonian Basin (Szekszárdi et al., 2022). The operating company MS Energy Solutions bought a well formerly owned by Kiha Földhő Ltd (Kiha-EK-14). The underground part of the project has been completed, but the well is still not producing. MS Energy Solutions plans to start a new reuse project with another well in Kiskunhalas (Kiha-D-7) as a follow up.

Figure C 10: Workover in Kiskunhalas (https://www.thinkgeoenergy.com/first-closed-cycle-geothermal-heat-plant-set-up-in-hungary/).

In Slovenia, two dry wells, which were originally drilled for hydrothermal energy production, were recompleted as deep borehole heat exchangers producing heat for the local community. They are both located in the Pannonian Basin. The well in Benedikt v Slovenskih Goricah has a TD of 1858 m with a BHT of around 85 °C. For the reuse application 1371 m were taken.

C.4.2. Deep Borehole Heat Exchanger projects in Europe outside the TRANSGEO region

Outside of the TRANSGEO working area in Europe, the countries, Spain, France, Italy, the Netherlands, Slovakia, Czech Republic, Ukraine, Finland and Sweden were checked about their inventory of DBHE projects (Tables C 6 and C 7).

Country	Site Name	Geological Unit	realised	Status	Date DBHE installed	Date abandoned	Well owner	Operator	Depth TD (TVD, m)	Depth used (TVD, m)
Czech Republic	Hrušky Z-40	Vienna Basin	Y	abandoned	2021	2022	MND	greenwell	1480	1020
Finnland	Jyväskylä	cratonic	N	modelled	not realised	--	N/A	--	N/A	600 1000 2000 3000
Finnland	Helsinki	cratonic	N/A	N/A	N/A	--	N/A	N/A	1300	N/A
Finnland	Rovaniemi	cratonic	N	modelled	not realised	--	N/A	--	N/A	600 1000 2000 3000
Finnland	Vantaa	cratonic	N	modelled	not realised	--	N/A	--	N/A	600 1000 2000 3000
France	Aigueperse	Limagnes	Y	producing	N/A	--	N/A	N/A	N/A	N/A
France	Hélions 1	Rhine Graben	Y	abandoned	N/A	N/A	N/A	N/A	1157	1157
France	Mios Le Teich	Aquitaine Basin	Y	producing	N/A	--	N/A	N/A	3758	2491
France	Pézenas	South-Est Basin	Y	producing	N/A	--	N/A	N/A	735	735
France	Sébastopol	Aquitaine Basin	Y	producing	N/A	--	N/A	N/A	2155	865
France	Sore 1A	Aquitaine Basin	Y	producing	N/A	--	N/A	N/A	3632	1646
Italy	Villafortuna 1 (Villafortuna-Trecate field)	sedimentary basin	N	modelled	not realised	--	N/A	--	N/A	N/A
Italy	Gela 38	sedimentary basin	N	modelled	not realised	--	N/A	--	N/A	N/A
Italy	Tempa Rossa	sedimentary basin	N	modelled	not realised	--	N/A	--	N/A	N/A
Netherlands	--	--	--	--	--	--	--	--	--	--
Norway	Gardermoen North	cratonic	Y	producing	2018	--	--	--	1485	1485
Norway	Gardermoen South	cratonic	Y	producing	2018	--	--	--	1497	1497
Poland	Sucha Beskidzka (R-1)	sedimentary basin	N	modelled	not realised	--	N/A	--	2436	2390
Slovakia	--	--	--	--	--	--	--	--	--	--
Spain	--	--	--	--	--	--	--	--	--	--
Switzerland	Weggis	Molasse Basin	Y	abandoned	1994	2000	N/A	N/A	2302	2300
Switzerland	Weissbad	Subalpine Molasse	Y	still producing?	1996		N/A	N/A	1600	1213
Ukraine	--	--	--	--	--	--	--	--	--	--
United Kingdom	Cornwall (Eden project; EG-1)	mafic	N	modelled	not realised	--	N/A	--	4871 (5277 MD)	4000
United Kingdom	Kirby Misperton	mafic	N	planned	not realised	--	N/A	CeraPhi	N/A	N/A
United Kingdom	Newcastle Science Central Deep Geothermal Borehole (NSCDGB)	mafic	N	modelled pump tested	not realised	--	N/A	--	1821	922

Table C 7: European DBHE projects outside the TRANSGEO partner countries.

Country	Site Name	Geological Unit	realised	Status	Date DBHE installed	Date abandoned	Depth TD (TVD, m)	Depth used (TVD, m)	Original use of well	Purpose	Pipeline distance to consumer (m)	System	Casing diameter (inch) at bottom DBHE	Tubing material and insulation	Temp bottomhole (°C)	Temp inlet (°C)	Temp outlet (°C)	Flow rate (l/s)	Total heating capacity (kWt)	Annual heat production (MWh/yr)
Czech Republic	Hrušky 2-40	Vienna Basin	Y	abandoned	2021	2022	1480	1020	HC well depleted	test site	N/A	co-axial	N/A	N/A	51	6-38	10-28	3-5	N/A	N/A
France	Aigueperse	Limagnes	Y	producing	N/A	--	N/A	N/A	hc well	Greenhouse	N/A	N/A	N/A	N/A	43	N/A	N/A	17	N/A	N/A
France	Hélions 1	Rhine Graben	Y	abandoned	N/A	N/A	1157	1157	hc well	District heating	N/A	N/A	N/A	N/A	65	N/A	N/A	3	N/A	N/A
France	Mios Le Teich	Aquitaine Basin	Y	producing	N/A	--	3758	2491	hc well	Fish farming	N/A	N/A	N/A	N/A	74	N/A	N/A	33	N/A	N/A
France	Pézenas	South-Est Basin	Y	producing	N/A	--	735	735	hc well	Fish farming	N/A	N/A	N/A	N/A	37.4	N/A	N/A	19	N/A	N/A
France	Sébastopol	Aquitaine Basin	Y	producing	N/A	--	2155	865	hc well	Thermal baths	N/A	N/A	N/A	N/A	46	N/A	N/A	36	N/A	N/A
France	Sore 1A	Aquitaine Basin	Y	producing	N/A	--	3632	1646	hc well	Fish farming	N/A	N/A	N/A	N/A	48	N/A	N/A	2	N/A	N/A
Italy	Villafortuna 1 (Villafortuna-Trecate field)	sedimentary basin	N	modelled	not realised	--	N/A	N/A	hc well	power generation	--	co-axial	N/A	steel, air	160-170	40	100.38	20	627.9	--
Italy	Gela 38	sedimentary basin	N	modelled	not realised	--	N/A	N/A	hc well	N/A	N/A	co-axial	N/A	N/A	160-170	50	58	3	110.5	N/A
Italy	Tempa Rossa	sedimentary basin	N	modelled	not realised	--	N/A	N/A	hc well	N/A	N/A	co-axial	N/A	N/A	160-170	50	56.0	3	75.3	N/A
Poland	Sucha Beskidzka (R-1)	sedimentary basin	N	modelled	not realised	--	2436	2390	uneconomic gas well	test site	N/A	co-axial	6 5/8	A single and a double, made of plastic, string of the inner pipes was analyzed, different materials tested	73.18 (at 2340 m)	16 (avg.)	18 (avg.)	0.8 1.7 2.5 3.3	N/A	N/A
Switzerland	Weggis	Molasse Basin	Y	abandoned	1994	2000	2302	2300	dry HE well	direct heating, warm water	N/A	co-axial	N/A	0-1780 vacuum	78	32 (100kW) 9 (250 kW)	40 (100kW) 28 (250 kW)	0.8-1.75	100	220
Switzerland	Weissbad	Subalpine Molasse	Y	still producing?	1996		1600	1213	Spa, then deepend well and tight	heat for spa and hotel complex of "Hof Weissbad	spa directly adjacent	co-axial	N/A	steel?	45 (at 1213 m)	9	15 expected 10.6 real	2.92	N/A	N/A
United Kingdom	Cornwall (Eden project; EG-1)	mafic	N	modelled	not realised	--	4871 (5277 MD)	4000	dry HE well (completed 2023)	Heat supply for Biomes (new commercial greenhouses and other buildings at the Eden Project)	N/A	co-axial	13 3/8	N/A	N/A	N/A	85 expected	N/A	N/A	N/A
United Kingdom	Kirby Misperton	mafic	N	planned	not realised	--	N/A	N/A	hc well	N/A	N/A	N/A	N/A	N/A	N/A	N/A	N/A	N/A	N/A	N/A
United Kingdom	Newcastle Science Central Deep Geothermal Borehole (NSCDGB)	mafic	N	modelled pump tested	not realised	--	1821	922	dry HE well (drilled in 2014)	Heat supply for Helix area, University of Newcastle (hybrid state-of-the-art quarter)	N/A	co-axial (CXC, CXA tested)	7 to 941 m (6 to TD)	N/A	N/A	N/A	3.46 - 3.83 (after 25yrs modelling)	8.33	50	569.4

Table C 8: European DBHE reuse projects outside the TRANSGEO partner countries.

C.4.2.1. Projects of well reuse for deep borehole heat exchanger energy production in Europe outside the TRANSGEO region

From the Czech Republic, there was one DBHE projects in an abandoned well realised in the northern part of the Vienna Basin, near Mikulov in 2021. The well has a TD of 1480 m, from which 1020 were used for energy production. The inflow and return temperatures were a test arrangement in which the return flow from the borehole was routed via air coolers, where different cooling capacities were used. The air temperature also played a major role. Due to the use of normal steel tubing, only a small temperature increase of 1 to 10°C was achieved (at very high temperatures, the well also cooled). A future potential candidate in the Czech Republic would be the freshly commenced SYNERGYS project in Litoměřice, where a DBHE is an exit strategy for the planned (new, not abandoned) 3.5 km deep EGS wells if they fail to create an EGS reservoir. These wells are planned to be drilled during 2025-2026 (https://rin-gen.cz/en/aktualne/strategicky-projekt-synergys-systemy-pro-energetickou-synergii-animace-technologickych-soucasti).

France has realised 6 reuse projects which are summarised and described in detail in Maurel (2019).

In Italy several potential studies for the revitalisation of depleted oil fields (Villafortuna, Gela, Tempa Rossa) exist (Facci et al., 2023; Gizzi et al., 2021). Villafortuna was numerically modelled by Alimonti et al. (2018) with a depth of 4000-5000 m, and it is the only DBHE planned in Europe (based on our review) to generate electricity.

For Poland one case study exists, which was not realised. The well is an uneconomic gas well, Sucha Beskidzka (R-1), with a TD of 2436 m, where 2390 m are modelled to be used as heat source (Sliwa et al., 2015).

Schwitzerland already started in the 1990s with the application of DBHE in existing wells. The projects are Weggis and Weissbad, which are documented in literature very well (e.g. Kohl et al., 2000; Falcone et al., 2018).

From the Ukraine there is information about several attempts to establish heat exchanger projects in different basins, mostly to repurpose abandoned or depleted petroleum wells. There were some technical assessments provided, but no project was approved for further investments.

In the United Kingdom, there is no operational DBHE. 3 reuse projects are in the planning phase, which are in Cornwall (Eden project; https://www.edengeothermal.com/the-project/drilling-and-operations/),

which has also recently re-completed a deep geothermal well as a coaxial DBHE to ca. 4 km, delivering water at 85◦C. Another project is realised in the Kirby Misperton gas field retrofitting a well (Kolo et al., 2024 and references cited therein), with an independent study suggesting that a thermal power of just under 300 kW over a typical UK heating season can be achieved (Nibbs et al. 2023; Kolo et al., 2024 and references cited therein). In Newcastle a 50 kW pilot experimental borehole is planned (Brown et al., 2023; Kolo et al., 2023; Kolo et al., 2024 and references cited therein).

C.4.3. Deep Borehole Heat Exchanger projects outside Europe

Outside Europe, there are DBHE projects mainly in USA and China. In the USA, 2 projects are reusing existing wells. From the others no information could be found. In China, at least 4 of the projects are designated as test sites with a limited amount of production duration (72 hours to 138 days). One project (iHarbour in Xian) consists of new drilled arrays of 91 DBHEs with a depth of 2500 m each (Kolo et al., 2024).

Country	Site Name	Geological Unit	realised	Status	Date DBHE installed	Date abandoned	Well owner	Operator	Depth TD (TVD, m)	Depth used (TVD, m)	Well reuse	Original use of well	Purpose	Pipeline distance to consumer (m)	System	Casing diameter (inch) at bottom DBHE	Tubing material and insulation	Temp bottomhole (°C)	Temp inlet (°C)	Temp outlet (°C)	Flow rate (l/s)	Total heating capacity (kWt)	Annual heat production (MWh/yr)
China	Jimo	N/A	Y	producing	N/A	--	N/A	N/A	2600	N/A	N/A	--	N/A	N/A	N/A	N/A	N/A	83.2	N/A	14.5	8.5	N/A	N/A
China	Qingdao	N/A	Y	shut-in	N/A	N/A	N/A	N/A	2605	N/A	N/A	--	138 days test site with fixed inlet temperature	N/A	N/A	N/A	N/A	87.4	5	< 20	8.3	N/A	N/A
China	Songyuan	N/A	Y	shut-in	N/A	N/A	N/A	N/A	2044	N/A	N/A	--	60 days experimental test site	N/A	N/A	N/A	N/A	107.3	36,7 (1st day) 29,1 (60th day)	58,2 (1st day) 43 (60th day)	8.3	N/A	N/A
China	Xi'an	N/A	Y	producing	N/A	--	N/A	N/A	1962	N/A	N/A	--	N/A	N/A	N/A	N/A	N/A	75.6	N/A	> 25	7.8	N/A	N/A
China	Xi'an	N/A	Y	shut-in	N/A	N/A	N/A	N/A	2100	N/A	N/A	--	72h experimental test site	N/A	u-type	N/A	N/A	70.3	19.5	> 29,5	11.3	N/A	N/A
China	Xi'an	N/A	Y	shut-in	N/A	N/A	N/A	N/A	2000	N/A	N/A	--	106 days experimental test site	N/A	5 DBHE arry	N/A	N/A	80.8	13,6 (avg.)	20,8 (avg)	31.9	N/A	N/A
China	Xi'an (I Harbour)	N/A	Y	producing	N/A	--	N/A	N/A	2500	N/A	N/A	--	heating University	N/A	91 DBHE array	N/A	N/A	N/A	N/A	N/A	N/A	N/A	N/A
China	Yulin	N/A	N	planned	N/A	N/A	N/A	N/A	N/A	N/A	N/A	--	N/A	N/A	N/A	N/A	N/A	N/A	N/A	N/A	N/A	N/A	N/A
USA	California	N/A	N	planned	not realised	--	N/A	N/A	N/A	N/A	N/A	--	N/A	N/A		N/A	N/A	N/A	N/A	N/A	N/A	N/A	N/A
USA	Hawaii	volcanic	Y	producing	1991	--	N/A	N/A	N/A	N/A	Y	abandoned geothermal well	N/A	N/A	inner dual vacuum tube	N/A	N/A	110	30	98	1.3	N/A	N/A
USA	Newberry, Oregon (T2Well/EOS1)	volcanic	N	modelled	not realised	--	N/A	--	N/A	N/A	Y	N/A	N/A	N/A		N/A	heat conduction filler: graphite	N/A	N/A	N/A	N/A	N/A	N/A

Table C 9: Overview of Deep Borehole Heat Exchanger projects worldwide (outside Europe) with parameters.

There are general studies to the topic of reuse potential for Turkey (Kaplanoğlu et al., 2017). Similar studies have been reported for abandoned oil wells in Pakistan (Mehmood et al., 2017; Mehmood et al., 2019), Iran (Noorollahi et al., 2015; Noorollahi et al., 2016), Qatar (Madiseh SAG, 2013) and India (Singh, 2020).

C.5. Parameters

The parameters that influence the performance of the system are divided into three categories. The first category, operating conditions can be actively changed by the operator and is dependent on the use of the energy that is extracted by the DBHE. The well design parameters are set prior to construction of the system and can in some cases only be restrictively changed, depending on the limiting factors of an existing borehole that is re-purposed. Geological conditions also have a large impact on the efficiency of the system but are pre-defined by the nature surrounding the wellbore. It is important to carefully investigate whether the prevailing conditions at the desired location where the system should be implemented are favourable. The parameters, subdivided into their respective category are shown in an overview in **Error! Reference source not found.** and are further discussed below.

Geological Conditions	Operating Conditions	Well Design Parameters
Depth	Heat and cold demand	In-/Outlet configuration
Geothermal gradient	Flow rate	Working fluid
Thermal properties	Fluid inlet temperature	Pipe and borehole properties (thermal and geometrical)
**Groundwater flow*	Variability of heat extraction	Grout
		Well location (Heat demand)

Table C 10: Categorisation of parameters. **) The impact of groundwater was not investigated, but if present, should be taken into account.*

C.5.1. Geological conditions

The depth of the DBHE has a fourfold effect on the performance, as the contact surface which enables heat transfer, and the residence time of the fluid in the hot environment both increase and a higher formation thermal conductivity is typically found at deeper locations. This is important, as effluent fluid temperature is directly proportional to the thermal conductivity and inversely proportional to the square root of thermal diffusivity (Alimonti et al., 2018). Furthermore, the geothermal gradient ensures higher temperatures with greater depth (Gascuel et al., 2022). Compared to the thermal properties of various formations in the near wellbore region, the latter is more commonly known and accessible for different sites which makes it a good first point of reference for evaluating possible locations. As mentioned before, the closed-loop DBHE is not directly dependent on a suitable aquifer to work properly. However, the eventual impact of groundwater flow that might influence the efficiency of the system should be addressed (see Chapter C.6.5). In terms of thermal energy yield and the specific heat rate, deeper boreholes with higher subsurface temperatures generally result in better thermal production (Piipponen et al., 2022).

C.5.2. Operating conditions

Generally, the user profile gives quite narrow limits for the operating conditions of the system. Especially the heat and cold demand represents a hard limitation. Flow rate and temperature limits can be adapted to the needs within certain limits. Roughly speaking, the lower the flow rate the higher the temperature output of the DBHE. The completion of the well – especially the inner pipe diameter – has to be designed accordingly to the desired flow rates and temperature level.

The generally expected correlations between the flow rate and other operational parameters are:

Higher Flow Rate

→ Lower temperature output

→ Higher power output

→ Higher pressure drop → More pumping power

Hence, the user needs to find the best trade-off for the use case. This can be achieved through numerical modelling and a sensitivity analysis.

C.5.3. Well design parameters

As already mentioned, the annular inlet coaxial configuration is considered best for DBHE applications, making it the system of reference for the whole chapter. The geometrical properties of the pipes also significantly influence the performance of the system. By increasing the outer diameter (if possible) the overall heat transfer is improved which is even more impactful when considering small diameters (e.g., 180 mm and 220 mm). On the other hand, an increase of the inner pipe diameter (outlet pipe) leads to a decrease in performance. Keeping this in mind, decreasing the inner pipe diameter for an optimal thermal performance, the pressure drop that is increased at the same time needs to be considered which results in additional power consumption and ultimately operating costs. The thermal conductivity for the inner and outer pipe should be low and high, respectively. High thermal conductivity of the outer pipe enables the system to extract heat from the near wellbore region, while the low thermal conductivity of the inner pipe prevents thermal losses of the ascending fluid to the descending fluid, an effect that is called thermal short-circuiting (TSC). TSC is further favoured by great depths and low flow rates. Gascuel et al. (2022) also showed that the effect of the change in thermal conductivity of the inlet pipe is more prominent at low values (e.g., 1-5 W/m/K) but negligible for higher values (e.g., 10 W/m/K). The thermal properties of the inlet pipe depend on the material that is used, which for example can be high density polyethylene (HDPE), vacuum insulated tubing (VIT), insulated coil tubing; glass fibre reinforced plastic – in German: "Glasfaserverstärkter Kunststoff" (GFK).

The grout represents a challenge for DBHEs, especially when old wells are to be repurposed. The thermal conductivity should be high, for the same reason that applies to the outer pipe. The grout commonly used in oil and gas wells has a thermal conductivity of 0.7 W/m/K which presents an obstacle to heat transfer. In the case that a new well is drilled, the grout, additionally to its thermally enhanced properties needs to ensure well stability and provide an impermeable layer to prevent leakages or fluid inflow. Fulfilling these characteristics while having the ability to be poured easily creates a huge challenge (Gascuel et al., 2022). A 2500 m deep well in Germany (Aachen) used grout with a thermal conductivity of 2.02 W/m/K (Dijkshoorn et al., 2013; Sapinska-Sliwa et al., 2015). Water as a working fluid is commonly applied due to its thermal properties (i.e., high heat capacity) and low cost. An evaluation is ongoing where additives are tested that increase the efficiency of the system (e.g., adding 3%$_{vol}$ of aluminum oxide to increase the heat exchange by 1%; Alimonti et al., 2018) Last but not least, the well location needs to provide the ability of a DBHE to supply heat where it is demanded, by linking the system to a customer that is nearby heat losses in surface flow lines and investments for surface infrastructure are decreased.

C.6. Numerical simulation

C.6.1. Method

A dual continuum model (FEFLOW) is used for the modelling tasks in TRANSGEO. The DBHE is embedded as 1D analytical element in a finite element model. For these kinds of models, the correct discretisation around the wellbore is essential for a correct calculation of in- and outlet fluid temperature. This "ideal element size" is about 6 times the borehole radius (Diersch et al., 2010). In the case of retrofitted or depleted hydrocarbon wells with large drilling diameters this ends up with elements being too large considering the sharp thermal gradient around the DBHE, resulting in unstable model conditions. The work-around for this case is the fine discretisation of the DBHEs interior as homogeneous high thermally conductive medium with a discrete 1D element as BHE in the centre. This approach represents a compromise between the computationally easy dual continuum model and computationally expensive full discretisation including a Computational Fluid Dynamics (CFD) simulation of the BHEs interior and also enables the consideration of telescopic well design. The latter is not implemented in the Landau model.

C.6.2. Model validation on reference site Landau

Because data on implemented DBHE projects is very often company property and therefore not publicly accessible, the choice fell on 2 projects in "Landau an der Pfalz", which have been successfully operated for heating purposes for over 10 years.

Figure C 11: Location of Landau in der Pfalz in Germany (turquoise point).

In Landau, two former oil production wells that were no longer sufficiently productive, were converted into deep geothermal probes. The oil field with the two wells was operated by Wintershall Holding GmbH

at the time of this conversion and was later taken over by RDG GmbH (now ONEO GmbH). Both projects were initially realised in cooperation between EnergieSüdwest AG and Wintershall Holding GmbH (LBEG report, 2021).

The dataset provided by ONEO GmbH contains borehole data (including geological profile, lithology, casing scheme) and monitoring data of the DBHE operation through time. The monitoring data is quite sparse; these are the monthly sum of heat output [kWh] and daily measured temperature values. Values like heat extraction and flow rate had to be calculated (see Chapter C.6.3).

Site description

The hydrocarbon wells in Landau were drilled to bring oil and gas of the sediment filling (Figure C 13) of the Rhine Graben into production in the 1950s. The internal structure of the reservoirs is dissected by various faults. Therefore ca. 150 wells were drilled since the beginning to produce from every reservoir compartment.

The well La-044 was converted into a closed, coaxial deep geothermal probe by installing a 909 metre long inner pipe made of glass fibre reinforced plastic (GFK) in order to supply geothermal heat for heating a swimming pool at the LaOla leisure pool with the support of a heat pump. The heat output obtainable from the borehole was 88 kWt (LBEG report, 2021).

In order to convert the borehole La-049 into a closed, coaxial deep geothermal probe, a 794 metre long inner pipe made of PE-Xa was installed. The aim was to utilise the geothermal energy from this borehole directly without a heat pump in order to operate the floor heating in a car dealership. The heat output that could be obtained from the borehole was 80 kWt (LBEG report, 2021).

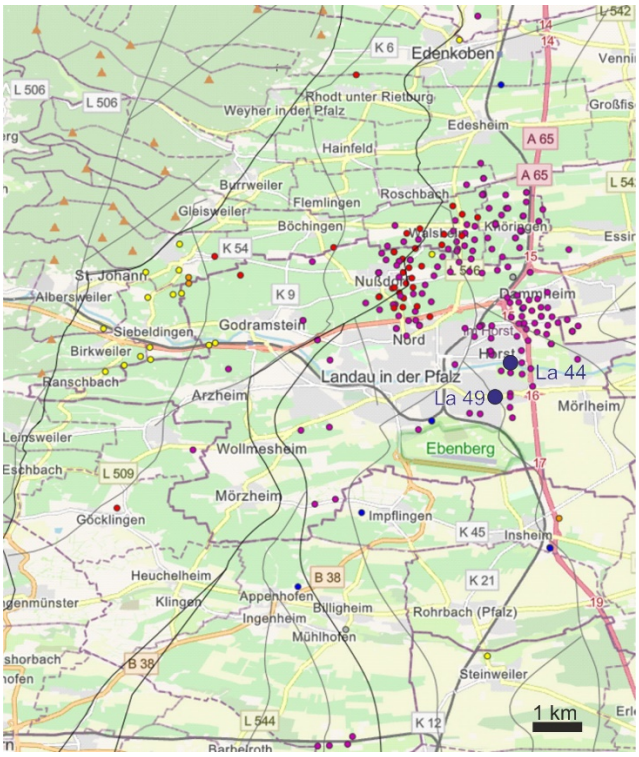

Figure C 12: Locations of hydrocarbon wells in the vicinity of Landau/Pfalz (magenta points). The dark-blue points mark the wells La 44 and La 49 which are used as deep borehole heat exchangers after hydrocarbon production was suspended.

Well details can be found at: https://geo.geopotenziale.eu/geonetwork/srv/de/main.home and via WMS service.

GEOLOGISCHES PROFIL		MAECHTIGKEIT
	DILUVIUM = PLEISTOZAEN	62.5
	PLIOZAEN	0.0
	OBER-MIOZAEN	22.5
	OB. HYDROBIEN SCH.	506.5
	UNT. HYDROBIEN SCH.	59.0
	CORBICULA SCHICHTEN	135.0
	CERITHIEN SCHICHTEN	150.5
	BUNTE NIEDERR.-SCHICHTEN	63.0
	STOERUNG----------S.A.150 m---	0.0
OELFUENDIG	CYRENENMERGEL	101.0

Figure C 13: Typical geological cross section of a well bore in Landau showing the Neogene sediment fill of the Rhein Graben with their thickness ("Schichten" means "layer"; "Stoerung" means "fault; "oelfuendig" means "oil-bearing"; "Maechtigkeit" means "thickness").

As displayed in Figure C 14, the temperatures in the Rhine Graben are favouring geothermal applications. The geothermal gradient is high with 80 °C/km, which lead to temperatures at -500 m of 45-75°C in Landau and at -1000m of 90-100 °C.

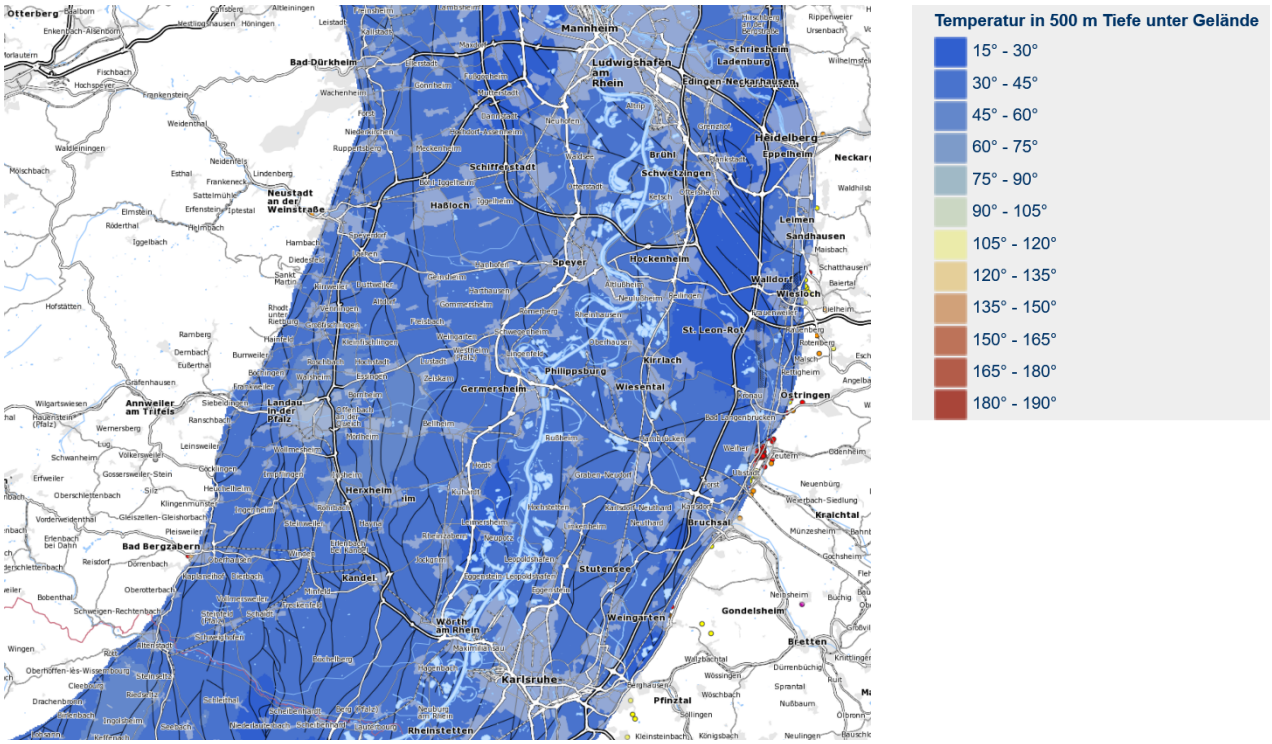

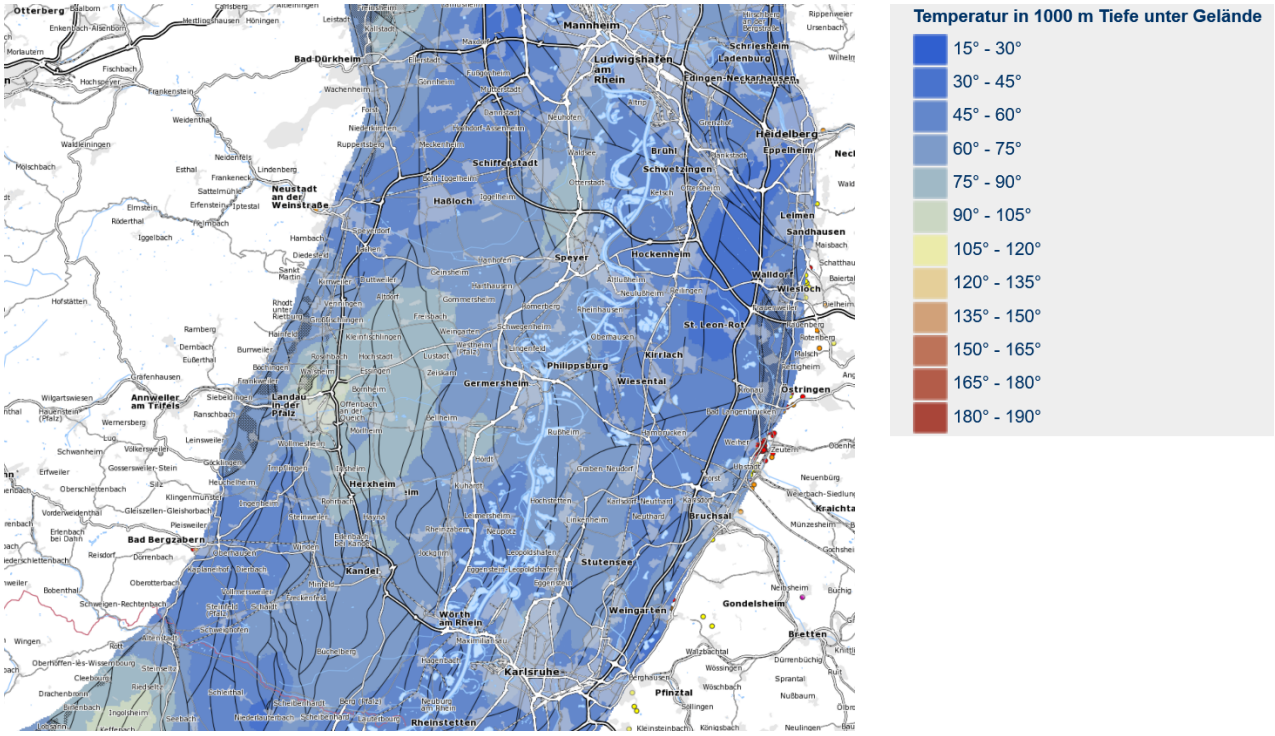

Figure C 14: Temperature in the Upper Rhein Graben at -500 m (NN) (top) and -1000 m (NN) (bottom) depth; maps from https://geo.geopotenziale.eu/geonetwork/srv/de/main.home. The geothermal gradient is higher than the average: 80 K/km.

Well Landau 44 (DBHE for LaOla swimming pool)

The calibration site in Landau is well Landau 44, drilled in 1957 to a total depth 1100 m MD (964 m TVDSS), which found oil and produced in the Cyrenenmergel (marls).

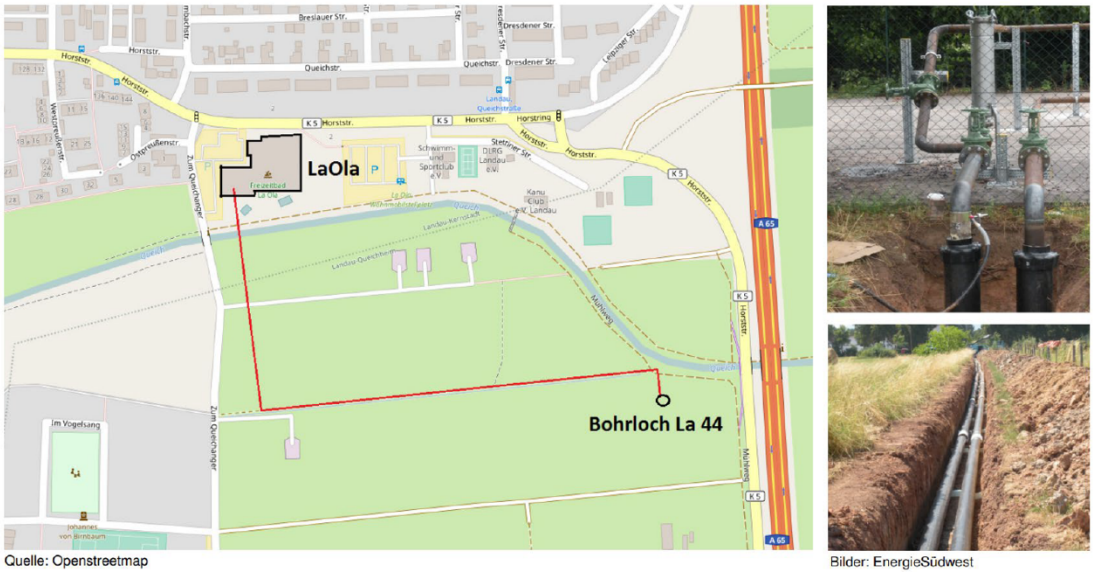

Figure C 15: Location of well Landau ("Bohrloch La 44") in relation to heat consumer swimming pool ("LaOla"). A 500 m pipeline was needed to connect producer and consumer.

Numerical model setup

To establish the mesh in FEFLOW the „Ideal Element Size“ around the DBHE was taken, which is 6.3 x borehole radius (10 cm). That leads to an element size of 63 cm which is too large for the steep thermal gradient around the DBHE. Therefore the DBHE was discretised with high conductivity inside. This represents an accurate, stable solution, but requires high computing power and time. As tubing in the CXC design was applied, where colder fluid is injected through central pipe and warmer fluid is produced through the annulus. The other dimensions used for modelling are displayed in **Error! Reference source not found.**.

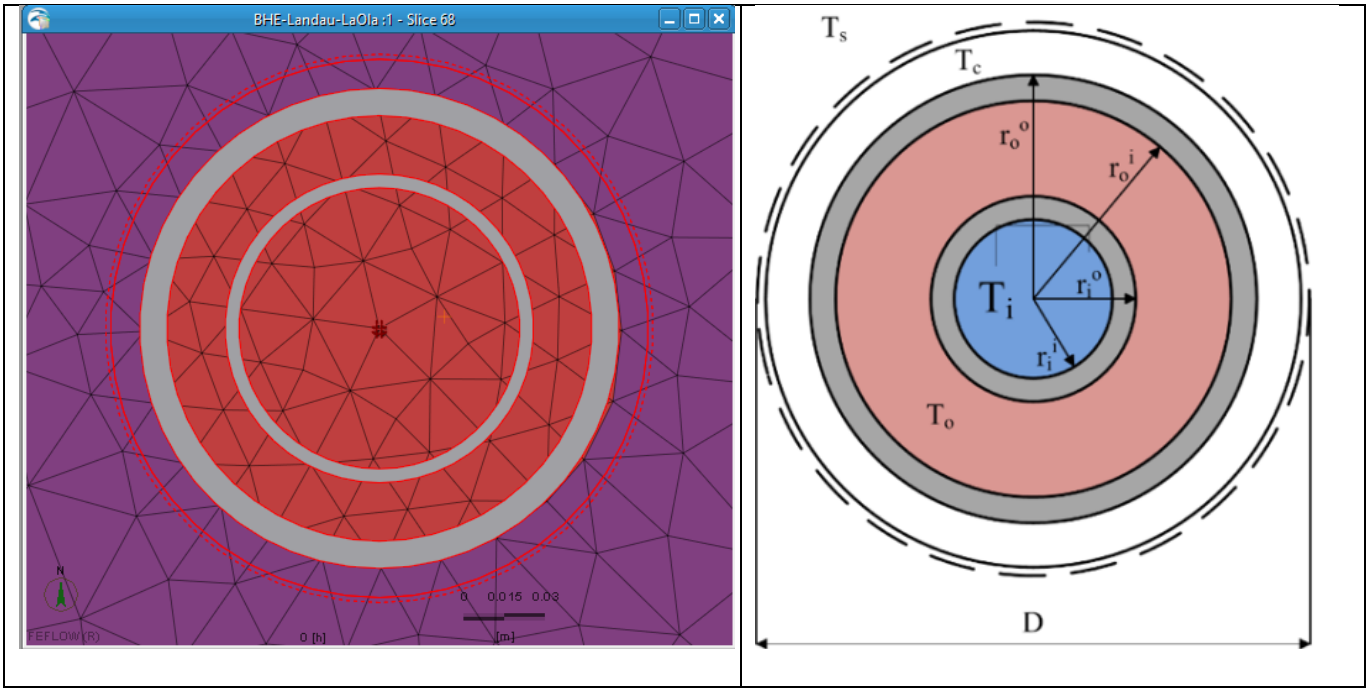

Figure C 16: Model setup in FEFLOW with CXC fluid flow configuration (right picture taken from Macenic et al., 2020).

Parameters	Value	Unit	Value	Unit
Depth			**900**	**m**
Borehole diameter	**8 1/2**	**inch**	**21,6**	**mm**
Outer diameter - outer pipe	**7**	**inch**	**177.8**	**mm**
Thickness casing	**--**		**8.05**	**mm**
Inner diameter - outer pipe	**--**		**169.75**	**mm**

Table C 10: Geometrical properties of the coaxial borehole heat exchanger used in the case study (see also Chapter C 6.5).

C.6.3. History matching

Based on the available monitoring data from well La-044 (LaOla) an attempt of a model-history matching was executed. The monitoring data is quite sparse and contain only the monthly sum of heat output [kWh] and daily measured temperature values (Figure C 17). It is unknown whether the temperature is a daily mean or measured once a day. In either case, assuming a 24/7 operation of the system, the fluid circulation rate q can be estimated based on the equations below:

$$q = \frac{P_{th}}{\Delta T * c_P}$$

$$P_{th} = \frac{monthly\ Heat\ demand}{1\ month\ (730\ h)},$$

where P_{th} is the heat output, ΔT is the temperature, c_P heat capacity coefficient.

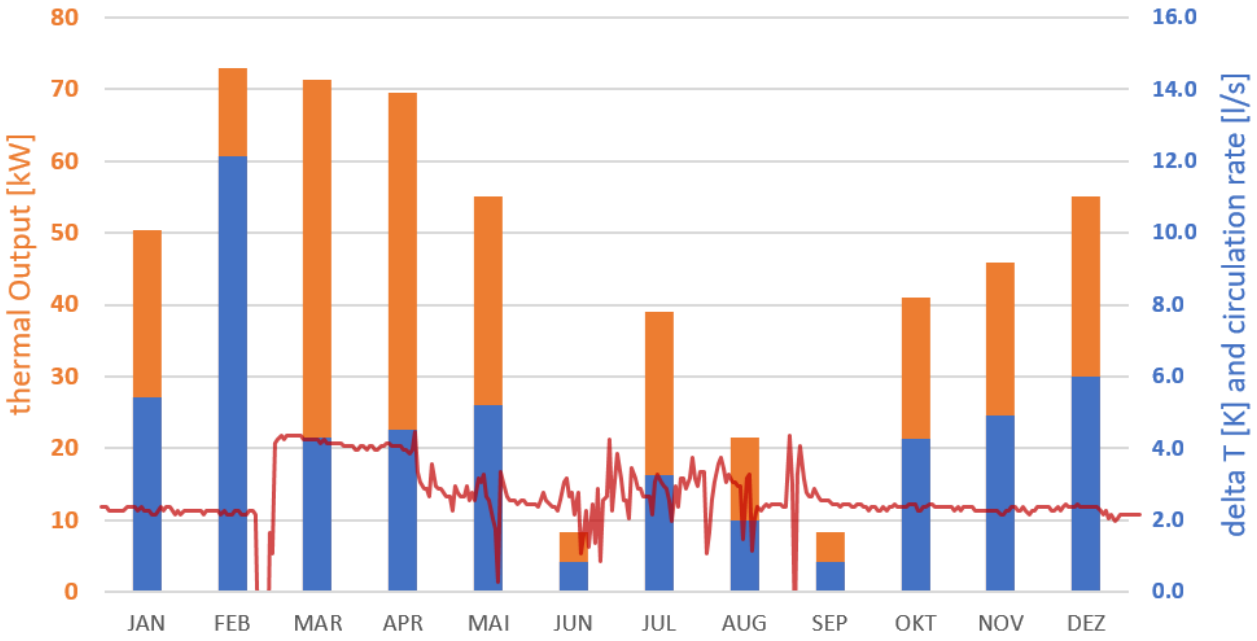

Figure C 17: Monitoring data (input data) from one year of well Landau 44; blue bar: flow rate (l/s), orange bar: heat capacity 24/7 (kWt). The red line represents ΔT [K].

The implemented history matching is based on a simplified procedure, where the underground thermal conductivity is adopted manually to produce a reasonable fit between measured and modelled temperature in- and output. The calculated heat output of the DBHE is considered as fixed.

Figure C 18 shows the results of the history matched model, considering the uncertainties of the input data the results are satisfying. A constant heat load (blue line in Figure C 18) is used for further calculations of the proof of concept (base case) and sensitivity analysis.

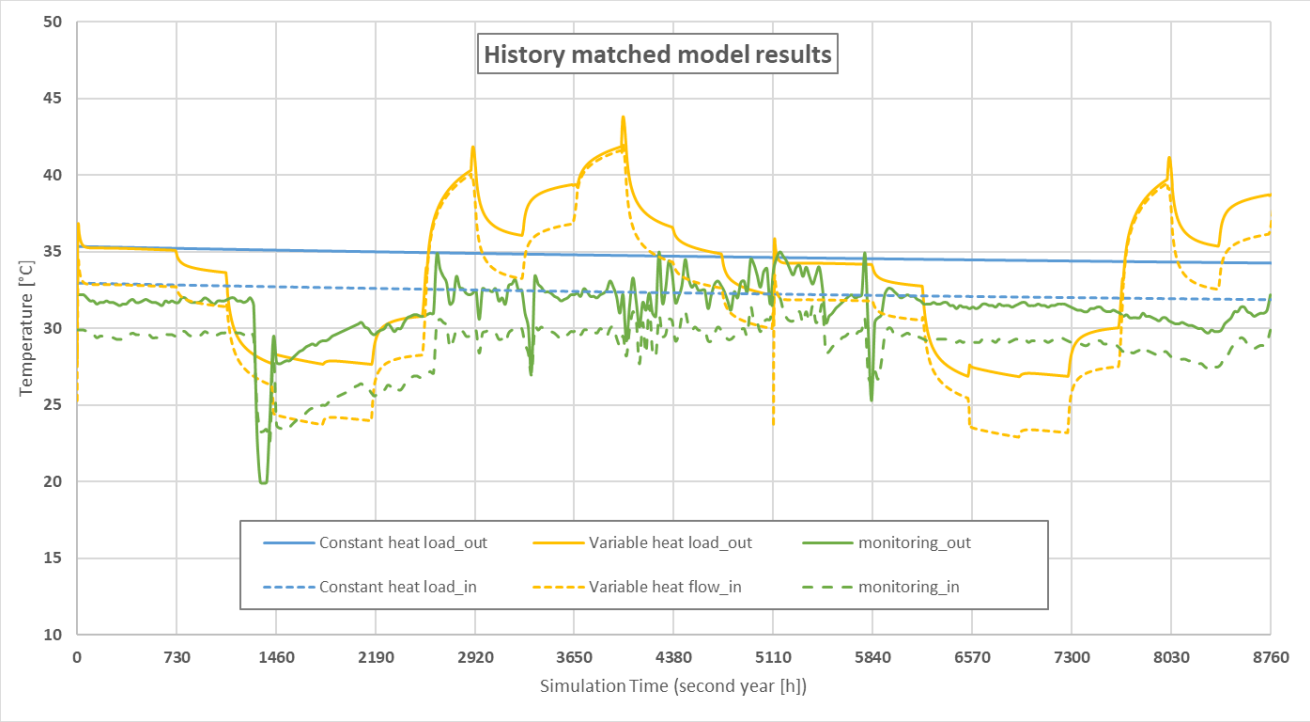

Figure C 18: History matched model results of the base case (Landau case). Inflow temperature is marked with stippled lines and outflow temperatures with solid lines. The blue lines represent constant heat load modelled, the yellow lines variable heat loads modelled and the green lines the monitored real data of the Landau well.

C.6.4. Proof-of-concept (base case)

A constant heat load over a period of 25 years is calculated to predict the long-term behaviour of a DBHE based on the "base case" site Landau. While in the first year of operation a significant temperature drop appears, this drop is approximately 0.5 K/a in the third year, further reducing with time to about 0.2 K/a in the 25th year of operation. In total numbers, this means a reduced production temperature of ca. 34 °C, starting from about 45 °C at the beginning of operation. This has to be taken into account for the planning and layout of the installation.

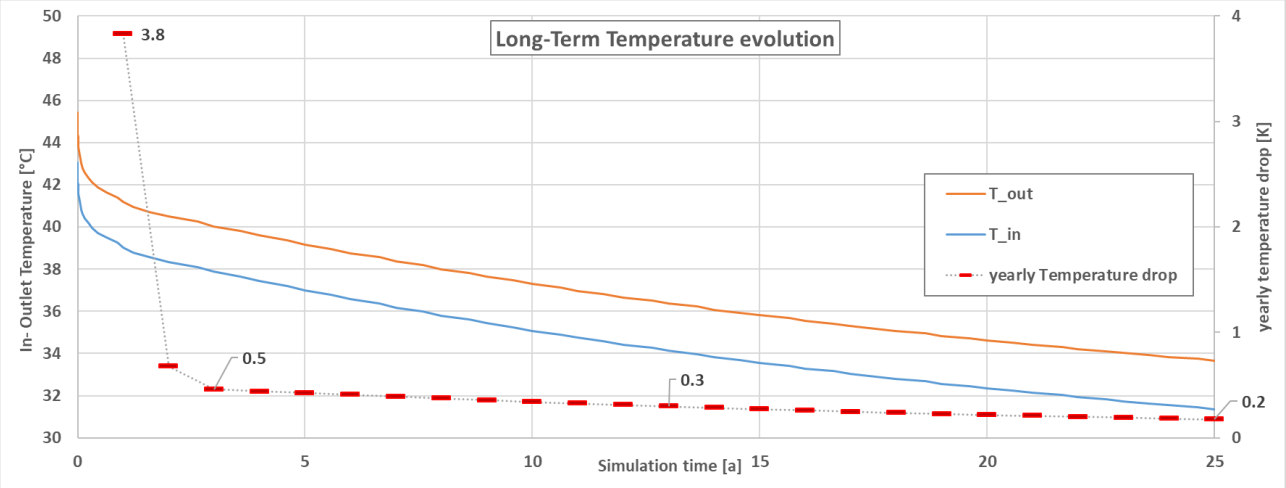

Figure C 19: Long-term temperature evolution.

C.6.5. Sensitivity analysis

The sensitivity analysis uses the history matched model from the site at Landau that has been described in the previous chapter as a base case. The simulation-time control has been adapted to reduce the computational time to investigate the influence of the relevant parameters within a reasonable amount of time. The final simulation time is 43 800 h (corresponding to 5 years), as the further course of output data can be estimated for longer times of operation, based on the history matched model. The goal of the sensitivity analysis is to determine the parameters that have the most impact on the sustainable use of the system over five years, which is more specifically defined as a system outlet temperature of more than 25 °C.

Parameter	Low	Base	High	Unit	Comment
Flow rate	2.67	4.48	6.27	[l/s]	
Heat output(Heat demand)	26.91	44.85	62.79	[kW]	
Thermal conductivity working fluid	0.51	0.59	0.8	[W/m/K]	Thermal parameters of working fluid have been changed simultaneously, representing three different fluids
Volumetric heat capacity working fluid	3920	4191	4200	[kJ/m3/K]	
Outlet pipe diameter (inner pipe)	0.09	0.11	0.14	[m]	Wall thickness is adjusted accordingly
Thermal conductivity outlet (inner) pipe	0.03	0.34	0.40	[W/m/K]	
Depth	728	910	1092	[m]	
Geothermal gradient	30	80	45	[°C/km]	
Groundwater flow		unknown			At top and bottom of the well profile

Table C 11: Simulation matrix used for the sensitivity analysis.

The change in flow rate and the amount of heat extraction is defined as 40% deviation from the base case. The three working fluids that are investigated are water for the base case, water mixed with an antifreeze additive for the low case, and water mixed with nanoparticles (nanofluid) for the high case. The respective values have been estimated in this case as there is a lack of satisfying literature but correspond to realistic properties of such fluids. A -20% and +20% change in the outlet pipe diameter is assumed for the low and the high case, respectively. Additionally, the wall thickness has been adopted to fulfil estimated requirements for the minimum strength of the pipes to ensure integrity. The thermal conductivity of the inner pipe is chosen for VIT and HDPE, while it is worth mentioning that an insulated coil tubing might even have a lower thermal conductivity than the VIT. The depth and geothermal gradient are also included in the sensitivity analysis, as they might differ significantly for different re-purposing projects throughout Europe. As the influence of groundwater flow on DBHE is not investigated thoroughly yet, a case where groundwater flow is prominent in the upper, and one in the lower part of the well length is included. The inlet configuration (e.g., annular inflow and centred outflow) is not changed,

as the annular inflow configuration has been shown to be most effective within the literature review. Also, the effect of an increased outer pipe diameter has been shown to be superior to smaller diameters which is why it is not included in this study. As these outer pipes are not interchangeable in the re-purposing of an old well, the thermal conductivity is not altered, too.

Flow Rate

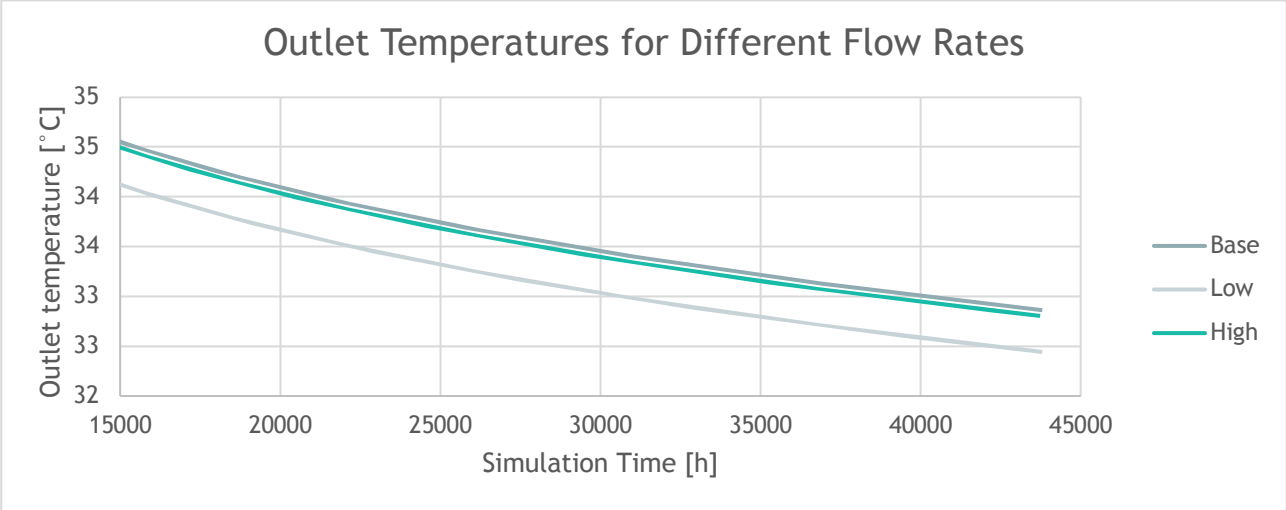

Figure C 20: Impact of different flow rates on outlet temperature. Flow Rate: Base: 4.48 l/s, Low: 2.67 l/s, High: 6.27 l/s.

Figure C 20 only shows the simulation time from 15000 h onwards, to better visualize the results after ten years. The final outlet temperatures are 32.44°C, 32.86°C, and 32.8°C for low, base, and high case, respectively. Both a higher and a lower flow rate result in a decreased outlet temperature after five years of operation. This leads to the conclusion that for a given well setup, there is an optimum flow rate to use the system in the most sustainable way. Though most literature describes an increase in temperature by a decrease in flow rate, attributed to a longer residual time of the working fluid in the hot environment of the borehole, this effect is countered by an increased cooling time of the upwards flowing fluid by the downwards flowing fluid. This effect is shown by the Figure C 21, where the temperature along the well is plotted. The blue line corresponds to the fluid in the downwards pathway, while the red represents the fluid on its way to the surface. The upper graph shows the low case, while the high case temperature profile is shown on the lower graph.

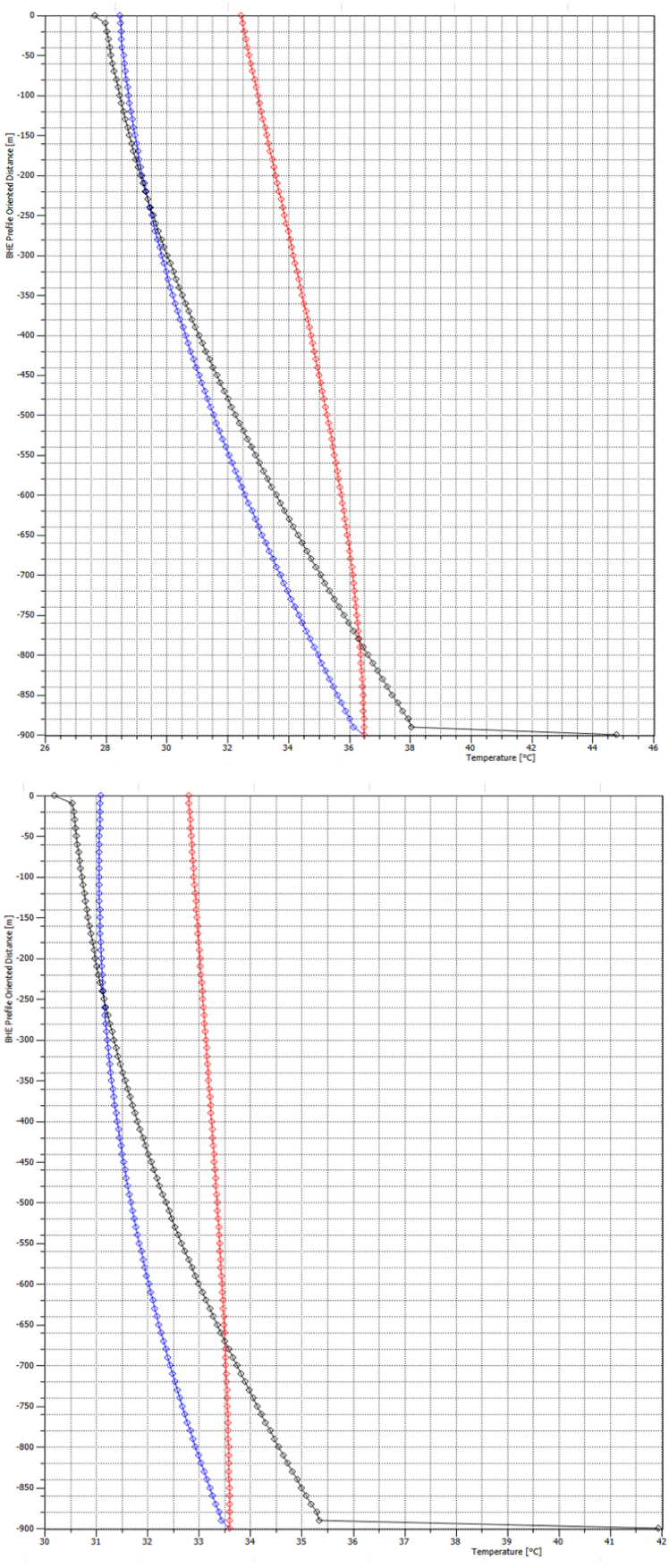

Figure C 21: Simulated temperature profiles along the borehole with a low fluid circulation rate (upper graph) and a high fluid circulation rate (lower graph).

The blue line shows the temperature of the downwards moving fluid in the annulus, the red line shows the temperature of the upward moving fluid inside the coaxial pipe and the black line shows the temperature of the immediate surroundings of the well.

Though the fluid with a lower flow rate reaches a higher BHT, the temperature drops comparably more from bottom to top, induced by the thermal short-circuiting between the colder downward flowing fluid inside the annulus and the warmer upward flowing fluid inside the pipe. In Figure C 22, the different outlet temperatures according to the respective flow rates are shown.

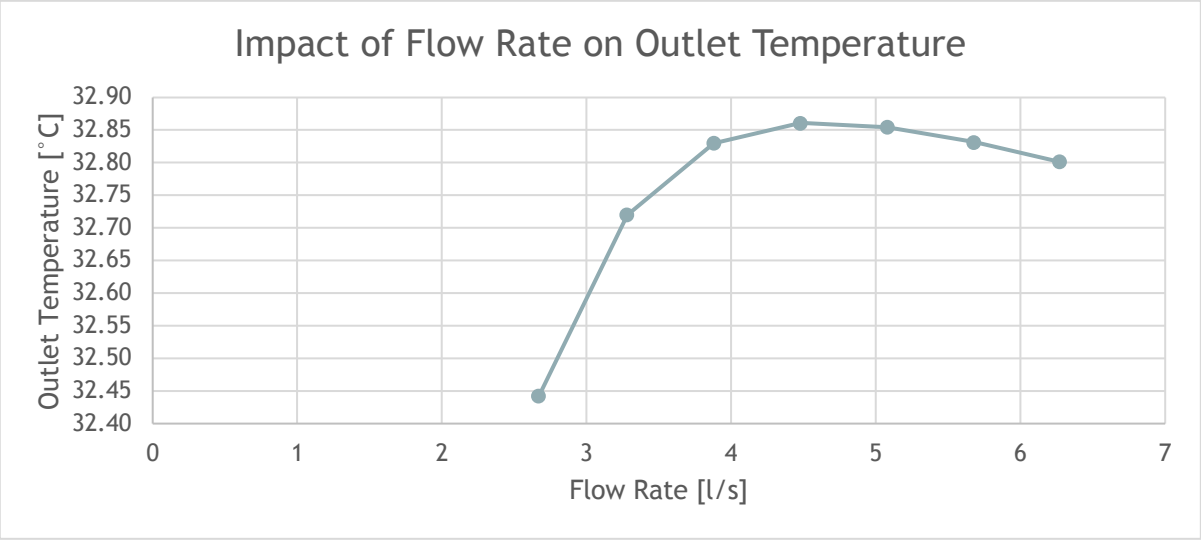

Figure C 22: Influence of flow rate on outlet temperature.

Heat extraction (Heat demand)

As might be expected, the heat extraction rate has the strongest influence on the temperature output. While the circulation rate is fixed, the heat extraction rate is varied by +/- 40 % of the base case. For the Landau case study, this yields a variation of the temperature output from ~ 27 °C for the "High" case and 40 °C in the "Low" Case. This can make the difference whether a heat pump has to be implemented or not and "free heating" can be considered. Hence, this trade-off might have a strong impact for the economics of the project.

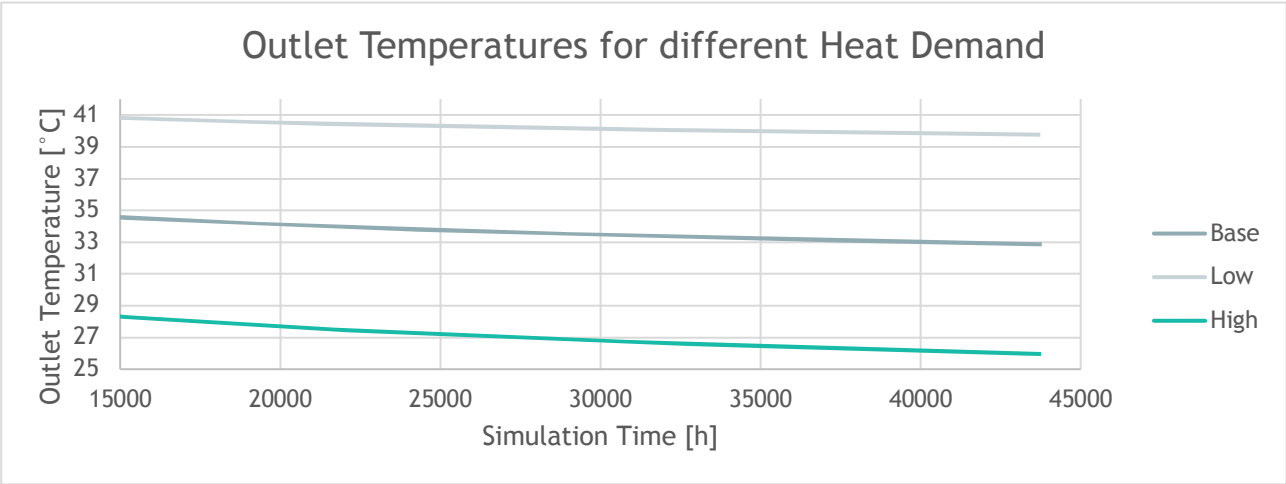

Figure C 23: Outlet temperatures for different heat output values. Base: 44.85 kW, Low: 26.91 kW, High: 62.79 kW.

Working Fluid

Different working or circulation fluids have been considered. While pure water is most common for DBHE installations, there are also cases where antifreeze is considered and implemented. While antifreeze has a negative impact on the thermal and hydrodynamic properties of the fluid, an evaluation is ongoing where additives are tested that increase the efficiency of the system (e.g., adding 3%$_{vol}$ of aluminum oxide to increase the heat exchange by 1%; Alimonti et al., 2018). The sensitivity analysis is carried out implementing the values from Table C 12 and a constant heat load. Our results show no mayor influence of the choice of working fluid on the obtained temperature (Figure C 24).

Fluid types	Outlet temperature [°C]	
Water with antifreeze	32.85	Low Case
Water	32.86	Base Case
Nanofluid	32.87	High Case

Table C 12: Application of different working fluids.

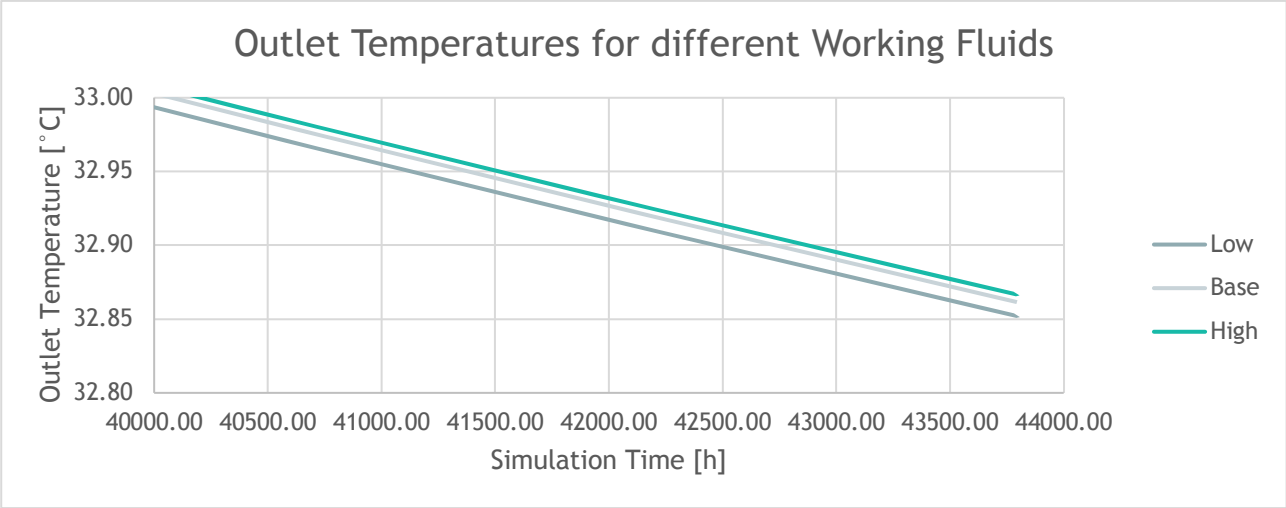

Figure C 24: Variations of outlet temperatures by using different working fluids, water with antifreeze (low case), water (base case) and a nanofluid (high case).

Outlet Pipe Diameter (Inner Pipe Diameter)

In accordance with the results by Doran et al. (2021), variation of the outlet pipe diameter shows no big effect on the outlet temperature, but in our simulations the effect appears to be negligible. The reason for this could be in the used methodology: Doran et al. (2021) implemented a 2D axisymmetric CFD model, with which the effect of enhanced or reduced turbulence within the BHE pipes is considered. With the semi analytical model implemented in FEFLOW the geometry changes, but the change in turbulence of the flow pattern is not considered.

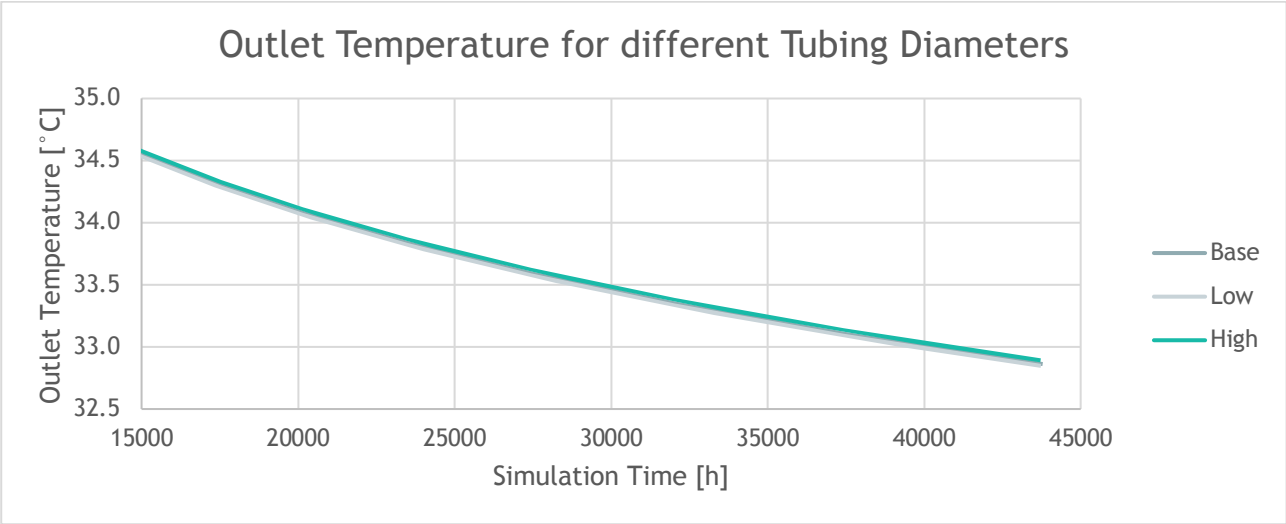

Figure C 25: Influence of tubing diameter (outlet pipe, inner pipe) on outlet temperature. Diameter Base: 0.11 m, Low: 0.09 m, High: 0.14 m.

Outlet Pipe Conductivity (Inner Pipe)

The thermal conductivity of the inner pipe is chosen to represent VIT and HDPE, while it is worth mentioning that insulated coil tubing might even have a lower thermal conductivity than the VIT. With the VIT inner piping, the output temperature can be elevated by ca. 1 °C, as shown in Figure C 26.

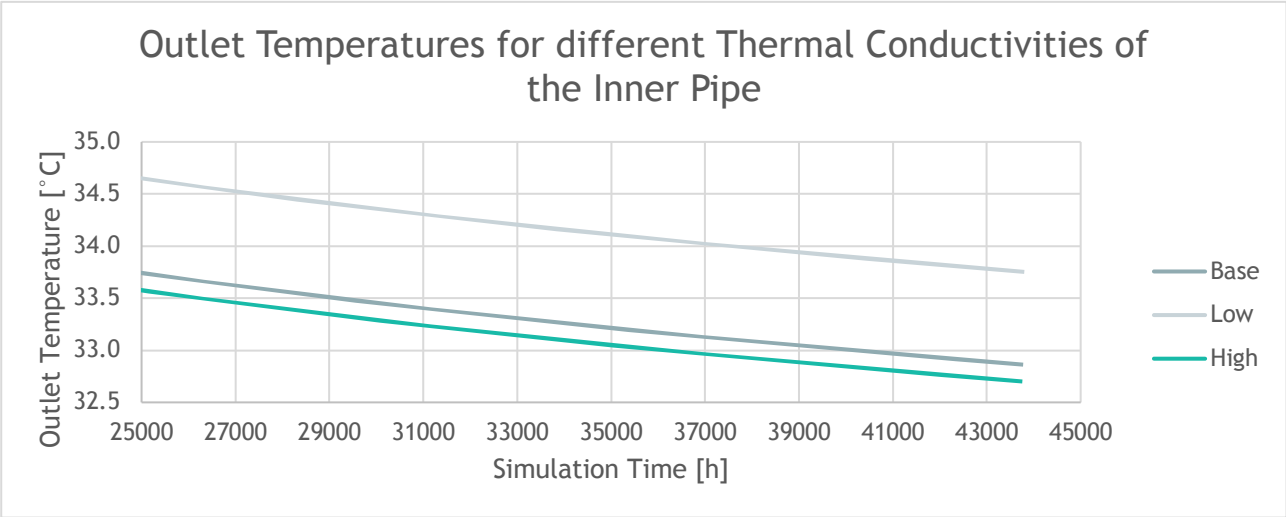

Figure C 26: Influence of thermal conductivity of the inner pipe on the outlet temperature. Thermal Conductivity of the outlet (inner) pipe: Base: 0.34 (W/m/K), Low: 0.03 (W/m/K), High: 0.40 (W/m/K).

Depth

In retrofitting projects, the well depth is not really a design parameter, as the well is already drilled. Anyhow it can be of interest how deep the cementation should be placed. In the Landau case study the highest perforation lies at 991 m. Therefore this interval has been cemented and the usable depth interval is 900 m (internal report, 2010).

Geothermal Gradient

Obviously, a high geothermal gradient is favourable for heat extraction and the temperature level. In the case of Landau, where an extraordinary high geothermal gradient of 80 °C/km is observed, the base case is considered as “high conditions”. The “low” case represents the global mean 30 K/km and the higher case 45 K/km. The high observed gradient in Landau leads to an extraction temperature of above 30 °C, even after 25 years of operation. Considering the standard geothermal gradient of 30 K/km the temperature would drop to below 10 °C; assuming the same amount of heat extraction.

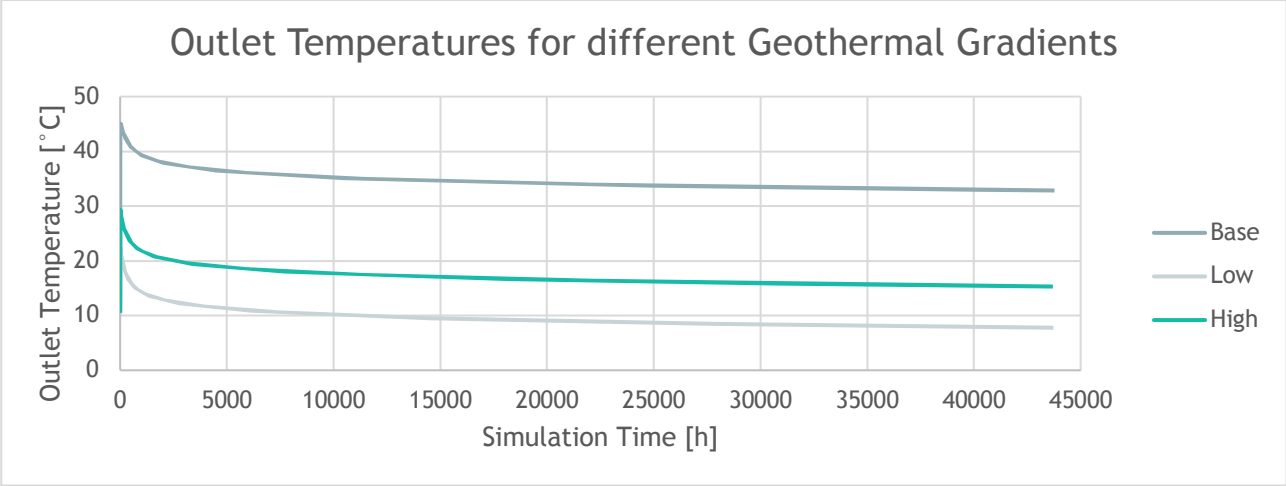

Figure C 27: Outlet temperatures for different geothermal gradients. Base: 45 K/km, Low: 30 K/km, High: 80 K/km.

C.7. Requirements to reuse hydrocarbon wells as Deep Borehole Heat Exchangers

The parameters that influence the efficiency of the system are generally divided into categories (see Table C 13). “Initial well properties” are fixed. Variability is only possible if a well is deep enough to reduce the needed depth interval. The "geological conditions" can only be influenced by where the project is implemented, as the basic geological conditions cannot be changed. The "well design parameters" can only be partially adjusted before the system is commissioned. After that the "operating conditions" can be actively optimised by the operator of the heat exchanger. Most of the parameters are also considered in the sensitivity analysis in order to draw conclusions about which parameters are to be categorised as very critical and which as negligible.

C.7.1. Initial well properties

Well location is important because the application purpose can be determined by this, among other things (excessive distances to the consumer would lead to high heat losses in the pipes).

The distance from the DBHE to the consumer should not exceed 3 km (Koltzer et al., 2024). The main reason for preferring short distances is the high cost of heating networks. With larger distances, the heating costs for the consumer increase rapidly and the system becomes uneconomical (Koltzer et al., 2024). In the sensitivity analysis of this report, this factor was not tested.

The casing size at the deepest point of the DBHE use is a fixed factor and can have influence on the net depth and can be a decision maker if a well is reused or not. Koltzer et al. (2024) recommend that “Idle wells where the 7” surface casing is deepest should be the main target to repurpose as DBHE”.

C.7.2. Geological conditions

When it comes to old boreholes, the depth cannot be influenced, as this is obviously limited. The geothermal gradient should of course be high, as should be the thermal conductivity of the rock. It would be prudent to investigate the presence of thick, shallow aquifers, even if they were not tested in the present study. If there is a strong groundwater flow, it could influence the temperature behaviour of the circulating fluids.

C.7.3. Well design parameters

The inner tube or the configuration of the tubes (co-axial with annular or centred inflow, or U-tube) can be optimised before commissioning the BHE. The co-axial annular inlet is used in DBHE. This has proven to be the most efficient because the U-tube has too high pressure losses (with the same diameter) and the thermal contact with the environment is better.

For the working fluid, research is being carried out into possible additives that can increase efficiency with a small addition. For example, Alimonti (2016) tested the feasibility of maximising the heat extracted. Two different heat transfer fluids were tested: diathermic oil and water, the latter having better heat transfer properties. Furthermore, Melinder (2007) has shown that the values of thermal conductivity and volumetric heat capacity of water are higher than those of the fluids commonly used as secondary working fluids.

In the case of pipes, both the size and the thermal properties are of interest. In principle, the outer pipe should have a high thermal conductivity (good thermal energy exchange for heating the fluid with the rock) and the inner pipe should have a low thermal conductivity to prevent thermal short-circuiting. Different insulations for the inner pipe could be HDPE (high-density polyethylene) or VIT (vacuum insulated tubing). VIT is much more expensive, but performs better in certain applications and operating conditions.

The thermal conductivity of the cement should again be high, as this improves heat exchange between the borehole and the subsurface. Unfortunately, this is often not the case when it comes to retrofitting old oil wells, as bentonite (0.7 W/m/K) is often used. There should also be good cement contact to ensure better heat exchange.

C.7.4. Operating conditions

The flow rate has a major impact on the longevity of the system and strongly depends on the thermal use of the well. High flow rates achieve a higher overall performance, but the output or production temperature is lower than with low flow rates.

The extraction rate at the wellhead has to be designed within an extensive district heating system, including other energy converters and storage units, and taking into account the demand structure, to ensure sufficient temperatures at the domestic stations. Koltzer et al. (2024) recommend that the temperature at the consumer should not be lower than 60 °C for a 4th or 5th generation heat grid to operate as a base load. The reason is, if more heat is consumed, the heat generation costs decrease while the operating hours increase.

The duration of operation is a variable parameter. Koltzer et al. (2024) posit that in order to ensure optimal economic performance, the heat source should be operated continuously throughout the year with 8 000 operating hours. This approach minimises the costs associated with heat generation and makes the DBHE comparable to other heat sources. The DBHE can be operated throughout the year, provided that the heat demand is uniform or that the heat source is integrated into a fourth or fifth-generation heat grid as a base load contribution. In the sensitivity analysis of this report, the operational duration was set at five years, with 8 760 hours per year (43 800 hours in total).

	Impact on other parameters	Min-Max Value	Opt. Value	Literature references	Min-Max Value	Opt. Value	Variability of parameter
		from literature			based on sensitivity analysis		
Initial well properties							
Well location	Geothermal gradient Temperature Distance to energy consumer	--	--	--	--		fixed
Distance to energy consumer (pipeline, km)	--	0-3	0	Koltzer et al. (2024)	--		fixed
Depth	Geothermal gradient Outlet temperature	with the global mean gradient: 30 K/m a minimum depth of a well (usable depth interval for DBHE) is required: 1000 m (30 °C)					fixed/ variable
Casing diameter at DBHE base (inch)	--	6 5/8	>7	Projects: Prenzlau (GER), Sucha Beskidzka (R-1, PL) Koltzer et al. (2024)	--		fixed
Casing-Formation contact	Heat transfer	no exact numbers available		Kohl et al. (2000): Weissbad: 1 cm thick loose contact zone extending over 1/3 of the total borehole has influence	--		fixed
Casing material	--	Thermal conductivity of carbon steel = 54 W/m/K					fixed
Geological conditions and reservoir properties							
Geothermal Gradient (K/km) Heat Flow	Outlet Temperature	the higher the better global mean gradient: 30		Heat Flow Viewer and Database https://ihfc-iugg.org/viewer/	30 - 80 (Landau)		fixed
Well design parameters for DBHE							
Tube configuration	co-axial (annular or centred inflow)						variable
Working fluid (W/m/K)	Amount of heat extraction	water additives		Alimonti et al. (2018)	no impact 0.51 - 0.8		variable
Outlet pipe diameter (m)	--	variation of the outlet pipe		Doran et al. (2021)	neglectable 0.09 - 0.14		variable

		diameter shows no big effect on the outlet temperature				
Outlet pipe conductivity (W/m/K)						variable
HDPE (high density polyethylene)	Costs Amount of heat extraction	0.4		Gascuel et al. (2022)	output temperature can be elevated by ca. 1 °C with a VIT	
VIT (vacuum insulated tubing)		0.03 - 0.037				
Insulated coil tubing		0,022				
Grout (thermal conductivity; W/m/K)	Amount of heat extraction Costs	0.7 (bentonite; used for O&G)	2.02 - 2.7	Dijkshoorn et al. (2013); Gascuel et al. (2022); Pascual-Munoz et al. (2018); Sapinska-Sliwa et al. (2015)	--	variable
Operational properties						
Flow rate (l/s)	--	3-10		Gascuel et al. (2022)	2.67 - 6.27	variable
Outlet temperature (°C)	Amount of heat extraction	--	60	Koltzer et al. (2024)	29 - 41	variable
Duration of operation (h/yr)	--	8000	--	Koltzer et al. (2024)	8760 (43 800 h in 5 yrs)	variable

Table C 13: Parameters to reuse hydrocarbon wells in sedimentary basins as deep borehole heat exchangers based on literature review and sensitivity analysis of this report.

C.7.5. Examples of modelling configurations from literature

As there are various project configurations existing in various geothermal settings, depth and technical conditions (e.g. borehole diameters), Tables C 14 and C 15 give an overview of parameter relations.

C.8. Engineering workflow to reuse hydrocarbon wells as Deep Borehole Heat Exchangers

The engineering workflow to reuse hydrocarbon wells starts when a well is selected to be suitable (e.g. status, location, depth, consumer, liability) for recompletion. At this project stage, the following steps have to be done (compiled from Bräuer, 2011; Macenić, 2020; Sliwa et al., 2015):

1. Checking the well's condition to ensure that the casing is intact and that there are no barriers in the borehole

The integrity of the borehole is checked for the installations in accordance with the well integrity in relation to the formation. These steps require workover equipment.

2. Preparation of the borehole for recompletion (conversion to geothermal equipment)

The sections of the casing strings, where the fastening of the mechanical plug is planned to take place should be cleaned with a scratcher, the sealing sections should be filled with properly selected cement slurry.

After fastening the mechanical plug, the wellbore must be checked for leaks, when the slurry is bonded, the top of the cement plug must be located and checked for leaks (e.g. cement bond log). A pressure test can be carried out in order to ensure a tight seal against the formation and any formation water. This rules out the possibility of mass transport between the outer pipework and the rock.

3. Conversion of the borehole – Installation of new tubing

After well integrity checks and workover, the new tubing can be installed. For the most common BHE types, a coaxial system, a double pipe is installed, which protrudes openly into the casing at the bottom. The double pipe consists of an inner pipe, which can be thermally insulated by an insulating gas (e.g. N_2) and is separated from the outer double pipe against thermal bridges by means of a centring piece. For the install of plastic pipes no workover winch is needed. The tubing can just let down in the well and comes rolled on trucks. The installation of steel pipes requires a workover rig, which is much more expensive.

	Configuration	Borehole diameter (bottom of DBHE, mm)	Outer pipe				Inner pipe			
			Material	Thermal conductivity ($W\,m^{-1}K^{-1}$)	Outside diameter (mm)	Inside diameter (mm)	Material	Thermal conductivity ($W\,m^{-1}K^{-1}$)	Outside diameter (mm)	Inside diameter (mm)
Scenario A	HDPE-A	156	Steel - Carbon. 0.5% C	54	114	102	HDPE	0.4	60	49
	HDPE-B	156			114	102		0.4	89	73
	VIT-1	156			114	102	VIT	0.037	89	57
	VIT-2	156			114	102	Insulated coil tubing	0.022	89	57
Scenario B	HDPE-A	222	Steel (pre-existing casing)	54	178	162	HDPE	0.4	89	73
	HDPE-B	222			178	162		0.4	114	96
	VIT-1	222			178	162	VIT	0.037	89	57
	VIT-2	222			178	162	Insulated coil tubing	0.022	89	57
	VIT 3	222			178	162	VIT	0.036	102	62

Table C 14: Dimensions for different scenarios of DBHE configurations (Gascuel et al., 2022). Scenario A: Inserting an outer pipe inside the existing casing in order to cover the lower open section, Total depth = 2000 m. Scenario B: Using the pre-existing casing as the outer pipe, while its lower open section is cemented; Depth used = 1000 m.

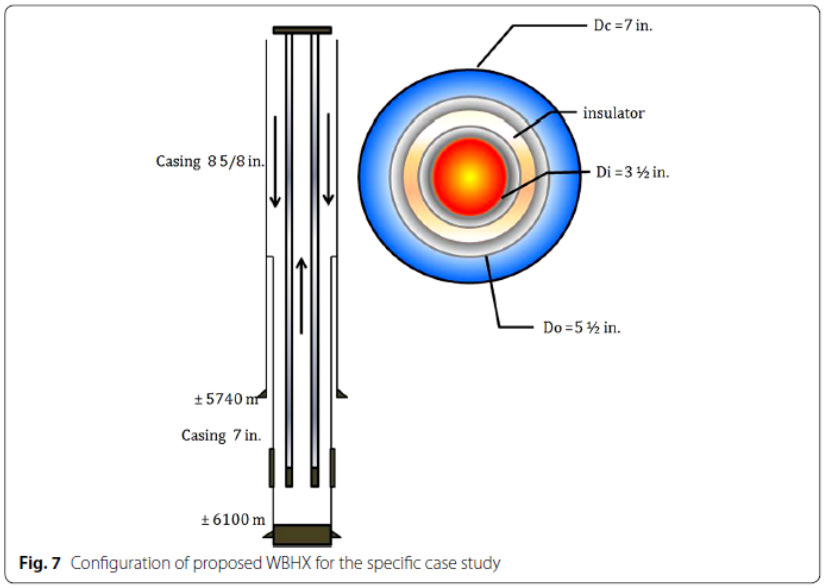

Fig. 7 Configuration of proposed WBHX for the specific case study

Table 1 WBHX tube sizing

	Internal diameter (mm)	External diameter (mm)
D_i 3½ in.	77.9	88.9
D_o 5½ in.	121.4	139.7
D_c casing 7 in.	150.4	177.8

Table C 15: Casing and tubing dimensions of DBHE reuse of a very deep well (Villafortuna 1) with a DBHE interval of > 5700 m, modelled by Alimonti, 2016 (WHBX = Well Heat Borehole eXchanger).

4. Installation of the surface facilities with the heat exchangers

The pumping system for circulating the working fluid (in most cases water or a water-glycol mixture) pumped in the well in a circuit is located in a closed special container that has been specially adapted for connection to the well. The drill head connections with inlet and outlet are connected directly to the container via a drill head shut-off valve for maintenance and safety purposes.

The container or fixed shed contains circulation pumps for circulating the working fluid as well as thermal equalisation vessels for the circulating mixture. A control unit for the flow rate is attached to a heat exchanger, which absorbs the heat energy pumped from the borehole and transfers it via a local heating network to the consumers or a recooler for test purposes.

5. Installation of the local heating network to determine the technical availability

The local heating network has to be constructed from the borehole via roads and meadows to the customer. A heat exchanger has to be installed on the consumer side of the heating network. The heat taken can be raised to the appropriate temperature level using gas to the appropriate temperature level using gas heat pumps.

6. Connection to the consumer

7. Start of heat consumption and improvement of the software used and calibration of the newly obtained results

After installation and commissioning of the measurement data acquisition system, the data can be analysed. It should be possible to stabilise the temperature and output after a certain period of time. This means that sustainable geothermal utilisation is possible with balanced heat dissipation.

8. Optional steps: Improvement of the control technology - Start of measurement analysis if operations are conclusive

C.9. References

Alimonti, C., D. Berardi, D. Bocchetti, and E. Soldo. 2016. Coupling of Energy Conversion Systems and Wellbore Heat Exchanger in a Depleted Oil Well. *Geothermal Energy* 4(1).

Alimonti, C., E. Soldo, D. Bocchetti, and D. Berardi. 2018. The Wellbore Heat Exchangers: A Technical Review. *Renewable Energy* 123: 353–81.

Blasi, A., and M. Menichetti. 2012. Thermal Conductivity Distributed from a Thermal Response Test (TRT) in a Borehole Heat Exchanger (BHE). *Acque Sotterranee - Italian Journal of Groundwater* 1(3): 033–041.

Bräuer, Leopold. 2011a. Energie Aus Erde, Luft, Wasser-Wärmepumpen und Geothermie. *Klima- und Energiefonds*. (https://www.klimafonds.gv.at/wp-content/uploads/sites/16/KLIEN_2011_ScienceBrunch_Energie-Erde-Luft-Wasser.pdf (July 18, 2024).

Bräuer, Leopold. 2011b. Geothermie aus Sonden. *Blue Globe Report* 26.

Brown, Christopher S., and Louis Howell. 2023. Unlocking Deep Geothermal Energy in the UK Using Borehole Heat Exchangers. *Geology Today* 39(2): 67–71.

Brown, Christopher S., Isa Kolo, Gioia Falcone, and David Banks. 2023. Investigating Scalability of Deep Borehole Heat Exchangers: Numerical Modelling of Arrays with Varied Modes of Operation. *Renewable Energy* 202: 442–52.

Bußmann, Werner. 2014. Geothermie-Energie für die Zukunft. Geothermische Vereinigung e.V..

Cai W., F. Wang, S. Chen, C. Chen, J. Liu, J. Deng, O. Kolditz, and H. Shao. 2021. Analysis of heat extraction performance and long-term sustainability for multiple deep borehole heat exchanger array: A project-based study. Applied Energy. 289:116590.

Caulk, Robert A., and Ingrid Tomac. 2017. Reuse of Abandoned Oil and Gas Wells for Geothermal Energy Production. *Renewable Energy* 112: 388–97.

Deng, J., Wei, Q., He, S., Liang, M., Zhang, H., 2019a. What is the main difference between medium-depth geothermal heat pump systems and conventional shallow-depth geothermal heat pump systems? Field tests and comparative study. Appl. Sci. 9 (23), 5120. https://doi.org/10.3390/app9235120.

Dijkshoorn, Lydia, Simon Speer, and Renate Pechnig. 2013. Measurements and Design Calculations for a Deep Coaxial Borehole Heat Exchanger in Aachen, Germany. *International Journal of Geophysics*.

Doppelreiter, David. 2012. Geothermische Nachnutzung Der Kohlenwasserstoffbohrung Mühlleiten 2 in Oberösterreich. In *Pangeo Austria 2012 Conference Proceedings*.

Doran, Hannah R. et al. 2021. Modelling an Unconventional Closed-Loop Deep Borehole Heat Exchanger (DBHE): Sensitivity Analysis on the Newberry Volcanic Setting. *Geothermal Energy* 9(1).

Duggal, Rohit, Ramesh Rayudu, John Burnell, and Jim Hinkley. 2022a. Analytical and Numerical Modelling of a Coaxial Borehole Heat Exchanger to Extract Geothermal Energy. In *Proceedings 44th New Zealand Geothermal Workshop*, https://www.researchgate.net/publication/365814932.

Dürnegger, Thomas. 2009. Integration eines Bohrlochwärmetauschers in ein bestehendes Heizsystem. MSc Thesis, University Leoben. https://pureadmin.unileoben.ac.at/ws/portalfiles/portal/2490657/AC07895871n01vt.pdf (July 18, 2024).

Eden project; Webpage. https://www.edengeothermal.com/the-project/drilling-and-operations/. (July 18, 2024).

Enerchange. 2009. Neue Wege bei OMV. Webpage. https://www.tiefegeothermie.de/news/neue-wege-beim-omv (July 18, 2024).

Energieatlas Rheinland Pfalz. Energieatlas_Rheinland_Pfalz_Praxisbeispiel_Erdwaerme_aus_stillgelegter_Erdoel_Bohrung_in_Landau_Pfalz_2014-1. Webpage. https://www.energieatlas.rlp.de/earp/praxisbeispiele/projektsteckbriefe/projekt-steckbriefe/anzeigen/unternehmen/1 (July 18, 2024).

Eugster, Walter, and Hans Fügister. 2003. Weggis - Final Report.

Facci, Marina, Eloisa di Sipio, and Antonio Galgaro. 2023. Energy Transition and Deep Geothermal Solution Role: A Screening Procedure for the Retrofitting and Reuse of Ex Oil&Gas Wells as Deep Closed-Loop Borehole Heat Exchangers in Italy. In EGU, https://meetingorganizer.copernicus.org/EGU23/EGU23-14599.html; https://doi.org/10.5194/egusphere-egu23-14599.

Falcone, Gioia et al. 2018. Assessment of Deep Geothermal Energy Exploitation Methods: The Need for Novel Single-Well Solutions. Energy 160: 54–63.

Fritsche, Johann-Gerhard. 2012. Geologische Und Geothermische Ergebnisse Aus Dem Projekt Mitteltiefe Erdwärmesonde Heubach. In 7. Tiefengeothermieforum Hessen – Proceedings.

Gascuel, Violaine et al. 2022. Design and Optimization of Deep Coaxial Borehole Heat Exchangers for Cold Sedimentary Basins. Geothermics 105.

Geothermieforum Niedersachsen. 2021. Geothermische Nachnutzung von Bohrungen. Landesamt für Bergbau, Energie und Geologie (LBEG), Bundesverband Erdgas, Erdöl und Geoenergie e.V (BVEG) in Zusammenarbeit mit dem Niedersächsischen Ministerium für Wirtschaft, Arbeit und Verkehr.

Gizzi, M., Glenda Taddia, and Stefano lo Russo. 2021. Reuse of Decommissioned Hydrocarbon Wells in Italian Oilfields by Means of a Closed-Loop Geothermal System. Applied Sciences 11(5).

Gola, G. et al. 2022. Geothermal Deep Closed-Loop Heat Exchangers: A Novel Technical Potential Evaluation to Answer the Power and Heat Demands. Renewable Energy 198: 1193–1209.

Hinsch, 2012. https://www.yumpu.com/de/document/view/1770506/heimische-erdgas-und-erdolforderung-in-bayern.

Holmberg H., Acuna J., Nass E., Sonju OK. 2016. Thermal evaluation of coaxial deep borehole heat exchangers. Renew Energy. 97:65–76.

Kalmar, L., Medgyes, T., Szanyi, J., 2020. Specifying boundary conditions for economical closed loop deep geothermal heat production. Energy 196, 117068. https://doi.org/ 10.1016/j.energy.2020.117068.

Kaplanoğlu MA., Baba A., Gokcen Akkurt G. 2019. Use of abandoned oil wells in geothermal systems in Turkey. Geomech Geophys Geo-energ Geo-resour. 6(1):2. doi:10.1007/s40948-019-00125-0

Karasalihović Sedlar, Daria, Tomislav Kurevija, Marija Macenić, and Ivan Smajla. 2022. Regulatory and Economic Challenges in the Production of Geothermal Brine from a Mature Oil Field. Energy Sources, Part B: Economics, Planning and Policy 17(1).

Kohl, T., M. Salton, and L Rybach. 2000. Data Analysis of the Deep Borehole Heat Exchanger Plant Weissbad (Switzerland). In Proceedings World Geothermal Congress 2000, https://www.researchgate.net/publication/237304492.

Kolo, Isa et al. 2024. A Comprehensive Review of Deep Borehole Heat Exchangers (DBHEs): Subsurface Modelling Studies and Applications. Geothermal Energy 12(1).

Kolo, Isa, Christopher S. Brown, Gioia Falcone, and David Banks. 2023. Repurposing a Geothermal Exploration Well as a Deep Borehole Heat Exchanger: Understanding Long-Term Effects of Lithological Layering, Flow Direction, and Circulation Flow Rate. Sustainability 15(5).

Koltzer, Nora et al. 2024. Repurposing idle wells in the North German Basin as deep borehole heat exchangers. Geothermal Energy 12 (35). https://doi.org/10.1186/s40517-024-00315-4.

Kurnia, Jundika Candra et al. 2022. Geothermal Energy Extraction Using Abandoned Oil and Gas Wells: Techno-Economic and Policy Review. International Journal of Energy Research 46(1): 28–60.

Kvalsvik, Karoline H, Kirsti Midttømme, and Randi K Ramstad. 2019. Den Haag Geothermal Energy Use, Country Update for Norway.

Law, R., Bridgland, D., Nicholson, D., Chendorain, M., 2014. Heat extraction from deep single wells. In: Proceedings World Geothermal Congress. Thirty-Ninth Workshop on Geothermal Reservoir Engineering. Stanford, California (USA), pp. 19-25. https://pangea.stanford.edu/ERE/pdf/IGAstandard/SGW/2014/Law.pdf.

Ledet, D. et al. 2023. Leveraging oil and gas infrastructure using closed-loop geothermal technologies. In: Der Geothermiekongress 2023, https://www.der-geothermiekongress.de/Tagungsband2023/www.conftool.net/geothermiekongress2023/indexd67f.html?page=browseSessions&print=export&ismobile= false&form_session=13#paperID244 (July 18, 2024).

le Lous, Morgan, François Larroque, Alain Dupuy, and Adeline Moignard. 2015. Thermal Performance of a Deep Borehole Heat Exchanger: Insights from a Synthetic Coupled Heat and Flow Model. Geothermics 57: 157–72.

Lund, John W., Tonya L. Boyd. 2016. Direct utilization of geothermal energy 2015 worldwide review, Geothermics, Volume 60, 66-93, ISSN 0375-6505, https://doi.org/10.1016/j.geothermics.2015.11.004.

Lund, A., Karvinen, T., Lehtonen, M., 2020. Analysis of deep-heat energy wells for heat pump systems. In: Proceedings of the IEEE PES Innovative Smart Grid Technologies Europe (ISGT-Europe) 26-28 October 2020. The Hague, Netherlands, pp. 574–578.

Lund, Andreas E.D. 2024. Performance Analysis of Deep Borehole Heat Exchangers for Decarbonization of Heating Systems. Deep Underground Science and Engineering.

Macenić, Marija, Tomislav Kurevija, and Kristina Strpić. 2020. Analytical and Numerical Modelling of Heat Extraction Rates in the Coaxial Heat Exchanger for a Retrofitted Deep Oil and Gas Wells. In 4th SEE Sdewes Conference Sarajevo 2020, https://www.researchgate.net/publication/366249809.

Madiseh SAG. Geothermal energy extraction from petroleum wells in Qatar. In: Vol 2013. Hamad bin Khalifa University Press (HBKU Press); 2013: EEP-075. doi:10.5339/qfarf.2013.EEP-075

Maurel, Camille et al. 2019. Inventory and First Assessment of Oil and Gas Wells Conversion for Geothermal Heat Recovery in France. https://brgm.hal.science/hal-02306770.

Mehmood A, Yao J, Yan Fun D, Zafar A. 2017. Geothermal Energy Potential of Pakistan on the Basis of Abandoned Oil and Gas wells. *Journal of Petroleum Environment Biotechnology*. 08(03): 1000332. doi:10.4172/2157-7463.1000332

Mehmood A, Yao J, Fan D, Bongole K, Liu J, Zhang X. 2019. Potential for heat production by retrofitting abandoned gas wells into geothermal wells. *PLOS ONE*. 14(8): e0220128. doi:10.1371/journal.pone.0220128

Melinder A. 2007. Thermophysical properties of aqueous solutions used as secondary working fluid. Doctoral thesis. Dept. of Energy Technology School of Industrial Engineering and Management, Royal Institute of Technology, KTH Stockholm, Sweden.

Miocic, Johannes, Jan Drenth, and Pieter van Benthem. 2024. Reutilising Hydrocarbon Wells as Deep Heat Exchangers to Decarbonise Heating in the Northern Netherlands. In EGU General Assembly 2024, 24-7761. https://doi.org/10.5194/egusphere-egu24-7761.

Nash, Susan Smith, Patrick L. Friend, and Marit Brommer. 2022. A Fully Integrated and Updated Geothermal Gradient Atlas of the World. In Proceedings of the Annual Offshore Technology Conference, Offshore Technology Conference.

Nibbs, W et al. 2023. Repurposing Onshore Wells for Geothermal Use in the United Kingdom: Application as Deep Borehole Heat Exchangers. In World Geothermal Congress, World Geothermal Congress. http://eprints.gla.ac.uk.

Noorollahi Y., Pourarshad M., Jalilinasrabady S., Yousefi H. 2015. Numerical simulation of power production from abandoned oil wells in Ahwaz oil field in southern Iran. *Geothermics*. 55:16-23. doi:10.1016/j.geothermics.2015.01.008

Noorollahi Y, Mohammadzadeh Bina S, Yousefi H. 2016. Simulation of Power Production from Dry Geothermal Well Using Down-hole Heat Exchanger in Sabalan Field, Northwest Iran. *Natural Resource Reservoir*. 25(2):227-239. doi:10.1007/s11053-015-9270-3

Piipponen, Kaiu, and et al. 2022. The Deeper the Better? A Thermogeological Analysis of Medium-Deep Borehole Heat Exchanger EEciency in Crystalline Rocks - Not Peer Reviewed. Reserarch Square. https://doi.org/10.21203/rs.3.rs-1196300/v1.

Press release RAG 2012. Einzigartiges Regionales Energie-Projekt Aus Kombination von Erdwärme Und Biomasse Neukirchen a.d. Vöckla Eröffnet. Webpage. https://www.ots.at/presseaussendung/OTS_20120503_OTS0111/einzigartiges-regionales-energie-projekt-aus-einer-kombination-von-erdwaerme-und-biomasse-fuer-neukirchen-ad-voeckla-eroeffnet (July 18, 2024).

Raymond, J., Malo, M., Tanguay, D., Grasby, S., Bakhteyar, F., 2015a. Direct utilization of geothermal energy from coast to coast: a review of current applications and research in Canada. In: Proceedings of the World Geothermal Congress. Melbourne, Australia

Renaud, Theo et al. 2021. Numerical Analysis of Enhanced Conductive Deep Borehole Heat Exchangers. Sustainability (Switzerland) 13(12).

Renaud, Theo, Patrick Verdin, and Gioia Falcone. 2019. A Numerical Study of Deep Borehole Heat Exchangers Efficiency in Unconventional Geothermal Settings. In European Geothermal Congress 2019, European Geothermal Congress 2019 Den Haag, 11–14.

Richter, Alexander 2021: First closed-cycle geothermal heat plant set up in Hungary. Webpage. https://www.thinkgeoenergy.com/first-closed-cycle-geothermal-heat-plant-set-up-in-hungary/ (July 18, 2024).

Rock Energy. 2018. Ingeniously Sharing the Everlasting Warmth of Mother Earth Experience from Deep Geothermal Drilling Oslo Airport.

Rybach, Ladislaus, and Harald L Gorhan. 2005. Proceedings World Geothermal Congress Country Update for Switzerland. https://www.researchgate.net/publication/228773954.

Schneider, D., E. Brossmann, H. Wetzel. 1997. Erdwärmetiefensonde Prenzlau, Technisches Konzept Und Betriebserfahrungen. Tagungsband der 4. Geothermischen Fachtagung.

Singh HK. Geothermal energy potential of Indian oilfields. 2020. Geomechanics and Geophysics for Geo-Energy and Geo-Resources. 6(1):19. doi:10.1007/s40948-020-00148-y

Sliwa, Tomasz et al. 2015. Applicability of Borehole R-1 as BHE for Heating of a Gas Well. In Proceedings World Geothermal Congress, World Geothermal Congress, 19–25.

Szekszárdi, Adrienn et al. 2022. WeHEAT Project WeHEAT SYSTEMS: A Sustainable Closed Loop Heating Technology in the Field of Geothermal Energy. In European Geothermal Congress, https://www.researchgate.net/publication/362733458.

Ungemach, Pierre, Raul Hidalgo, and José S Sanchez. 2010. Proceedings World Geothermal Congress Multiple Use Assessment of the Madrid Basin (Spain) Geothermal Potential.

Wang, Z., Wang, F., Liu, J., Ma, Z., Han, E., Song, M., 2017. Field test and numerical investigation on the heat transfer characteristics and optimal design of the heat exchangers of a deep borehole ground source heat pump system. Energy Convers. Manag. 153, 603–615. https://doi.org/10.1016/j.enconman.2017.10.038.

D. Borehole Thermal Energy Storage (BTES)

D.1. Authors

Tomislav Kurevija	UNIZG-RGNF	tomislav.kurevija@rgn.unizg.hr	Croatia
Luka Perković	UNIZG-RGNF	luka.perkovic@rgn.unizg.hr	Croatia
Marija Macenić	UNIZG-RGNF	marija.macenic@rgn.unizg.hr	Croatia
Daria Karasalihović Sedlar	UNIZG-RGNF	daria.karasalihovic-sedlar@rgn.unizg.hr	Croatia
Ivan Smajla	UNIZG-RGNF	ivan.smajla@rgn.unizg.hr	Croatia

D.2. Borehole Thermal Energy Storage (BTES)

Decarbonization of heating with the use of geothermal energy can be divided into deep geothermal and shallow geothermal energy sources. While there are many publications related to using shallow geothermal for borehole thermal energy storage (BTES), there are not many published papers related to deep geothermal BTES. Seib et al. (2024) presented an assessment of medium-deep BTES for location Lichtwiese Campus, Darmstadt with specific focus on optimization of drilling methods and investigation of lithology of the reservoir. Brown et al. (2023) performed statistical modelling and sensitivity analysis for repurposing deep geothermal exploration well for BTES application and concluded that operational parameters were more influential on deep BTES systems than thermal conductivities of materials indicating that timeseries analysis has to be conducted. Ma et al. (2024) performed analysis of operational characteristics for heating and storage of medium-deep borehole heat exchangers and concluded that heat transfer and power consumption of circulating pump can be optimized. The benefits of thermal recovery of deep geothermal reservoirs is investigated by Fu et al. (2024). The goal of this study is to establish a workflow the possible repurposing of the Savica-1 well as a BTES between the seasonal heating demand and waste heat from nearby industry.

D.2.1. Description of technology

Borehole thermal energy storage is a system that utilizes boreholes (often referred to as borehole heat exchangers) for transferring heat or cold to the surrounding ground material (rock, soil, or clay) (Gehlin, 2016). During charging the rock is heated. During discharging parts of this heat is recovered. Heat is transferred to the rock by heat conduction when water (or another working fluid) circulates in a closed loop through the well during the charging period (Nordell, 1994). The working fluid circulates inside plastic U-tube pipes or co-axial pipes placed in closely spaced boreholes, which are typically 2 – 5 m apart, 20 – 200 m deep and often sealed with grout. Thermal losses depend on subsurface properties, borehole layout, regional groundwater flow and surface heat losses. This type of storage is suitable for using excess heat from industries and renewable sources (like solar thermal) when no aquifer for Aquifer Thermal Energy Storage (ATES) is present, but the storage capacity is limited. BTES also integrates wells with heat pumps and combined heat and power (CHP) plants (Kallesøe, A.J. & Vangkilde-Pedersen, 2019).

D.2.2. Technical design

D.2.2.1. Storage geometry

Storage geometry is an important parameter to prevent heat loss. Storage capacity is proportional to storage volume, while heat losses are proportional to surface area. Therefore, a design with a small surface-to-volume ratio is desirable. Also, to minimise heat losses to the surface, shallow BTES borehole field is usually insulated on top (Gehlin, 2016). The insulation can be done with a BTES field covered with a layer of XPS and covered with 2-3 m of soil (Reuss, 2015). Borehole spacing is typically uniform. Compact shapes of the storage reduce heat losses. Most commonly, boreholes are drilled in rectangular, hexagonal, or circular arrays. To minimize land use and heat losses, boreholes are occasionally drilled obliquely, giving the storage a broom-like shape. Depth, spacing and configuration must be optimized for each project (Nordell, 1994). The outer shape of the BTES storage is determined by the pattern and depth of the boreholes. The distance between boreholes is crucial for efficiency (Kallesøe, A.J. & Vangkilde-Pedersen, 2019). Number of BHEs in the BTES fields range from a few dozen to over 100 boreholes.

D.2.2.2. Borehole installations

Borehole heat exchangers (BHE) for BTES are drilled to a certain depth in hard or soft formations, at the common depth of 20 – 200 m. They are usually grouted as grout stabilizes and seals boreholes and enables good thermal contact between ground material and the collector pipes. Most used types of collectors are single and double U-tube pipes since they are reliable, simple to install and have the lowest cost. There are also various types of coaxial collectors, with hard and soft shells, which are more expensive, more complicated to install and have a higher risk of leakage (Gehlin, 2016). Boreholes and pipe installations are crucial components of the store because they facilitate efficient heat transfer between the heat carrier fluid and the rock volume. Every installation should balance cost and effectiveness. U-tubes are often connected in series to form circuits for fluid flow, with flow direction designed to maximize efficiency and minimize heat loss (Figure D 1). Field tests have shown that double U-tubes are more efficient than single ones, although coaxial collectors should be most effective (Kallesøe, A.J. & Vangkilde-Pedersen, 2019).

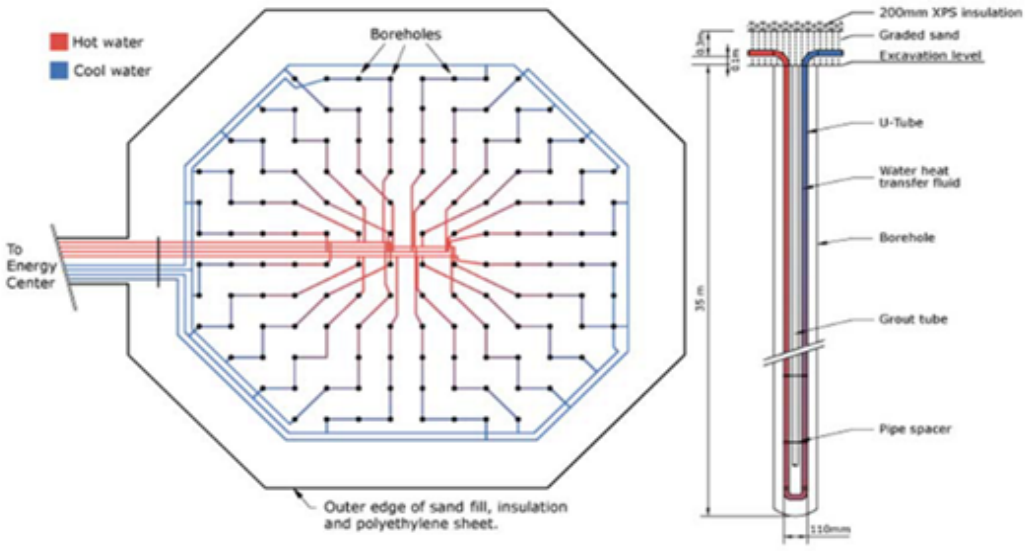

Figure D 1: Layout of a borehole thermal energy storage and cross-section of a single borehole and U-tube (Sibbit & McClenahan, 2015).

D.2.2.3. Rock properties

BTES is based on the ground materials' ability to store (heat capacity) and conduct (thermal conductivity) heat. These properties are affected by factors such as mineral composition of the surrounding rocks, temperature and fluid content. Thermal properties can be estimated by using geological maps and rock samples, while laboratory tests on samples like drill cuttings or cores yield more accurate values (Nordell, 1994). Higher heat capacity allows more heat to be stored in the BTES. While high thermal conductivity aids in charging heat into the storage volume, it also increases heat conduction away from storage, leading to lower temperature near the storage during discharge. Lower conductivity retains higher temperatures near the boreholes, enabling better heat recovery. Studies have shown that BTES efficiency increases with decreasing rock thermal conductivity, as lower conductivity leads to higher efficiency in heat extraction (Catolico et al., 2016). But still, low thermal conductivity may decrease the ability to charge the storage efficiently. Therefore, medium thermal conductivities are often considered desirable for thermal energy storage systems. Performing a Thermal Response Test at the BTES site provides essential data for design calculations, including thermal conductivity and borehole thermal resistance. This test involves heating fluid in the borehole and monitoring heat transfer into the surrounding ground as the fluid circulates in the tubes (Kallesøe, A.J. & Vangkilde-Pedersen, 2019). High thermal conductivity is desirable as poor heat transfer in the collectors will affect the storage efficiency both at injection and production.

D.2.2.4. Geology and hydrogeology

Preferred geological conditions for BTES include drillable ground with high heat capacity and low natural groundwater flow. A preliminary screening of local geology is essential, typically based on existing well records, to assess depth, soil and rock type, groundwater flow and water table depth. This information guides the selection of drilling and grouting techniques. Based on this screening, estimates of the thermal properties of the geological layers can be made using existing table values for heat capacity and thermal conductivity. However, regional geological variations may affect these values, requiring careful evaluation and consideration of uncertainty (Kallesøe, A.J. & Vangkilde-Pedersen, 2019).

A thorough investigation of local hydrogeological conditions including groundwater level and flow is crucial. Water flow through or around the storage volume can cause heat loss by advection, which should be minimized. Ideally, a BTES should be placed above the groundwater table or in geological conditions with low hydraulic conductivity, such as tight clay, till, limestones, sediments with low permeability, or un-fractured crystalline rocks. For zones with unavoidable high groundwater flow, insulation with thermally reducing grout can minimize heat loss. Thermally enhanced grout is typically used in other zones to increase heat transfer from the borehole to the storage volume. Groundwater flow is not desirable as convective heat transport with groundwater flow will negatively affect heat storage performance, because the stored heat would be transported away from the storage by the moving groundwater (Gehlin, 2016).

D.2.2.5. BTES field monitoring process

During BTES operation, measuring the ground and subsurface temperatures needs to be carried out, because heat transport in the storage involves three thermal processes: within each borehole, locally between boreholes and surrounding area and globally in the storage area. Heat transfer from the fluid to the rock mass and related heat losses are key concerns. That is why usually some boreholes are drilled inside of a storage for subsurface temperature measurement, including at least one outside, but near the storage. Those data, combined with values of injected (charged) and produced (discharged) heat give a good insight into storage efficiency considering heat losses and overall functioning of the storage.

D.3. Literature review

From the literature review it can be concluded that there is no operational medium-deep to deep BTES system in the world. The research is mainly theoretical with few pilot projects, such as SKEWS and PUSH-IT projects done in TU Darmstadt, Germany. The TU Darmstadt BTES explores operational conditions of medium-deep BTES with three boreholes drilled to depths of around 750 m. The results of the operation of this BTES project are yet to be published since the investigations and measurements are ongoing. So far, operational BTES systems are found in shallow geothermal projects, and some of them are described below.

D.3.1. HT-BTES in Luleå - Sweden

The heat storage in Luleå, built in 1982-83, was the first high-temperature Borehole Thermal Energy Storage (HT-BTES) constructed in bedrock. Its purpose was experimental and demonstrational for Lulea University of Technology. It got waste heat from a gas-fired co-generation plant which was transferred to the storage by the district heating system (delivered temperature was 70-82°C during summer). The BTES was separated from the district heating system by a heat exchanger and heat pumps were used for 20% of the extracted heat. The storage system heated one building at the University during winter (Hellström, 1991).

D.3.1.1. Technical design

The heat storage consisted of 120 vertical boreholes (10×12 holes) placed in a rectangular shape. The distance between the boreholes was 4 m, giving a drilled area of 36 m × 44 m. Boreholes were 65 m deep, with a diameter of 152 mm, which gives total rock storage volume of 120 000 m^3 (Table D 1) The boreholes were connected to a heat exchanger by a plastic pipe system. Open coaxial type of collectors were used (Nordell, 1994).

HT-BTES in Luleå			
Years of operation	1983-90	**Storage shape**	Rectangular
Storage volume [m3]	115 000	**Ground type**	Rock
Number of boreholes	120	**Thermal conductivity ground [W/(m*K)]**	3.42
Borehole depth [m]	65	**Volumetric heat capacity ground [MJ/(m3*K)]**	2.28
Total borehole length [m]	7800	**Insulated [Yes/No]**	No
Borehole spacing [m]	4	**Insulation material**	-
Borehole diameter [mm]	152	**Insulation thickness [mm]**	-
Collector type	Open Coaxial	**Source of charge**	Waste heat
Collector diameter [mm]	Unknown	**Injected energy/year (expected) [GWh]**	2.3 (2.8)
Collector material	Unknown	**Extracted energy/year (expected) [GWh]**	1.0 (1.6)
Collector temperature resistance	Unknown	**Charging temp [°C]**	70-85
Thermal stratification [Yes/No]	Yes	**Storage maximum temp [°C]**	65
Number of boreholes in series	5	**Storage minimum temp [°C]**	30
Total collector length in series [m]	325	**HP for extraction [Yes/No]**	Yes

Table D 1: Design parameters for the HT-BTES in Luleå, Sweden (Malmberg, 2017).

D.3.1.2. Geology and Hydrogeology

The bedrock consists of folded medium-grained gneiss, with an overburden of silty clay and sulfidic soil (5-10 m thick). Seismic investigations confirmed the depth of soil cover and didn't detect larger fracture zones running through the site. The core borehole of 48 m was drilled, as an inclined borehole in order to pass through the storage site and to perform core mapping (Table D 2). This method discovered some fractures and smaller crushed zones in bedrock (twelve shear zones with a total width of 2.7 m). The core borehole was later used for measuring permeability by pressure testing. Some groundwater flow was noticed, with a gradient of 2 ‰ (Andersson et al., 1983).

ROCK					
Type of rock	Volumetric heat capacity	Thermal conductivity	Density	Hydraulic conductivity	Initial temperature
folded medium-grained gneiss	2.03 MJ/m^{3}K	3.7 W/mK	2742 kg/m^3	2x10^{-7} m/s	3.5°C

SOIL						
Type of soil	Thickness of cover	Groundwater level	Volumetric heat capacity	Thermal conductivity	Bulk density	Hydraulic conductivity
sulfide soil	5 - 10 m	0.7 m	3.49 MJ/m^{3}K	0.75 W/mK	1540 kg/m^3	10^{-9} - 10^{-11} m/s (estimated)

Table D 2: Physical data for the a) rock and b) soil cover (Andersson et al., 1983).

D.3.1.3. Operational data

The temperature was measured inside and outside of the storage volume at 33 points at different depths in observation wells (Figure D 2). Observation wells T1-T6 were filled with sand after installing temperature-measuring devices, to avoid convection movements of the water. In wells M1-M4 only one temperature-measuring device was installed per well. The wells were filled with water, except for about 1 m of sand filling around the measuring device (Nordell, 1994).

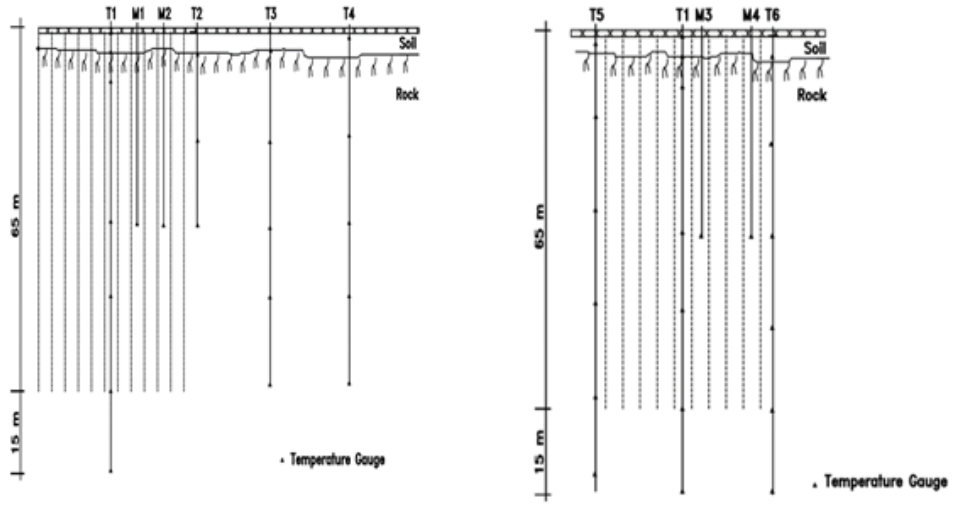

Figure D 2: Sections of the BTES system with locations of the temperature gauges (Nordell, 1994).

D.3.1.4. Results

Operation cycle lengths varied during the first five years of use. The first charging period was longer (seven months) to raise the original rock temperature of 3.5°C as much as possible. After five years of operation, about 2800 MWh of charging energy during summer and 1600 MWH of recovered energy during winter were planned, but not fulfilled. The water flow rate was 12.5 l/s during charging periods (0.5 l/s through each borehole), while during the extraction period the water flow rate was 6.5 l/s since it was controlled by the water flow rate of the building to which the stored heat was supplied. Supply temperatures during charging were 70-80°C while leaving temperatures were 15-20 °C lower. During extraction, the water supply temperature entering the storage was 30-45°C. While passing through the storage, the temperature of water was raised by a maximum of about 10°C, so the supply temperature to the building was 35-55°C (Nordell, 1994).

D.3.1.5. Conclusion and discussion

Due to unfavourable control strategies and mistakes during the construction leading to lower performance than expected, the storage was taken out of operation in 1990. According to Nordell (1994), major problems were the operation and maintenance of the installed heat pumps. Problems may have occurred because of groundwater impact which includes scaling and erosion. This could be avoided by using some closed-loop collector types (such as U-tube for example). Also, from the economic side, it would be more profitable to drill fewer deeper boreholes, instead of a lot of shallow ones (64 boreholes 125 m deep, instead of 120 boreholes 65 m deep). This change would reduce costs by 13%, because of reduced storage land area. During the extraction period, the thermal resistance in the boreholes was unexpectedly high. This was because of the low water flow rate and the borehole pipe not being centered. By increasing the flow rate and centering the borehole pipe charged energy would increase by 30% and recovered energy by about 51% (Nordell, 1994). Also, using insulation material would reduce heat losses and affect the heat recovery efficiency of the storage.

D.3.2. HT-BTES in Emmaboda – Sweden

The HT-BTES in Emmaboda presents as a larger copy of the Lulea heat storage. It is used for both energy research projects and as a system to increase the storage capacity of the Xylem Water Solutions AB plant

(Malmberg, 2017). The objectives of this project were to document the original construction/design and measures taken to improve its operation (Nordell et al., 2015).

D.3.2.1. Technical design

The storage consists of 140 boreholes, each 150 m deep. The spacing between boreholes is 4 m and they are aligned in a rectangular shape (36 × 52 m). A 0.4 m thick layer of foam glass insulation is put on top of the storage. Considering overburden thickness, the effective depth of the storage is 144 m which gives a storage volume of 323 000m^3. The collector type used is open coaxial, made of polypropylene (PPE), 40/90 diameter (Nordell et al., 2015).

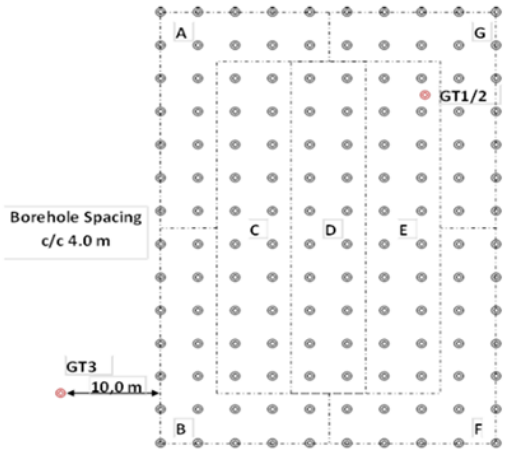

Figure D 3: Plan of drilled boreholes. The seven sections and the location of the 140 boreholes and monitoring holes are indicated. The red rings show the location of monitoring holes (Nordell et al., 2015).

D.3.2.2. Geology and Hydrogeology

Geology was indicated by drilling. Bedrock was made of reddish grey to light grey granodiorite with overburden which mainly consists of glacial till, 2-8 m thick. Towards the bottom of the holes, there was an increasing number of amphibolite dykes (2-5 m thick). The bedrock surface was slightly dipping towards the west. The thickness of the overburden decreased towards the east. Borehole drilling also revealed several water-filled fractures and unstable cross zones in the bedrock, which therefore has a fracture permeability. Around 30% of the boreholes produced more than 500 L/min. The groundwater table was 2 m below borehole heads (Nordell et al., 2015). The BTES area has not been affected by regional groundwater flow according to a thermal response test. A large fracture zone in the west was present at 30 m depth in UB1 (GT3) (Ramstad et al., 2023; Figure 5).

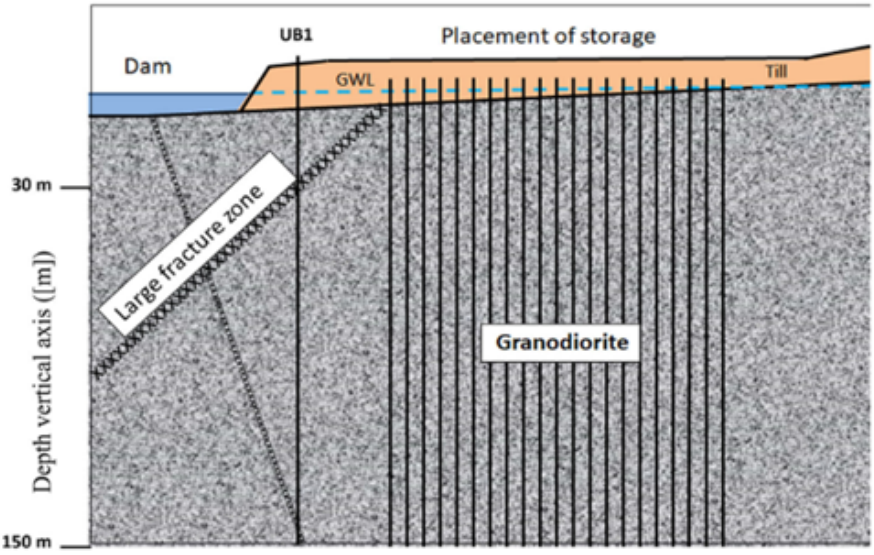

Figure D 4: Hydrogeological and geological conditions in the east-west cross-section of the BTES (Ramstad et al., 2023).

D.3.2.3. Measured operational data

The system is designed to reverse flow direction depending on the mode of operation (charging and discharging) for water flow rates between 5 and 20 L/s. Many temperature and pressure gauges were installed throughout the storage to help operate the storage and detect operational problems automatically. Two monitoring boreholes were drilled, one inside the storage and the other outside. Also, temperature measurements were performed on the top and bottom of the insulation to monitor the insulation efficiency (Nordell et al., 2015).

D.3.2.4. Results

- 2010 – 2015

The energy was calculated based on the water flow rate and water temperature difference between the inlet and outlet temperature to and from the storage system. Heat was extracted for two years in a test run. Overall, 198 MWh of energy was extracted from the HT-BTES system over 5 years (Nordell et al. 2015). The injection temperatures varied over 5 year period, ranging from as low as 15 °C up to 65 °C. The overall injection temperature was presumed to be at 60 °C constantly, however it varied significantly and was lower majority of the time (Nordell et al., 2015). Therefore, the production temperatures were also lower than anticipated, ranging from as low as around 16 °C up to around 45 °C as seen in Figure D 5 (Nordell et al., 2015).

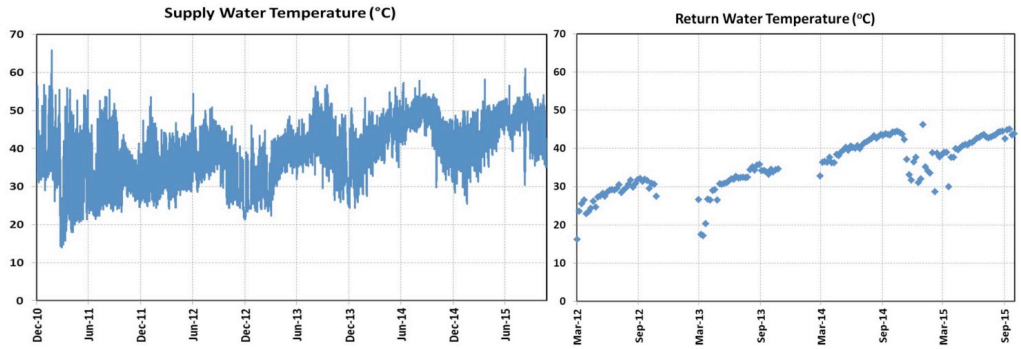

Figure D 5: Measured injection (supply) and extraction (return) water temperatures from 2010 to 2015 at the Emmaboda HT-BTES (Nordell et al., 2015).

From the start of operation until the end of the evaluation period, 11875 MWh of energy has been injected into the storage volume, while only 198 MWh has been extracted. Most of this heat has been conducted into the surrounding bedrock, which has been warmed up. Temperatures were measured in three locations in the bedrock inside and outside the storage volume (Figure D 6). Two temperature gauges were installed inside the GT1-2 observation borehole, at the depth of 70 and 117 m. The third device was put in observation borehole GT3, 10 m outside of the storage (Nordell et al., 2015).

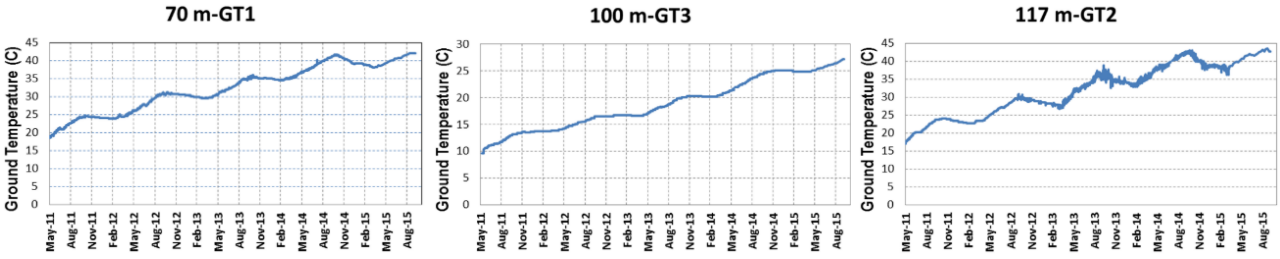

Figure D 6: Measured temperature at a depth of 70,100 & 117 m below surface (Nordell et al., 2015).

The measured ground temperature at 117 m shows small sudden deviations from the expected slow temperature change that should take place. This phenomenon cannot occur in the storage volume if heat is only transferred by conduction. A similar observation was made in the Lulea heat store, where it was correlated to precipitation in the form of rain. This most probably isn't the case in Emmaboda, but open circulation through the boreholes causes convection in the bedrock and fractures (Nordell et al., 2015).

The efficiency of the insulation layer on top of the storage was also measured by measuring the temperature under and on top of the insulation layer. The mean temperature difference measured was between 11°C and 13°C. It was calculated that annual heat loss through the thermally insulated surface on top of the storage is 63 MWh, which makes up 6% of the total heat loss (Nordell et al., 2015).

- 2018 – 2021

After a few years, a heat pump system, consisting of 8 parallel connected heat pumps was installed. This enabled drastically increasing accumulated heat extraction from the storage (figure D 7). Installing heat pumps lowered the average temperature of the storage to (20-40°C), which enabled significantly higher cooling capacity during summer and reduced heat losses due to the lateral flow of stored heat (Andersson et al.,2021).

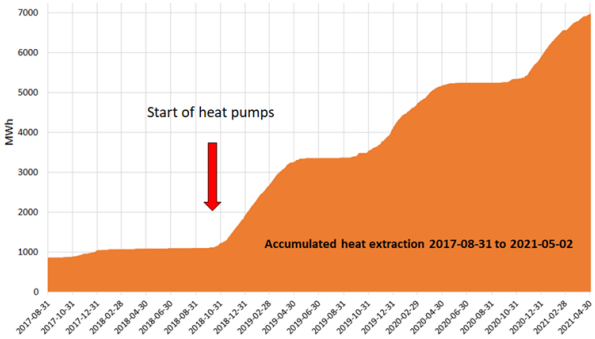

Figure D 7: The accumulated heat extraction from the storage from 2017 to 2021 (Andersson et al., 2021).

D.3.2.5. Conclusion and discussion

During the construction of the HT-BTES in Emmaboda (Table D 3), unexpected drilling problems occurred, which could have been avoided with a small number of test drillings. This storage functions just fine by lowering the working temperatures of the storage to about 40°C and installing a heat pump system to support the discharge of heat from the storage.

Although a coaxial borehole exchanger has helped to obtain a thermally favorable temperature profile in the storage, it's not sufficient to prolong a high temperature when extracting heat. It was presumed that various technical problems, such as vacuum pressure and stripping of gas could be prevented by using conventional borehole heat exchangers, such as thermal-resistant U-tubes.

HT-BTES in Emmaboda			
Start of operation	2010	Storage shape	Rectangular
Storage volume [m3]	323 000	Ground type	Rock
Number of boreholes	140	Thermal conductivity [W/(m*K)]	3
Borehole depth [m]	150	Volumetric heat capacity [MJ/(m3*K)]	2.34
Total borehole length [m]	21 000	Insulated [Yes/No]	Yes
Borehole spacing [m]	4	Insulation material	Foam glass
Borehole diameter [mm]	115	Insulation thickness [mm]	400
Collector type	Open Coaxial	Source of charge	Waste heat
Collector diameter [mm]	40/90	Injected energy/year (planned) [MWh]	3 271* (3 600)
Collector material	Polypropylene (PPE)	Extracted energy/year (planned) [MWh]	89* (2 700)
Collector temperature resistance	80	Charging temp [°C]	30-60
Thermal stratification [Yes/No]	Yes	Storage maximum temp [°C]	45
Number of boreholes in series	2	Storage minimum temp [°C]	Unknown
Total collector length in series [m]	300	HP for extraction [Yes/No]	Considered

Table D 3: Design parameters for HT-BTES in Emmaboda, Sweden (Malmberg, 2017).

D.3.3. BTES in Neckarsulm - Germany

In Neckarsulm solar district heating is used for space heating and domestic hot water for a new housing estate. To keep up with the development of residential areas over several years, solar collector fields and storage were increased in several stages. Due to geological and hydrogeological conditions, BTES is selected for seasonal heat storage (Reuss, 2015).

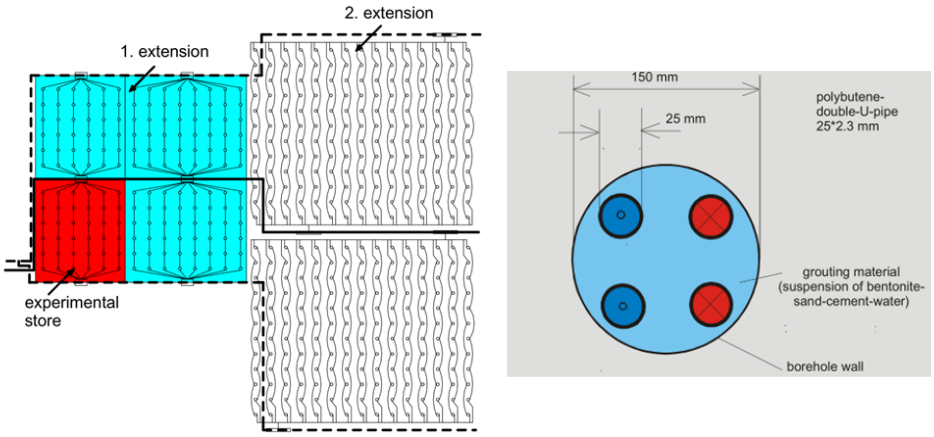

Figure D 8: Scheme of the duct heat store in Neckarsulm (left) and of a borehole heat exchanger (right) (Heidemann et al., 2003).

D.3.3.1. Technical design

The first pilot storage was made of 36 boreholes in 1997. After two extensions, storage was made of 528 boreholes in 2011, with a storage volume of 63360 m^3. Due to geological conditions, boreholes are 30 m deep. The geometry was rectangular, to allow extension in several stages (Figure D 8). Spacing in the first extension was 2 m. Spacing in the second extension was 1.5 m in the center and 2.5 m at the edges to reduce heat losses to the sides (Figure D 8). To avoid heat losses through the top, a 20 cm thick insulation layer of XPS was used to cover the top of the storage. Above the insulation, there is a 2-3 m thick layer of soil. Double U-tubes made of polybutene (PB) were used as collector type (Reuss, 2015; Figure D 9).

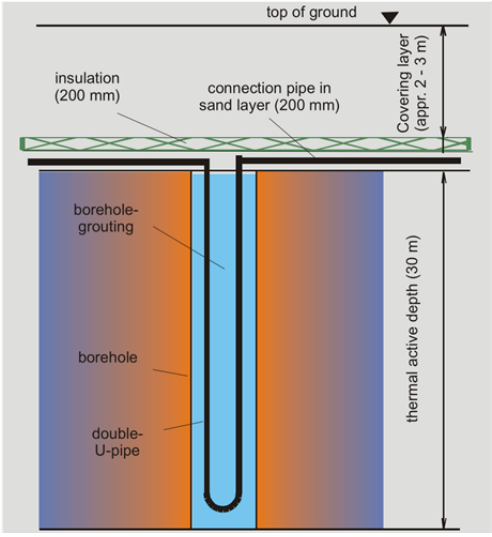

Figure D 9: Scheme of a borehole heat exchanger in Neckarsulm (Heidemann et al., 2003).

D.3.3.2. Geology and hydrogeology

Under the first 2-3 m of soil, there is a 30-35 m thick layer of clay. That layer of clay is followed by highly permeable dolomite. Because of low hydraulic conductivity ($k \approx 10^{-8}$m/s), favourable volumetric heat capacity ($c = 2.85$ MJ/m^3K) and thermal conductivity ($\lambda = 2.2$ W/mK), clay is suitable for BTES. Since under

clay, there is dolomite with much higher hydraulic conductivity with groundwater flow, the maximum depth of boreholes is 30 m (Reuss, 2015).

D.3.3.3. Measured operational data

Temperatures were measured at different depths in the middle of the first and second extensions of the heat store. The highest measured temperature was 57°C at a depth of 20 m in the middle of the first extension in 2000 (Figure D 10 - left). Temperature was also measured above the thermal insulation layer (-0.2 m), which is not only dependent on charging periods but also the ambient air temperature. The temperature below the thermal insulation (2-3 m below ground surface) was around 15 K lower than in the layers above the insulation. The insulation effect was decreased due to increased moisture in the polysterene that was used as the insulation. The temperature at 2 m below the storage (at 32 m) increased in the first extension by 15 to 20 K when compared to undisturbed ground temperature due to heat losses (Heidemann et al., 2003). The second extension had a different construction of insulation was done which ensured long-term insulation effect of the top of the field. Figure D 10 (right) shows temperature monitoring at different layers of the second extension where it is seen that the highest temperature measured was at around 54°C at the top of the store (2-3 m below the ground). Also, the temperature above the thermal insulation does not exceed circa 28 °C (Heidemann et al., 2003).

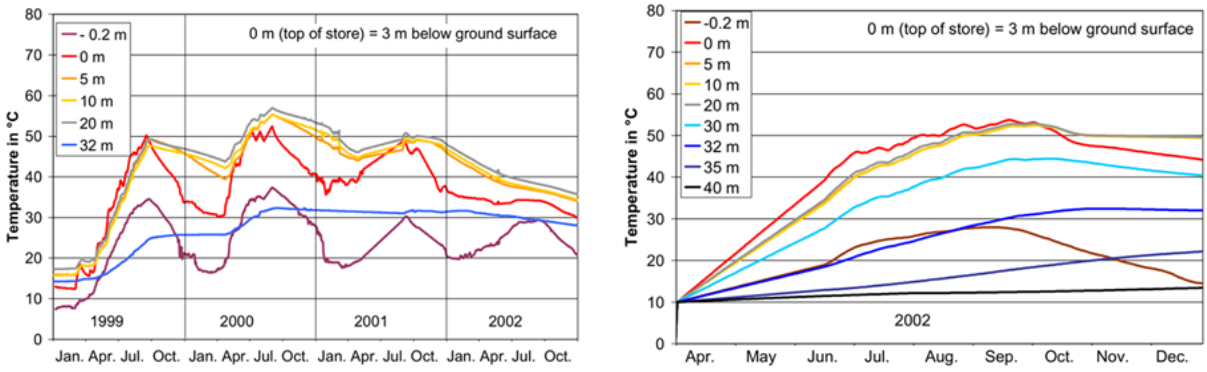

Figure D 10: Temperatures in the middle of the first extension (left) and the second extension (right) of the duct heat store in Neckarsulm (Heidemann et al., 2003).

The development of solar collectors, duct heat store and their heat delivery and heat losses from 1999 to 2002 can be seen in Table D 4 and from 2003 to 2007 in Table D 5 and field design parameters in Table D 6.

		1999	2000	2002
Collector area	m²	2636	3090	5007
Heat delivery of solar collectors	MWh/a	802	577	1696
per m²	kWh/m²	304	219	331
Solar heat delivery to heat distribution net	MWh/a	250	213	822
per m²	kWh/(m²·a)	95	81	164
Total heat delivery to heat distribution net	MWh/a	1241	1247	1720
Heat losses in net (calculated)	MWh/a	349	242	533
Heat delivery by gas boiler	MWh/a	1028	1034	1303
Solar fraction (based on total heat demand)	**%**	**18**	**17**	**39**

Table D 4: Data of the heat balances in Neckarsulm (Heidemann et al., 2003).

		2003	2004	2005	2006	2007
Solar yield of collectors	[MWh]	2050[1)] 71[2)]	1629[1)] 38[2)]	1634	1805	1854
per m² collector area	[kWh/m²]	406[1)]	318[1),3)]	310.5	343	336
Solar heat into district heating network	[MWh]	700[1),2),4)]	755[1),2),4)]	1221	1011	1204
per m² collector area	[kWh/m²]	126[1)]	143[1)]	232	185	218
Overall heat delivery into the district heating network	[MWh]	1810 +81[5)]	2236[1)] +120[5)] 879[2)]	4825	2647	2807
Heat delivered by the gas boiler	[MWh]	1109	1481[1)] 879[2)]	3311	1510	1485
Solar fraction	[%]	39	34[1]	26.7	39.6	44.8

[1)] District heating system "Grenchenstraße" (CSHPSS with BTES)
[2)] District heating system "Eugen-Bolz-Straße" (adjacent district heating system)
[3)] 5007 m², collector field „Pflegeresidenz" (256 m³) connected during the year
[4)] Heat losses of the solar network were subtracted. Only the solar heat delivery of the district heating system "Grenchenstraße" but not of "Eugen-Bolz-Straße" is included. For 2003 the heat losses of the solar network are not included within the calculation of the solar heat into the district heating system.
[5)] Heat losses of the solar network.

Table D 5: Heat balances for the years 2003 to 2007 for the CSHPSS Neckarsulm (Nußbicker-Lux et al., 2009).

HT-BTES in Neckarsulm			
Start of operation	1997/99/2002-	**Storage shape**	Rectangular
Storage volume [m3]	63 360	**Ground type**	Clay
Number of boreholes	528	**Thermal conductivity [W/(m*K)]**	2,2
Borehole depth [m]	30	**Volumetric heat capacity [MJ/(m3*K)]**	2,85
Total borehole length [m]	150 840	**Insulated [Yes/No]**	Yes
Borehole spacing [m]	2	**Insulation material**	Polystyrene
Borehole diameter [mm]	150	**Insulation thickness [mm]**	200
Collector type	Double U-tube	**Source of charge**	Solar thermal
Collector diameter [mm]	25	**Injection power [GJ]**	Not found
Collector material	Polybutene (PB)	**Extraction power [GJ]**	Not found
Collector temperature resistance	85	**Charging temp [°C]**	60 (66*)
Thermal stratification [Yes/No]	Yes	**Storage maximum temp [°C]**	65
Number of boreholes in series	6	**Storage minimum temp [°C]**	45
Total collector length in series [m]	360	**HP for extraction [Yes/No]**	No

* As of monitored operation in 2002 (Mangold, et al., 2003).

Table D 6: Design parameters for HT-BTES in Neckarsulm, Germany (Malmberg, 2017).

D.3.4. TU Darmstadt medium deep BTES

Currently, there are no deep or medium-deep BTES systems operating in the world. The first project that is currently researching a medium-deep borehole thermal energy storage (MD-BTES) is a pilot project implemented at the Technische Universität Darmstadt (TU Darmstadt). The first research that showed the potential of constructing an MD-BTES at the TU Darmstadt was carried out in 2016. Welsch et al. (2016) emphasized that in the field of energy storage using MD-BTES there is still no operational experiences which presents a challenge in broad implementation of such systems. In the study the advantage of the MD-BTES is seen in storing high temperature heat in greater depths when compared to shallow BTES (Welsch et al., 2016). This mitigates the problem of disrupting the temperatures in shallow aquifers which can be affected by significant change in temperature if shallow BTES is used. Furthermore, less area is needed since fewer boreholes are drilled with MD-BTES to ensure the same heat storage levels due to MD-BTES operating at higher temperatures. Welsch et al. (2016) considered MD-BTES to be of 100 m to 1000 m of depth with less than 50 BHEs in a field. Numerical simulations with different storage geometrical setup (position of BHEs), BHE configuration (number and BHE length), injection and production temperatures (spanning from 70 – 110 °C for injection and from 10 – 50 °C for production) as well as different rock properties, were performed to establish an optimal design and favourable temperatures to operate the MD-BTES storage (Figure D 11). The simulations showed that the storage efficiency ranges from 32% to almost 84%, due to heat diffusion, while specific heat extraction rate ranges from 49 W/m to 113 W/m. The study concluded that by increasing BHE length and the number of BHEs the storage capacity and storage efficiency are both increased. Also, the dissipation effect of the occurrence of the groundwater flow is recognized as a significant factor of MD-BTES performance and it should be limited to avoid stored heat dissipation.

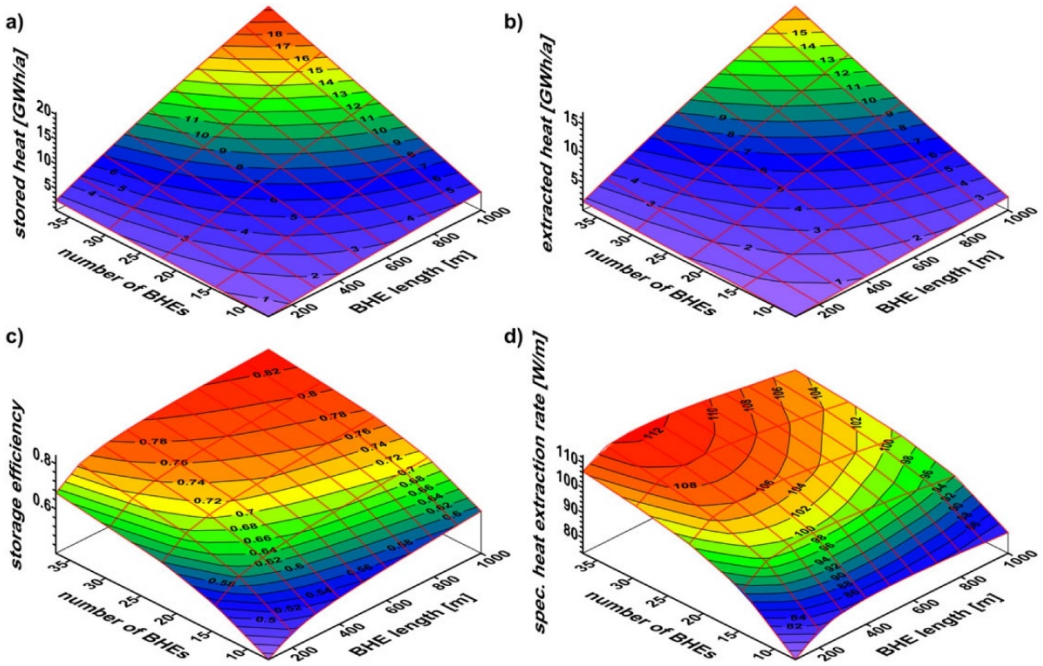

Figure D 11: (a) Amount of stored heat, (b) amount of extracted heat, (c) storage efficiency and (d) specific heat extraction rate in the 30th year of operation depending on a change in the number of borehole heat exchangers (BHEs) and the BHE length for storage systems with a BHE spacing of 5m (Welsch et al., 2016).

Within the SKEWS project three boreholes were drilled and completed as borehole heat exchangers (BHE) from 18.7. to 25.10.2022 (Krusemark et al., 2024) in the western part of the Lichtwiese Campus, at TU Darmstadt (Figure D 12). The drilled BHEs are 750 of lenght and have spacing of 6.88 m (Seib et al., 2024). The geological profiles show that Permian basaltic and sedimentary rocks interbedded with sedimentary mudstones are present in the first 200 m of depth, followed by reddish granite from 200 m to 470 m and ending with gray granodioritic material from 470 m to final depth of 750 m (Figure D 13).

Figure D 12: Site location of the MD-BTES at the pilot site Campus Lichtwiese, TU Darmstadt (www.push-it-thermalstorage.eu/pilots/darmstadt/).

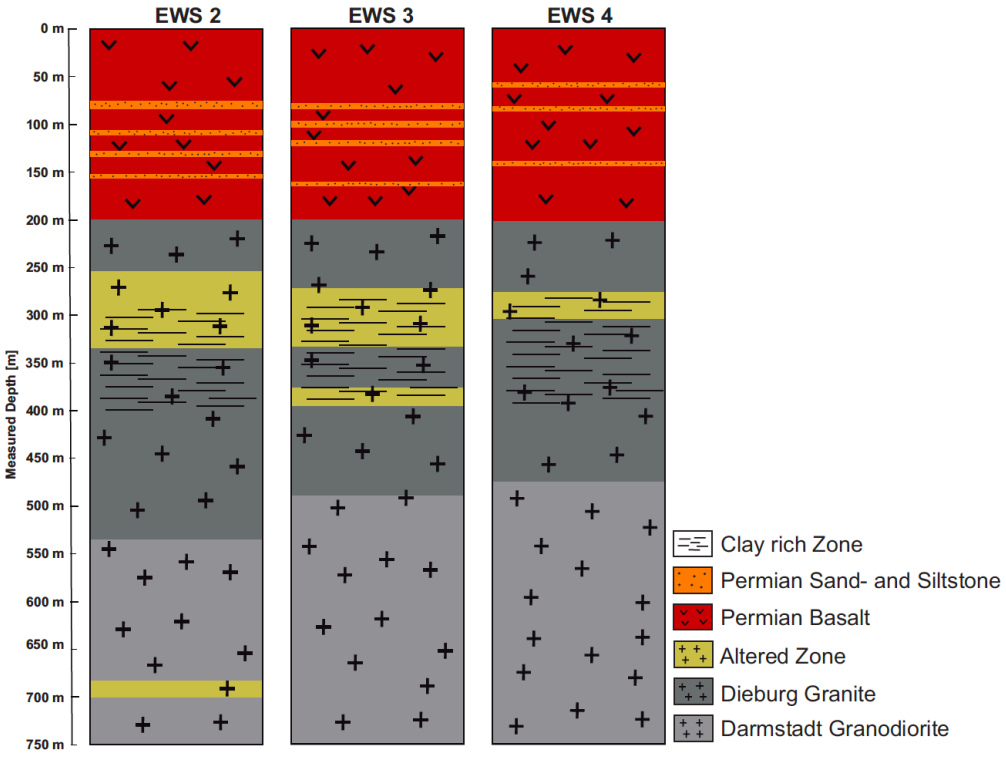

Figure D 13: Geological profiles of three BHEs at pilot site identified on cutting samples and mud logging data (Seib et al., 2024).

Before drilling commenced extensive surveys, such as conductivity tomography profiles, gravity measurements, 2D seismic profiles and petrophysical data on nearby outcrops, were gathered and analysed to identify possibilities for improvement of constructing MD-BTES systems in crystalline environment.

D.3.5. Conclusion

Initial feasibility screening must consider geological conditions, heat load and system modelling. Key geological parameters include geology, groundwater flow and thermal properties. Significant groundwater flow should be avoided to prevent advective heat loss. Higher heat capacity is preferable. Optimal borehole layout and system design maximize efficiency. Drilling and grouting should be carefully executed, considering costs and environmental impact. Top insulation is necessary to reduce heat loss. System efficiency depends on input/output parameters, thermal properties and integration and is favoured by a small surface-to-volume ratio. Each project must adapt to specific geological parameters. Pre-design tools should be utilized for optimization. Larger storage volumes tend to be more financially viable.

Annual heat loss for a given annual mean temperature of the store is a function of the volume, shape and ground properties. Storage efficiency is defined by the ratio between extracted and stored thermal energy.

BTES applications have primarily been designed for larger building complexes, residential communities and district heating networks. These systems often utilize solar panels, industrial waste heat and, for smaller systems, cooling of buildings during summer. Future applications may include heat from waste heat incineration and power-to-heat setups.

D.4. Numerical simulation

D.4.1. Method

- **The conceptual model**

The modelling framework is based on transient simulation of energy balance flows in the surface equipment, borehole heat exchanger (BHE) and the geothermal reservoir. The simulation is done in a coupled approach for all three system components modelled by separate balance equations. The modelling framework for the BHE is built on 1D energy balance for coaxial BHE with annular inlet (CXA exchanger – coaxial annular inlet). The modelling framework for the geothermal reservoir is finite element analysis (FEM). Both BHE and reservoir modelling approach are done in a commercially available software FeFlow (Diersch, 2014). For finite element groundwater flow in FeFlow, relevant data and case studies can be found in (Diersch, 2014) or in the FeFlow online documentation (FeFlow 8.0 Documentation). Surface equipment is modelled with user-defined scripts in which all model features are combined with a set of specific equations describing each of the component. The full coupling is done with a Python-Feflow interface.

The framework is tested on a hypothetical case study for a single-well BHE (acting as a single-well deep BTES) integrated into a district heating (DH) network of the city of Zagreb. The location of the BHE corresponds to the existing Savica-1 well located in the industrial zone of the city of Zagreb, but also in a relative proximity to the potential heat demand. The conceptual scheme of the problem is presented in Figure D 15. As a transition towards the 4th generation district heating (Lund et al., 2021) and decarbonized heating, the BTES is introduced. During the winter period, the DH is supplied directly from the BHE and industrial waste heat, where BHE is used first. During the summer period industry is rejecting the excess heat due to limited flexibility. In combination with this waste heat and lack of thermal demand, the BHE could now be used to reject the heat into the reservoir to enhance its thermal recovery before the new heating season starts.

Since in this work only a single deep BHE is considered, it can balance heat flows for only one minor part of the DH, i.e. DH covering residential object in the proximity of the BHE and source of industrial waste heat. Therefore, the DH network is divided into DH-1 and DH-2, where only DH-1 has the direct access to the BHE as a part of the BTES in seasonal balancing between industrial waste heat and heat demand. The waste heat thermal power is few tenths to few hundreds of megawatts, while a single BHE can be used to accept up to a few hundreds of kilowatts, depending on the configuration. From the modelling point of view, the effects of a single well would not be visible in the modelling results if the division between DH-1 and DH-2 was not done. In this report, all further modelling and analysis of results will refer only to DH-1, where the effect of single BHE of the BTES can be visible.

The detailed scheme of the process is presented in Figure D 16. As already mentioned, only the DH-1 (the one containing the BHE) is relevant for the analysis. The system consists of three heat exchangers (HX): the main heat exchanger for direct heating with geothermal energy (HX) and two waste heat exchangers (WH-1 and WH-2) for utilization of industrial waste heat. The WH-1 is used to additionally heat the DH-1 during the heating season if the geothermal reservoir fails to supply sufficient heat in terms of both DH-1 and leaving load temperature (LLT). The WH-2 is used to reheat the geothermal reservoir during the summer time when there is excess heat from the industry and no heat demand. A high temperature heat pump (HTHP) is used to elevate the temperature level of the low-enthalpy geothermal heat. As a final heating supply for the DH-1 there is a possibility to use the electric heating (EH). Electric heater should be used only if there is not enough heat supply from the WH, heat pump or direct use of geothermal heat from HX.

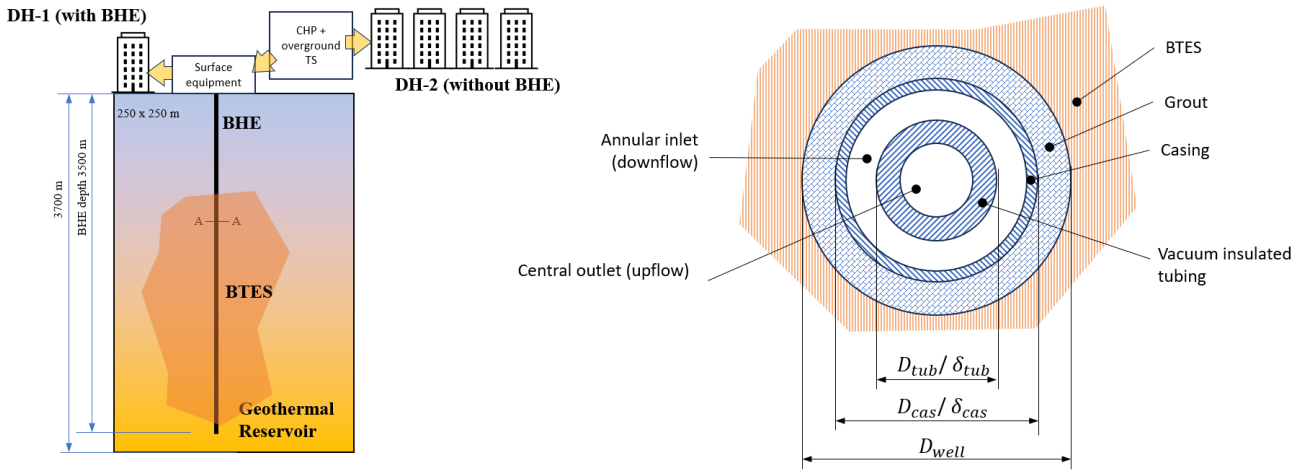

Figure D 15: The conceptual scheme of the simulation problem (left) and cross-section of the borehole heat exchanger with annular inlet BHE-CXA (right).

All three HX's can be bypassed with the use of three separate two-way valves V-HX, V-WH1 and V-WH2, which are used to control the mass flow at the „hot" side of the HX and consequent heat transfers in heat exchangers.

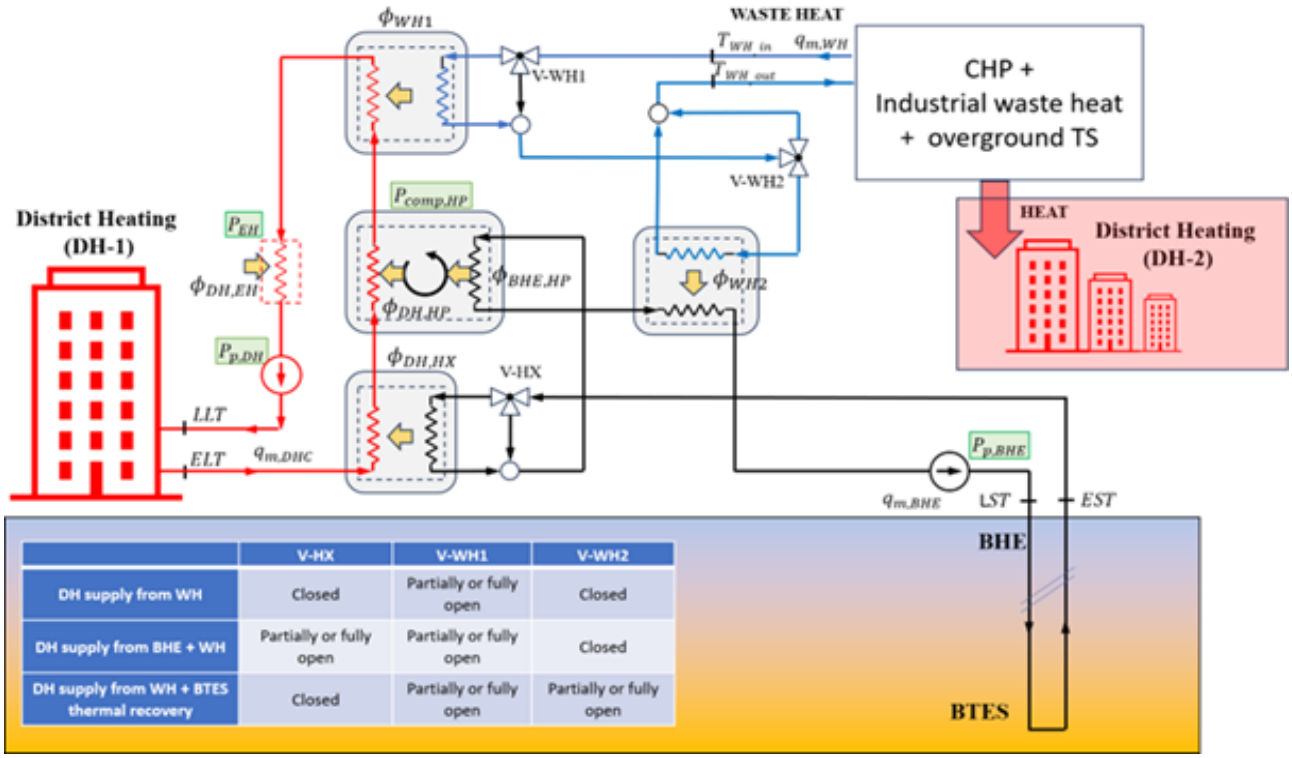

	V-HX	V-WH1	V-WH2
DH supply from WH	Closed	Partially or fully open	Closed
DH supply from BHE + WH	Partially or fully open	Partially or fully open	Closed
DH supply from WH + BTES thermal recovery	Closed	Partially or fully open	Partially or fully open

Figure D 16: The scheme of the surface equipment with energy flows of heat and electricity.

The mass flow rate on the „hot“ side of the HX is determined by the valve openness ratio x_v (Equation 1).

$$x_v = \frac{q_{m,HX}}{q_m} \quad (1)$$

which is a ratio between the mass flow rate going through the heat exchanger $q_{(m, HX)}$ and total mass flow rate q_m (Equation 2).

$$q_m = \underbrace{x_v q_m}_{q_{m,HX}} + \underbrace{(1 - x_v) q_m}_{q_{m,HX,bypass}} \quad (2)$$

The value of valve openness ratio x_v lies between 0 and 1.

The role of the surface equipment is to ensure the best possible way to:

- Supply heat to DH-1 from the BHE-CXA (direct heating and heat pump)
- Supply heat to DH-1 from the WH-1
- Store excess heat from WH-2 into the geothermal reservoir through the BHE-CXA into the rock mass.

The overall energy balance consists of the heat and power balance. Heat balance has to satisfy temperature constraints, meaning that inlet temperature from waste heat is $T_{wh,in}$ and is determined by the operation of the industrial burners. The leaving source and entering source temperatures, LST and EST, are determined by the operating strategy of the surface equipment and is described in detail in the following chapters. The leaving load and entering load temperatures, LLT and ELT, are determined by the heat demand of the system, which can be high-temperature or low-temperature, depending on the heating system DH-1.

Future DH systems will eventually evolve into the low-temperature systems with temperatures in the system lower than 60 °C, but the full transition will take a few decades. The overall modelling framework is presented in Figure D 17.

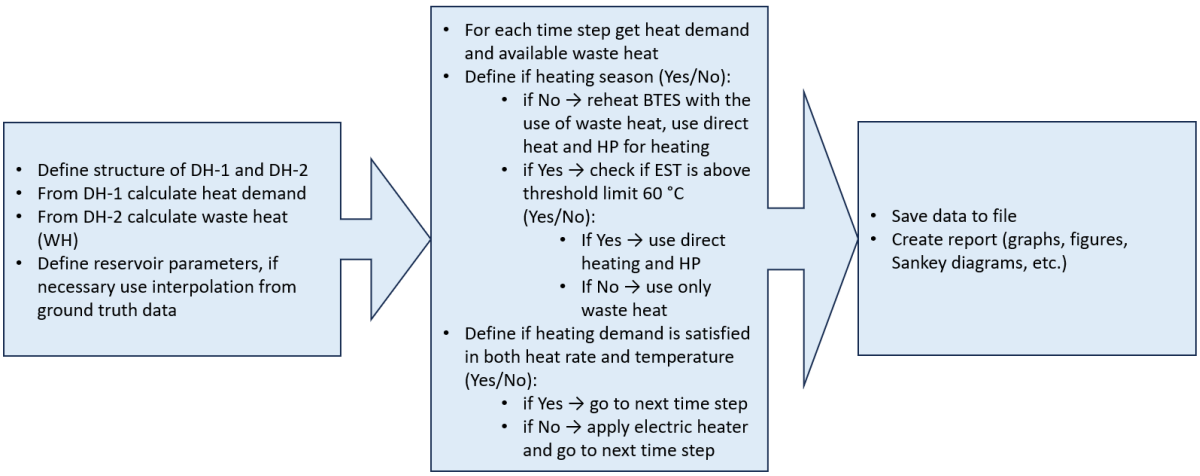

Figure D 17: The overall modelling framework of the BTES assessment method.

The modelling is done with transient simulation, since seasonal variations in energy flows have to be captured. The control of the surface equipment combining waste heat and BHE is done with control valves V-HX, V-WH1 and V-WH2. The coupling between the surface operation and reservoir modelling is done with the use of a Python-Feflow interface.

The detailed description of the mathematical modelling of heat exchangers, together with optimization of the valve openness x_v is given below.

- **The Python-FeFlow interface**

The Python v3.10 (Pilgrim & Willison, 2009) interface is written in Spyder Python IDE, and dynamic update of FeFlow BHE boundary conditions is done with the use of FeFlow's Interface Manager (IFM) (IFM FEFLOW Model Class). The interface is based on a time-stepping algorithm that takes into account pre-time step and post-time step processes that govern the operating parameters of the BHE-CXA prior to FEM calculation.

In the pre-time step the mass flow rate ($q_{m,BHE}$) and leaving source temperature (LST) are calculated from the balance of the overall surface equipment. In the post-time step the resulting entering source temperature (EST) is obtained from the FEM calculations in the current time step and all results for the current time step are saved into the result file. The complete interface is presented in Figure D 18.

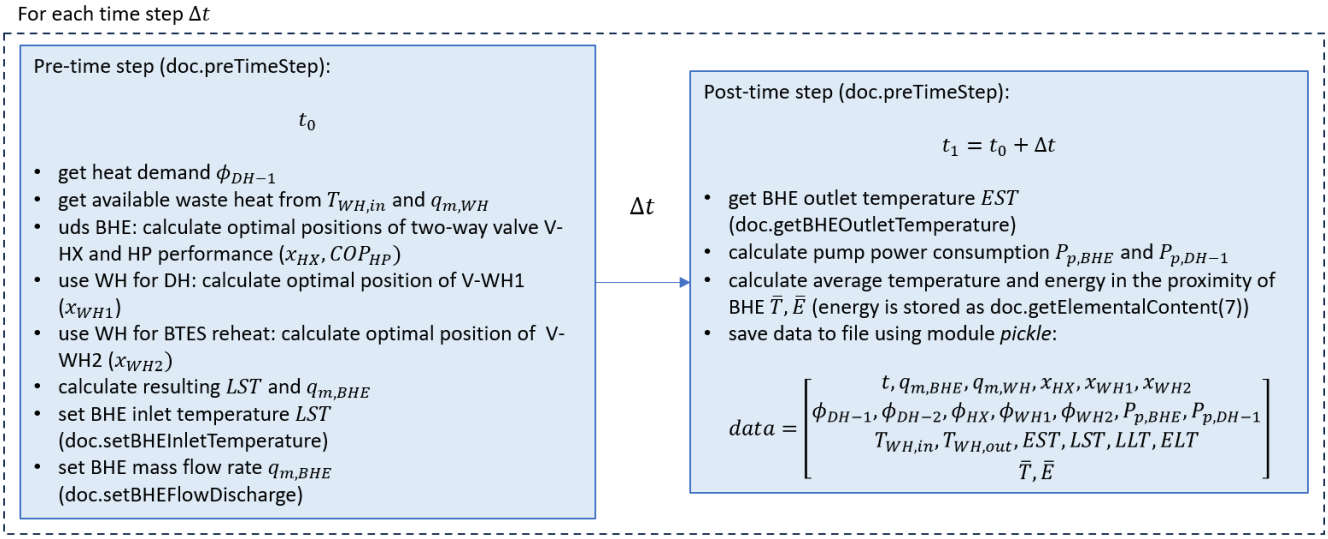

Figure D 18: The Python-Feflow interface.

Available waste heat is provided as available inlet temperature ($T_{WH,in}$) at given mass flow rate ($q_{m,WH}$). The coupling between the surface equipment and the FeFlow is done with optimization of mass flow rates which control heat transfer in each of the heat exchanger. Mass flow rates are directly dependent on the openness of control valves ($x_{v,HX}, x_{v,WH1}, x_{v,WH2}$). The detailed description and mathematical model of heat demand and heat exchanger is provided in following chapters.

- **The DH-1 heat and power demand**

The heat demand is calculated from the formula (Equation 3):

$$\phi_{DH-1} = q_{m,DH-1} c (LLT - ELT) \qquad (3)$$

where LLT is determined by the ambient temperature and heat to be delivered ϕ_{DH-1} is determined by the mass flow rate of the DH-1 system $q_{m,DH-1}$. The parameter *c* is specific heat of the water.

Power demand is determined by the consumption of circulation pumps which are function of mass flow rate, density and pressure drop in the system. There are two circulation pumps, one for primary fluid that ensures the flow rate between the BHE and surface equipment $P_{p,BHE}$, and other one for DH-1 mass flow rate between surface equipment and heating demand $P_{p,DH-1}$. The power consumption is calculated according to the Equation (4):

$$P_p = \frac{q_m}{\rho}\Delta p \tag{4}$$

Pressure drop Δp is calculated from the Bernoulli equation, where pressure drop dominantly depends on linear pressure drop that is calculated from the Equation 5:

$$\Delta p_{lin} = \frac{fL}{D}\frac{1}{2}\frac{1}{\rho}\left(\frac{q_m}{A}\right)^2 \tag{5}$$

The friction factor f is calculated iteratively from the Colebrook-White relation.

- Water-to-water heat exchanger (WTW-HX)

The water-to-water (WTW) heat exchangers (HX) are modelled based on NTU method. The role of the WTW HX model is to find outlet hot (H) and cold (C) stream temperatures according to Figure . Implicit statement of the problem can be written as (Equation 6):

$$F\left(q_{m,H}, T_{H,in}, T_{H,out}, q_{m,C}, T_{C,in}, T_{C,out}, \phi\right) = 0 \tag{6}$$

Variables $\left(q_{m,H}, T_{H,in}, T_{H,out}, q_{m,C}, T_{C,in}, T_{C,out}, \phi\right)$ are operating parameters and (c_C, c_H, k, A) are physical parameters and constants. Depending on the unknowns to be found, the explicit formulation can be derived. For example, if the inlet temperatures of the cold $T_{C,in}$ and hot $T_{H,in}$, stream as well as cold stream mass flow rate $q_{m,C}$ and heat demand ϕ are known, then the problem becomes (Equation 7):

$$\left(q_{m,H}, T_{H,out}, T_{C,out}\right) = f\left(T_{H,in}, q_{m,C}, T_{C,in}, \phi\right) \tag{7}$$

Usually there are practical limits to of outlet temperatures $T_{H,out}$ and $T_{C,out}$ and in that case the heat transfer rate ϕ cannot be known in advance, but becomes a solution of a constrained nonlinear optimization problem where the outlet temperature of the cold stream is now a part of the goal function. The scheme of the problem is presented in Figure D 19.

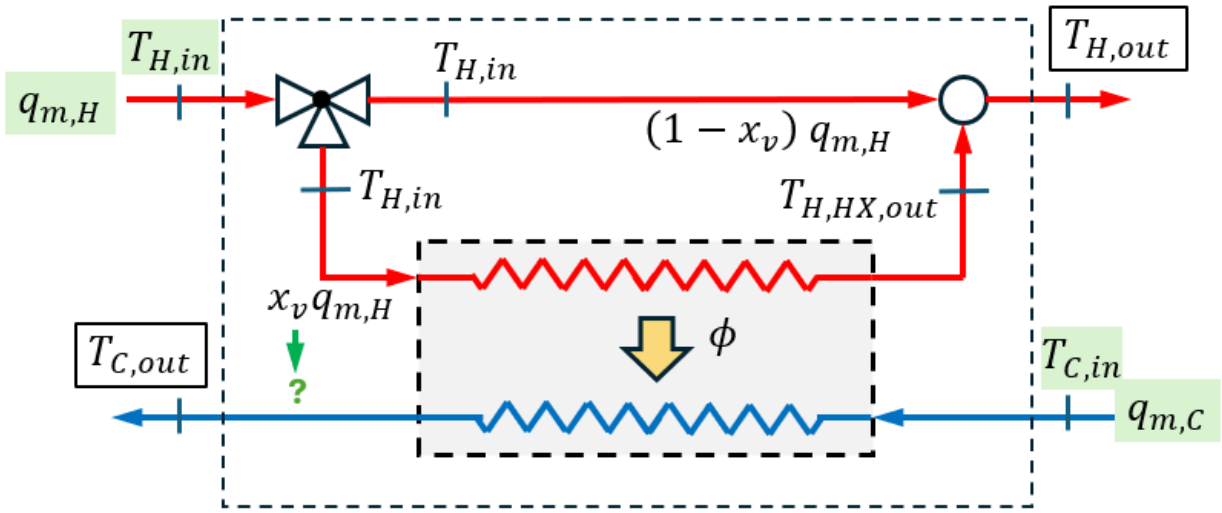

Figure D 19: Scheme of the optimization problem.

The problem statement referring to Figure is: find the position of a two-way valve x_v which will ensure that $T_{C,out}$ is as close as possible to predefined value $T_{C,out,set}$ without violating the minimum outlet temperature of the hot stream $T_{H,out,min}$ or maximum outlet temperature of the cold stream $T_{C,out,max}$. The goal function is (Equation 8):

$$min\left(\left|T_{C,out} - T_{C,out,set}\right|\right) = f(x_v)$$
$$0 \le x_v \le 1 \tag{8}$$

subject to constraints (Equation 9):

$$T_{H,out} > T_{H,out,min}$$
$$T_{C,out,max} > T_{C,out} \tag{9}$$

Variables $\left(T_{C,out,set}, T_{H,out,min}, T_{C,out,max}, q_{m,H}, T_{H,in}, q_{m,C}, T_{C,in}\right)$ should be know in advance. The goal function brings $T_{C,out}$ as close as possible to $T_{C,out,set}$ by changing the bounded variable x_v which should be low enough to avoid $T_{H,out}$ below the minimum value of $T_{H,out,min}$ or $T_{C,out}$ above the minimum value of $T_{C,out,max}$, but high enough to minimize the goal function.

The goal function is calculated from the following expression (Equation 10):

$$min\left(\left|T_{C,out} - T_{C,out,set}\right|\right) \tag{10}$$

where $T_{C,out}$ and resulting ϕ can be calculated from the following set of equations for ϕ and x_v (Equation 11):

$$T_{C,out} - T_{C,in} - \frac{\phi}{C_C} = 0$$

$$\left\{ \frac{1 - e^{\left[-\frac{kA}{C_{min}}\left(1-\frac{min(C_C, x_v q_{m,H} c_H)}{max(C_C, x_v q_{m,H} c_H)}\right)\right]}}{1 - \frac{min(C_C, x_v q_{m,H} c_H)}{max(C_C, x_v q_{m,H} c_H)} e^{\left[-\frac{kA}{C_{min}}\left(1-\frac{min(C_C, x_v q_{m,H} c_H)}{max(C_C, x_v q_{m,H} c_H)}\right)\right]}} \right\} \times min(C_C, x_v q_{m,H} c_H)(T_{H,in} - T_{C,in}) - \phi = 0 \quad (11)$$

If the temperature at the exit of the HX on the side of the hot stream is noted as $T_{H,HX,out}$, then the resulting temperature at the hot side can be calculated from the mixing balance (Equation 12 & 13):

$$T_{H,out} = x_v T_{H,HX,out} + (1 - x_v) T_{H,in} \quad (12)$$

with

$$T_{H,HX,out} = T_{H,in} - \frac{\phi}{x_v q_{m,H} c_H} \quad (13)$$

The constraints can be calculated from the expressions (Equation 14):

$$T_{C,out,max} - T_{C,in} - \frac{\phi}{C_C} \geq 0$$
$$x_v \left(T_{H,in} - \frac{\phi}{x_v q_{m,H} c_H} \right) + (1 - x_v) T_{H,in} - T_{H,out,min} \geq 0 \quad (14)$$

The mass flow rate through the hot side of the HX is (Equation 15):

$$q_{m,H,HX} = x_v q_{m,H} \quad (15)$$

The x_v represents the openess ratio of the valve and is calculated as (Equation 16):

$$x_v = \frac{q_{m,H,HX}}{q_{m,H}} \quad (16)$$

- High temperature heat pump model (HTHP)

District heating heat pumps for 4th generation district heating systems must increase the temperature level of heat from temperatures of 10-15 °C up to 60-65 °C. This represents the high-temperature heat pump (HTHP) category. In this work the detailed modelling of HTHP will not be presented, since it is out of the scope, but simple model based on temperature difference is presented in Figure D 20.

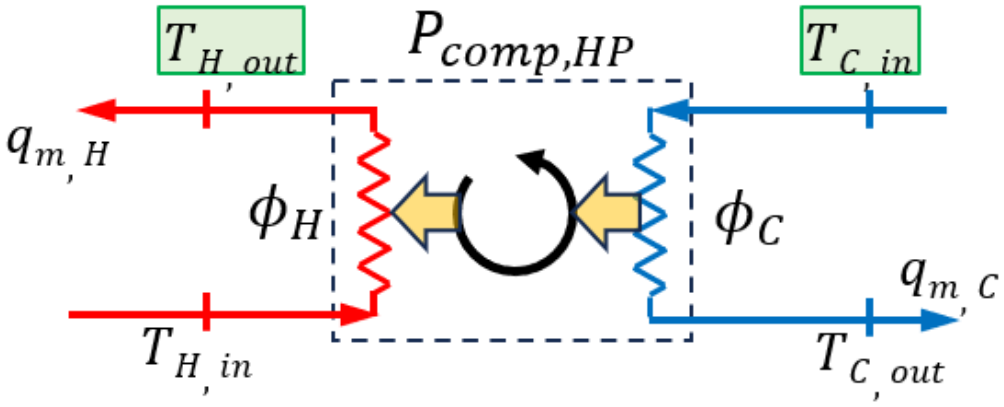

Figure D 20: Scheme of the heat pump as a reference to simple HP model.

The model is based on coefficient of performance (COP), which can be defined, according to Figure D 19, as (Equation 17):

$$COP_{HP} = \frac{\phi_H}{P_{comp}} = f(\Delta T_{HP}) \tag{17}$$

The heat pump temperature lift, ΔT_{HP}, can be calculated as difference between outlet of hot stream minus inlet of cold stream (Equation 18):

$$\Delta T_{HP} = T_{H,out} - T_{C,in} \tag{18}$$

The aim of the HTHP model is to maximize the heating rate ϕ_H with finding the optimal temperatures $T_{C,out}$ and $T_{H,out}$ which satisfy temperature constraints (Equation 19):

$$\begin{gathered} \max(\phi_H) \\ \phi_H = q_{m,H} c_w (T_{H,out} - T_{H,in}) \\ P_{comp,HP} = \frac{\phi_H}{COP_{HP}} \\ \phi_C = \phi_H - P_{comp,HP} \\ T_{C,out} = T_{C,in} - \frac{\phi_C}{q_{m,C} c_w} \end{gathered} \tag{19}$$

These temperature constraints are (Equation 20):

$$\begin{gathered} T_{H,out} \leq T_{H,out,max} \\ T_{C,out} \geq T_{C,out,min} \end{gathered} \tag{20}$$

The temperatures $T_{H,in}$ and $T_{C,in}$, as well as mass flow rates $q_{m,H}$ and $q_{m,C}$ need to be known in advance. An overview of HTHP's with corresponding functions $COP = f(\Delta T_{HP})$ is provided in Royo et al. (2021).

- Model of the borehole thermal energy storage (BTES) energy balance

In order to evaluate the possibility of a reservoir to store thermal energy, energy balance has to be done. Energy balance is based on energy conservation law (Equation 21):

$$\left(\frac{dE_R}{dt}\right)\Big|_{r\leq r_{set}} = \phi_R|_{r=r_{set}} - \phi_{BHE} \quad (21)$$

Where the temporal term dE_R/dt and the heat exchange with the BHE ϕ_{BHE} can be obtained from FeFlow simulations for the domain around then BHE satisfying the spatial condition $r \leq r_{set}$. If the temporal term is positive, heat is accumulated, and vice versa. The recovery heat power of the reservoir can be calculated (Equation 22):

$$\phi_R|_{r=r_{set}} = \left(\frac{dE_R}{dt}\right)\Big|_{r\leq r_{set}} + \phi_{BHE} \quad (22)$$

This parameter is important since it reflects the inflow or outflow of heat from the proximity of the BHE. It depends on temperature regime in the BHE, as well as thermal and hydraulic properties of the reservoir and groundwater movement. It reflects both conductive and convective term, and if the convective term is known, the conduction term can be calculated.

D.4.2. Model validation on reference site Savica

D.4.2.1. Site description and model setup

The setup of the BTES domain, as well as the setup of all parameters is briefly described here. Results are presenting the comparison between all cases in terms of geothermal heat and waste heat supply and circulation pump and heat pump power demand. All simulations have been performed with two-year time horizon and a maximum timeseries integration time step of three hours.

In this work two BHE configurations for Savica-1 well will be tested. According to insulated tubes that can be placed in a well casing, the two possibilities are tested: one that is inserted in a shallower, but wider well and can be placed up to 1800 m depth and another that is inserted in deeper, but narrower well and can be placed up to 2200 m depth. The main parameters of these two BHE options are listed in Table D 7.

Parameter	Unit	Values		Description
		BHE2200	BHE1800	
L_{well}	m	2200	1800	well depth

D_{well}	in	6,00	8,50	well diameter
	mm	152,40	215,90	
$D_{cas,OD}$	in	5,50	7,00	tubing OD
	mm	139,70	177,80	
δ_{cas}	in	0,24	0,50	tubing thickness
	mm	6,20	12,65	
$D_{cas,ID}$	in	5,01	6,00	tubing ID
	mm	127,30	152,50	
$D_{tub,OD}$	in	3,50	4,50	vacuum tube OD
	mm	88,90	114,30	
$D_{tub,ID}$	mm	50,60	76,00	vacuum tube ID
δ_{tub}	mm	19,15	19,15	vacuum tube thickness
A_{ann}	mm2	6518	8001	annulus area
A_{cen}	mm2	2010	4534	central tube area
w_{ann}	m/s	0,77	0,62	annulus area fluid velocity based on 5 kg/s
w_{cen}	m/s	2,49	1,10	central area fluid velocity based on 5 kg/s

Table D 7: Borehole heat exchanger parameters for 1800 and 2200 m depth.

Moreover, BTES will be compared to cases with no BTES reheating. Reheating is done from the second waste heat HX (see Figure D 15). So, for no-reheat the valve V-WH2 is fully closed at all times. The complete list of all cases is presented in Table D 8.

Case name	*Deep borehole heat exchanger*	*Waste heat source*	*BTES reheating*
BHE1800-Ind-RehY	BHE1800	Industrial	Yes
BHE2200-Ind-RehY	BHE2200	Industrial	Yes
BHE1800-Ind-RehN	BHE1800	Industrial	No
BHE2200-Ind-RehN	BHE2200	Industrial	No

Table D 8: Setup of Savica-1 well test cases.

- Setup of Savica-1 in FeFlow

The thermal conductivity of the casing is taken as 50 W/m/K, for the grout 2.3 W/m/K and for the vacuum insulated tubing 0.015 W/m/K (class D grade of insulation). Thermal rock properties were calculated using Jelić correlations for thermal conductivity, heat capacity and density for Sava subbasin (Jelić, 1987) and temperature from the geological report for Savica-1 to determine geothermal gradient and graphically presented in Figure D 21.

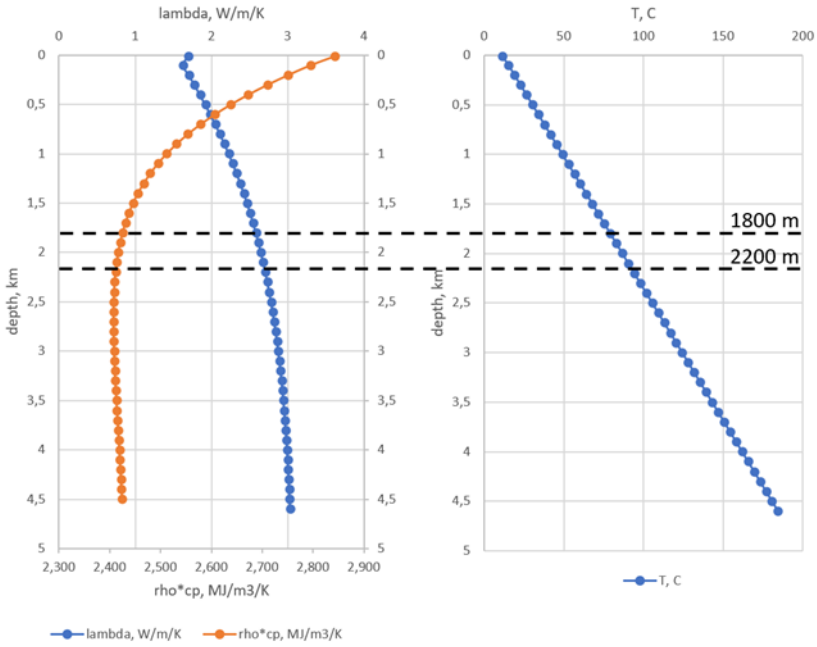

Figure D 21: Thermophysical rock properties at Savica-1 well based on Jelić correlations for Sava subbasin (Jelić, 1987) and geological report for Savica-1 well.

The boundary conditions of the Feflow domain are no-flow isothermal, where boundary temperature corresponds to the static temperature. The assumption is that reservoir is isothermal at the boundaries,

with bottom temperature equal to 160 °C, temperature at the top equal to 12 °C and lateral boundaries at linear distribution between the top and the bottom (Figure D 22). This results in thermal gradient of approx. 40 °C/km. The mesh is triangular in x-y plane and resolution is approximately 0.5 meters around the BHE and 10 m on the lateral boundary. Depth is set to 2500 m and layers are equidistant in z-direction. The domain is modelled as a dry rock, with porosity of 5% and zero hydraulic conductivity.

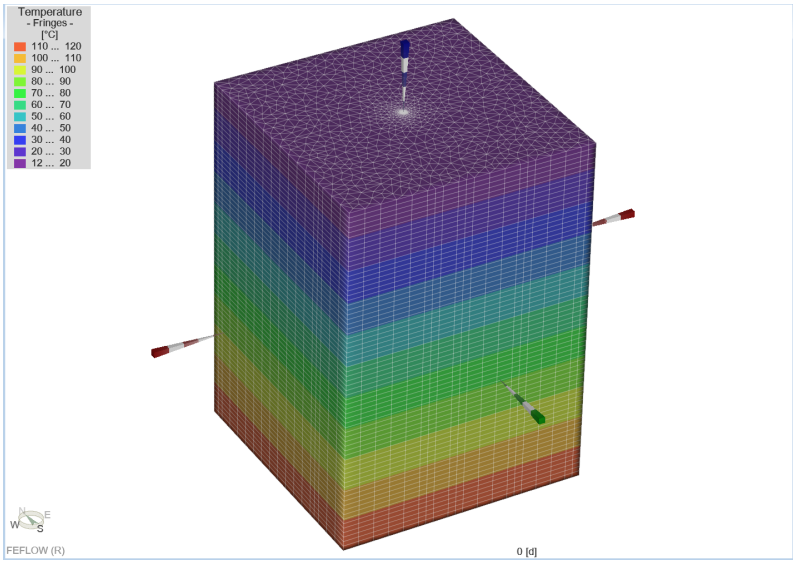

Figure D 22: FeFlow domain around Savica-1 well with isothermal boundary conditions.

- Setup of parameters in Python interface for modelling industrial waste heat and heat demand

The total heat demand of DH-1 is calculated as 2 GWh. The hourly distribution of thermal demand is calculated as (Equation 23):

$$\phi_{DH,t} = \delta_t \phi_{dem,tot} \tag{23}$$

where δ_t is a fraction of heat demand in time „t“ calculated as (Equation 24):

$$\delta_t = \frac{d_t}{\sum_{t=1}^{8760} d_t} \tag{24}$$

and $d_t = 0.627 - 0.0258 \times T_{amb,t}$. Therefore, hourly distribution of heat demand depends on hourly distribution of ambient temperature $T_{amb,t}$.

The LLT of the DH-1 depends also linearly on the ambient temperature (Equation 25):

$$LLT = 80 + \frac{65 - 80}{20 - 5}\left(T_{amb,t} - 5\right) \tag{25}$$

The values are cropped between $65 \leq LLT \leq 80$. The sliding parameter is mass flow rate of the waste heat hot water (Equation 26):

$$q_{m,WH,t} = \frac{\phi_{DH,t}}{(LLT - ELT)4200} \quad (26)$$

Industrial waste heat is modelled with a constant temperature of 80 °C. The timeseries of input setup variables for DH-1 for a single year are presented in Figure D 23.

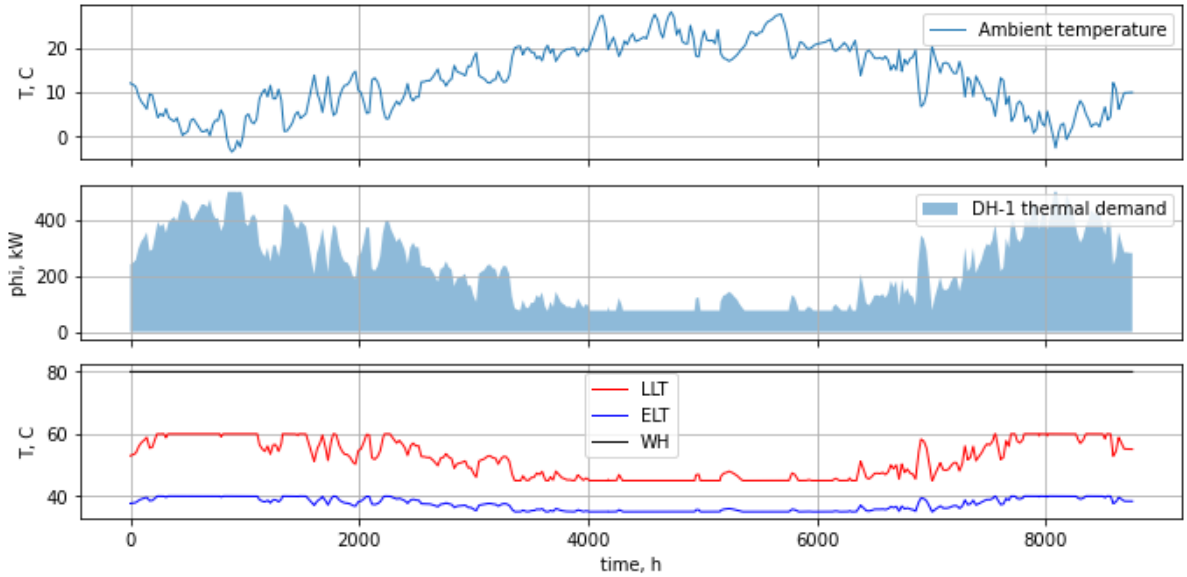

Figure D 23: Annual timeseries of input variables.

The peak thermal demand is around 500 kW during the winter season for heating and hot water demand and less than 100 kW during the summer season for hot water demand. For a muti-Year analysis the annual timeseries of input data are repeated.

D.4.2. Simulation results

- **Analysis of results: annual energy balance for all cases**

Annual energy results are presented in Figure D 24 for the second year of simulation. Results differ substantially between configurations and whether reservoir reheating was included into the system. Power balance, where power source from the import is positive and consumption breakdown is negative on the graph (a) shows big difference between power consumption between BHE1800 and BHE2200 configurations, which was expected due to hydraulic losses for longer BHE with smaller tubing diameter for case BHE2200. However, the power consumption for the electric heater was larger for BHE1800, while power consumption of the HTHP compressor was larger for BHE2200. Electricity consumption shows little difference between reheating and no reheating. DH balance (b) shows that DH supply is dominated by HTHP in all cases, while direct heat supply from the BHE is negligible for cases with no reheating. Second largest heat supplier is waste heat WH-1, while electric heating generally has minor influence on heat supply. The total annual heat demand equals the predefined value of 2GWh. BHE balance (c) shows that the reservoir is the main supplier of heat towards the BHE, while for the reheating cases this is additionally increased by waste heat WH-2 stored in the BTES. Withdrawal of heat from the BHE is dominantly used for the HTHP, while for reheating there is also a smaller portion used for direct heating for domestic hot-water supply, which occurs also outside the heating season. WH balance (d) shows that the lowest waste heat supply is for the case of

BHE2200 with no reheating and that using waste heat for reheating the BTES, WH-2, is similar for both BHE configurations.

	BHE1800-Ind-RehY	BHE2200-Ind-RehY	BHE1800-Ind-RehN	BHE2200-Ind-RehN
E_EH	0,060	0,007	0,065	0,008
E_pump	0,026	0,166	0,026	0,166
E_HTHP	0,180	0,242	0,222	0,275
demand	0,266	0,414	0,313	0,449

	BHE1800-Ind-RehY	BHE2200-Ind-RehY	BHE1800-Ind-RehN	BHE2200-Ind-RehN
E_DH_EH	0,060	0,007	0,065	0,008
E_DH_WH1	0,675	0,367	0,707	0,382
E_DH_BHE	0,276	0,310	0,000	0,086
E_DH_HTHP	0,990	1,322	1,238	1,536
demand	2,0	2,0	2,0	2,0

	BHE1800-Ind-RehY	BHE2200-Ind-RehY	BHE1800-Ind-RehN	BHE2200-Ind-RehN
E_WH2_BHE	0,520	0,472	0,000	0,000
E_R_BHE	0,566	0,918	1,015	1,347
E_BHE_HTHP	-0,810	-1,081	-1,016	-1,261
E_BHE_DH	-0,276	-0,310	0,000	-0,086

	BHE1800-Ind-RehY	BHE2200-Ind-RehY	BHE1800-Ind-RehN	BHE2200-Ind-RehN
E_WH2	0,520	0,472	0,000	0,000
E_WH1	0,675	0,367	0,707	0,382
WH supply	13,8%	15,4%	0,0%	4,3%

Figure D 24: Annual energy results for all cases.

The annual results of energy flows show that majority of heat is supplied from the BHE, around 60 % for BHE1800 and 80 % for BHE2200 cases. However, electricity demand and ratio between BHE direct supply and BHE-HTHP supply are different if reheating of the BTES (dry rock) is used, which is presented in Figure D-25.

The electricity demand is reduced by 15 % for the BHE1800 cases and by 8 % for the BHE2200 cases if reheating is used. This reduction comes from the increased ratio of direct-to-HTHP supply from the BHE, where percentage of direct heating increases from 0 to 15 % for the case 1800BHE and from 4 to 15 % for the case BHE2200. At the same time the HTHP heating will be reduced from 61 to 50 % for the case BHE1800 and from 76 to 66 % for the case BHE2200.

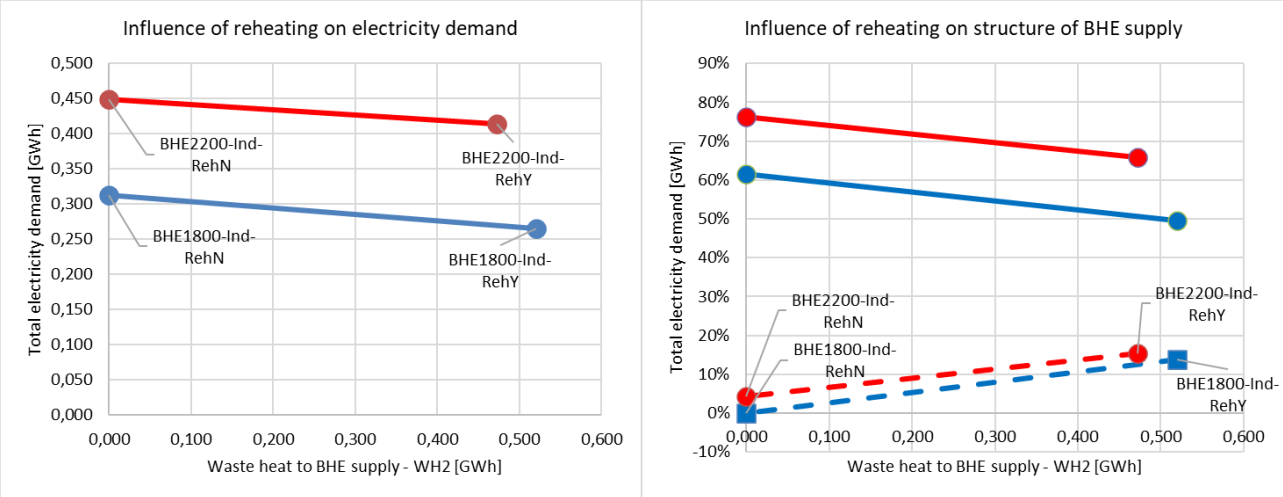

Figure D 25: Influence of reheating of the BTES on electricity demand and structure of the BHE supply.

- Analysis of results: estimation of BTES performance and system efficiencies

In order to see the dynamics of BTES, the timeseries of BTES energy is presented in Figure 26. The energy is estimated from Equation 24 as integral of the derivation of reservoir energy within a certain radius from the BHE. Reservoir energy is obtained from the FeFlow internal IFM functions (Equation 27):

$$E_{BTES} = \int_{t=0}^{8760h} \left(\frac{dE_R}{dt}\right)\Big|_{r \le r_{set}} \quad (27)$$

In this work a radius of r_{set} = 4 m around the BHE is considered as a BTES volume. Results show that without reheating BTES can regenerate naturally from the surrounding geothermal heat. Without reheating energy recovery starts at - 100 MWh and ends at + 100 MWh for BHE1800 and at +180 MWh for BHE2200 meaning that natural regeneration can add approximately 200 and 280 MWh, respectively. If reheating (WH-2) is included, then additional 250 MWh for BHE1800 and 220 MWh for BHE2200 can be added to the BTES. For a 400 kW demand this corresponds to approx. 625 and 550 additional hours of heating, respectively. That is under the condition that this heat can be extracted.

The efficiency comparison will be done according to the parameters COP_{HTHP} and COP_{tot}. They are defined according to the Equation 28 & Equation 29:

$$COP_{HTHP} = \frac{\phi_{DH,HTHP}}{P_{HTHP,komp}} \quad (28)$$

$$COP_{tot} = \frac{\phi_{DH}}{P_{HTHP,komp} + P_{BHE,pump} + P_{EH}} \quad (29)$$

which define internal HTHP efficiency and overall efficiency of the heating system. Efficiency results are presented in Figure D 271D 26.

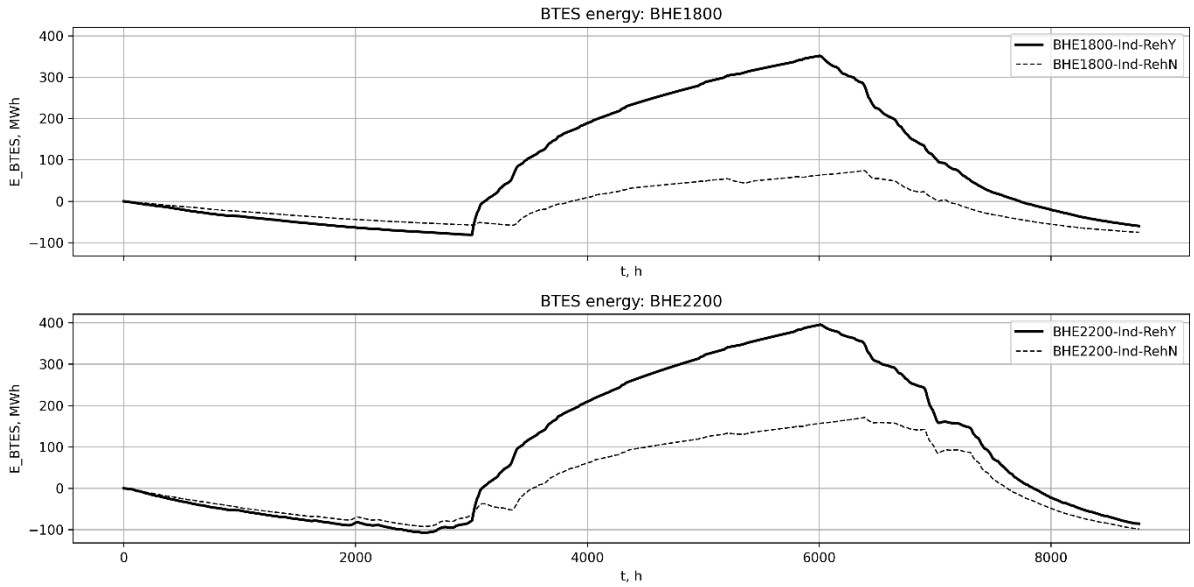

Figure D 26: Timeseries of BTES energy for the two BHE configurations (BHE1800 and BHE2200) with (RehY) and without (RehN) reheating.

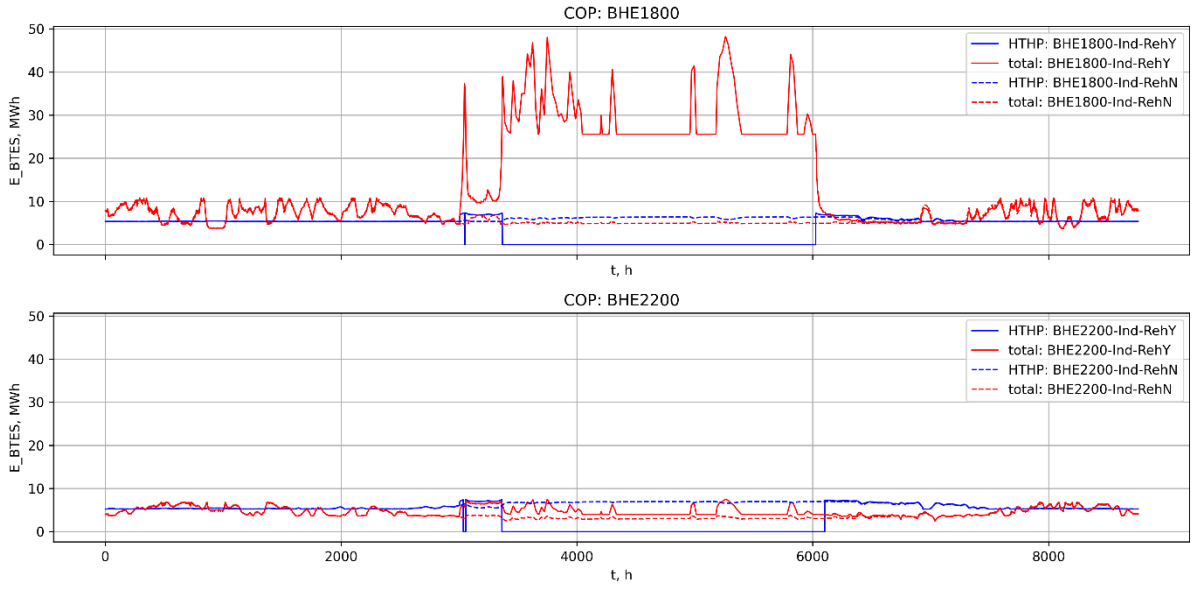

Figure D 271: Comparison between system efficiencies for all cases.

For the BHE1800 values of total COP are slightly higher than for the BHE 2200. On the other hand, HTHP COP is around 7 for all cases, since it depends only on temperature difference, as described in the method chapter.

- **Analysis of results: detailed timeseries results for the 1800 m deep BHE with reheating (case BHE1800-Ind-RehY)**

To illustrate the dynamics of the energy flows, the detailed timeseries for the second year of simulation is presented in the Figure D 27.

The analysis shows that direct heating from BHE is dominant when heat demand is low. This is during the summer for covering the hot water demand. Direct heating will be applied only when EST is above 5 °C difference from the LLT. Valve openness (*x*) also shows that reheating valve WH-2 is open during the summer period, while for winter heating season WH-1 covers the heat demand above baseload BHE supply. Electric heaters are supplying only peak thermal demand. Electricity demand is largest for HP. For this configuration the HP (or multiple HP's) should have thermal output power of at least 180 kW-th, while electric heaters should have at least 100 kW-el.

D.5. Requirements to reuse hydrocarbon wells for Borehole Thermal Energy Storage

A total of four configurations have been tested with difference in length and diameter of the casing and whether reheating is included or not. All four tested cases showed different annual energy flows, indicating the need for a-priori testing presented in this report.

Main conclusions are that longer tubing leads to higher hydraulic losses and higher power consumption, but reduces the need for the waste heat, which is favourable if waste heat comes at high cost. Also, longer tubing can reach reservoir depths with higher temperatures which can result in higher amount of direct heating in the overall heating. The influence of BTES is seen at the higher heat supply from the waste heat for reheating and higher supply of direct heating from the geothermal for district heating supply.

The well reservoir properties that define a well/reservoir as suitable for BTES are the same as for deep borehole heat exchangers (DBHE). We therefore refer to section C for a description of these parameters.

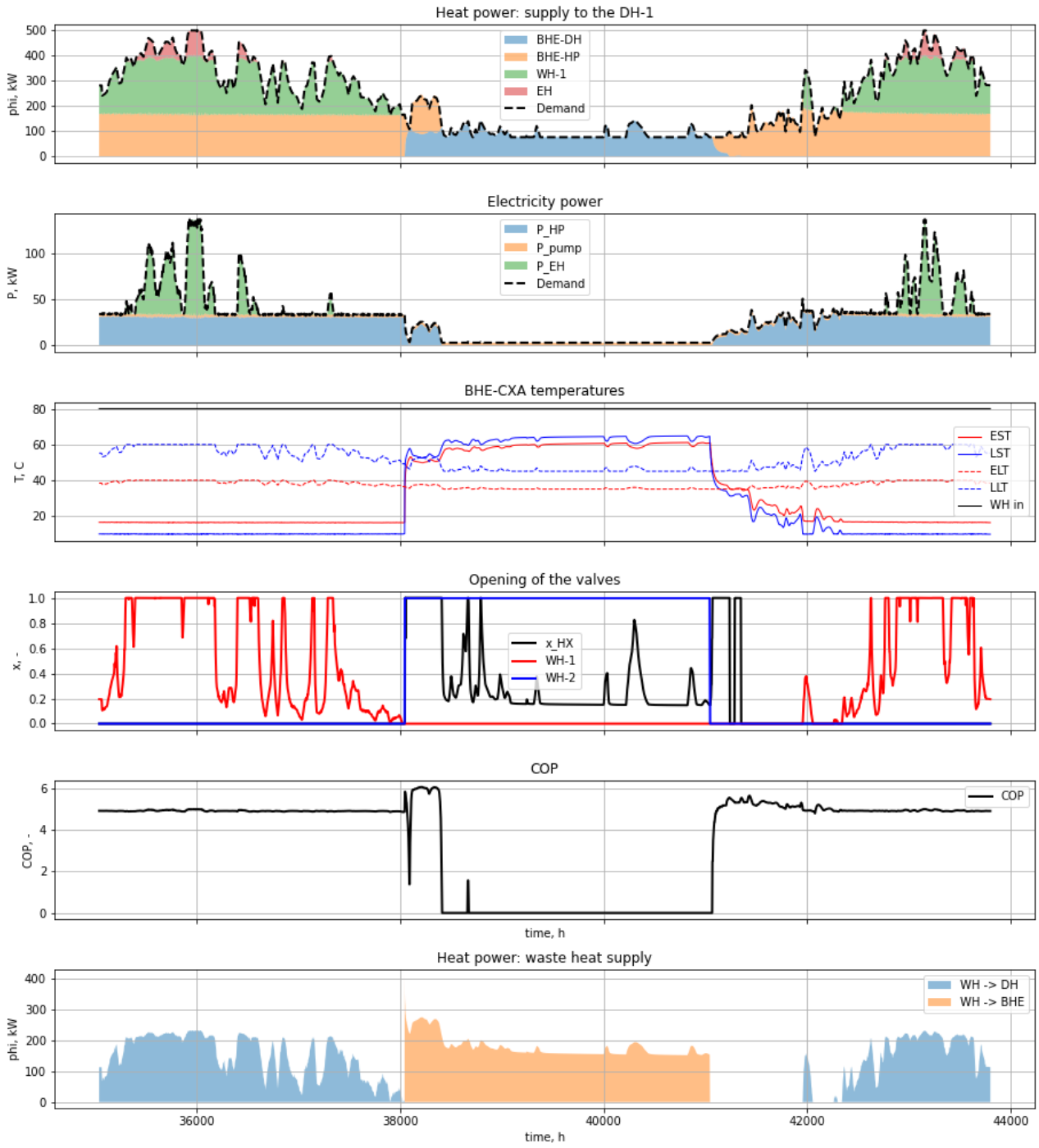

Figure D 27: Detailed timeseries analysis for the second simulation year for the 1800 m deep BHE with reheating (case BHE1800-Ind-RehY). Legend: BHE-DH – borehole heat exchanger-district heating; BHE – borehole heat exchanger; BHE-HP – borehole heat exchanger-heat pump; WH-1 – waste heat-1; WH-2 – waste heat-2; EH – electric heater; EST – entering source temperature; LST – leaving source temperature; ELT – entering load temperature; LLT – leaving load temperature; WH in – waste heat in; WH – waste heat; DH – district heating; x – valve openness; x_HX – heat exchanger valve openness; COP – coefficient of performance.

D.6. Workflow to reuse hydrocarbon wells for Borehole Thermal Energy Storage

Liquidated wells that could be chosen for BTES/DBHE applications are usually old wells in which several cement plugs are set at several different depths, to prevent the breakthrough of formation fluid and communication with the surface or existing aquifers. Also, the casing is cut off at minimally 3 m below the ground surface to ensure the return of the preexisting environment. Temporarily abandoned wells are wells that no longer fulfil their purpose (e.g. extraction of reservoir fluid) but are still not cemented or cut off at the surface. In the case of a mature oilfield wells with high water cut, these wells usually are classified as monitoring wells.

Therefore, temporarily abandoned wells are potentially better candidates for revitalization, unlike liquidated wells. To describe a workflow to reuse such wells as BTES, the conversion of temporarily abandoned oil and gas wells is almost identical to deep BHE process and consists of several steps. After selecting the well, it is necessary to determine its construction parameters, primarily the diameters and casing installation depths, as well as check for potential retained drilling equipment. Workover is then carried out on the selected well which includes lowering working tubing into the well, which circulates the fluid, installs plugs, and cleans casing pipes. After cleaning process, a packer is installed at the bottom to close the well and isolate it from possible inflow of fluid from the reservoir rock and outflow of the working fluid from the well. After that, it is necessary to remove any remaining fluid, clean the casing from possible impurities (e.g. scale, etc.) and check the mechanical and hydraulic integrity of the well channel. The installation of the tubing finishes the installation of the deep BHE (DBHE) for BTES. The installed tubing, although closed at the bottom, is perforated which enables closed circulation within the DBHE. The choice of the way in which the individual installation of the deep BHE will be carried out depends on the individual well and its structural characteristics. If the hydraulic calculation shows that the flow surface is adequate (e.g. at smaller depths), it is possible to use a circulation tool instead of installing tubing closed at the bottom.

The casing columns represent the outer pipe, while the tubing represents the inner pipe of the deep borehole heat exchanger. The most common application in the oil industry for flexible tubing is as a working string, which is used to perform maintenance work on wells (e.g. flushing, drilling, etc.), and it is also used as a production, ascending column. It is available on the market up to a maximum of 0.127 m (5") outer diameter. For projects of relatively shallow oil and gas wells, up to approximately 2000 m, the use of such an ascending column is optimal from the point of view of optimal pressure drop and necessary flow, but for projects of greater depth (>2000 m) it is necessary to consider the use of classic threaded columns up to 0.152 m (6 ") whose inner diameter is different than that of flexible tubing. The reason for considering this kind of application is the fact that during fluid circulation in the coaxial system, most of the pressure drop is related to the inner tube. In order to minimize the pressure drop, thus saving electricity for the circulation pump and investment costs, it is necessary to make an analysis of the unit pressure drop for different combinations of the diameter of the inner pipe and the outer pipe. In general, the characteristics of wells, that is, their constructional features, can usually be found in well logs or final drilling reports. Additionally, to minimize the heat transfer between circulating fluid in the annular and tubing, it is assumed that additional inner pipe is installed with slightly larger diameter than the first tubing in order to achieve insulation with vacuum pump. Other option is to install vacuum insulated tubing (VIT) which can have thermal conductivity as low as 0,01 W/m°C, while achieving 0,1 W/m°C is considered as good insulation.

D.7. References

Andersson, O., N. Håkansson, and L. Rydell. (2021). Heat pumps rescued Xylem's heat storage facility in Emmaboda, Sweden. The REHVA European HVAC Journal 58 (4):23–7.

Andersson, S., Johansson, A., Nordell, B., Åbyhammar, T. (1983). A Borehole heat store in rock: pilot trials in Luleå and preliminary design of a full-scale installation. Swedish Council for Building Research, Stockholm, Sweden.

Brown, C. S., Kolo, I., Falcone, G., & Banks, D. (2023). Repurposing a deep geothermal exploration well for borehole thermal energy storage: Implications from statistical modelling and sensitivity analysis. *Applied Thermal Engineering*, *220*, 119701.

Catolico, N., Ge, S. & McCartney, J.S., (2016). Numerical modeling of a soil-borehole thermal energy storage system. Vadose Zone Journal, 15(1), pp.1-17.

Diersch, H. J. G. (2013). *FEFLOW: finite element modeling of flow, mass and heat transport in porous and fractured media*. Springer Science & Business Media.

FeFlow 8.0 Documentation. www.feflow.info/html/help80/feflow/01_Introduction/intro.htm (accessed 30 March 2024)

Fu, H., Yu, M., Liu, J., Cui, P., Zhang, W., Mao, Y., & Zhuang, Z. (2024). Influence of heat storage on performance of multi-borehole mid-deep borehole heat exchangers. *Journal of Energy Storage*, *90*, 111718.

Gehlin, S. (2016). Borehole thermal energy storage. In Advances in Ground-Source Heat Pump Systems (pp. 295–327), Elsevier. https://doi.org/10.1016/b978-0-08-100311-4.00011-x

Heidemann, W., Nußbicker, J., Mangold, D., & Müller-Steinhagen, H. (2003). Solar Assisted District Heating System with Duct Heat Store in Neckarsulm-Amorbach (Germany). In ISES Solar World Congress.

Hellström, G. (1991). Ground heat storage: thermal analyses of duct storage systems, Lund: University of Lund, Department of Mathematical Physics.

IFM FEFLOW Model Class, dhi.github.io/ifm/api_doc.html (accessed 30 March 2024).

Jelić, K. (1987): Stacionarna geotermijska energija u Savskoj i Dravskoj potolini Panonskog bazena SR Hrvatske. Nafta.

Kallesøe, A.J. & Vangkilde-Pedersen, T. (eds). 2019: Underground Thermal Energy Storage (UTES) – state-of-the-art, example cases and lessons learned. HEATSTORE project report, GEOTHERMICA – ERA NET Cofund Geothermal. 130 pp + appendices.

Krusemark, M., Seib, L., Bossennec, C., Wang, F., Schubert, G., Wasmer, G. and Sass, I., 2024. Chemical analysis and data logging of groundwater quality from three monitoring wells at the SKEWS Site, Campus Lichtwiese of TU Darmstadt.

Lund, H., Østergaard, P. A., Nielsen, T. B., Werner, S., Thorsen, J. E., Gudmundsson, O., ... & Mathiesen, B. V. (2021). Perspectives on fourth and fifth generation district heating. *Energy*, *227*, 120520.

Ma, J., Wang, H., Li, Y., Ren, J., Sun, H., Du, S., & Wen, H. (2024). Heating and storage of medium-deep borehole heat exchangers: Analysis of operational characteristics via an optimized analytical solution model. *Journal of Energy Storage*, *90*, 111760.

Malmberg, M. (2017). Transient modeling of a high temperature borehole thermal energy storage coupled with a combined heat and power plant. KTH Industrial Engineering and Management. Master thesis.

Mateu-Royo, C., Arpagaus, C., Mota-Babiloni, A., Navarro-Esbrí, J., & Bertsch, S. S. (2021). Advanced high temperature heat pump configurations using low GWP refrigerants for industrial waste heat recovery: A comprehensive study. *Energy conversion and management*, *229*, 113752.

Nordell, B. (1994). Borehole heat store design optimization, Luleå: Luleå University of Technology.

Nordell, B., Andersson, O., & Scorpo, A. L. (2015). Long-term Performance of the HT-BTES in Emmaboda, Sweden – Operation and Experiences. Luleå: Luleå University of Technology.

Nußbicker-Lux, J., Bauer, D., Marx, R., Heidemann, W. & Müller-Steinhagen, H. (2009). Monitoring results from German central solar heating plants with seasonal thermal energy storage. EFFSTOCK 2009, Stockholm, Sweden, June 14-17.

Ramstad, R.K., Justo Alonso, M., Acuña, J., Andersson, O., Stokuca, M., Håkansson, N., Midttømme, K. & Rydell, L., 2023. The borehole thermal energy storage at Emmaboda, Sweden: First distributed temperature measurements. Science and Technology for the Built Environment, 29(2), pp.146-162.

Reuss, M. (2015). The use of borehole thermal energy storage (BTES) systems. In Advances in Thermal Energy Storage Systems: Methods and Applications (pp. 117–147). Elsevier Inc. https://doi.org/10.1533/9781782420965.1.117

Pilgrim, M. & Willison, S., 2009. Dive Into Python 3, Springer.

Sass, I., Krusemark, M., Seib, L., Bossennec, C., Pham, T. H., Schedel, M., ... & Homuth, B. (2015). Medium-Deep Borehole Thermal Energy Storage (MD-BTES): from Exploration to District-Heating Grid Connection, Insights from SKEWS and PUSH-IT Projects.

Seib, L., Frey, M., Bossennec, C., Krusemark, M., Burschil, T., Buness, H., Weydt, L. & Sass, I. (2024). Assessment of a medium-deep borehole thermal energy storage site in the crystalline basement: A case study of the demo site Lichtwiese Campus, Darmstadt. *Geothermics*, *119*, 102933.

Sibbitt B. & McClenahan D. Seasonal Borehole Thermal Energy Storage – Guidelines for design & construction, IEA-Solar Heating & Cooling TECH SHEET 45.B.3.1, page 1-15.

Welsch, B., Rühaak, W., Schulte, D. O., Bär, K., & Sass, I. (2016). Characteristics of medium deep borehole thermal energy storage. International journal of energy research, 40(13), 1855-1868.

E. Hydrothermal Energy Production (HE)

E.1. Authors

Dr. Ferenc Fedor	University of Pécs	Hungary
Catarina C. Castro	University of Pécs	Hungary
Dr. János Szanyi	University of Szeged	Hungary
Dr. János Kovács	University of Pécs	Hungary
Dr. Hannes Hofmann	GFZ Potsdam	Germany

E.2. Hydrothermal Energy Production

E.2.1. Description of technology

In hydrothermal energy systems a geothermal fluid (hot water/brine, steam or both), which is stored in a permeable and often porous geothermal reservoir and which carries the heat, is produced through wells. These wells are open in the reservoir section. Thus, we refer to hydrothermal energy as open systems. The produced hot water is usually reinjected into the same formation for pressure maintenance reasons through injection wells. A typical hydrothermal system in central Europe produced hot water from a porous and permeable sedimentary or carbonate aquifer. After heat extraction at the surface the hot water is then re-injected into the same reservoir for pressure maintenance and fluid disposal reasons. With one production and one injection well such a system is called well doublet (Figure E 1), which has a typical well spacing at the surface of only a couple of meters to couple of hundred meters (to minimize cost, space requirements and heat losses on the surface) and at the bottom of the well of often more than 1 km (to avoid thermal breakthrough of the cold injected water at the hot production well).

Depending on the enthalpy/temperature we can distinguish between low enthalpy (low-medium temperature) systems and high enthalpy (high-temperature) systems. Depending on the water phase we distinguish between liquid-dominated, two-phase and vapour-dominated hydrothermal systems. In Central Europe, and especially in the context of well reuse we typically have liquid-dominated low enthalpy systems (Table E 1).

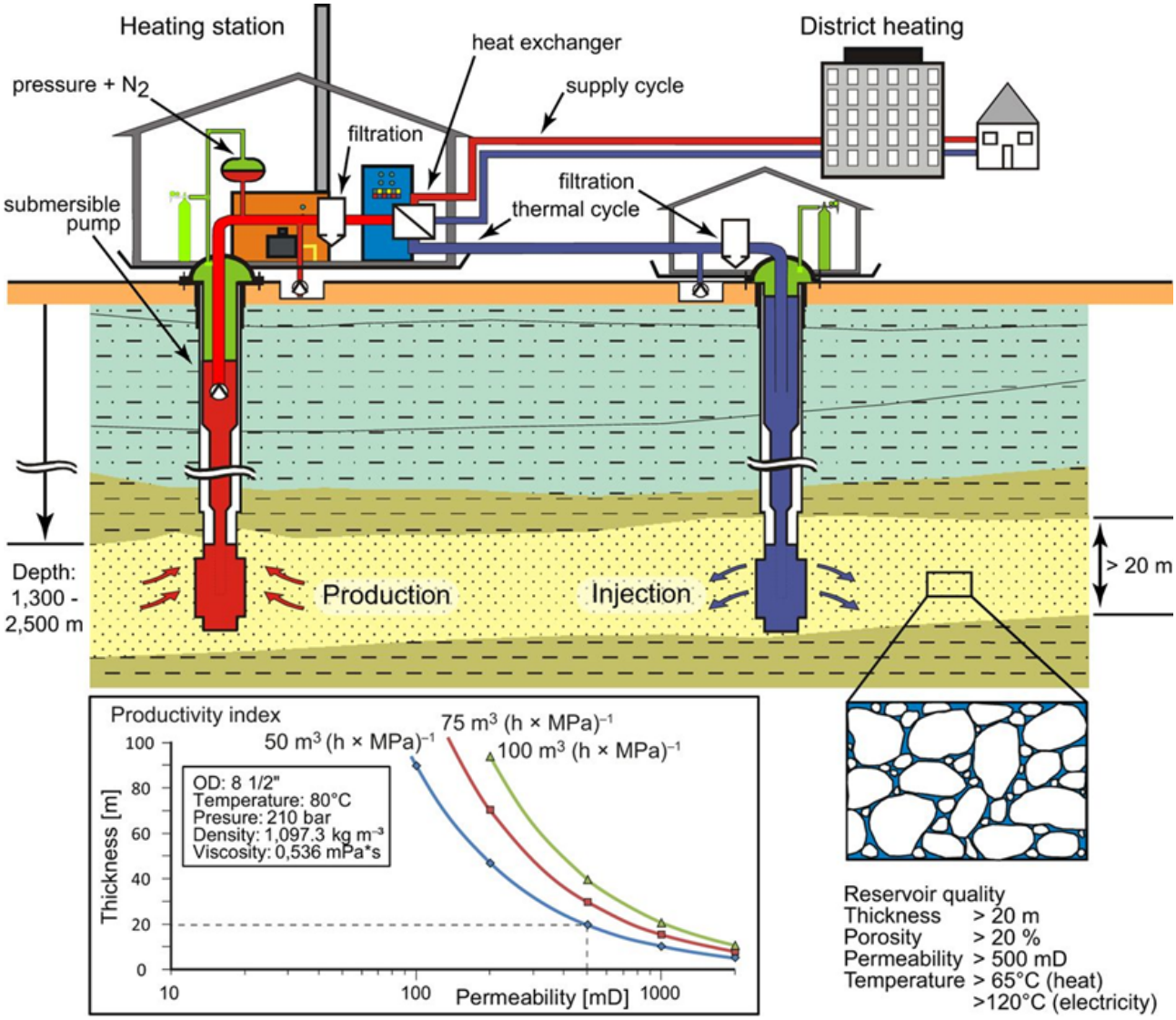

Figure E 1: Typical utilization of a low-enthalpy liquid-dominated hydrothermal energy system in Central Europe. Hot water is produced by at least one production well and the cold water is re-injected by at least one injection well. The main requirement for a hydrothermal system is a sufficiently thick porous and permeable reservoir (productivity index) with the temperature required for a specific application (Franz et al., 2018).

Low-temperature (LT) systems with reservoir temperature at 1 km depth below 150°C. Often characterised by hot or boiling springs.	***Low-enthalpy*** geothermal systems with reservoir fluid enthalpy less than 800 kJ/kg, corresponding to temperatures less than about 190°C.	***Liquid-dominated*** geothermal reservoirs with the water temperature at, or below, the boiling point at the prevailing pressure and the water phase controls the pressure in the reservoir. Some steam may be present.
Medium-temperature (MT) systems.		
High-temperature (HT) systems with reservoir temperature at 1 km depth above 200°C. Characterised by fumaroles, steam vents, mud pools and highly altered ground.	***High-enthalpy*** geothermal systems with reservoir fluid enthalpy greater than 800 kJ/kg.	***Two-phase*** geothermal reservoirs where steam and water co-exist and the temperature and pressure follow the boiling point curve.
		Vapour-dominated geothermal where temperature is at, or above, the boiling point at the prevailing pressure and the steam phase controls the pressure in the reservoir. Some liquid water may be present.

Table E 1: Classifications of geothermal systems on the basis of temperature, enthalpy, and physical state (Bödvarsson, 1964; Axelsson and Gunnlaugsson, 2000).

E.2.2. Hydrothermal heat and power production

Geothermal projects follow a carefully crafted exploration and development program and by testing the potential outputs of the related well, the kind of utilization suitable for the well can be determined. According to Nardini (2022) high-temperature resources (>200°C) are suitable for dry steam or flash geothermal power plants. Medium temperature resources (<200°C) are suitable for binary power plants. Low-temperature geothermal resources (<150°C) are suitable for direct uses (recreation, heating and drying). Generally, geothermal energy utilization is commonly divided into two categories: electric energy generation and direct uses (Table E 2).

RESERVOIR TEMPERATURE	FLUID TYPE	APPLICATION	TECHNOLOGY
HIGH -T >150°C	water, vapour	electricity generation	▪ DRY STEAM TURBINE ▪ SINGLE/DOUBLE/TRIPLE FLASH
		direct heat use	❖ HEAT EXCHANGER
MEDIUM-T 90-150°C	water	electricity generation	▪ BINARY CYCLE
		direct heat use	❖ HEAT EXCHANGER ❖ GEOTHERMAL HEAT PUMP
LOW-T <90°C	water	direct heat use	❖ HEAT EXCHANGER ❖ GEOTHERMAL HEAT PUMP ❖ DIRECT HEAT USE

Table E 2: Simplified scheme of geothermal resources, application, and technology (Nardini, 2022).

E.2.2.1. Electricity generation

There are three main types of geothermal power plant technologies: dry steam, flash steam, and binary cycle (Figure E 2). The type of conversion is part of the power plant design and generally depends on the state of the subsurface fluid (steam or water) and its temperature. Direct dry steam, flash cycles, binary cycles, and hybrid cycles that are coupled with a Rankine cycle or combined with various heat sources, such as concentrated solar power, are the four major energy conversion mechanisms used to generate geothermal power (Moya et al., 2021). Back-pressure type energy production is an additional basic method used in dry steam geothermal energy systems, generally providing temporary power generation. Figure E 3 shows the percentage of energy produced based on the classification of prevailing power plants (Colpan et al., 2021).

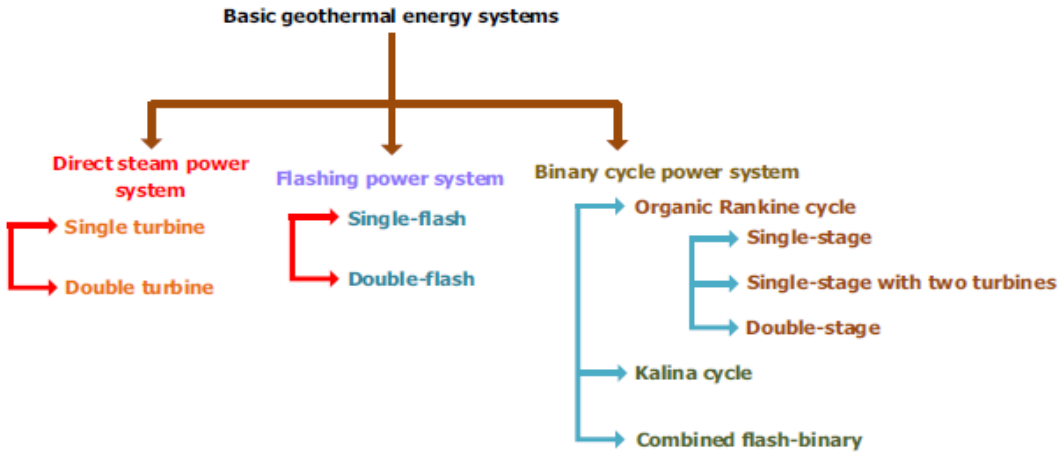

Figure E 2: Schematic diagram of geothermal conversion technologies (Dincer and Ozturk, 2021).

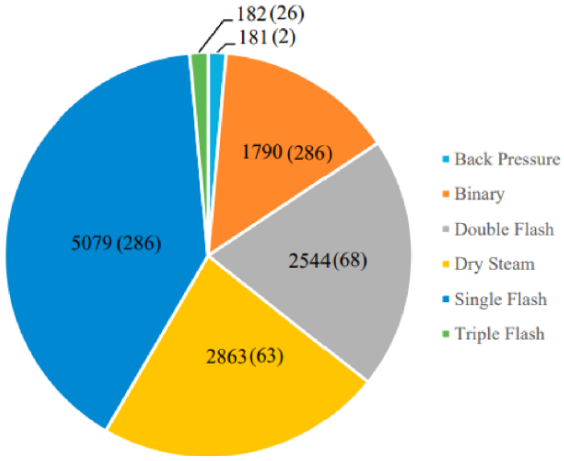

Figure E 3: Share of different geothermal conversion technologies for electricity production (Colpan et al., 2021, modified by Sharmin et al., 2023).

Dry steam power plants

Dry steam power plants are used at high temperature (>200°C) vapor-dominated (or dry-steam) reservoirs. These types of reservoirs are rare. Major fields are located in Larderello, Italy, and the Geysers in California, USA (Bayer et al., 2013).

These plants draw from underground resources of steam, in which the conversion device is a steam turbine designed to use the low-pressure, high-volume fluid produced in the steam field. The steam is piped directly from underground wells to the power plant, where it is directed into a turbine/generator unit. Dry steam plants commonly use condensing turbines. The condensate is re-injected (closed cycle) or evaporated in wet cooling towers (Nardini, 2022). Dry steam plants range in size from 8 MWe to 140 MWe (S&P Global Platts, 2016).

The first instance of geothermal electric power generation using dry steam systems occurred in Larderello, Italy, with an experimental plant developed in 1904 and commercial operations beginning in 1913. The geothermal field at Larderello is one of the few that produces superheated steam, created by significant heat transfer from rocks to the fluid. This small Tuscan village became the epicenter of industrial geothermal energy development, both for electricity generation and various non-electrical uses. Over the years, the dry steam power plant in Larderello expanded and now consists of 34 plants. The site's total capacity is now 800 MWe, contributing to Italy's status as the sixth-largest producer of geothermal energy globally, with geothermal power making up nearly 2% of the country's energy mix.

Back-pressure-type energy production is another method utilised in dry steam geothermal energy systems. While these systems are cost-effective, they have lower thermal efficiency compared to traditional condensing systems. Back-pressure systems are primarily used for temporary power generation and are often integrated into setups that provide both electricity and heating. Unlike conventional systems, back-pressure geothermal power generation does not include condensers or cooling mechanisms. In these systems, steam is released at atmospheric pressure, and the fluid remains uncondensed. The cost of back-pressure geothermal power production is lower, but the power output is less efficient than in condensing systems. Despite their lower efficiency, back-pressure systems hold potential for various applications (Dincer and Ozturk, 2021).

Steam technology remains effective and is currently used at The Geysers in California, the world's largest single source of geothermal power (IEA, 2022). Dry steam plants account for approximately 23% of global geothermal capacity, with 63 plants collectively producing 2863 MWe. Among all geothermal power plants, dry steam plants are the most cost-effective and efficient (Sharmin et al., 2023).

Flash steam power plants

Flash steam plants are the most common type of geothermal electricity plant in operation today. They are similar to dry steam plants; however, the steam is obtained from a separation process called flashing. The technology uses water from high-heat, overpressurised geothermal reservoirs. As it flows upwards, the pressure decreases and some of the hot water boils into steam. The steam is then separated from the water and directed to the turbines. The fluid fraction exiting the separators, as well as the steam condensate (except for condensate evaporated in a wet cooling system), is usually re-injected. The temperature of the fluid drops if the pressure is lowered, so flash power plants work best with well temperatures greater than 182 °C. Flash plants vary in size depending on whether they are single- (0.2–80 MWe), double- (2–110 MWe), or triple-flash (60–150 MWe) plants (S&P Global Platts, 2016).

The Coso Geothermal Power Plant in California is an active producer of geothermal electrical power in the United States. Hot geothermal fluid (brine) travels up wells, some as deep as 3.350 m, and flashes into steam that drives turbines which in turn drive electrical power generators. Brine that does not flash into steam, along with condensed steam from the turbines, is collected and injected back into the geothermal

reservoir through injection wells. The project has produced as much as 270 MWe, enough power to supply 250.000 homes (COSO Energy, 2024).

The single-flash steam GPSs form the basis in geothermal energy systems. The fluid used in geothermal energy systems is supplied from the underground. This fluid is available as a mixture of steam and liquid. The most basic energy system that can produce electricity by making use of this mixture is the single-flash steam geothermal energy system.

The double-flash steam GPS can be defined as one that occurs when the single-flash is upgraded in terms of performance. Looking at the double-flash system, the difference that can be seen directly from the single-flash steam geothermal system is that the working fluid enters the flashing process twice. In this way, considering geothermal fluid with the same amount and temperature, more power can be obtained from this system compared to a single-flash system.

Binary-cycle power plants

Binary-cycle geothermal power plants can use lower-temperature geothermal resources, making them an important technology for deploying geothermal electricity production in more locations. Binary-cycle geothermal power plants differ from dry steam and flash steam systems in that the geothermal reservoir fluids never enter the power plant's turbine units. Low-temperature (below 180°C) geothermal fluids pass through a heat exchanger with a secondary, or "binary," fluid. This binary fluid has a much lower boiling point than water, and the modest heat from the geothermal fluid causes it to flash to vapor, which then drives the turbines, spins the generators, and creates electricity. Two types and variants are used in practice: the Organic Rankine cycle (ORC) and the Kalina cycle (KC).

Organic Rankine Cycle power plants

The Organic Rankine Cycle (ORC) is a closed thermodynamic cycle that uses high molecular weight organic liquids with a lower evaporation temperature than water to take thermal energy from lower temperature heat sources (biomass, geothermal, solar and waste heat) and convert it into electricity.

The principle of ORC technology was first established by T. Howard in 1826 (Tartière and Astolfi, 2017) when he experimented with building an engine using "alcohol" or "ether" as the working fluid in a power cycle. The first geothermal binary ORC power plant was installed in 1967 on the Kamchatka Peninsula in the Soviet Union, providing the first practical evidence of the efficiency of power generation by binary cycle plants using low-boiling organic compounds (Tomarov et al., 2015). Today, ORC systems are the most prevalent, accounting for 43% of total installations and representing 21.7% of the total installed capacity worldwide with an average capacity factor of nearly 65% (Gutiérrez-Negrín, 2024).

Numerous studies have examined the performance of ORC power plants in oil fields, utilizing both abandoned wells and co-produced water (Yang et al., 2017). There are three implemented examples globally of using this technology to generate electricity from medium-temperature co-produced water at oil fields (Wang et al., 2018). In the United States, two projects demonstrate this application: the first in the Wyoming oil field, where an ORC power plant generates 180 kWe from co-produced water with temperatures of 90.6-98.9°C and a flow rate of ~55 L/s (Nordquist & Johnson, 2012). The second is the first commercial project in North Dakota, which uses water at 98°C and a flow rate of ~40 L/s to generate 250 kW of net power (Gosnold et al., 2019). Another project in the Huabei oil field of China generates 310 kW of net power from geothermal water at 110°C with a flow rate of ~25 L/s (Xin et al., 2012).

Kalina Cycle power plants

The Kalina cycle (KC) is an innovative thermodynamic cycle that can be utilized for the conversion of thermal energy from a comparatively low heat source temperature to mechanical power. Introduced by Aleksandr

Kalina in 1984, this power cycle can be an attractive alternative to a simple Rankine cycle in power plants. KC plants use a water-ammonia mixture, where the ammonia concentration changes throughout the cycle. During the boiling phase, the ammonia begins to vaporize first leaving a low-concentration mixture, which increases its boiling temperature. This results in reducing the temperature difference between the exhaust gases and the bottoming cycle, which allows more effective heat transfer. This provides efficiency comparable to a combined cycle with less complexity. By appropriate choice of the ratio between the components of the solution, the boiling point of the working solution can be adjusted to suit the heat input temperature. Because of this ability to take full advantage of the temperature difference between the heat source and sink available, it finds applications in the reuse of industrial process heat, geothermal energy, solar energy, and the use of waste heat from power plants (Bottoming cycle). Even at lower pressure, a Kalina cycle may have higher efficiency than a comparable Rankine cycle.

Germany is the first country to use KC to convert geothermal energy to electrical power from medium-temperature sources. Although the Kalina cycle presents some theoretical advantages when compared to ORC, this technology did not gain market favor. It has been applied only rarely on a geothermal resource (Table E 3), e.g., the 2 MWe plant in Husavík, Iceland, has encountered some serious issues and failures during its operation (Asgeirsson, 2009). The Husavík unit was commissioned in June 2000 and exploits a brine source at 124°C, cooled to 80°C. The geothermal fluid is then used further for heating purposes in the local district heating system (Spadacini et al., 2017).

Plant and location	T_{geo} (°C)	Cycle	Working fluid	Gross capacity (kWe)	Specific brine consumption [(kg/s)/MW]	Cooling tower
Husavik, Iceland	124	Kalina	NH3-H2O	2030 (1700)	53	Wet
Unternhaching, GER	122	Kalina	NH3-H2O	4000 (3400)	44.2	Wet
Bruchsal, GER	120	Kalina	NH3-H2O	610 (550)	51.8	Wer

Table E 3: Small binary power plants using low-temperature geothermal resources or non-conventional working fluids (modified by Franco, 2011).

Combined flash/binary power plants

The combined flash/binary power plants produce electricity and other useful outputs using energy from a renewable energy source. As can be seen from the schematic diagram of the system in Figure E 4, the geothermal fluid is transferred to the flash chamber with flow 1, and the system starts to function. The pressure of the geothermal fluid coming to the flash chamber is reduced, and the geothermal fluid is converted into a mixture of liquid and steam. Then this liquid-steam mixture is sent to the separator with flow 2. The incoming fluid is divided into two as steam and brine in the separator. The steam coming out of the separator is sent to the purifier with flow 3 to increase the performance of the fluid. The fouling part in the fluid is removed from the system by flow 4. The steam fluid with increased quality is sent to the turbine with flow 5 to obtain the electrical output. The incoming steam is expanded between flow 5 and flow 6 to generate electricity. Then the steam coming out of the turbine is sent to the condenser with flow 6 to be condensed. The condenser is used for the heating output, which is a beneficial product. The fluid coming out of the condenser is sent to the three-way valve with the number 7 flow. While the geothermal fluid is circulating in the system, a binary cycle is also performed. While the process up to this point is taking place, at the same time, the other fluid leaving the separator is sent to the evaporator with flow 11. By using the evaporator, heat energy in the geothermal fluid is transferred to the organic working fluid in the ORC cycle. This energy transfer is carried out by heat transfer between the geothermal fluid and the ORC working fluid. The energy-laden organic working fluid is sent to the turbine with flow 13 for electricity generation. The incoming steam is expanded between flow 13 and flow 14 to produce electricity. Then ORC

operating fluid coming out of the turbine is sent to condenser 2 with flow 14 to be condensed. The condenser is used for the heating output, which is a useful product. The ORC working fluid from condenser 2 is sent to the pump with flow 15 to increase its pressure. To increase the temperature of the pressure-enhanced ORC fluid, this fluid is sent to the evaporator with flow 16. The process of increasing the temperature here takes place within the geothermal fluid coming from a separator with flow 11. Then the geothermal fluid coming out of the evaporator is sent to the three-way valve with flow 12. Fluids combined with the three-way valve are sent to the ground with flow 8. The combined flash/binary GPS generally works this way.

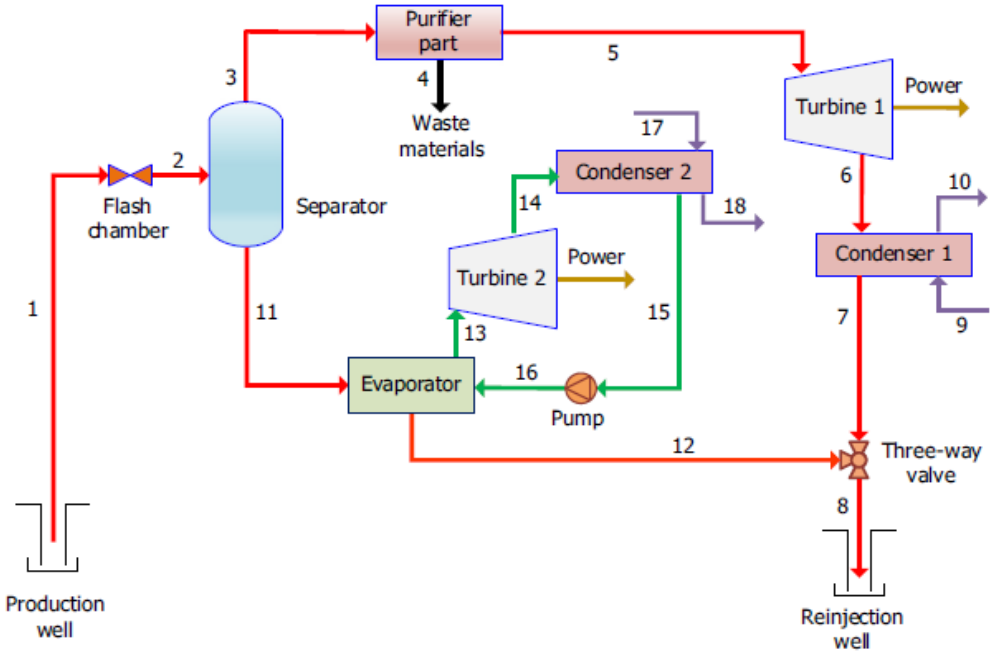

Figure E 4: Simplified flow diagram of a combined flash/binary geothermal power system (Dincer and Ozturk, 2021).

E.2.2.2. Direct use of heat

Direct or non-electric use of geothermal energy refers to the immediate use of the energy for both heating and cooling applications. Typically, the heat is transferred from the geothermal brine to a working fluid (e.g., water) through a heat exchanger. Globally, direct utilization of geothermal energy for applications requiring heating or cooling increased by 50% between 2015 and 2020. However, geothermal heating and cooling is difficult to assess as a global market, especially because its data collection is challenging (EGEC, 2023). More than 88 countries use geothermal energy for heating and cooling, in which geothermal energy is used 58.5% for ground-source heat pumps, 18.0% for bathing and swimming, 16.0% for space heating, 3.5% for greenhouse and covered ground heating, 1.6% for industrial applications, 1.3% for aquacultural pond and raceway heating, 0.4% for agricultural drying, 0.2% for snow melting and cooling, and 0.2% for miscellaneous applications (Figure E 5). The installed capacity and thermal energy available worldwide today are 107,727 MWt and 1,020,887 TJ/yr (283,580 GWh/yr), respectively (Lund & Toth, 2021).

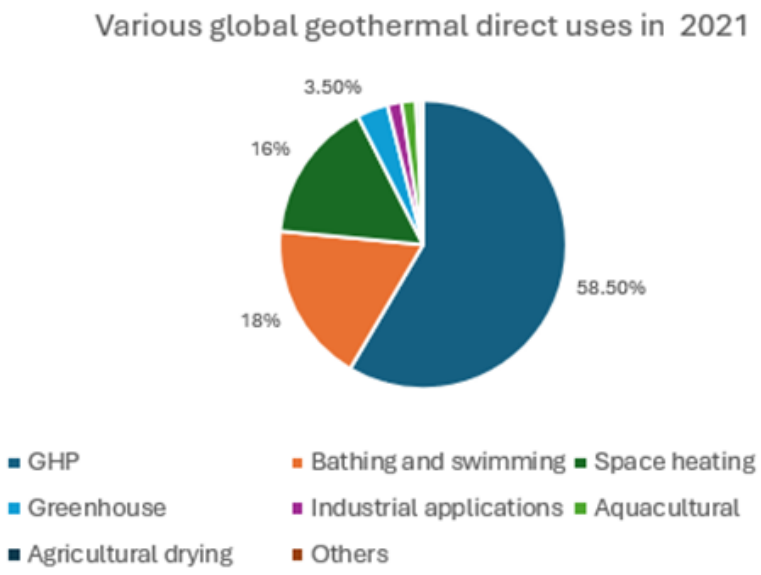

Figure E 5: Various global direct uses of geothermal heat in 2021 (Lund and Toth, 2021).

Geothermal direct use goes back to when people used hot springs for bathing, cooking food, and loosening feathers and skin from games. One of the main advantages of the direct use of geothermal energy is that it can use low-to-moderate resource temperatures (<150°C) very efficiently.

Generally, direct-use systems are typically composed of three components:

- A production facility – usually a well – to bring the hot water to the surface;
- A mechanical system – piping, heat exchanger, controls – to deliver the heat to the space or process
- A disposal system – injection well, storage pond, or river – to receive the cooled geothermal fluid.

Heat demand represents a significant share of final energy consumption for space heating, especially in cold countries, for agricultural and for industrial processes. Geothermal heat production systems may meet the demand by simply providing fluids at the required temperature. For example, the water circulating through the network of pipes, beams and panels of the heating systems of a building may be kept constant in the summer by exchanging heat with groundwater fluids at a temperature of 18°C. If a groundwater fluid temperature of 30°C is discharged, it can be used to pasteurize milk in a cheese factory (Manzella, 2017).

The versatility of direct use can take advantage of the same resource to meet thermal requirements or to base combined heat and power configurations (CHP) (USAID, 2015). In CHP, the thermal content of either 'waste heat' or geo-fluid after the power generation process is used to meet the required temperature in direct-use applications. Geothermal heat pumps play a vital role in space heating in cold zones (Naili et al., 2016; Antonijevic & Komatina, 2011). Additionally, district heating by using low-enthalpy geothermal resources is another very mature technology (Aslan et al., 2011; Pujol et al., 2015).

Recent research has demonstrated the positive impacts of cascade applications in geothermal development. The use of geothermal resources in cascade configurations includes not only electricity generation but also the direct use of thermal energy (Pujol, et al., 2015; Shortall et al, 2015), drying and dehydration processes, heat pumps, fish farming and swimming pools for recreational activities. Cascading systems allow multiple

applications of CHP linked to the same geothermal resource. In the cascade design, different temperatures of the same geothermal heat flow are used in staging and successive applications in a sequence that requires lower temperatures downstream (Bloomquist et al., 2013; Glassley, 2015). Gudmundsson (1988) exemplifies the cascade system by a facility that uses geo-fluid for different applications. The geo-fluid leaving the power plant at an optimum temperature is used to heat a cucumber and tomato greenhouse, then piped through cabbage, carrots, and other vegetable fields. This is an example of power generation, greenhouse, and soil heating as cascading uses. Figure E 6 provides an example of a combined heat and power configuration in a multipurpose cascade design. In Figure E 6, Valdimarsson (2015) illustrates how the same geothermal heat flow (at 202 °C and 162 °C) is used to produce electricity, then, when it leaves the power plant (at 81 °C), is used for district heating purposes and finally at a lower temperature, the geo-fluid is applied in other direct uses. In Figure E 7 the temperature-dependent range of different direct geothermal applications is shown.

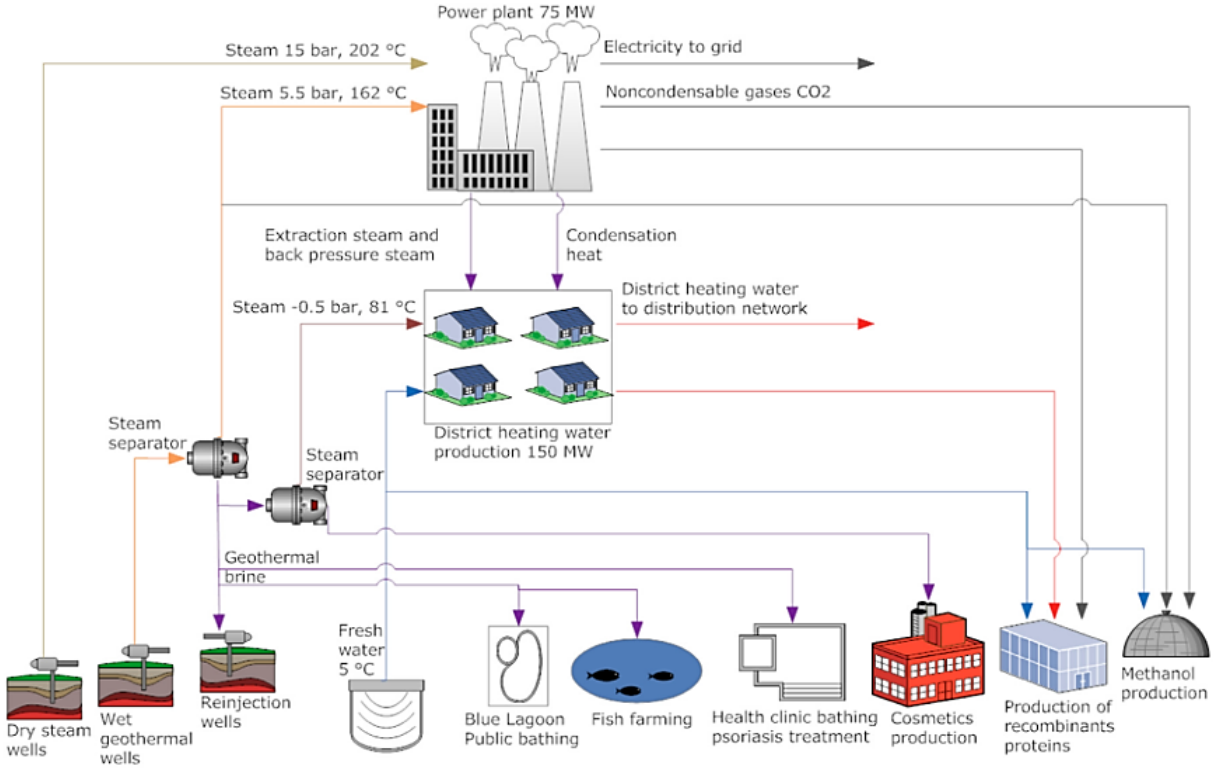

Figure E 6: Cascade application of geothermal resources for the example of the Blue Lagoon, Iceland (Valdimarsson, 2015).

Spas, balneology, tourism

Geothermal heat and water have been utilized for therapeutic and recreational purposes for many thousands of years, offering a unique and sustainable resource for spas, balneology, and tourism worldwide. The first written records of geothermal spa use date back to 500 BC. The therapeutic effects of thermal water have been known even in ancient times. In ancient Greece, there was a high level of thermal bath culture (Szabó et al., 2013). This tradition has been continued by the Romans. In numerous Western-European states thermal spa tourism and thermal water treatments are an important engine of local and regional development. In the 19th century, famous spa resorts of Europe became the favorite destinations of the

rich and were functioning as places that combined relaxation with balneology and electrophototherapy (Tabbachi, 2008).

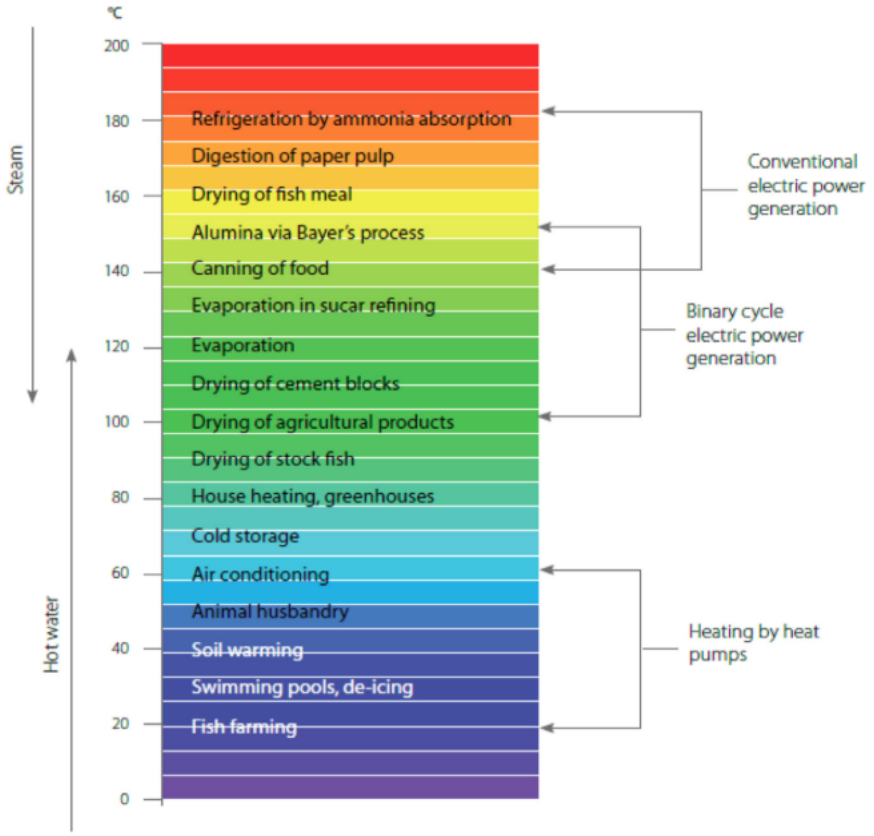

Figure E 7: Lindal diagram illustrating the range of direct geothermal applications depending on the temperature of the procuced fluid (USAID, 2013).

The spa industry continued to develop, absorbing and combining customs and traditions of many national cultures along the way (Cohen, M., & Shivdasani, S., 2010). By the middle of the 1980s, resort hotels developed spa centers (Monteson, & Singer, 2004) in order to respond to the growing demand of their customers and, in the process, increase their competitiveness. At about the same time, many destinations appeared specifically targeting the health/wellness market segments, both in Europe and more exotic places in south-east Asia (Tabbachi, 2008).

Currently, in the international context, countries such as Japan, New Zealand, Turkey, France, Spain, Greece, Tunisia, Italy, Iceland, Czech Republic, Hungary, and Portugal are some of those with a stronger tradition of using mineral waters for the treatment of various pathologies. An estimation of 34,099of thermal/mineral springs establishments are operating in 130 countries, with revenues of ~$64 billion in 2019 (GWI, 2021).

In the 21st century, mainly in Europe, the use of geothermal waters suffers particular attention in Tourism, and the resolution of the European Parliament of November 29, 2007, mentions in one of its chapters thermal tourism and recommends the "use of European programs to promote thermal tourism and stresses the relevance of cross-border cooperation in the definition of financing solutions for this tourism product". In 2011 it underwent an update with the publication of the Parliament Resolution of September 27, and a new

policy framework for Tourism in Europe is defined, which states and recognizes that due to "demographic developments in Europe, health tourism will show growth in health tourism, in particular, spa tourism".

In Europe, balneology, including spas and thermal baths, accounts for 25% of geothermal production (Toth, 2020). Hungary stands out as one of the richest countries in the world in water resources with 162 active thermal baths. Balneology is historically the country's most important geothermal application, with 102 wells yielding thermal and sometimes medicinal waters. According to Toth (2020), these thermal well productions represented a total installed capacity of 249,5 MWt with an annual use of about 3,684 TJ/yr.

When it comes to exploitation fields for heating purposes, the geothermal fields Ivanić and Bizovac in Croatia are examples of the formerly hydrocarbon exploratory or oil production wells being used for geothermal exploitation in the present, including balneology, as is the case in the Bizovac hotel and spa complex.

As for tourism, spas, and balneology can significantly enhance tourism by offering unique, sustainable wellness experiences that attract health-conscious travellers and promote the natural beauty of geothermal regions. Industrial tourism is also a recent form of tourism that has been growing among destinations. In addition to having an on-site experience to visit oil and natural gas resource sites, inoperative and abandoned industrial heritage sites can be accessed. This attracts new inhabitants and helps potentially abandoned areas to revitalize since old buildings can be reused, and new services for visitors and locals can emerge. Active industrial tourism is potentially a direction for further strategic development and differentiation of local offers (Pavlakovič et al., 2021).

District heating, municipalities

Heating residential buildings or stand alone commercial buildings with geothermal fluid from a produced well (potentially combined with a heat pump) is a simple process. The hot water of geothermal sources is pumped to the structure from the well, where a heat exchanger transports the heat energy from the geothermal hot source to the in-building system (O'Brien, G. et al, 2020). The geothermal hot water is then disposed of to the surface or injected into the aquifer by an injection well. The utilization of geothermal heat resources for direct space heating accounts for about 37% of all direct utilization development. The first known commercial utilization of geothermal heat energy was in Chaudes-Aigues Cantal, France, which was constructed in the 14th century. Despite geothermal resources, temperatures in surplus of 50°C are generally advised for space heating, but resources as low as 40°C could be utilized in certain space heating requirements and circumstances (Bloomquist, 2003).

The mass flow rate and the temperature of the geothermal source determine the reliability and the potential of the geothermal fluid in district heating applications. Similarly, the chemical composition of the brine, which might comprise some ingredients such as silica, hydrogen sulfide, chlorides, and oxygen is essential for choosing suitable materials required to design the energy conversion system. The mineral concentration in the geothermal fluid rises correspondingly with increasing temperature and the depth of the geothermal resource (Dincer and Ezzat, 2018).

Geothermal fluid with a limited concentration of 150 mg/kg for silica, less than 50 mg/kg for chlorides, and oxygen below 5 µg/kg is considered uncontaminated and can be used directly for space heating and hot tap water. Hot water is delivered to the consumers at temperatures varying from 60 to 90°C and returned at a temperature varying from 30 to 35 °C. The thermal power obtained from geothermal hot water with a mass flow rate of 6 kg/s with a temperature drop from 90 to 50 °C is around one megawatt. Geothermal district heating systems are classified into two types depending on the utilization of the geothermal energy. If it is used indirectly by transferring the geothermal heat to the secondary system via heat exchanges, the district heating system is called the primary system. If the geothermal energy is used directly in the house heating

system, the district heating system is called the secondary system (Figure E 8) (Björnsson, 1999; Dickson & Fanelli, 2013).

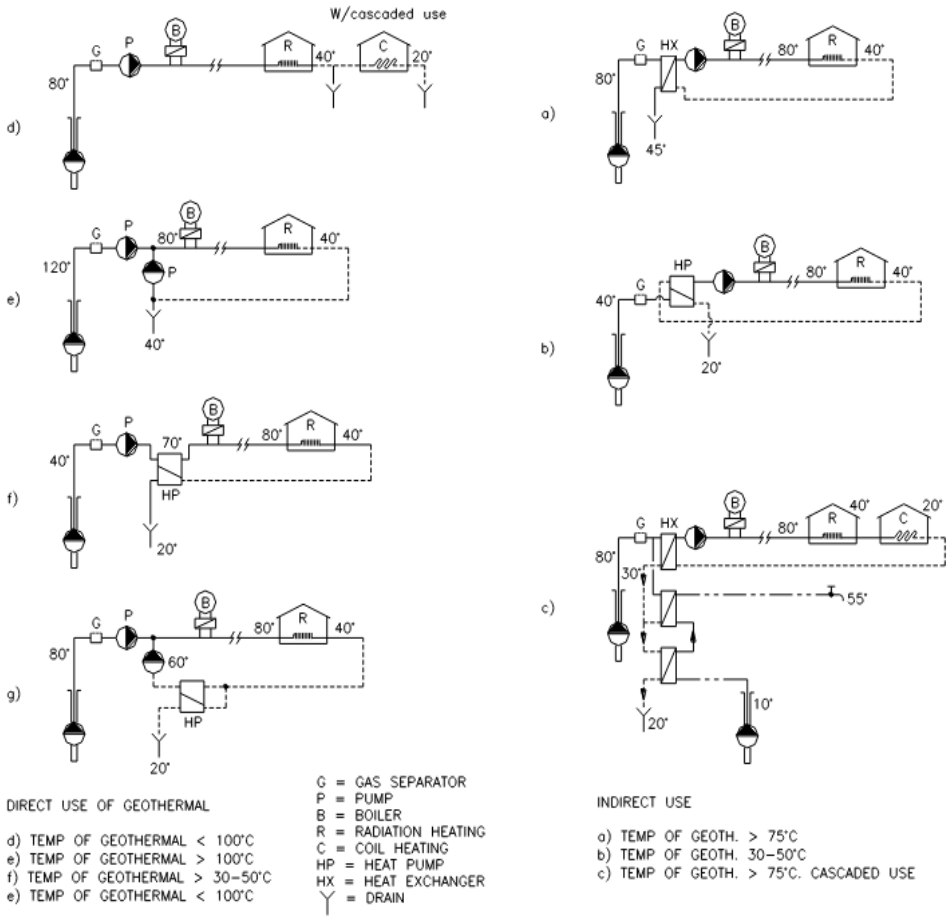

Figure E 8: Examples of direct and indirect district heating networks with geothermal water (Björnsson,1999).

In order to improve thermal efficiency, cascade systems are common in geothermal district heating systems. It refers to the sequential use of geothermal energy at multiple temperature levels to maximize efficiency. In this system, high-temperature fluid is first used for applications requiring the most heat, such as electricity generation or industrial processes. The partially cooled fluid is then cascaded to successively lower temperature applications, such as district heating, ensuring that the geothermal resource is utilized to its fullest potential before being reinjected into the ground. There are several ways to use the geothermal cascade in actual engineering: directly through multiple plate heat exchangers, use at the end to improve the geothermal heat, use a plate heat exchanger and water source heat pump, or plate heat exchange and absorption heat pump.

Countries like Iceland, Italy, the United States, France, Hungary, Austria, and China effectively utilize cascade systems to maximize geothermal energy benefits. Initially used for district heating, the geothermal fluids are then employed for greenhouse heating, promoting agricultural productivity, followed by aquaculture to maintain warm water conditions for fish farming. Additionally, residual geothermal heat supports industrial processes such as food drying and processing. Finally, the lowest temperature fluids are used in thermal spas, offering wellness treatments and enhancing tourism. In Austria, Bad Blumau, a 250kW

Binary cycle plant, uses 85°C “waste” water fed to district heating for Rogner Bad Blumau Hotel and Spa (Legmann, 2003).

The reuse of abandoned oil and gas wells for district heating systems is an innovative and sustainable approach being explored worldwide. These wells, often found in sedimentary basins rich with geothermal potential, can be repurposed to harness residual geothermal energy for heating purposes. In Canada, projects like the one in Hinton, Alberta, aim to utilize geothermal energy from old oil and gas wells to provide heat for the local community, showcasing a practical example of this approach. Similarly, in the United States, there are several projects seeking to repurpose oil fields. In North Dakota, Williston Basin, more than 73 oil and gas wells drilled in the Inyan Kara sandstone formation are approaching the end of their useful lives for the petroleum industry. They are being studied to produce geothermal energy. Preliminary mapping indicates the reservoir temperature of 82 and 85°C at 1600m, hence, a viable source of heat for district heating systems (Eagle-Bluestone et al., 2022).

In Europe, Hungary has the most significant district heating system, available in a total of 21 settlements out of a total of 94 district heating systems (Barcs, Bóly, Cserkeszőlő, Csongrád, Gárdony, Győr, Hódmezővásárhely, Kistelek, Makó, Miskolc, Mórahalom, Nagyatád, Orosháza, Szarvas, Szeged, Szentes, Szentlőrinc, Szigetvár, Szolnok, Vasvár, Veresegyház) where thermal water partially replaces gas-based heating. In addition, a large project is in operation in the city of Szeged. It aims to convert nine district heating systems to geothermal operation, with the goal of replacing natural gas with geothermal energy for heating 27,000 dwellings (block houses apartments) and 500 public buildings. With a nominal capacity of 224 MWt, the project involves drilling 9 production and 18 injection wells into the Late Miocene (Dunántúli Group) sandstone, producing thermal water at an average temperature of 90°C (Nádor et al, 2019).

In the global distribution of thermal energy used, space heating accounts for 16%, of which 91% is for district heating. Space heating, including individual space heating and district heating, has increased 68.0% in installed capacity and 83.8% in annual energy use over WGC2015. The installed capacity now totals 12,768 MWt, and the annual energy use is 162,979 TJ/yr. In comparison, 91% of the installed capacity and 91% of the annual energy use is in district heating (29 countries). The leaders in district heating in terms of both capacity and annual energy use are China, Iceland, Turkey, France, and Germany, whereas in the individual space heating sector in installed capacity (MWt), the leaders are Turkey, Russia, Japan, United States, and Hungary. In annual energy use (TJ/yr), the leaders are Turkey, Japan, Russia, the United States, and Switzerland, a total of 29 countries. These five leaders account for about 90% of the world’s total use in district heating and about 75% of the world’s individual space heating. (Lund & Toth, 2021).

Agriculture (greenhouses)

Agricultural applications of geothermal fluids include temperature control of crop growth in open fields and greenhouses. Thermal water can be used in open-field agriculture to heat the soil and, sometimes, to irrigate it where ponds and rivers are not available. The most common application of geothermal energy in agriculture is, however, in greenhouse heating, which has been developed on a large scale in many countries. Opening costs for heating greenhouses, which in some cases account for 35% of the cost of the croatian product (vegetables, flowers, indoor plants, and tree seedlings), can be considerably reduced by using geothermal heat (Manzella, 2017).

Countries like Iceland and the Netherlands have pioneered the use of geothermal energy in agriculture. Iceland, for instance, derives approximately 90% of its greenhouse heating from geothermal sources, while the Netherlands utilizes over 500 hectares of greenhouse space heated by geothermal energy, accounting for about 10% of its total greenhouse area. Where agricultural users are concerned, it should be noted that almost all the known technologies were developed in Europe and then spread around the world.

In Hungary most of the geothermal energy production is used as direct heat supply, with 40% for agriculture business. Croatia and Slovenia have lower but still notable shares. France's agricultural sector played a pivotal role in unlocking low-enthalpy geothermal heat for greenhouse applications. Similarly to France, and Alberta in Canada, other sacred sectors of Alberta's economy that can be engaged in geothermal co-creation include water, fishing, and eco-tourism. To strengthen this agricultural-geothermal sector, the resourcing can also be linked through policy incentives for geothermal heat technologies like retrofitted oil wells at the small and medium business levels (Nadkarni et al., 2022).

As for heat optimization, several applications of the cascade utilization of geothermal energy for agriculture have been operating worldwide, especially in the United States. In the region of Klamath Falls, Oregon, 6 geothermal wells with temperatures ranging from 27 to 93C and depths around 90m provide energy to agriculture and aquaculture. The main well is used for greenhouse heating at 93C. A similar application is in Cotton City, New Mexico, where the installation of a Kalina cycle plant with a net power of 1 MWe was planned to supply electricity to a facility of fish hatchery, and the waste heat will also be used to maintain the temperature of the hatchery. The geothermal resource, in this case, comes from a well with a depth of 120m, with a temperature between 115 and 120, and a flow of 63 l/s (Rubio-Maya et al., 2015).

Worldwide use of geothermal energy for greenhouse and covered ground heating has grown significantly, with a 24% increase in installed capacity and a 23% rise in annual energy use. The installed capacity is 2,459 MWt, with an annual energy utilization of 35,826 TJ/yr. A total of 32 countries report geothermal greenhouse heating, with Turkey, China, the Netherlands, Russia, and Hungary accounting for approximately 83% of the global total annual energy use. This data is based on country update papers submitted to the World Geothermal Congress 2020 (WGC2020) and comparisons with data from the World Geothermal Congresses held in 1995, 2000, 2005, 2010, and 2015 (Lund & Toth, 2021).

Industry (automotive industry, food industry)

The utilization of geothermal energy in the industry dates back to the early 20th century, but its widespread adoption has gained momentum in recent decades as concerns over fossil fuel dependency and climate change have increased. Heating is by far the largest form of energy used in industrial processes. Geothermal heat can provide a continuous energy supply with many temperature levels, at different loads and capacities, at low operational cost. This makes it suitable for a vast range of industrial processes.

Geothermal energy provides heat for a range of industrial uses, depending on the temperature of geothermal fluids. Industrial processes such as milk pasteurization and food dehydration require higher-temperature geothermal fluids, which are therefore often developed in association with or cascaded with electricity-producing geothermal fields, as they are in El Salvador, Iceland, Kenya, Mexico, and New Zealand. In industrial applications, geothermal energy in the temperature range being considered here (below 150°C) is used in the basic processes of preheating, washing, peeling and blanching, evaporation, distilling, drying, and refrigeration (Popovska, 2001).

Preheating and heating

Geothermal energy can be effectively used to preheat boilers and other process-feed water in a wide range of industries. This imposes a considerable load on the boiler for feed-water heating of incoming water at typically 10-16 °C up to the temperature at which it is introduced into the boiler, typically 90-150 °C, depending on the system. The geothermal resource can be used to offload the boiler of some or all this preheating load. A wide variety of industries use for various processes large quantities of feed water which can be preheated or heated geothermally to the use temperature (Popovska, 2001).

Washing

Large amounts of low-temperature energy (35-90°C) is consumed in several industries for washing and clean-up. One principal consumer is food processing, with major uses in meat processing for scalding; soft drink production for container and returnable bottle washing (77°C); in poultry dressing, as well as canning and other food processes. Textile industry finishing plants are another large consumer of wash water at 90°C. Smaller amounts are used in the production of plastics (85-90°C) and leather (50 °C). Sizable amounts of hot water and other hot fluids at temperatures under 90 °C are used in several metal-fabricating industries, machinery, and transportation equipment for parts digressing, bouldering, and washing processes (Popovska, 2001).

Peeling and blanching

In the typical peeling operation, the product is introduced into a hot bath, which may be caustic, and the skin or outer layer, after softening, is mechanically scrubbed or washed off. Peeling equipment is a continuous-flow type in which the steam or hot water is applied directly to the product stream or indirectly by heating the product bath. In most instances, the product contact time is short. Blanching operations are similar to peeling. The product is usually introduced into a blancher to inhibit enzyme action, produce coating, or for cooking. Blanching may be either a continuous or batch operation. Typical blanching fluids require closely controlled properties. Thus, it is unlikely that geothermal fluids could be used directly in blanchers and peelers because of the water quality. Geothermal fluids could, however, provide the energy through heat exchangers. The temperature range for most of the peeling and blanching systems is 77-104 °C (Popovska, 2001).

Evaporation and distillation

Evaporation and distillation are basic operations in many processing plants to aid in concentrating a product or separating products by distillation. The source temperature requirements vary with the product being evaporated. However, in a majority of agricultural processes, water is being driven off, and in these cases, operating temperatures of 82-120 °C are typical. In some circumstances, the evaporators operate at reduced pressures, which decreases temperature needs and improves product quality. Evaporators are commonly found in sugar processing, mint distilling and organic liquor processes. Evaporators, depending upon temperature and flow rate requirements, can be readily adapted to geothermal energy as the primary heat source. The energy can be transferred through secondary heat exchangers to the working fluids or, in some instances, used directly at the evaporator, depending upon existing plant designs or adaptations to new plant expansions (Popovska, 2001).

Sterilizing

Sterilizers are used extensively in a wide range of industries and include applications such as equipment sterilization for the canning and bottling industry. Most sterilizers operate at temperatures of 104-120°C and utilize geothermal energy with the use of heat exchanger and potable sterilizer water. Many sterilizers operate in a continuous mode. Equipment washdown and sterilization, however, may occur periodically or at shift changes (Popovska, 2001).

Several countries have successfully integrated geothermal energy into their industrial sectors. Iceland uses geothermal energy for various industrial applications, including aluminum smelting and fish processing. The Hellisheidi geothermal power plant, one of the largest in the world, supplies both electricity and hot water to industrial facilities (Jónsson et al., 2019). In New Zealand, in addition to its dairy industry, uses geothermal energy in timber drying and pulp and paper manufacturing, leveraging the high temperatures available from geothermal sources to reduce drying times and energy costs. In 2020, the global installed geothermal capacity for agri-food and industrial uses was 14 GWth, 35% more than in 2015. This sector grew at an annual rate of 4-7% between 2000-2020 and is expected to continue growing at similar rates. Market

opportunities are expected from using geothermal energy to provide refrigeration in the supply chain and desalination using geothermal heat (EGEC, 2023).

In the automotive industry, the push for greener manufacturing processes aligns well with the use of geothermal energy. As electric vehicles (EVs) become more prevalent, geothermal energy can provide a sustainable energy source for the electricity demands of EV production facilities. In addition, some countries that have been using—or plan to use—geothermal systems to provide the heating needs of manufacturing facilities.

In Germany, the automotive manufacturing company Stellantis NV (Stellantis) has signed a binding term agreement with Vulcan Energy Resources (Vulcan) for the first phase of a multiphase project that aims to decarbonize the Opel main plant of Stellantis in Rüsselsheim, Germany through the development of a geothermal system. Based on current assumptions, the project can provide a portion of the facility's energy needs by 2025. In addition, in Munich, BMW is using geothermal energy for heating. Beyond Germany, a new plant in Debrecen, Hungary, which BMW has said will be the world's first auto factory to run entirely without fossil fuels, will rely heavily on solar and geothermal.

In Hungary, geothermal energy has found a valuable application in the automotive industry, particularly in heating manufacturing facilities. Automotive manufacturing plants in Hungary utilize geothermal heating to maintain optimal indoor temperatures, ensuring consistent production conditions year-round. In addition to BMW, companies like Audi have taken significant steps in incorporating geothermal energy into their production processes. In 2012 Audi's Hungarian plant opened a geothermal facility in the city of Győr to supply most of its heat requirements. Audi Hungaria is thus the second of five Audi sites to achieve a neutral carbon balance. The geothermal plant in Győr meets approximately 70 percent of the demand. The remaining heat is generated through natural gas, with carbon neutrality assured thanks to bio-gas certificates. Audi Hungaria is the biggest user of industrial geothermal energy in Hungary. The plant has an annual output of at least 82,000 megawatt-hours of thermal energy. Since 2015, the company has made use of 250 gigawatt-hours of geothermal energy, reducing emissions of CO_2 by 50,000 tonnes.

The BMW factory in Debrecen and the Mercedes factory in Kecskemét, as well as LEGO factory in Nyíregyháza are also planning to switch to partial geothermal heating. Intensive drilling is underway in Kecskemét and Nyíregyháza.

Slovenia is the leading consumer of energy for industry purposes, accounting for nearly 46.8% of the total final energy consumption, followed by Germany, with 29%.

The food industry uses a third of the world's energy during production in all the processes involved. Fossil fuels are the most common sources for generating electrical energy for the food industry; however, using geothermal energy would not only reduce operational costs but also support food security by enabling more efficient processing and preservation methods.

Geothermal energy can be used throughout the food supply chain to improve the sustainability of the entire food sector. It can be applied across a broad spectrum of food applications, such as the following:

- Heating of greenhouses (25 – 100 °C) to grow fruits, vegetables, flowers, and plants
- Aquaculture (20 – 40 °C) or fish farming
- Cultivation of algae (35 – 37 °C)
- Soil heating (20 – 40 °C) to grow crops such as carrots, cabbage, and asparagus
- Irrigation (40 – 75 °C)
- Drying of food or crops (40 – 100 °C)
- Pasteurization of milk (70 – 100 °C)
- Evaporation and distillation (80 – 120 °C) for processing of milk and preparation of spirits
- Sterilization (> 105 °C)

- Refrigeration (> 120 °C)

Geothermal energy plays a growing role in the global industrial energy market. Its sustainability, reliability, and cost-effectiveness make it an attractive option for industries seeking to reduce their carbon footprint and adhere to stricter environmental regulations. The International Renewable Energy Agency (IRENA) reports that geothermal energy could contribute significantly to industrial decarbonization efforts, particularly in sectors requiring continuous and stable heat supplies.

E.3. Literature review

E.3.1. Hydrothermal Energy systems in selected countries

For a hydrothermal geothermal resource to be viable, a large heat source, a permeable reservoir, a supply of water, an overlying layer of impermeable rock, and a reliable recharge mechanism are essential. These geological features must be naturally present. These hydrothermal resources are distributed throughout the world, not restricted to volcanic regions, but also occur as hot water in sedimentary formations.

This review focuses on low to medium-enthalpy hydrothermal systems. A total of 7 countries are currently utilizing ORC binary power plants for the extraction of hydrothermal energy from these systems: the United States, Australia, Iceland, Croatia, Germany, and Hungary (Table E *4*).

Country	Number of units	Capacity installed 2022*	Gross electric production	Temperature of production well	Flow rate	Depth of wells
		[MWe]	[GWh]	[°C]	[L/s].[Kg/s]	[m]
Australia	1	150kWe	-	98	27	1230
United States (Ayling, 2020)	24	662.35	3763.657	97 - 187	130	
Iceland (Ragnarsson, 2021)	1	0.6	-	-	116	-
Austria (EGEC, 2024)	2	1.2	0.5	105	80	2500
Croatia (EGEC, 2024)	1	16.5	93.7	170	208	-
Germany (EGEC, 2024)	10	43.5	179	113 - 152	28 - 185	3500
Hungary (EGEC, 2024)	1	3.35	-	125	-	-
*Summ of all units capacity installed						

Table E 4: Hydrothermal energy systems using orc binary power plants worldwide in 2023 (Gutiérrez-Negrín, 2024).

Australia

The use of geothermal waters in Australia is limited. Exploratory wells have been drilled, and pilot projects developed, however, all of them have been abandoned. Direct use of geothermal waters provides heat to many of the municipal buildings and public facilities, as well as to supply spas water in the city of Portland, western Victoria. The water is pumped from a 1400 m deep bore at a temperature of 58°C. The only existing geothermal power generation in Australia is a small, 120kW net binary-cycle plant at Birdsville in southwest

Queensland. This power plant utilizes a low-temperature hydrothermal-type geothermal resource, accessing 98°C groundwater from a 1,230 m deep artesian bore that taps a confined aquifer in the underlying Great Artesian Basin. The Great Artesian Basin spans 22% of the Australian continent and has wellhead temperatures ranging from 30°C to 100°C (Habermehl & Pestov, 2002).

United States

The United States is a global leader in geothermal energy production, with significant contributions to both direct-use applications and electricity generation, reflecting a century-long journey of exploration and innovation. Among the 168 hydrothermal systems in the country, excluding systems in National parks, there are three power projects of 13.500 MWe operating based on geothermal resources in the 100°C and 150°C temperature range (Sanyal, 2005). These hydrothermal systems are mainly explored in the State of Nevada, with mean estimates of identified and undiscovered hydrothermal resources totalling 5,755 MWe.

Croatia

Most of the currently known geothermal potential locations in Croatia were discovered during oil and gas exploration and exploitation from the mid-twentieth century. Since then, geothermal resources have mainly been used for balneology in numerous spas. In the last decade, low-temperature geothermal resources have also been used in agriculture (two geothermal greenhouses in Bošnjaci and Sveta Nedelja) and for district heating (Zagreb geothermal site). With Croatia's first geothermal ORC power plant, Velika 1, commissioned in 2019, the interest in developing geothermal projects is seen in the current 10 exploration and 23 exploration licenses assigned.

With a capacity of 16.5 Mwe and a gross electric production of 93.7 GWh, this Binary power plant has been operating at full capacity since March 2019, but recently it operates at lower capacity due to technical problems supplying electricity to almost the entire city of Bjelovar. The reservoir was discovered in 1990 by INA-Naftaplin during an underground exploration for oil. The oil was never found, instead, a promising potential for geothermal energy was discovered. The Velika Ciglena project exploits steam and hot water at 170 oC to produce electricity to feed the local power grid (Rašković et al., 2013).

Germany

In Germany there are about 190 geothermal installations for direct use of geothermal energy. This number includes facilities for district heating, thermal spas, and combination with space heating. The installed geothermal capacity of these facilities amounts to 406.3 MWth, with a geothermal heat production of 5,378.6 TJ in 2018. District heating plants accounted for the largest portion of the geothermal capacity with 346.2 MWth and a heat production of 3,634.9 TJ.

Geothermal electricity generation in Germany is based on the use of binary systems (Kalina cycle or ORC). Due to favorable geological conditions, geothermal district heating and power plants are mainly located in the Molasse Basin in Southern Germany, in the North German Basin, or along the Upper Rhine Graben. In addition to installations using "deep" geothermal energy, numerous small- and medium-sized decentralized geothermal heat pump units are in use for heating and cooling of individual houses and office buildings (Weber et al., 2022).

At the end of 2021, eleven geothermal plants with an installed capacity of 47.6 MWe fed electricity into the German grid. The geothermal power production in 2020 summed up to a total of 190.6 GWh. According to the EGEC Market Report (2023), there are currently 10 hydrothermal power plants operating with Binary cycles (ORC or Kalina) in Germany, as per Table E ***5***.

State/power plant name	Year commisioned	Turbine	Capacity installed 2022	Gross electricity production	Temperature of production well	Flow rate
			[MWe]	[GWh]	[°C]	[Kg/s]
Baden-Württemberg - Bruchsal	2009	B-Kal	0.5	-	131	28
Bavaria - Holzkirchen	2019	B-ORC	3.6	23	152	55
Bavaria - Taufkirchen	2014	B-Kal	4.3	-	136	120
Bavaria - Kirchweidach	2021	B-ORC	4.4	1.8	127	50
Bavaria - Garching a. d. Alz	2021	B-ORC	4.9	27.5	125	-
Bavaria - Oberhaching-Laufzorn-Grünwald	2014	B-ORC	4.3	18	127	140
Bavaria - Sauerlach	2014	B-ORC	5	26.4	140	110
Bavaria - Traunreut	2016	B-ORC	5.5	27.6	113	185
Bavaria - Dürrnhaar	2013	B-ORC	5.5	31.2	141	135
Bavaria - Kirchstockach	2013	B-ORC	5.5	23.5	141	135

Table E 5: Binary orc power plants in Germany 2022 (EGEC, 2023).

Hungary

Hungary's excellent geothermal potential is well known. Traditionally, the country's geothermal energy production has been used mostly for direct heat utilization. There are approximately 1700 hot water wells, of which 1000 are active thermal wells. District heating systems provide geothermal heat to about 93 towns or settlements (Toth et al., 2019). In 2019, more than 900 active thermal water wells produced about 90 million m^3 of thermal water in Hungary, representing 1023.7 MWt or 10,701 TJ/yr.

The agriculture sector is still a key player in direct use, especially in the southeast of Hungary, where the heating of greenhouses and plastic tents has long traditions. These account for ~ 358 MWth installed capacity and ~ 2,891 TJ yearly production. Geothermal district heating and thermal-water heating cascade systems represent a major part of Hungary's direct use, available in 23 towns representing about 223,4 MWth installed capacity and 2,288 TJ annual production.

Major new projects have been established in Győr and Szeged. In Szeged, the geothermal project aims to convert nine district heating systems to geothermal operation, with the goal of replacing natural gas with geothermal energy. Currently, the project supplies heat and domestic hot water to 27,256 apartments and 433 public buildings. Individual space heating (mostly associated with spas) is available in nearly 40 locations, representing an estimated installed capacity of about 77,2 MWth and 299 TJ/yr production.

Balneology is historically the country's most important geothermal application, with more than 250 wells yielding thermal and sometimes medicinal waters. These represent a total installed capacity of 249,5 MWt with an annual use of about 3,684 TJ/yr. Recently, the first Hungarian geothermal power plant project was implemented in Tura in 2017. This Binary ORC power plant has a 3 MWe capacity and a temperature of 125° C (Toth, 2020).

E.3.2. Reuse of hydrocarbon wells for hydrothermal energy production

The oil industry has left and will leave many hydrocarbon wells behind, which could be prepared to produce geothermal energy. Facing with declining reserves, increasing operation costs, volatile oil prices, and green energy trends, oil and gas companies started to explore and utilize oilfield geothermal energy from existing assets, seeking for solutions to reduce operation costs, extend the economic life of aging fields and achieve environmental and social benefits (Wang et al., 2018). As the geothermal resources in oil and gas reservoirs has been continuously studied, a considerable amount of geothermal reserves is reported in worldwide oilfields (Wight & Bennett, 2015; Erdlac et al., 2007; Liu et al., 2018; Wang et al., 2016). More importantly, oilfields possess unique economic and technical advantages to utilize associated geothermal resources. Existing wellbores, surface facilities, and useful data empower the oilfield geothermal project with reduced cost, minimized risk, and significant convenience (Liu et al., 2018; Wang et al., 2017).

The geothermal gradient of hydrocarbon fields demonstrates the potential for direct-use applications and for electricity generation in some cases. Converting these wells eliminates the need for new drilling, thereby reducing the environmental impact associated with drilling footprints and carbon emissions (Aydin et al., 2024). Oil reservoirs typically exhibit normal geothermal gradients and are encountered between 1000-3000 meters depths. Consequently, bottom-hole temperatures in repurposed wells generally range from 40-200 °C. As a type of resource that co-exists with hydrocarbon in sedimentary basins, oilfield geothermal resources fall into the intermediate to low-temperature category, given that the produced fluid temperatures mostly range between 65°C and 150°C (Liu et al., 2018).

Direct use of oilfield geothermal could be divided into two categories. One is the traditional direct-use applications, such as heating buildings, spas, greenhouses planting, drying crops, and several industrial processes. The other is special oilfield applications, including oil gathering, heat tracing, crude oil transportation, and geothermal water flooding. In Austria, the produced heat from abandoned oil exploration wells has been utilized for spa resorts. Likewise, in Albania, the required heat for greenhouses is supplied from abandoned wells with more than 65 °C temperatures. In Hungary, water flooding as a secondary oil production method and heating the gathering pipes in heavy oil production use geothermal water (Lund & Boyd, 2016). Extraction of energy in this case, is by means of either producing hot fluids or exploiting heat by closed-loop circulation.

The first geothermal power plant utilizing oil wells at 99°C was reported by Wang et al. (2018). For low-temperature resources, technologies like ORC and thermoelectric modules are mostly used. Thermoelectric modules exhibit efficiencies between 4-5%, while ORC units can achieve ~8-15% depending on the geothermal fluid.

Even though most geothermal power plants have been constructed in the last decades, conversion of oil and gas wells has occurred mainly in the recent decade. This conversion is an important initiative that is seriously considered and partly implemented by some governments and oil and gas companies. Feasibility studies of hydrocarbon well conversion have been conducted in several countries including Hungary (Toth et al., 2018), Pakistan (Farah, 2017), Poland, (Barbacki & Uliasz-Misiak, 2003), the United-States (Caulk & Tomac, 2017) and New Zealand (Reyes, 2007).

Economically, it should be noted that major modifications or facilities in abandoned wells may be needed, and some costs are incurred by retrofitting projects. However, a retrofitting project is estimated to cost only one-third of the cost required to make a new conventional geothermal well (Kurnia et al., 2022). Via retrofitting, a well can stay active for up to 30 (Van Erdeweghe et al., 2018) - 40 (Evans, 2010) years. However, prior to retrofitting, well integrity must be ensured; otherwise, the project life would be cut shorter, or there may be high associated costs due to potential problems such as leakage of oil, gas, or water.

In retrofitted geothermal projects, the bottom hole temperatures are often lower than in conventional geothermal wells. Due to these projects' low temperatures, improving work efficiency and optimization should be followed to the maximum to minimize cost and guarantee the economic advantage of the projects. Advances in science in recent years have led to optimization in various fields to the extent that production scenarios, new surface cycles, and working fluids are considered (Ashena, 2023).

Worldwide, repurposing oil and gas wells for geothermal energy is gaining traction as many innovative approaches to sustainable energy are in development. Unfortunately, many of these are pilot projects, e.g., Germany, in the Brandenburg State, has a project in the planning phase called Velten, Pritzwalk - a crude oil and natural gas drilling project, with an indication of a second use for geothermal energy, and Slovenia, with a pilot geothermal power plant on an existing gas well Pg08 in the village of Čentiba. The geothermal power plant, with an electrical power of 50 kWe, will provide 400 MWhr of electricity annually. Active or recent active geothermal energy systems operating from old oil wells seem to be restricted to Austria, Croatia, and Hungary.

In Croatia, the only ORC power plant. in the field Velika Ciglena, was originally drilled and equipped for hydrocarbon exploration. After discovering the geothermal reservoir, exploratory wells were added to the geothermal field and are now used for electricity generation. In addition, the geothermal fields Ivanic and Bizovac are examples where hydrocarbon exploratory wells are used for geothermal exploitation. The Ivanić field still remains to have wider applicability, however, the town is interested in using this potential for district heating, as well as adding new potential once the oil field is out of commission and using remaining wells. The Bizovac geothermal potential is another example and adds to the development of the town since the geothermal energy is used in balneology in the Bizovac hotel and spa complex. Some reuse projects are currently in the planning phase. All these exploration fields lie on medium-enthalpy resources, for example, the Lunjkovec-Kutnjak exploration field, in which the measured temperatures at the bottom of the wells range from 128 °C to 144 °C. The first phase of the project involves the ORC power plant of 2MWe, which will use geothermal brine from already existing wells. It is expected that thermal energy for heating in the future development of the project will be around 90 MWt. Other sites that are planning to re-use existing wells if overall exploratory phase goes positive are Merhatovec, Slatina and Babina Greda.

Recently, a reference project is ongoing for the Szentes geothermal field near the city of Szeged. Being one of the most active geothermal fields in Hungary, it currently has 32 active production wells and many abandoned ones that could be repurposed for geothermal.

For the geothermal extraction and utilization projects, the integrated risk/opportunity assessment and management requires complex steps conducted in a systematical framework, mainly including identification, assessment and ranking of events and associated actions (Yuan & Wood, 2018). The detailed workflow (Figure E 9) involves integrating qualitative, semi-quantitative, and quantitative risk and opportunity assessment of oilfield geothermal energy production actions and other potential risk sources, using a range of analysis tools, and applying performance indicators monitored for rigorous and holistic risk and opportunity management of oilfield geothermal projects. During oilfield geothermal projects, to identify and recognize risk and opportunity factors, extensive data from laboratory and field data in multiscale (including single well tests, pilot studies involving water injection and production well practice, and associated thermal energy utilization testing) are required (Yuan, B., & Wood, D. A. 2018).

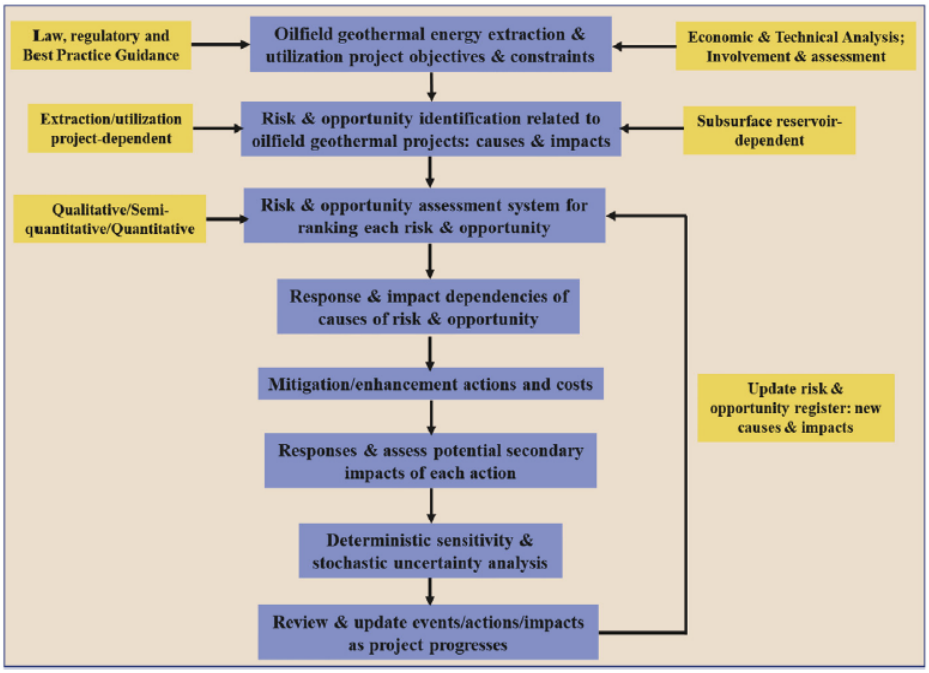

Figure E 9: An integrated workflow for risk and opportunity identification, assessment, and management of oilfield geothermal energy projects (Yuan and Wood, 2018).

E.4. Numerical simulation

The Szentes region is the largest and one of the oldest geothermal fields in Hungary. Geothermal operations started in the area more than 50 years ago. Due to the high production of thermal water from 45 wells, by the early 1990s the hydraulic water level in the aquifers had dropped by 25-40 m. Initially, most wells flowed freely up to 50 m, but nowadays the wells require continuous pumping. Currently there are no reinjection wells at all. A numerical model, based on pressure measurements and calibrated using data from wells in the area, was developed during the study to investigate the recharge process and the sustainability of the system.

The model was used to demonstrate that even a single injection well has a beneficial effect on reservoir recharge.

We have prepared our hydrodynamic model according to the above-mentioned aspects, taking into account the surrounding wells, the requirements of the relevant Hungarian regulations (Annex 2, point I/A of the Decree 18/1996 (VI.13) of the Hungarian Ministry of Health and Welfare, and the Government Decree 147/2010 (IV.29.). 4§ (3) a)-e).

It should be noted, however, that if a hydrocarbon exploration company such as MOL (Hungarian Oil Company) wants to use its own wells for geothermal purposes, it has much more sophisticated options, as it has a detailed geological model itself, including a database of measurements on which the model is based, that allows for hydrocarbon production. An experiment of this kind is presented by Abdulhaq et al. (2024). The study combined Multi-Criteria Decision Analysis (MCDA) with an Analytic Hierarchy Process (AHP) to decide how to reuse abandoned hydrocarbon wells. Reservoir parameters analysed geostatistically with an

integrated Pyton scripting and on the basis of stochastic simulation were identified the potential zones and their categories of suistainability.

E.4.1. Method

The hydrodynamic calculations were performed using the Processing MODFLOW Pro environment. The software is one of the MODFLOW clones, which is an internationally accepted version, similar to other clones (Visual MODFLOW, GMS, GW Vistas, MODFLOW-SURFACT, Processing MODFLOW for Windows, etc.), has extensive calibration references, supports more MODFLOW packages than other clones, and is well compatible with Surfer for Windows map editing and spatial modelling software. For modelling, Processing MODFLOW Pro software version 8.0.43 (© Simcore Software 1991-2013) was used.

Hydrodynamic calculations were performed using the public domain USGS versions of MODFLOW-96 and MODFLOW-2000. The PMPATH program version 8.0.42 (©W-H. Chiang & W. Kinzelbach, 1994-2002) was used to view and interpret the results and to determine the streamlines and path times. Surfer for Windows version 25.2 (© Golden Software Inc., 1993-2023) was used to edit the maps and perform interpolations from local data. To draw graphs, fit curves and determine the equations of fitted curves, we used Grapher for Windows version 21.2 (© Golden Software Inc., 1992-2023). The environment used is the internationally and nationally accepted computational framework, which uses finite difference solutions of the basic leakage equation[1] and finite difference and characteristic solutions of the transport equation.

Although not presented in detail later, a petrophysical model of the Szentes geothermal field has been prepared. The software used to analyse the correlation between wells and petrophysical facies was CycloLog. The conventional stratigraphic analysis approach is generally empirical. CycloLog is a standalone software that provides an analytical tool developed to help the well-log correlation while ensuring a data-driven and unbiased result when compared to model driven interpretation (Van der Vegt & Vinci, 2021). It uses the concept of Walters facies rule saying that the vertical variation in strata is controlled by known processes and is therefore predictable. The software contains several interesting applications, but the one highlighted here is the INPEFA ® (Integrated Prediction Error Filter Analysis) Log transformation, which is a subsurface tool for the analysis of vertical variations in the log data using a spectral analytic method to transform standard wireline log data. In this way, normally unseen information from routine log data can be extracted (Castro, 2022).

E.4.2. Reference site Szentes 8

For hydrothermal systems, especially when talking about abandoned oil and gas wells, we usually have to look at a pool of wells (or a pay zone, or a field). This means that it is not enough to look at one producing well and one injection well, but to look at the impact of production and injection on the entire reservoir. The modelling study has been carried out on this basis for the geothermal field in Szentes and contains a hydrodynamic simulation of a re-used hydrocarbon exploration well as geothermal production well and a newly drilled injection well and considers surrounding wells.

[1] The basic relation describing leakage is Darcy's law; this is combined with the continuity equation for the mass conservation of fluids flowing in a porous medium to give the basic equation for leakage. The resulting partial differential equation can be written in a slightly different form for permanent and non-permanent saturated medium flow, and can even be extended to unsaturated medium leaks.

E.4.3. Site description

The study area is located in the region of Szentes, in the southern part of the Hungarian Great Plain, on the left bank of the Tisza River, at an elevation of about 81-85 m above Baltic sea level. (Figure E 10). The geological structure of the area is determined by the sedimentary characteristics of the Hungarian Great Plain.

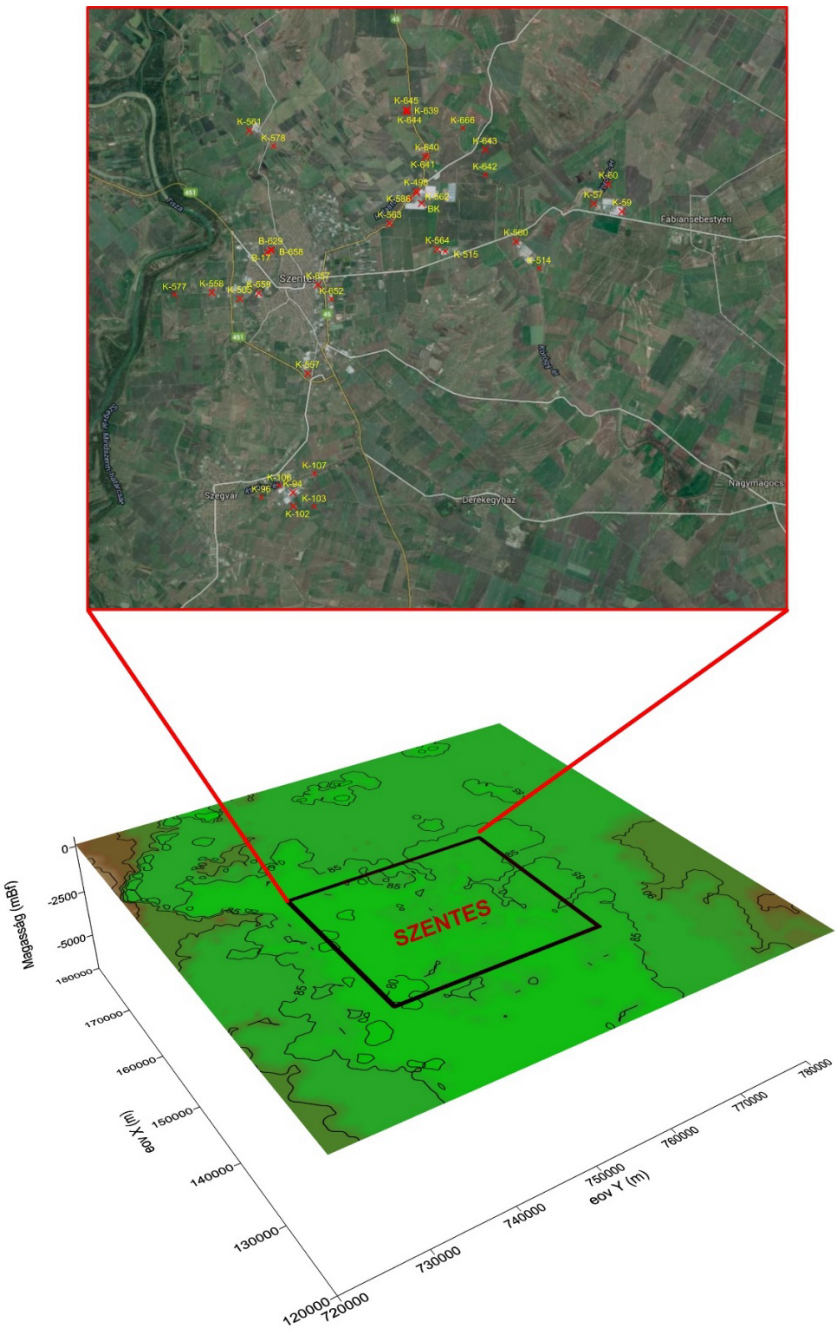

Figure E 10: Topography of the investigated area with the Geothermal wells.

The area under study belongs to the northern part of the structural geological unit known as the Makó Trench, where the basin of the Hungarian Great Plain is 3000-5000 m deep. A map of the bedrock elevation

in the wider area is shown in Figure E 11. The basin subsided at different rates over time, starting in the Miocene, when marly, aleuritic sediments typically accumulated in the basin. However, the most intense phase of subsidence occurred during the Pannonian period, resulting in a total thickness of sediments deposited in the Miocene of more than 4000 m, which are the result of sediment accumulation in the Pannonian Sea.

The sedimentation of the lower Pannonian is characterised by the predominance of clay-lime-marl and very fine quarzitic layers. The amount of coarser sandy material is relatively small compared to the sediment accumulation of the Upper Pannonian. The upper 300-400 m thick part of the sand-sandstone of the Danubian Formation Group (formerly called Upper Pannonian) contains mainly unconsolidated sand layers. While the deeper layers are of more consolidated sandstone development. The sandstones are subdivided by clay-aleuritic, lignite-rich layers deposited in deltaic plains, marshes and small bays.

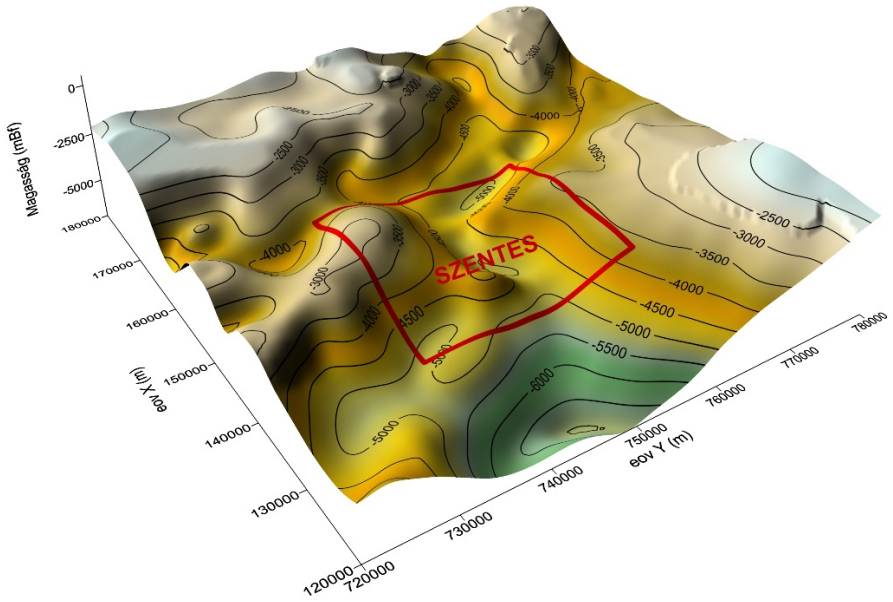

Figure E 11: Map of the Preneogene bedrock in the vicinity of the study area.

The lower boundary of the Transdanubia Formation Group (Upper Pannonian layers) lies between 2000 - 2500 m depth in the area, with a deepening trend from Szentes towards Szegvár (Figure E 12). The shallow marine, deltaic sediments are overlain by a finer sedimentary layer called the Levantien, which is covered by Pleistocene sediments. The Pleistocene fluvial layers, which are 400-600 m thick, develop from the Upper Pliocene overburden with sediment continuity. Coarse and medium-grained alluvium was formed in the Lower and Middle Pleistocene. The Upper Pleistocene sedimentation is characterised by a predominance of fine-grained sediments, with a predominance of clayey-silty sediments. A map of the depth of the Pleistocene sedimentary deposits is shown in Figure E 13.

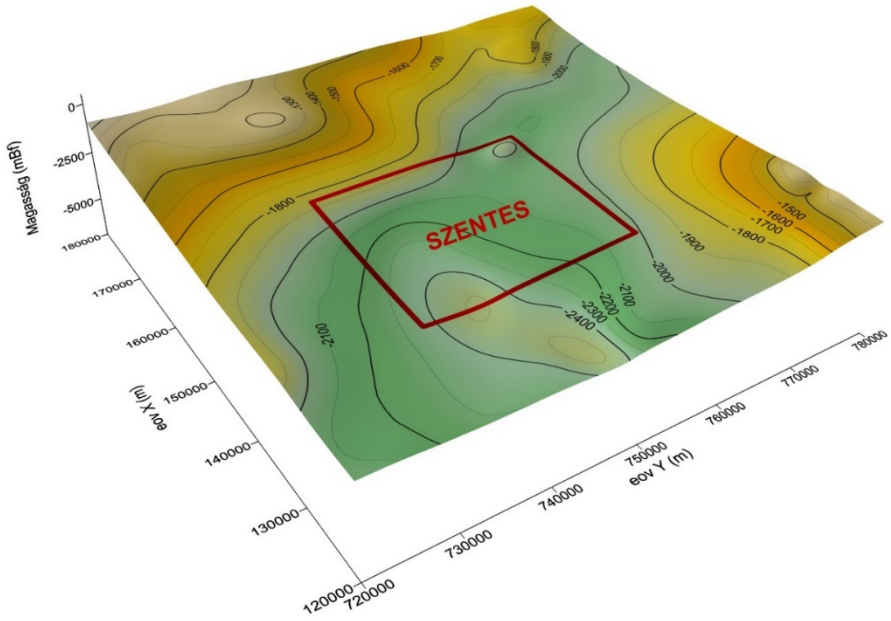

Figure E 12: Bedrock map of Upper Pannonian age formations in the vicinity of the study area.

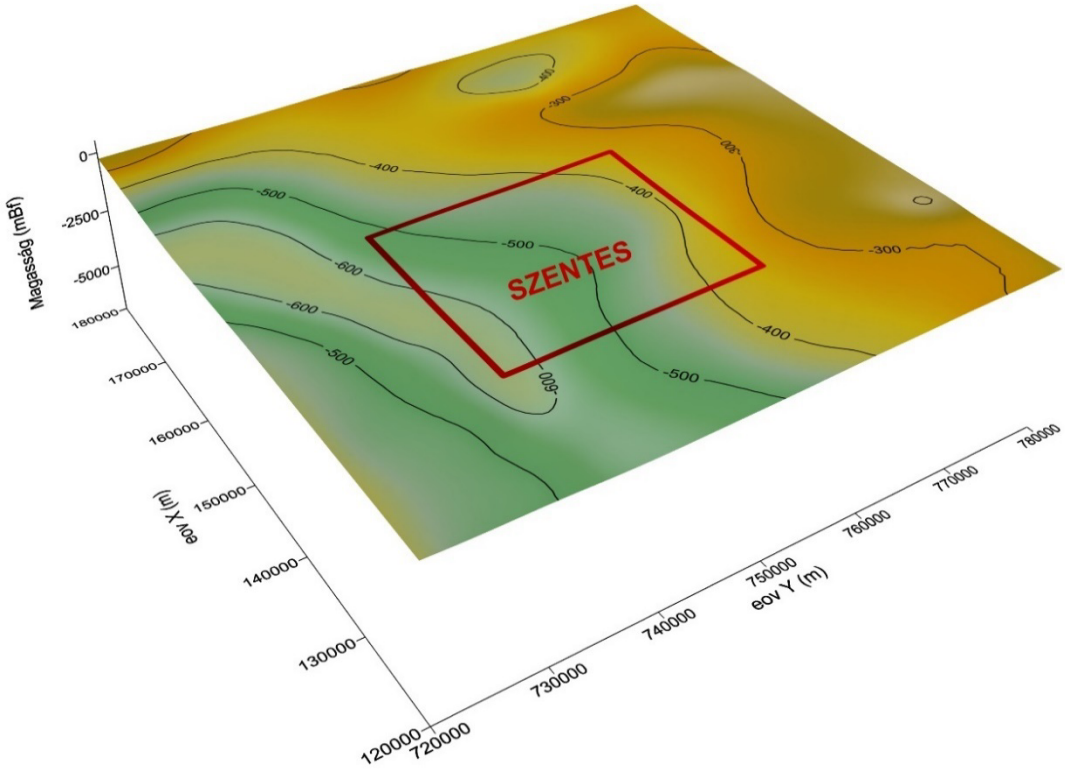

Figure E 13: Landscape map of Quaternary formations in the vicinity of the study area.

From the hydrogeological point of view, three major aquifer groups can be distinguished in the Szentes area. The first is the thick Quaternary aquifer, whose sandy, sometimes gravel layers also provide a significant part of the country's drinking water supply. In the area, the sand layers of the Lower-Middle Pleistocene, at a depth of 500-550 m, already yield warm thermal water. The sand layers forming the alluvium are good aquifers, with a sand content of over 50 % and a permeability of 1500 mD. The second aquifer is the sediments of the Levantian, which have a lower sand content (30-40 %) and a lower permeability (500 mD).

The main hydrothermal system is the sand-sandstone layers of the Upper Pannonian Újfalu Formation, which are hydrodynamically linked to the overlying layers. The Újfalu Formation is mainly fine to medium-grained sandstones with interbeds of clayey marl and aleurolite deposited in the delta front, delta plain environment. Fine-grained, aleurolite and clayey marl occur only in thinner layers, indicating that the rate of sedimentation and deposition was rapid, and therefore the delta front and delta plain cannot be separated from each other, but can only be classified as a single lithofacies unit.

The emerging sandstone bodies are of estuarine reef, deltaic basin fill and barrier reef origin. The fine-grained sediments of smaller thickness deposited between the sand bodies are mainly deposited between the deltaic, marsh-arroyal, lagoonal and bed-edge displacements or developed in the cutoff meander, or shallow Gulf of Brackwater. In the upper part of the formation, deposits of lignite and brown coal appear above the basement fillings.

In the vicinity of the study area, the sandstone layers of the Újfalu Formation were exposed in three (more or less distinct) depth ranges (Figure E 14).

- Upper layer (level A): filtered layers up to 1500-1800 m
- Middle layer (level B): filtered layers up to 1800-2000 m
- Lower layer (level C): filtered layers below 2000 m

The permeability of the well-conducting sand layers varies between 1000-2000 mD, with a sand fraction of 25-30 %. The shallower depths of the uppermost "A level" are less produced, but rather the well filters start from 1600-1650 m. The exception is the Szentes Strandfürdő (well B-693), which was drilled in 2015 and which has filtered sections from 1437 m to 1610 m. The 2 wells investigated in the present study, although filtering below each other[2], fall on the bottom of the middle layer (B) and on top of the bottom layer (C).

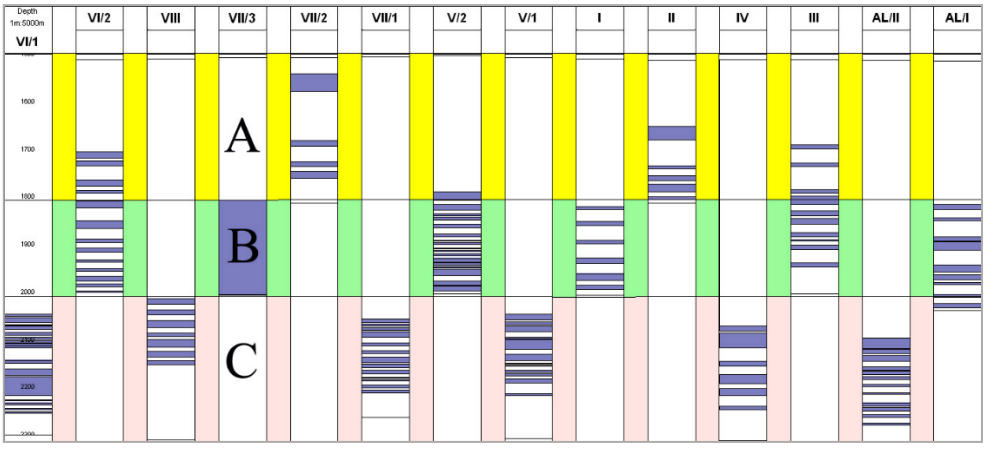

Figure E 14: Árpád-Agrár Zrt. perforated sections of wells at the Szent László site with indication of layer groups.

[2] filter sections in different reservoir layers

The pressure conditions in the study area are characterised by the fact that both in the Quaternary formations and in the Upper Pannonian layers the pressure is higher than the hydrostatic pressure, so the study area belongs to the outflow zone (Figure E 15). Figure E 15 shows the water level data of the wells in the Szentes area at the time of construction as a function of depth, which shows that the pressure in the Quaternary formations is 0.13 MPa higher than the hydrostatic pressure, while at the bottom of the Upper Pannonian it is 0.44 MPa higher. That is, in the natural state, the pressure increases with increasing depth, the pressure near the surface is hydrostatic, while at the bottom of the upper Pannonian the hydrostatic pressure exceeds the potentiometric pressure by approximately 40 m.

According to Almási (2001), the direction of seepage in the water reservoirs is E - W, due to recharge from the Maros alluvial cone, which is also confirmed by the Altnőder-Liebe stratigraphic water level map (Figure E 16). The Pleistocene and Pannonian strata show the same orientation.

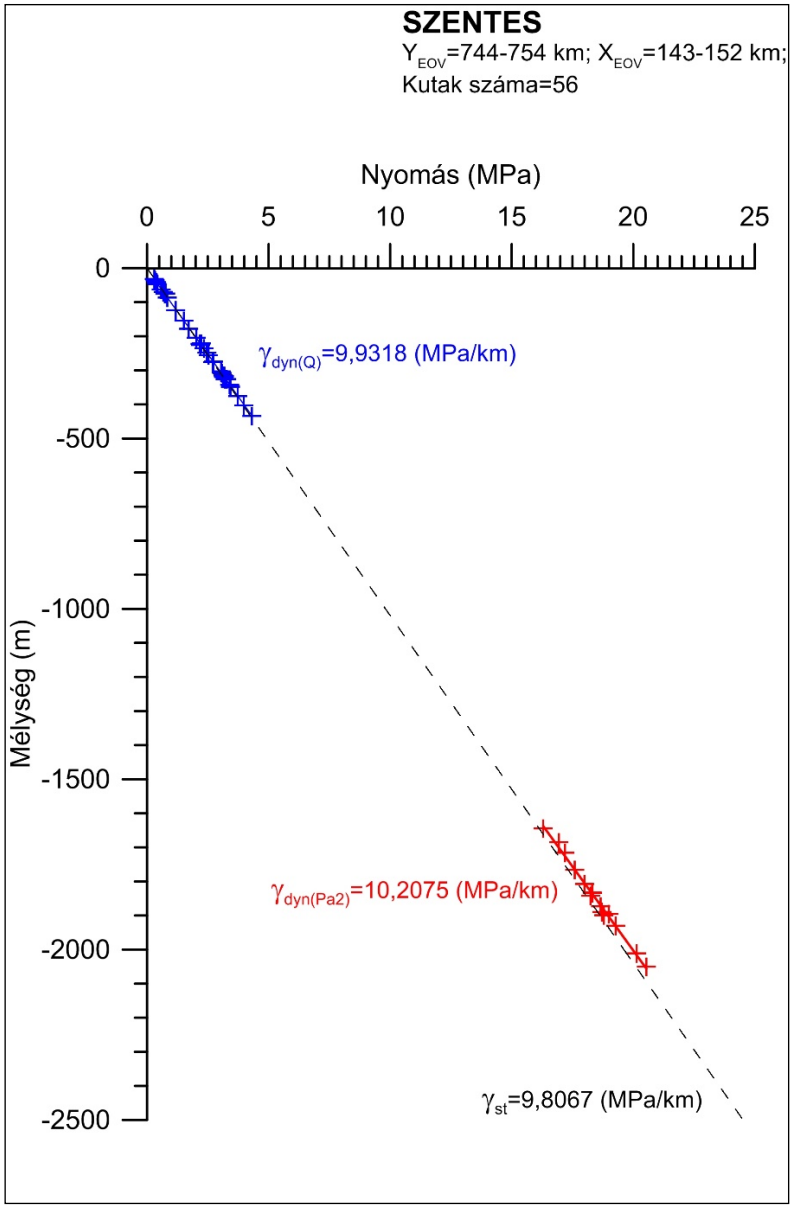

Figure E 15: Pressure-depth data from wells around Szentes (“mélység” means depth, “nyomás” means pressure).

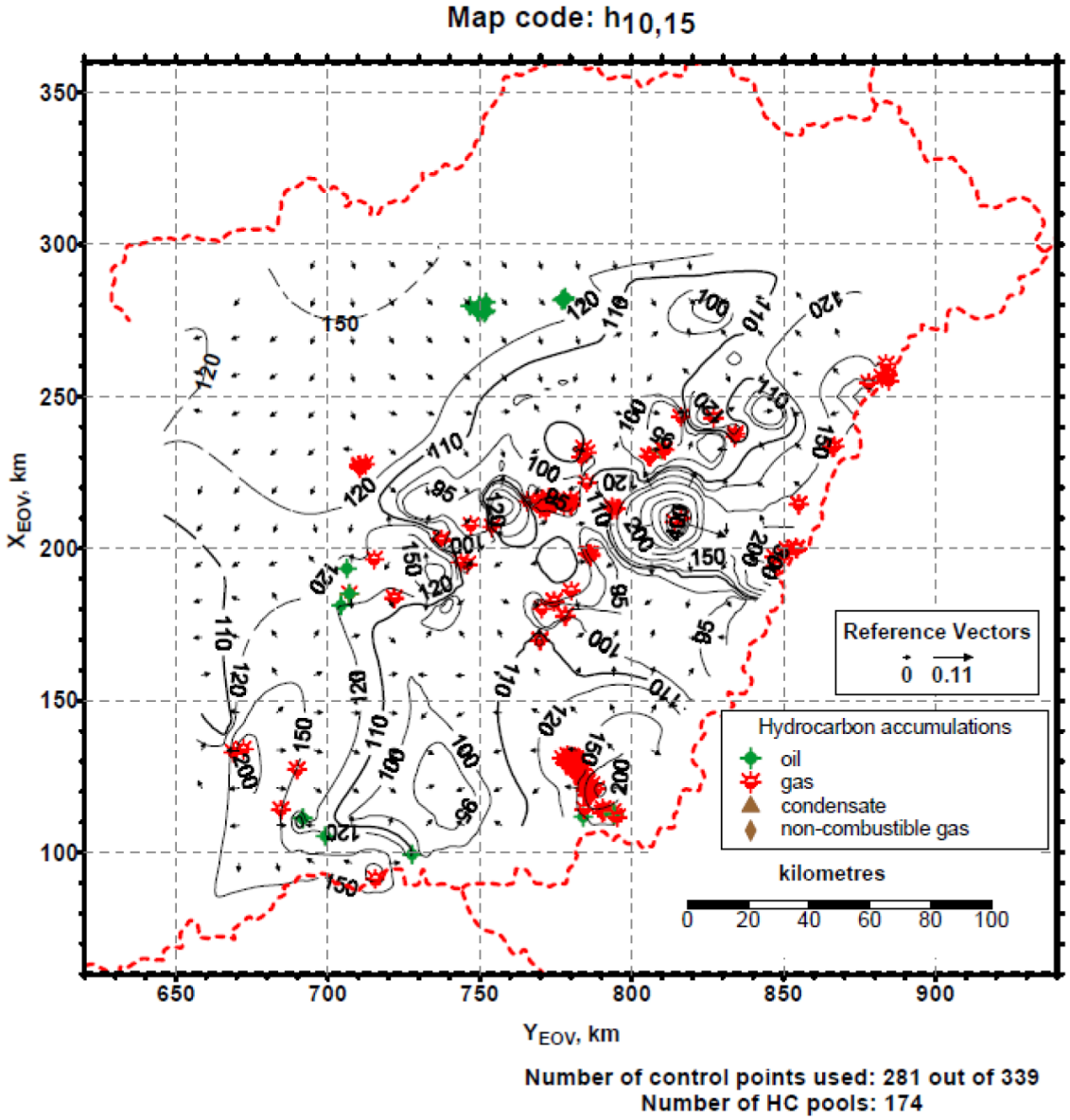

Figure E 16: Hydraulic head (in m a.s.l.), flow vectors and commercial hydrocarbon reservoirs in Szentes (Almási, 2001).

The regional hydrodynamic characteristics of the well environment were determined on the basis of complex well test measurements carried out in cooperation with Geo-Log Ltd. in the framework of the National Technology Programme (No. TECH. 08 A4 DA THERM) between 2009 and 2011. For the determination of the data of the 3 main stratigraphic groups, the most suitable data were the interaction test, the capacity test and the backfill measurement carried out on 3 wells of the Árpád-VII well group (K-644, K-639, K-645). The interaction test series consisted of detecting the wells during cyclic production in the monitoring wells. In this case, 6 production shutdowns were performed in well K-645. The planned 12 hours of production were followed by 6 hours of shutdown. Based on the evaluation, the hydrogeological parameters of the upper stratum (level A), middle stratum (level B) and lower stratum (level C) are given in Table E 6, Table E 7, and Table E 8, respectively.

Abbreviations	Hydrological parameters
$Q_{ü}$ - water flow before shutdown	1131,8 m^3/d
s - depression	4,74 m
q - specific water yield	239 $m^3/d/m$
k - permeability	$5638 \cdot 10^{-3}$ μm^2
K - hydraulic conductivity	13,0 m/d
T - transmissibility	701 m^2/d
S - storage factor	$99.5 \cdot 10^{-6}$
n_0 - porosity	0,25
a - piezo conductivity (diffusivity)	$7,05 \cdot 10^6$ m^2/d

Table E 6: Hydrogeological parameters of the upper stratum (level A).

Marking and naming	Hydrological parameters
$Q_{ü}$ - water flow before shutdown	1307,5 m^3/d
s - depression	10,2 m
q - specific water yield	128 $m^3/d/m$
k - permeability	$566 \cdot 10^{-3}$ μm^2
K - hydraulic conductivity	1,71 m/d
T - transmissibility	104 m^2/d
S - storage factor	$113 \cdot 10^{-6}$
n_0 - porosity	0,21
a - piezo conductivity (diffusivity)	$0,922 \cdot 10^6$ m^2/d

Table E 7: Hydrogeological parameters of the upper stratum (level B).

Marking and naming	Hydrological parameters
$Q_{ü}$ - water flow before shutdown	1375,2 m^3/d
s - depression	19,7 m
q - specific water yield	69,8 $m^3/d/m$
k - permeability	$340 \cdot 10^{-3}$ μm^2
K - hydraulic conductivity	1,22 m/d
T - transmissibility	99,8 m^2/d
S - storage factor	$154 \cdot 10^{-6}$
n_0 - porosity	0,2
a - piezo conductivity (diffusivity)	$0,647 \cdot 10^6$ m^2/d

Table E 8: Hydrogeological parameters of the upper stratum (level C).

The wells were also tested under the National Technology Programme. In the wider Szentes area there are currently 45 hot water wells, of which 35 operating wells in the study area were considered in the modelling (Figure E 17). The data on these wells at the time of their construction are shown in Table E 9.

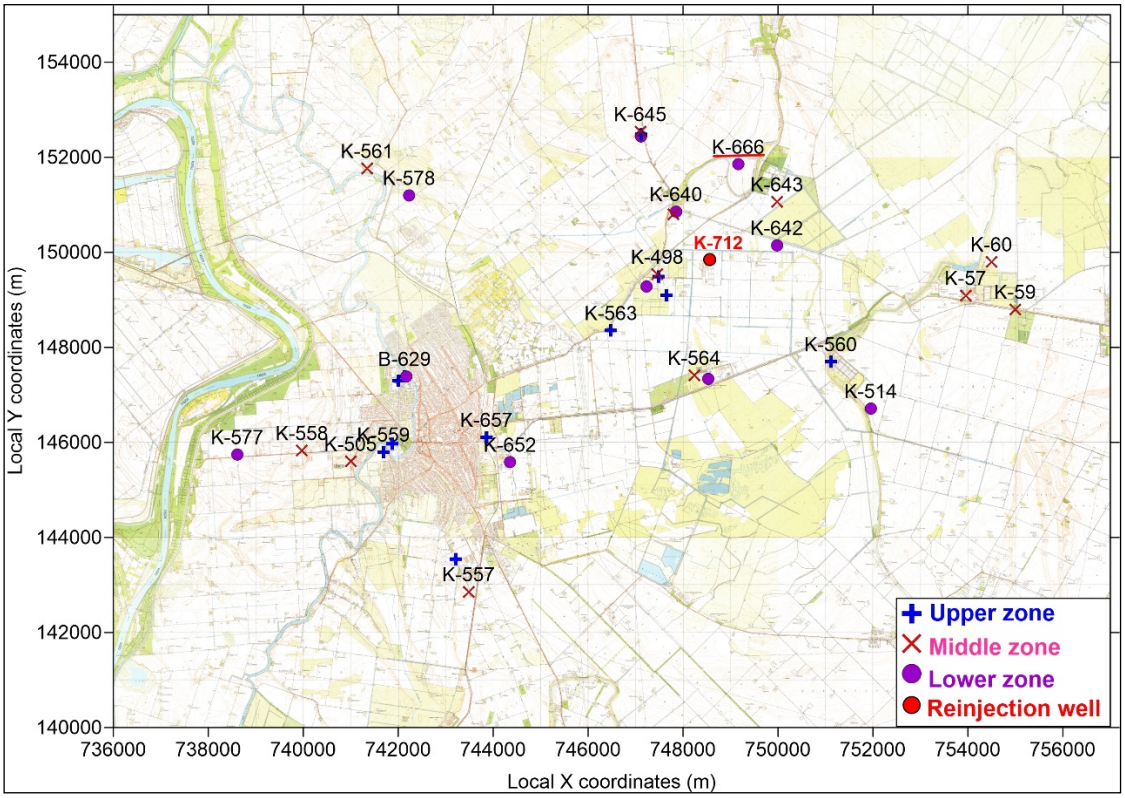

Figure E 17: Thermal wells in the Szentes area.

Cadastral number	EOV Y [m]	EOV X [m]	Bottom [m]	Filter top [m]	Filter bottom [m]	Production [m3 /year]	Model layer
K-561	741347	151764	2025	2025	1801	256000	19, 21
K-578	742231	151198	2401	2083	2266	256000	23
K-562	747489	149493	1798,5	1640	1793	150850	13, 15, 17
K-640	747855	150857	2239,5	2046,5	2209,3	134800	23
K-643	749982	151063	1998	1694	1989	189000	17, 19, 21
K-644	747112	152442	2257	2053	2205	156900	23
K-498	747458	149539	1995	1809	1983	154860	17, 19, 21
K-563	746484	148355	1992,5	1678	1936	170150	15, 17, 19
K-586	747234	149283	2303	2060	2235	178604	23
K-641	747800	150800	2000	1785,5	1993	155100	17, 19, 21
K-642	749981	150148	2398	2046	2255,5	172500	23
K-639	747111	152480	1806	1534	1755	174300	13, 15, 17
K-645	747101	152539	1999	1800,5	1998,7	194100	17, 19, 21
K-666	749166	151854	2893	2004	2143	131400	23

Cadastral number	EOV Y [m]	EOV X [m]	Bottom [m]	Filter top [m]	Filter bottom [m]	Production [m3 /year]	Model layer
BK	747655	149100	1450	1320	1450	130000	9
K-557	743485	142855	2000,5	1755	1995	200000	17, 19, 21
B-658	742169	147389	2344,7	2093,7	2300,7	255000	23
K-657	743863	146106	1997	1674,5	1885,5	110000	15, 17, 19
K-514	751957	146712	2199	1829	2192	125000	19, 21, 23
K-560	751114	147698	1815	1593	1776	125000	13, 15, 17
K-60	754500	149800	2190	1603	2065	150000	17, 19, 21
K-59	755000	148800	2001	1751	1994	69100	17, 19, 21
K-505	741000	145600	2004	1850	1952	182500	19, 21
K-558	739973	145828	2001	1803	1984	182500	17, 19, 21
K-577	738612	145745	2500	2187	2323	219000	23
K-559	741695	145797	1796	1631	1699,5	146000	13, 15
K-652	744358	145584	2346	2006	2329	255000	23
B-17	742000	147300	1725	1633	1720	300000	11, 13
B-629	742136	147388	1593	1329	1510,18	166000	9
K-57	753956	149091	2004	1736	1929	69133	17, 19, 21
K-515	748528	147342	2203	1928	2172	250000	21, 23
K-564	748239	147413	1900	1690	1843	150000	15, 17, 19
B-693	741875	145973	1700	1437	1610	360000	9, 11
K-711	743214	143547	1765	1541	1753	220000	11, 13
K-712	748465	149886	2000	1931	1981	131400	21

Table E 9: Data of the hot springs in the Szentes area at the time of construction and layers in the numerical model.

E.4.4. Historical data – Sz-VIII and Sz-1

The well selected for production was Sz-VIII (Sz-ÉK-1). The injection was modelled to be into well Sz-1. The main parameters of the two wells and their variation over time are shown in Table E 10.

	Sz-VIII (Sz-ÉK-1 CH exploration well)	Sz-1 (new geothermal well)
Cadastral Nr.	K-666	K-712
Year of the drilling	1987	2020
EOV X	151 854.77	149 885.75
EOV Y	749 166.02	748 464.66
Z	84.48 mabsl[3]	83,42 mabsl

[3] meter above Baltic sea level

Drilled depth (MD)	3400 m	2000 m
Casing depth	2893 m	1998 m
Final bottom	2605 m (cement plug)	
Usable bottom	2275 m (OKTF (2006))	

Table E 10: Main data of two wells

E.4.4.1. Szentes Sz-VIII. (Sz-ÉK-1) well history

Tables E 11-E 19 and Figure E 18 summarise the completion and history of well Sz-VIII.

Sz-VIII (Sz-ÉK-1)					
Nominal well construction	**diameter**		**Position**		**Type**
stand of pipe	**outer**	**inner**	**top**	**bottom**	
I.	473,1	?	0	51,5	steel
II.	399,8	317,9	0	499	
III.	244,9	228,5	0	1799	
IV.	177,8	159,4	706	2893	

Table E 11: Sz-VIII (Sz-ÉK-1) well completion data.

Opened layers	**diameter**		**Position**		**Type**
	outer	**inner**	**top**	**bottom**	
I.	177,8	159,4	2004	2015	perforation
II.	177,8	159,4	2027	2038	
III.	177,8	159,4	2049	2064	
IV.	177,8	159,4	2076	2084	
V.	177,8	159,4	2090	2105	
VI.	177,8	159,4	2115	2126	
VII.	177,8	159,4	2134	2143	

Table E 12: Sz-VIII (Sz-ÉK-1) open (perforated) layers.

Previous production data	**discharge** [l/min]	**water level** [m]	**pressure in 2270 m** [bar]	**well capacity** [l/min/m]	**water T in wellhead** [°C]	**other data**		
original state - 1988	0	13		–	–	BHT (2200 m)	112	°C
	800	-20,8		23,74	90	Spec. CH4 volume	13	l/m^3
OKTF - 2006	0	15	213,99	–	–	Bottom	2275	m
	360	–	213,34	–	–	BHT (2275 m)	115,5	°C

	670	–	212,87	–	–			
	1070	–	212,31	–	97	backblowing in	142	m

Table E 13: Sz-VIII (Sz-ÉK-1) well history, workover activity 1.

Geo-Log Ltd. - 13 and 20-22.04.2010 Event log			
Date	**Time**	**Discharge**	**Activity, notes**
2010.03. month			shutdown at the end of the heating season
2010.04.20	4:30–		Start production
2010.04.20	10:00–15:00		installation, installation of flow meter
	15:10–16:10		replacement of failed flow meter
	16:10–17:10		KPT-02 probe installation at 2000 m depth
	17:10–19:15	196	Q1 yield step, with free flow, followed by compressor
	19:15–21:15	416	Q2 yield step with compressor
	21:15–		
2010.04.21	–09:22	717	Q3 yield step with compressor
	09:23–11:23	0	Measurement of pressure rise
	11:23–12:27	725	Production before pressure gradient measurement
	12:27–16:10	725	Pressure gradient and temprerature logging
	16:10–17:00		Deployment of KPT-02 probe
	17:00–18:00		FTRmO-43/053 probe installation
	18:00–22:00	716	Flow measurements
	22:00–23:20		Deployment of FTRmO-43/053 probe
2010.04.22	08:30–10:30		dismantling, unpacking

Table E 14: Sz-VIII (Sz-ÉK-1) well history, workover activity 2 (Geo-Log Ltd, 2010).

Geo-Log Ltd. - 13 and 20-22.04.2010		
Bottom	2261,2	m
BHT (2261,2 m)	113,8	°C

Table E 15: Sz-VIII (Sz-ÉK-1) basic data in 2010.

produced layer	**discharge**	**water level**	**pressure in 2000 m**	**water T in wellhead**	**water T in deep**	**surface depression**	**deep depression**
	[l/min]	**[m]**	**[bar]**	**[°C]**	**[°C]**	**[bar]**	**[bar]**
closed (production for 120 min)	0	8,5	190,228	–	104,6	–	–
Q1 (production for 120 min)	196	24,28	190,114	78	105,6	–	0,115
Q2 (production for 140 min)	416	24,99	189,699	82	105,6	–	0,529

Q3 (production for 700 min)	717	19,91	189,075	91	105,5	–	1,153

Table E 16: Sz-VIII (Sz-ÉK-1) production data in 2010.

Discharge rate within filters			
filter	**perforation**	**discharge**	
	[m]	**[l/min]**	**[%]**
I.	1998,2–2009,2	20	3
II.	2021,2–2032,2	390	55
III.	2043,2–2058,2	20	3
IV.	2070,2–2078,2	10	1
V.	2084,2–2099,2	135	19
VI.	2109,2–2120,2	50	7
VII.	2128,2–2137,2	90	13
Sum:	**80 m**	**715**	**100**

Table E 17: Sz-VIII (Sz-ÉK-1) production data by perforation in 2010.

Calculated parameters			
equation of calculated discharge	$Q = 3300\ \Delta p^{0.56}$		
effecitve permeability of well	k_s	$511{,}4 \cdot 10^{-15}$	m^2
effecitve permeability of production zone	k	$404{,}2 \cdot 10^{-15}$	m^2
productivity factor [-] (	PF	1,27	
geothermal gradient	GG	21,49	m/°C
gas/water ratio	GWR	199	l/m^3
Spec. CH_4 volume (2011)	SMV	82,5	l/m^3

Table E 18: Sz-VIII (Sz-ÉK-1) calculated parameters 2010.

Rotaqua 04-05.05.2020 - cement column checking	top	bottom	
probe - KAEH-43/8436 & KAS-2-43T/84249	1696 m	2135 m	
Rotaqua 04-05.05.2020 - injection	BHT (2260,8 m)	115,2	oC
	layer	top-bottom	injected water
		[m]	[l/min]
	II.	2022,0–2025,0	505
	V.	2090,0–2098,0	55
	VI.	2112,5–2116,0	20
	VII.	2128,0–2133,5	30

Test1 - 08.05.2020 – 12.05.2020	All perforations are tested (I-VII) with water		
Test2 - 23.05.2020 – 24.05.2020	Perforation interval II is tested with water		
Minifrac test on 24.05.2020			
Test3 - 24.05.2020 – 25.05.2020	Perforation interval II is tested with water		
Injection of gel + proppant sand on 28.05.2020			
Test4 - 28.05.2020 – 29.05.2020	Perforation interval II is tested with water on		
Acidization treatment on 03.06.2020			
Test5 - 04.06.2020 – 08.06.2020	Perforation interval II is tested with water		
Water production between 09.06.2020 and 12.06.2020			
Test6 - 13.06.2020 – 16.06.2020	Perforation interval II is tested with water after production		
Frack&Pack treatment on 30.06.2021			
Test7 - 03.07.2021 – 07.07.2021	Perforation interval II is tested with water after Frack&Pack		
effecitve permeability of well T2 experiment	k_s	$6639 \cdot 10^{-15}$	m^2
effecitve permeability of production zone T2 experiment	k	$8487 \cdot 10^{-15}$	m^2
effecitve permeability of well T3 experiment	k_s	$6013 \cdot 10^{-15}$	m^2
effecitve permeability of production zone T3 experiment	k	$8684 \cdot 10^{-15}$	m^2
effecitve permeability of well T5 experiment	k_s	$785{,}5 \cdot 10^{-15}$	m^2
effecitve permeability of production zone T5 experiment	k	$194{,}5 \cdot 10^{-15}$	m^2
effecitve permeability of well T6 experiment	k_s	$10553 \cdot 10^{-15}$	m^2
effecitve permeability of production zone T6 experiment	k	$9470 \cdot 10^{-15}$	m^2

Table E 19: Sz-VIII (Sz-ÉK-1) well history, workover activity 3 (Rotaqua/Geo-Log Ltd., 2020-21).

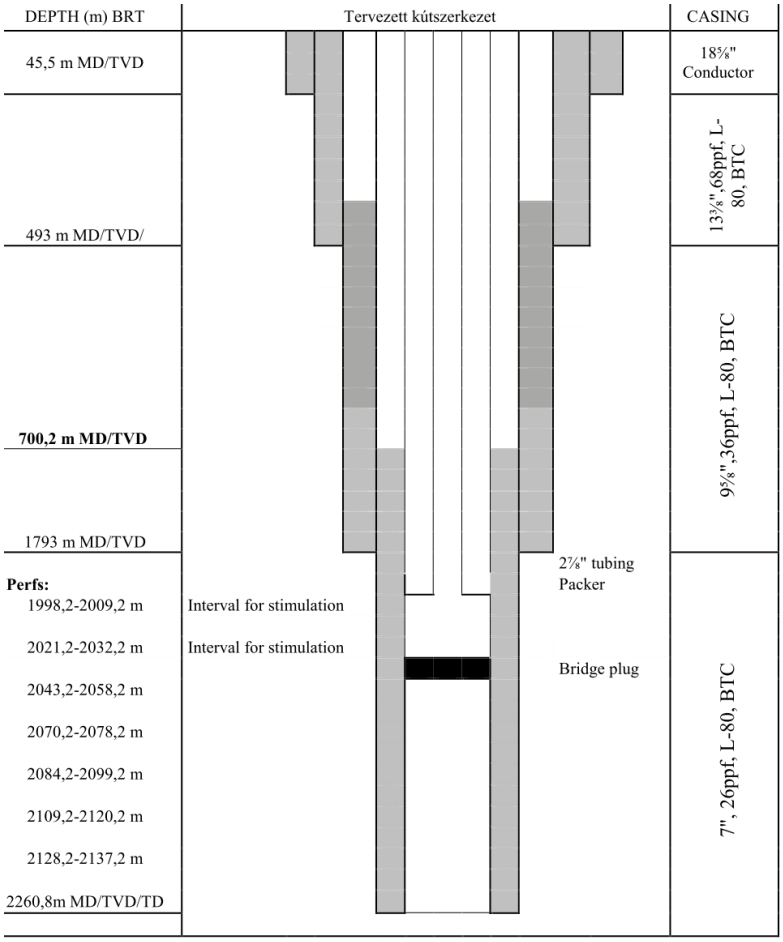

Figure E 18: Well data and planned simulation intervalls.

E.4.4.2. Szentes Sz-VIII. (Sz-ÉK-1) well history

Well Sz-1 was originally designed and registered as an injection well. The details of the production/injection data are the property of the Árpád-Agrár Zrt., Szentes.

Layer: 1934,0-1981,4 m upper-pannonian unconsolidated sandstone, marl

Discharge: 0 l/min

Water level (initial piezometric level): 2.75 m

Wellhead temperature: 84.1 oC

Bottomhole temperature: 101,7 oC

Spec. CH4 volume: 0.8-10 l/m3

TDS: 1-5 g/l

E.4.5. Model setup

The modelled area is 21x15 km, with the wells in the middle. The grid is oriented parallel to the main flow direction of the aquifer. The EOV coordinates of the model corner point are as follows: 736000, 140000; 757000, 140000; 757000, 155000; 736000, 155000.

The model was horizontally subdivided into 100x100 m elements, and the grid was progressively refined into 20x20 m elements near the wells (Figure E 19). The area was vertically subdivided into 23 layers from the surface to the base of the Transdanubian Formation Group (called the Upper Pannonian layers), based on the stratigraphic sequence of all Upper Pannonian wells and the filtered levels. The modelled area was assumed to be impermeable from below, given the more clayey layers of the Alföld Formation Group (formerly called Lower Pannonian). In the uppermost model layer, the cold aqueous Pleistocene strata were merged, resulting in a more detailed vertical resolution in the hot water bearing formations. The first model layer was overlain by the surface levels.

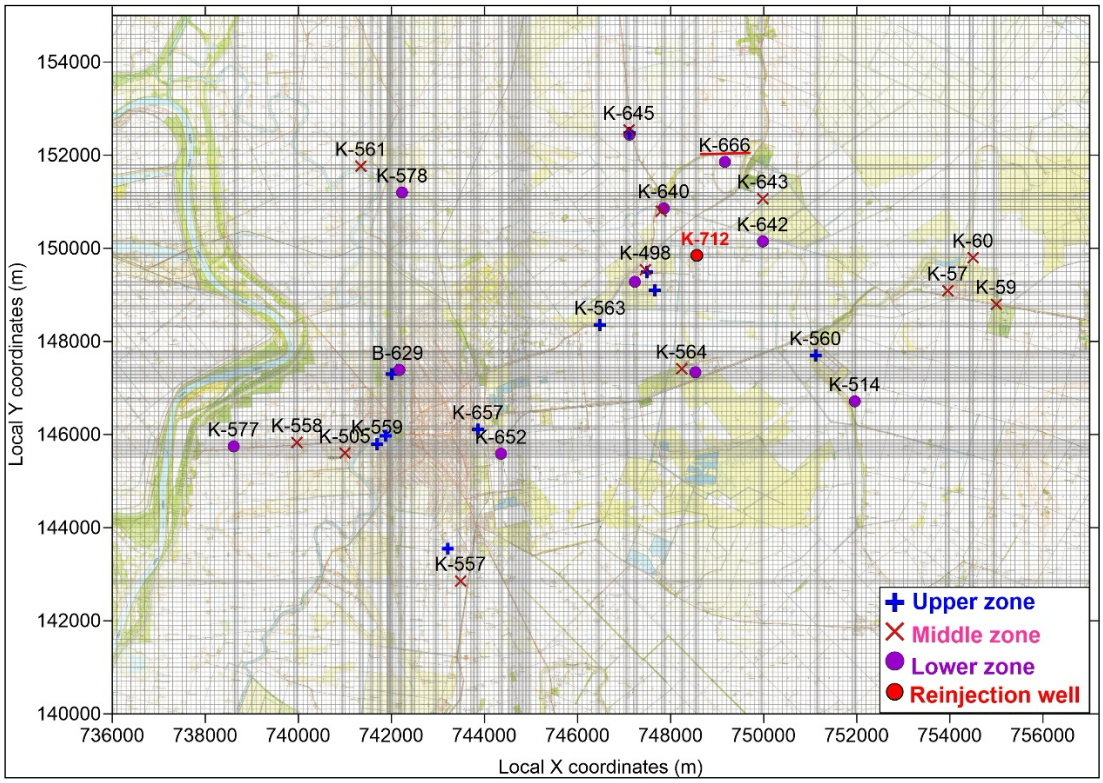

Figure E 19: Discretization of the numerical model.

The Quaternary and bedrock distributions of the Danubian Formation Group (formerly Upper Pannonian), presented in the geological setting, were also incorporated into the model. Thus the quaternary bedding plane gave the bedding plane of the 2nd model layer and the bedding plane of the last, 23rd model layer, the Transdanubian Formation Group. Basically, the wells of the upper stratigraphic group were placed in layers 11, 13 and 15, the wells of the middle stratigraphic group in layers 17, 19 and 21, while the wells of the lower stratigraphic group were placed in layer 23. It is understood that where the screening of a well extends across the boundary of the stratigraphic group, the stratum concerned also appears as a produced stratum at the well. The stratum classification of the wells is shown in **Error! Reference source not found.**. The geometric structure of the model - the model layers used and their depths - and the basic

hydrostratigraphic properties are given in **Error! Reference source not found.**. Behind each layer type, the percentage of clay or sand streaks contained is indicated in parentheses.

Nr.	Layer	overlaying level [mabsl.] (average)	underlaying level [mabsl.] (average)
1	clay-silty sand	84 (surface)	-420
2	clay-silty sand	-420	-495 (Quarter bedrock)
3	sand	-495	-660
4	clay	-660	-820
5	sand with clay (44%)	-820	-1000
6	clay, silty clay	-1000	-1130
7	sand, silty sand	-1130	-1170
8	clay with sand strips (19%)	-1170	-1380
9	sandy-sandstone with clay strips (40%)	-1365	-1396
10	clay	-1396	-1520
11	sandy-sandstone with clay strips (50%)	-1515	-1535
12	clay	-1535	-1593
13	sandy-sandstone with clay strips (50%)	-1593	-1624
14	clay	-1624	-1674
15	sandy-sandstone with clay strips (50%)	-1674	-1693
16	clay	-1693	-1763
17	sandy-sandstone with clay strips (50%)	-1763	-1791
18	clay	-1791	-1851
19	sandy-sandstone with clay strips (50%)	-1851	-1892
20	clay	-1892	-1933
21	sandy-sandstone with clay strips (50%)	-1933	-1952
22	clay	-1952	-2030
23	sandstone with clay and lignite strips (50%)	-2030	-2110 (lower Pannonian bedrock)

Table E 20: Layers used in the model.

The leakage coefficients of the aquifers in the surrounding wells of Árpád-Agrár Zrt. were determined on the basis of the test pumping data carried out in the framework of the above-mentioned National Technology Programme and well tests carried out in earlier wells with similar development (e.g. Hódmezővásárhely),

using also literature data. In Pleistocene aquifers, the hydraulic conductivity varies between 5-10 m/day. In the aquifers belonging to the Danubian Formation Group (formerly Upper Pannonian), the hydraulic conductivity and the free void volume (porosity) decrease gradually with depth. The horizontal hydraulic conductivity varies between 5.2 to 1.0 m/day in the "Level A" (model layers 11, 13, 15, 17), from 2.8 to 0.7 m/day in the "Level B" (model layers 19, 21) and from 2.5 to 0.4 m/day in the "Level C" (model layer 23). The hydraulic conductivity of 13 m/day measured in well K-639 in level A is an extremely high value due to the positive skin effect, and the maximum value is therefore lower. The clay streaks in the sands were included in the vertical hydraulic conductivity according to their percentage. The hydrological characteristics used in the model are shown in Table E 11.

Nr. of layer	Average hydraulic conductivity [m/day]		Free pore volume [-]
	Horizontal	Vertical	
1	6,2	0,01	0,27
2	1	0,001	0,1
3	9,3	0,5	0,27
4	0,001	0,00001	0,05
5	6,2	0,1	0,25
6	0,001	0,00001	0,05
7	5,2	0,1	0,25
8	0,001	0,00001	0,05
9	4,5	0,1	0,25
10	0,001	0,00001	0,05
11	4,5	0,1	0,25
12	0,001	0,00001	0,05
13	3,8	0,01	0,25
14	0,001	0,00001	0,05
15	2,5	0,01	0,25
16	0,001	0,00001	0,05
17	2,0	0,01	0,24
18	0,001	0,00001	0,05
19	1,7	0,01	0,22
20	0,001	0,00001	0,05
21	1,5	0,01	0,21
22	0,001	0,00001	0,05
23	1,2	0,01	0,2

Table E 11: Characteristics of the layers used in the model.

Among the 23 layers, the uppermost layer was considered to be open, the others closed. As shown in the characterisation of the hydrogeological conditions, the resting pressure levels in the area increase with depth in the initial state, i.e. the area is characterized as an upflow area. The regional flow direction in the area is E - W. The initial water tables in the model layers were derived from the initial water table data from wells screened to each depth, considering the initial state pressure-depth profile shown in Figure E 15. Data from wells outside the model area were also used in the generation of the initial water table distributions and the regional flow direction was considered as well.

As a boundary condition, GHB cells were used in the aquifer layers (model layers 1, 2, 3, 5, 7, 9, 11, 13, 15, 17, 19, 21 and 23) at the E and W edges of the model. The proportionality factor determining the rate of flow between the edge and adjacent cells varies between 4-16 m^2/day in the model. These were determined by considering the permeability of the layers and the size of the cells so that the calculated water levels reflect the initial water tables without simulating the wells.

A residual infiltration of 20 mm/year was assumed in the model. The wells included in the model are shown in Figure E 17. The production of the wells was determined by distributing their yields in proportion to the thickness of the layer between the model layers opened by the well. The annual production data per well and the number of model layers produced by each well are shown in Table E 9. First a steady-state model run, followed by a 20-year transient model consisting of 6 months of production followed by 6 months of shutdown cycles.

The 720 m3 of water extracted daily from well K-666, which was converted from an oil exploration well, was injected back into the newly trained well K-712. During this time, all other wells produced continuously at the yields shown in Table E 9.

E.4.6. Results

E.4.6.1. Proof-of-concept (base case)

In order to determine how much change the two selected wells will cause in the existing system, we first plotted the water levels during the production of all wells in layers 21 and 23 affected by the two wells and in layer 19 immediately above them, in the steady state case Figure E 20, Figure E 21 and Figure E 22.

The impact of the well pair under study on existing wells is best illustrated by the resulting pressure depression. In this case, the operating water level of the existing wells is taken as the baseline and the impact of the injection well on this water level is examined.

Only those aquifers are considered where a water level change of at least 1 m has occurred. This is only the 23rd layer (Figure E 23). Negative numbers in Figure E 23 indicate a rise in water level. It can be seen that the impact of the injection well under study is limited to model layer 21. Even this single recirculation well raises the water level by at least 1 m in most of the model area, which has a positive effect on the production of wells screened to this layer.

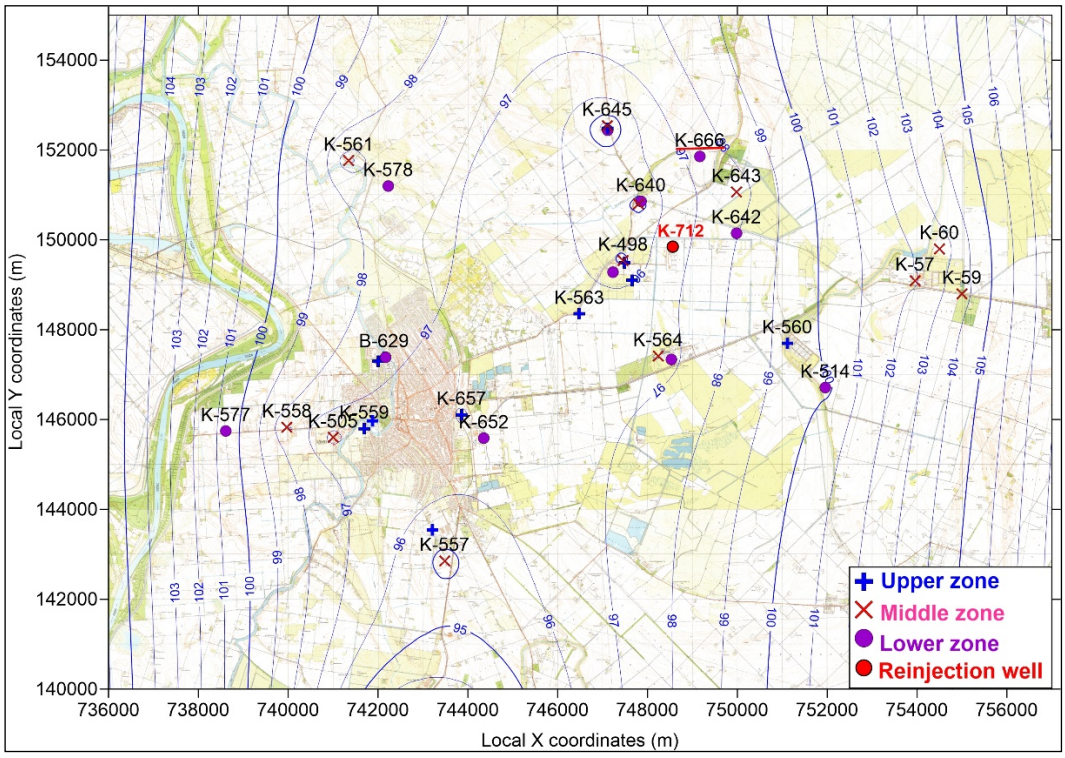

Figure E 20: Water levels affected by all wells in model layer 19 (mabsl).

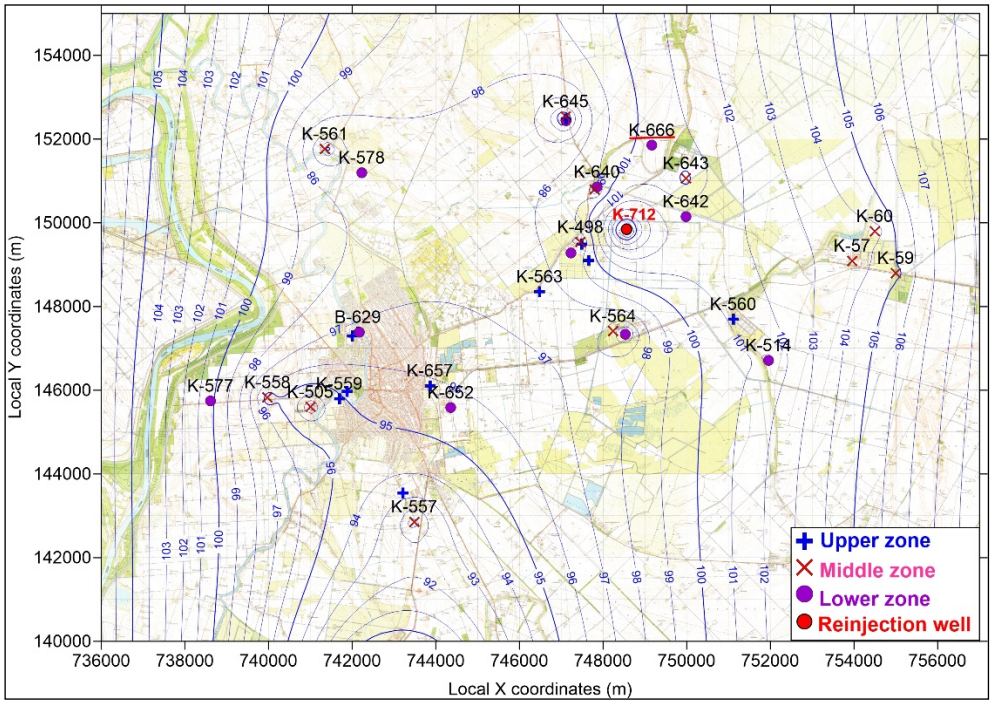

Figure E 21: Water levels affected by all wells in model layer 21 (mabsl).

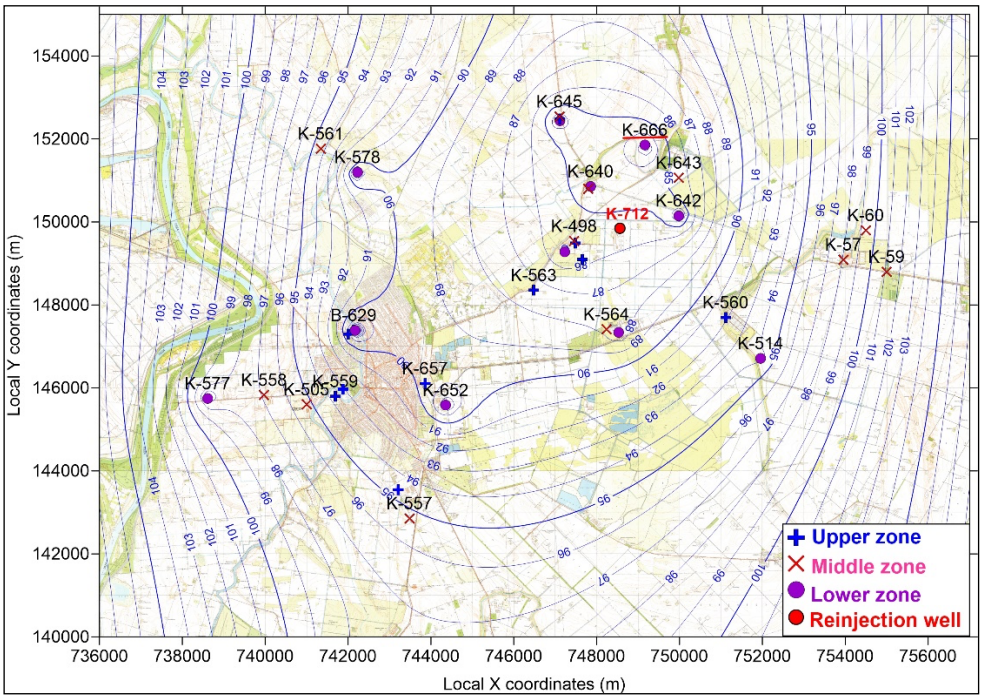

Figure E 22: Water levels affected by all wells in model layer 23 (mabsl)

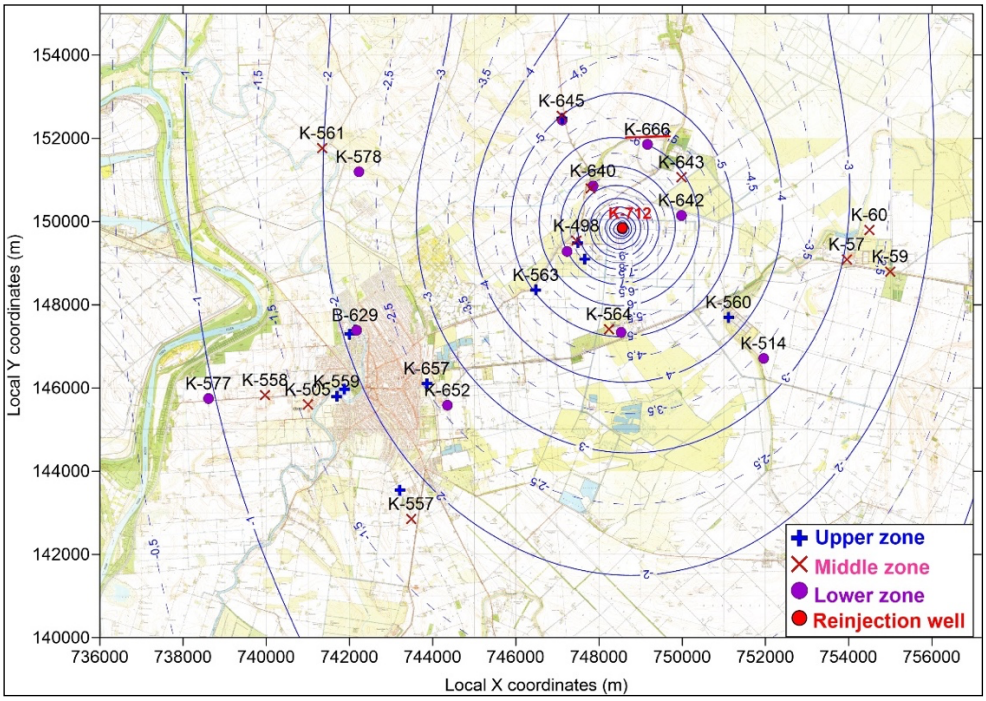

Figure E 23: Depression extent (m) of the tested well pair in model layer 21

In the transient case, we first show the water levels after 20 years of semi-annual production in layers 21 and 23 (Figure E 24 and Figure E 25), which are affected by the pair of wells under study. Compared to permanent production (Figure E 21 and Figure E 22), transient production results in a similar water level

distribution, but slightly higher in the produced layer and slightly lower in the re-injection layer 21, as expected in such a case.[4]

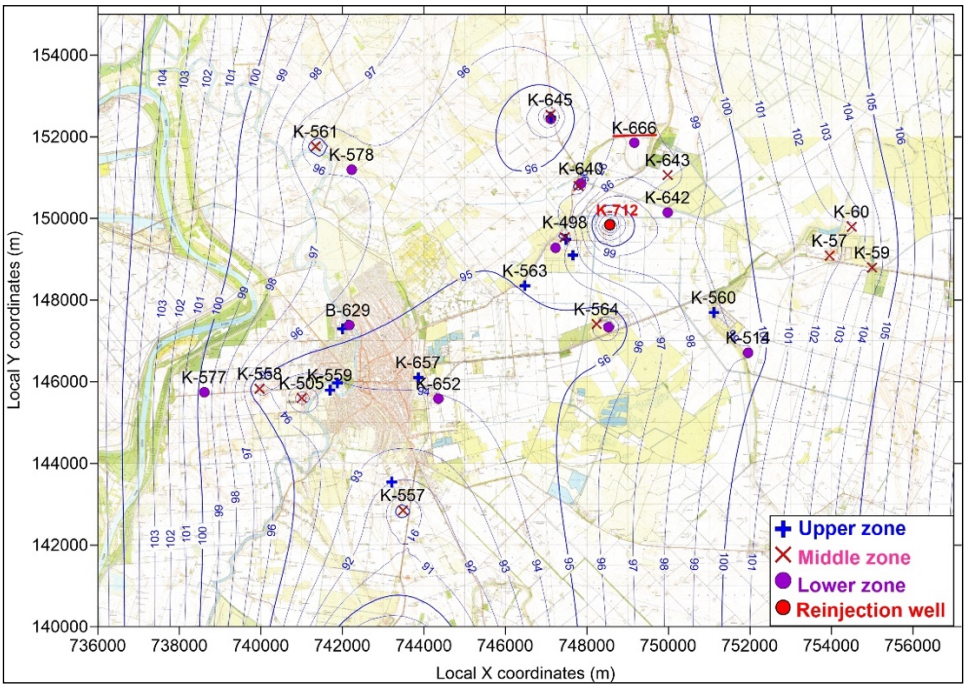

Figure E 24: 20-year transient production water levels in layer 21 (mabsl).

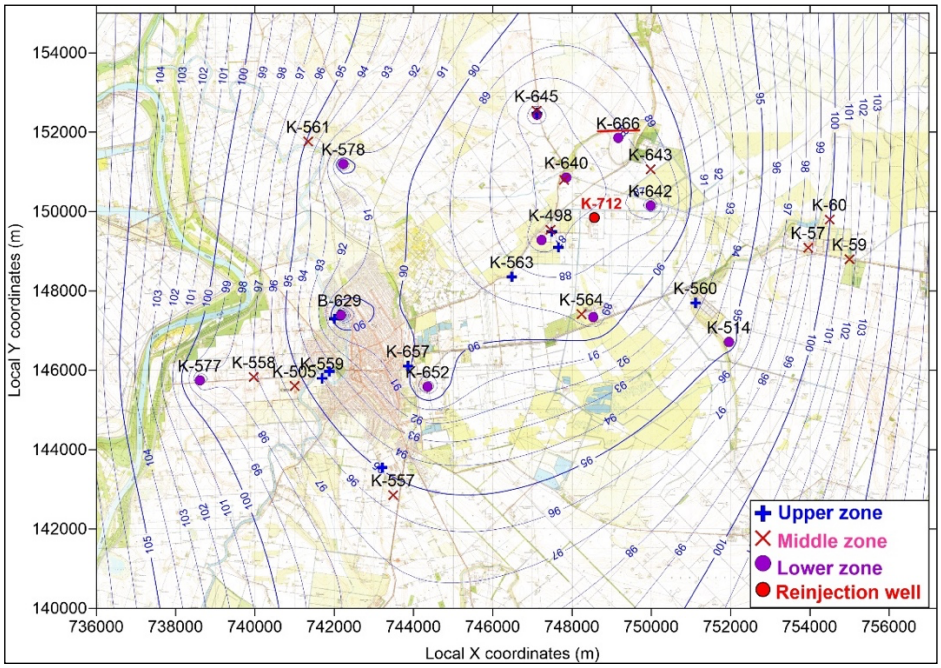

Figure E 25: 20-year transient production water levels in layer 23 (mabsl).

[4] The discrepancy is caused by the fact that the producing well (K666) produces from layer 23, while the injection well (K712) injects back into layer 21. These are real data, this is where the well screening was constructed. There is poor communication between the two layers, so the impact of the wells is barely visible in the layers they do not affect.

The distance between the two wells is about 2.9 km. The time it takes for the reinjected water to reach the production wells still needs to be examined. To do this, we have plotted the 10, 20, 30, 40 and 50-year circulation results (Figure E 26, Figure E 27, Figure E 28, Figure E 29, Figure E 30). Figure E 29 and Figure E 30 shows that the reinjected water reaches the production well B-17 after about 40 years and the production well K-333 after 50 years, so that no thermal breakthrough, i.e. temperature decrease, is expected in either well, since the reclaimed water has time to reheat during this time. The water from the injection well will be used in wells other than the production well. The temperature of the injected water is around 50 °C according to local practice. Previous heat transfer simulations in this environment have shown that the cooling effect after 50 years of injection has never reached 1 km. At a daily discharge of 720 m3/day (8.3 L/s) (low flux), no thermal breakthrough in the viscous system is expected. However, the recirculation has a positive effect on the water yield of the producing wells. It can be concluded that the impact of the system outlined is positive for existing wells.

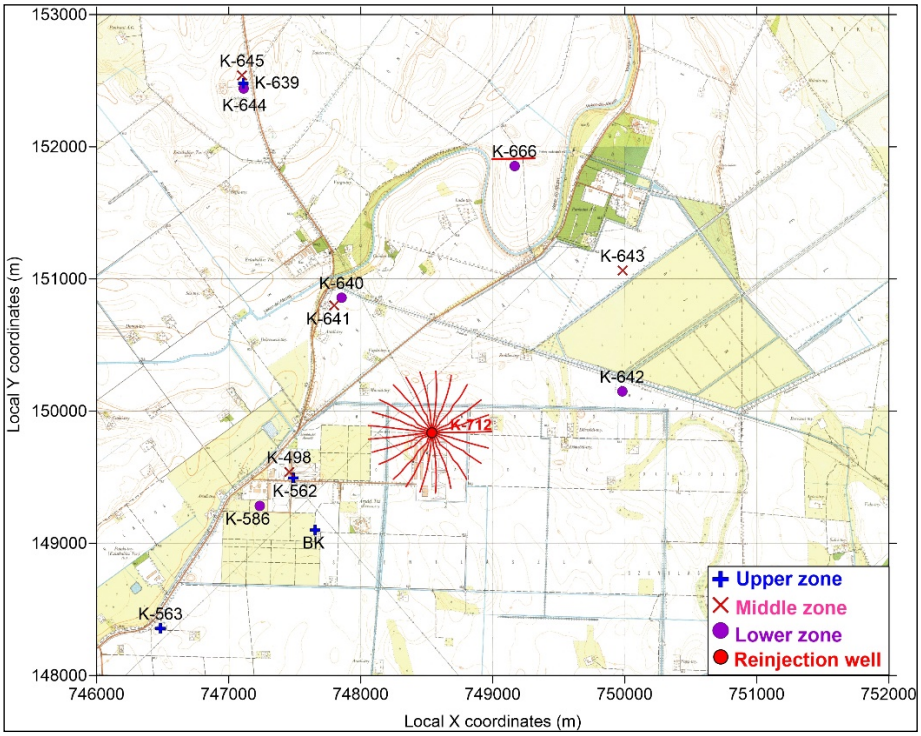

Figure E 26: Streamlines of the injection well for 10-year reach in layer 21

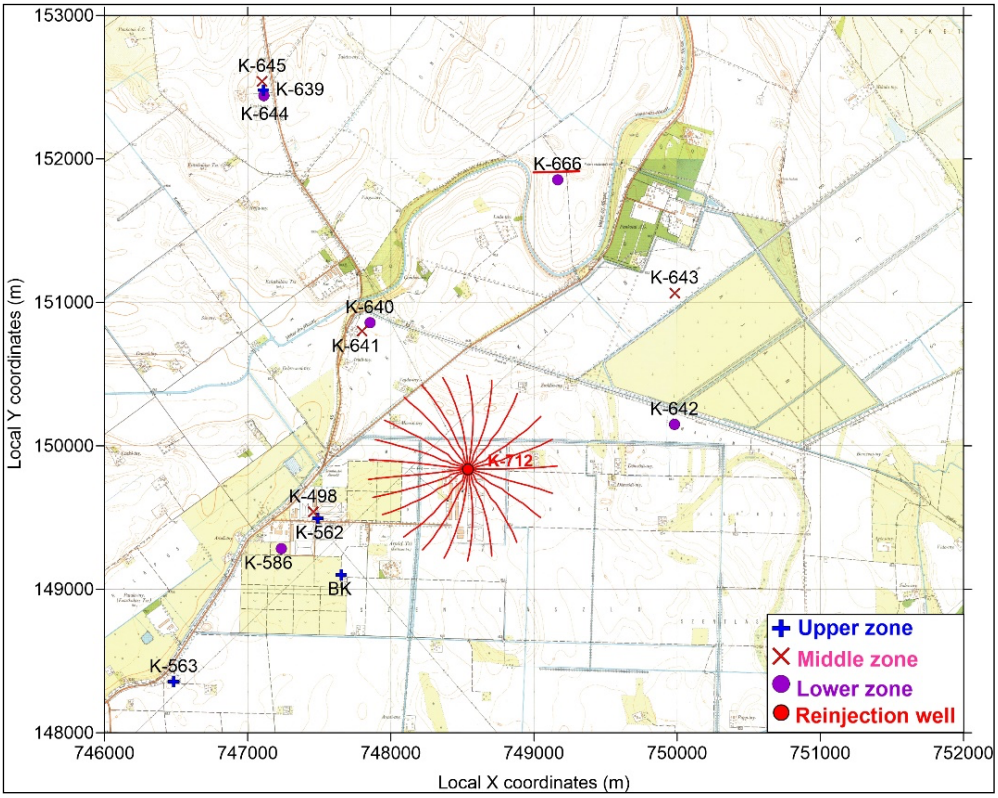

Figure E 27: Streamlines of the injection well for a 20-year continuous injection reach in layer 21.

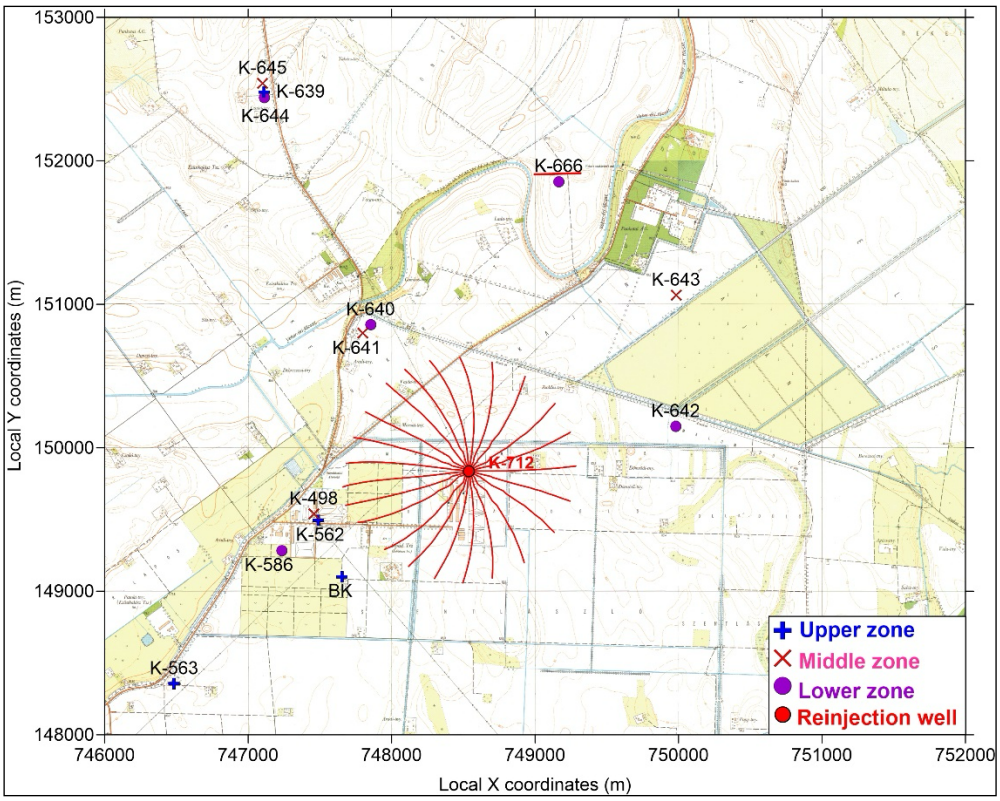

Figure E 28: Streamlines of the injection well for a 30-year continuous injection reach in layer 21.

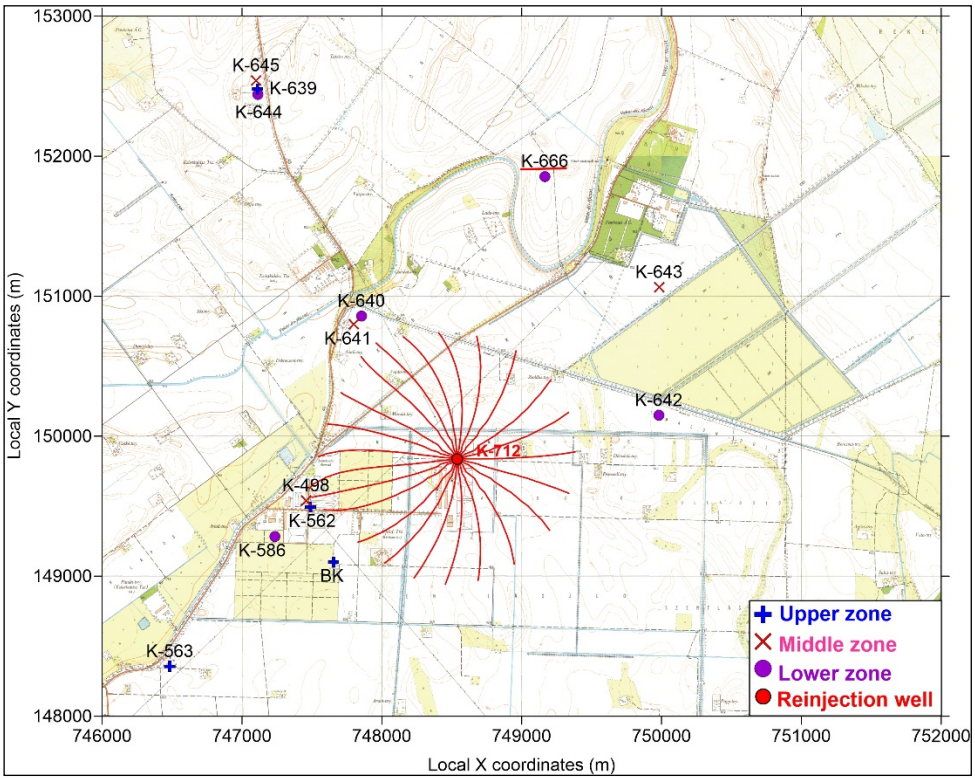

Figure E 29: Streamlines of the injection well for a 40-year continuous injection reach in layer 21.

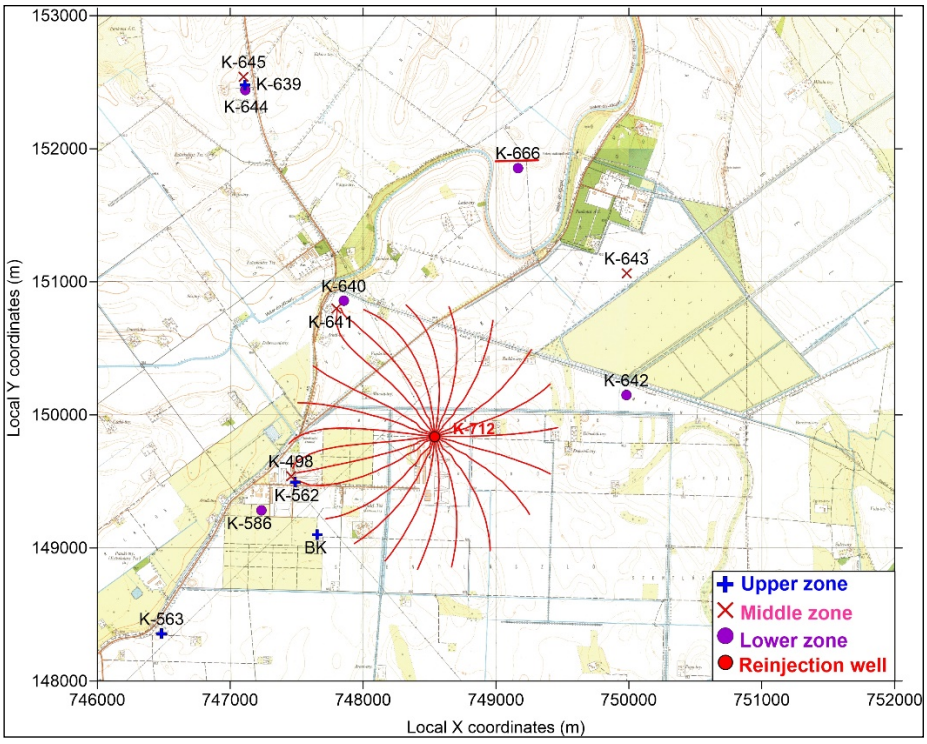

Figure E 30: Streamlines of the injection well for 50-year continuous injection reach in layer 21.

E.4.6.2. Impact of reservoir properties

Basically, three sets of parameters determine the heat/electricity generating capacity of a given well doublet. These are primarily the reservoir temperature, the produced water yield, and secondarily the chemical nature of the geothermal fluid. A fourth factor, although not related to the parameters of the well and reservoir, is the heat demand and its distance from the well.

The reservoir temperature is one of the most important factors in geothermal energy production. The temperature increases with depth, a measure of which is the geothermal gradient. The geothermal gradient for a particular area can be calculated from temperature measurements taken in thermal water wells and hydrocarbon exploration wells in that area. The water temperature measured at the wellhead is a function of a number of parameters, which should be taken into account in the design if only the reservoir temperature is given (e.g. new wells).

The trend curve plotted from the temperature-depth diagram of the temperature measured in wells at given depths in the vicinity of the planning area helps to determine the value of the geothermal gradient in the area. When estimating the discharge temperature, it should be kept in mind that there is a trade-off between the yield and temperature that can be achieved. Since reservoir temperature increases with depth, if shallower layers are opened to obtain higher yields, the temperature of the outflow will be lower. Assuming an average gradient of 50°C/km in the southern lowland area, the layer temperature is expected to be around 60°C at a depth of 1000 m and 110°C at 2000 m.

Well yield and productivity are determined by the reservoir's hydraulic parameters (porosity, permeability, reservoir pressure, storage capacity, etc.). The total reservoir space is made up of different units, permeable and impermeable layers, which vary according to grain size, density and sorting. In the case of old wells constructed several decades ago, the technical condition of the wells also severely limits the yield that can be achieved. In the Southern Great Plain porous aquifer series, the yields measured in existing thermal water wells are between 10 and 30 l/s.

When it comes to the chemical composition of the water produced from the well, the salinity and its quality and the gas content are the most important aspects. Knowledge of the chemical nature is necessary when designing the surface facilities and engineering in order to select the right quality of materials.

The total solute content of the waters stored in the Upper Pannonian reservoirs are mostly relatively low (around 500-1810 mg/l), with TDS and chemical composition varying with depth. In shallower than 600 m water depths, TDS and $NaHCO_3$, less frequently $CaMgHCO_3$, $NaCaMgHCO_3$ chemistry are mostly 500-750 mg/l, while deeper than this, TDS and $NaHCO_3Cl$, $NaClHCO_3$ chemistry are usually 1250-1810 mg/l, sometimes higher. The low solute TDS and chemical character indicate the presence of intense flows in the Upper Pannonian layers. Even high gas contents can be expected in the Southern Great Plain thermal water wells. If the gas/water ratio reaches 10 l/m^3 , a degassing device is required by regulation.

The heat market and the surface facilities, in particular the length of the pipeline, strongly influence the feasibility and economics of the project. It can be said that higher yields at lower temperatures or lower but still adequate yields at higher temperatures may be appropriate, but longer pipelines can significantly reduce the efficiency of the system. With knowledge of the heat market, the heat demand can be calculated and it can be used to calculate whether a given well is suitable to meet the heat demand and whether the market is large enough to make optimal use of the heat production from the well.

E.5. Requirements to reuse hydrocarbon wells for hydrothermal energy production

Error! Reference source not found. summarises all the factors that need to be considered for a hydrothermal project on an abandoned well. Key parameters are highlighted with dark background. For hydrothermal projects, with few exceptions, reinjection must be taken into account. In other words, it is always advisable to think in terms of two wells. In some cases, the abandoned oil/gas well may not be suitable for water production, but may be suitable for reinjection. The table also takes into account these factors. Basically, the parameters can be divided into three groups.

The first group describes the geological conditions of the reservoir near the well. Permeability, effective reservoir thickness and reservoir temperature largely influence the possible heat and thermal power a hydrothermal well can produce.

The second group lists well-related factors. The most important well parameters are the location, the well status, well age, well integrity, casing diameter and its productivity or injectivity. The well factors largely influence whether it is safe to reuse the well, how much effort it takes and if the anticipated flow rates and temperatures can be produced or injected.

The third group describes the market-related factors. Key parameter is the distance of a well from the users, which determines the maximum distance for transporting the produced energy for a given yield and temperature. In addition, information on the heat/electricity demand and heat/electricity transport infrastructure is essential.

Additional parameters may also be important from the point of view of the project's planning and long-term sustainability, however, they are not decisive in terms of the project's implementation. See Appendix A for a full list of parameters that may be considered in planning a new project.

Parameter	**Data source**	**Minimum/maximum value**	**Data availability (and accessibility)**
Reservoir parameters			
Effective reservoir permeability	Well tests, Production/injection data, Laboratory tests on rock cores, Calculated from porosity	Depends on the effective reservoir thickness (typically > 10^{-13} m^2)	Good (Very poor)
Effective reservoir thickness (geometry of the reservoir)	Geological well profile, Seismic survey, Geological model	Depends on the permeability (typically >20 m)	Very good (Very good)
Reservoir temperature	Temperature log/measurement	Depending on the application (typically >35°C)	Very good (Good)
Reservoir pressure	Pressure log	Hydrostatic or overpressurized (if not used as injection well)	Very good (Good)

Effective porosity of the reservoir	Well logs, Laboratory tests on rock cores, Well tests	Typically >15 % (if not fracture dominated)	Medium (Poor)
Structural geology of the reservoir (presence and properties of fractures and faults)	Seismic survey, Geological model, Well logs	Permeable fault, fracture network or karst required in low permeability rock	Medium (Poor)
Groundwater flow velocity and direction	Hydrostatic head measurements, Calculations	-	Poor (Very poor)
Water recharge	Production history	balanced	Poor (Very poor)
Salinity of reservoir fluid	Laboratory analysis of fluid samples	No limit, the lower the better	Good (Medium)
Gas/Oil-Water contact depth	Well logs	Best if no oil or gas is present in the geothermal reservoir	Very good (Very Poor)
Gas-Water ratio / Oil-Water ratio	Production data	Best when no oil or gas is produced	Very good (Very Poor)
Injected water salinity and temperature	Measurement, Laboratory analysis, Can be changed	Similar character than original water	Limited knowledge of behaviour in reservoir
Intercalated layers	Well logging	no or thin layers	Medium (Poor)
Mineralogy of the reservoir rock	Laboratory analysis of rock samples	Depending on the injected fluid	Medium (Poor)
Formation damage	Well tests, Partly repairable	Insignificant damage	Medium (Poor)
Well parameters			
Well location	GPS	Accessible, not located in a protected area	Very good (Very good)
Well status	Mining authorities	Shut-in or active is best, but also abandoned wells can be used	Very good (Very good)
Well age	Mining authorities, End of well report	<30-60 years	Very good (Very good)
Well integrity (wellhead, casing, cement quality along the well)	Well logging, Pressure testing	No leakage and no signs of significant casing or cement degradation	Good (Poor)
Casing diameters (inch)	End of well report, Well logging	>= 7 inch	Very good (Medium)
Productivity Index (L/s/MPa)	Well test, Production data	> 10 L/s/MPa	Very good (Very poor)
True vertical depth (TVD)	Well logging, Calculation, End of well report	> 1000 m	Very good (good)
Measured depth (MD)	Well logging, End of well report	-	Very good (Very good)
Perforation number, depth and quality	Given, changeable (e.g., re-perforating)	-	Medium (Very poor)

Surface facilities	Well owner	-	Very good (Medium)
Market parameters			
Distance to energy consumer (km)	GPS, Maps	0 - 10 km	Good (Good)
Required thermal/electrical power output of the hydrothermal system	Heat/electricity consumers	1-50 MW	Good (Good)
Existing infrastructure (e.g., heat transport lines)	Heat/electricity network operators	The more infrastructure that can be reused the better	Very good (Very good)
Possibility of multiple/cascade use	Heat/electricity consumers	yes	Medium (Medium)
Minimum lifetime of the hydrothermal wells and the heat demand	Economic analysis	> 20 years	-

Table E 22: Parameters determining successfull reuse of hydrocarbon wells for hydrothermal energy production. The most important parameters are highlighted with a dark background.

E.6. Workflow to reuse hydrocarbon wells for hydrothermal energy production

Investors have two options for the reuse of abandoned oil and/or gas wells. Either there is an abandoned well with twith suitable properties for geothermal use and they look for a geothermal market, or there is an existing market and they look for a well with the right parameters. The investor's objective may also be to generate electricity and/or heat. Electricity production is usually carried out by professional companies, often energy companies with significant capital, appropriate knowledge, geological models and professional background. Since these are high-risk projects and there are relatively few abandoned oil/gas wells that meet the necessary criteria, the following discussion will focus on the more common and more market-demanding thermal projects.

In all cases, it is worth starting from the assumption that the project is triggered on a strictly business basis, by investor demand. If the investor has a market, it is likely that they know the market well, has appropriate calculations and will be looking for wells with the right yield and temperature. However, in some aspects this is the relatively easier case. So, let us start from the assumption that a well (rarely a pair of wells) of unknown condition is available and the investor is looking for a market for it, i.e. the market has to be investigated.

1. First, it is worth obtaining information on the ownership of the well. The first step is to find out whether the well can be purchased or put to use.

2. This is followed by gathering information on the well and its surroundings, reviewing and interpreting well logs, surface geophysical surveys, well history, well structure, yield and temperature data, and if these indicate that the well is prospective, assessing the geothermal potential of the well and preparing a portfolio.

3. In parallel, a detailed assessment of the market demand for heat, identification of potential users and their heat demand, and, in the case of electricity generation, an assessment of the energy demand and available energy infrastructure are done.

4. If the market and well are available, a pre-feasibility study should be prepared for decision making. This should include an overview of the geology and hydrogeology of the area, the temperature, yield and chemistry of the water to be extracted, the technical conditions of the well as known from daily reports, documents and other sources (e.g. tacit knowledge), a list and evaluation of the workover activities required, an estimate of the amount of energy that can be extracted based on available production data, and an analysis and evaluation of the heat market and its economics.

5. On the basis of the pre-feasibility study, the investor can decide whether to proceed with the project and implement risk mitigation measures if required to proceed with the project.

6. If the investor wishes to proceed with the project, the investor must obtain the right to control the well (if it is not the owner of the well), and the necessary permits. On the basis of documentation in accordance with the regulatory requirements, it is advisable to inspect the well condition and production conditions, including cementing, well permeability, perforation quality, well at-rest measurement and test production, and in the case of injection wells, test injection (well logging and well tests).

6. On the basis of the above, it is advisable to prepare a feasibility study containing a detailed technical, market and economic analysis and a risk analysis for the construction of the well pair.

7. On the basis of the feasibility study, if the investor decides to launch the project, it is necessary to obtain the ownership of the well or the right to exploit the well if the investor does not own it. Subject to regulatory requirements, the investor must obtain a concession right or the necessary permit, with a few country-specific exceptions (e.g. balneology and agricultural use in Hungary), and must implement the project in accordance with the legal requirements.

Hydrocarbon wells can be reused for hydrothermal energy systems in the following ways:

1) Hot water can be co-produced with the oil or gas from the hydrocarbon reservoir towards the end of hydrocarbon production when the water-cut is high. This results in relatively low water flow rates (typically up to ~10 L/s) and energy output (few MWth) as the relative permeability of the water is reduced due to the residual oil or gas in the reservoir and sometimes due to the relatively low reservoir permeability, which is sufficient for gas production, but not sufficient for conventional hydrothermal energy production. Additionally, the pressure level may already be very low in the reservoir after many years of hydrocarbon production. To use the hot water that is produced anyway during hydrocarbon production, only a heat exchanger needs to be placed at the surface after water separation and it must be connected to the consumer.
2) Hot water can be produced from the hydrocarbon reservoir after the end of hydrocarbon production. In this case the production string should be removed from the well and an electrical submersible pump needs to be installed within the water column in the well. The potentially low flow rates/capacities resulting from relative permeability, absolute permeability and pressure described above also apply to this case.
3) The well is deepened below the hydrocarbon-water contact into the aquifer. This avoids at least the relative permeability problem, but results in a smaller well diameter, restricting the maximum flow rates due to frictional pressure losses in the well.
4) The well is cemented back to a potential shallower geothermal reservoir and the geothermal reservoir is accessed via perforations or a side-track.
5) A hydrocarbon exploration well, which did not find oil or gas, but hot water may be used right away as a hydrothermal production or injection well without the potential challenges described in (1-3) and without the need for expensive workover operations as described in (3-4).

E.7. References

Abdulhaq, H.A.; Geiger, J.; Vass, I.; Tóth, T.M.; Medgyes, T.; Szanyi, J. Transforming Abandoned Hydrocarbon Fields into Heat Storage Solutions: A Hungarian Case Study Using Enhanced Multi-Criteria Decision Analysis–Analytic Hierarchy Process and Geostatistical Methods. Energies (2024), 17, 3954. https://doi.org/10.3390/en17163954

Agemar, T., Alten, J., Ganz, B., Kuder, J., Kühne, K., Schumacher, S., & Schulz, R. (2012). The geothermal information system of Germany. Geotis, 165, 129-144.

Almási, I., 2001, Petroleum Hydrogeology of the Great Hungarian Plain, Eastern Pannonian Basin, Hungary. Doctor of Philosophy Dissertation, University of Alberta, Canada, 312 pages,https://era.library.ualberta.ca/items/7d5ade72-7101-42fb-b681-610b0350a727

Antonijevic, D., & Komatina, M. (2011). Sustainable sub-geothermal heat pump heating in Serbia. Renewable and sustainable energy reviews, 15(8), 3534-3538.

Asgeirsson, S.D., 2009. *Husavík Power Plant Corrosion and Erosion Experience,* 2008. from. P. Whittaker e Corrosion in the Kalina cycle.

Ashena, R. (2023). Analysis of some case studies and a recommended idea for geothermal energy production from retrofitted abandoned oil and gas wells. Geothermics, 108, 102634.

Aslan, A., Yüksel, B., & Akyol, T. (2011). Energy analysis of different types of buildings in Gonen geothermal district heating system. Applied thermal engineering, 31(14-15), 2726-2734

Axelsson, G., & Gunnlaugsson, E. (Eds.). (2000). *Long-term monitoring of high-and low-enthalpy fields under exploitation.* Japanese Organizing Committee for WGC2000.

Aydin, H., Yüksel, S., & Topuz, C. Utilization of Oil and Gas Wells for Geothermal Applications.

Barbacki, A. P., & Uliasz-Misiak, B. (2003). Geothermal energy of the Mesozoic Basin in The Carpathian Foredeep, Kraków Region, Poland. Applied energy, 74(1-2), 65-73.

Bayer, P., Rybach, L., Blum, P., & Brauchler, R. (2013). Review on life cycle environmental effects of geothermal power generation. Renewable and Sustainable Energy Reviews, 26, 446-463.

Björnsson, O. B. (1999, November). Geothermal district heating. In International Workshop on Direct Use of Geothermal Energy; Chamber of Commerce and Industry of Slovenia: Ljubliana, Slovenia

Bloomquist, R.G. (2003). Geothermal space heating. Geothermics Vol. 32. Issues 4-6, pp. 513-526

Bloomquist G, Lund J, Gehringer M. (2013) The world scientific handbook of energy. Geothermal Energy World Scientific Publishing Co Pte Ltd.

Bödvarsson G., 1964. Physical characteristics of natural heat sources in Iceland. Proc. UN Conf. on New Sources of Energy, Volume 2: Geothermal Energy, Rome, August 1961. United Nations, New York, 82-89.

Catarina, C. C., (2022). ” Fundamental steps in deriving a 3D Stratigraphical and Lithological Model of Zagyva formation in the Szentes region”, (Master's thesis). Eötvös Loránd University (ELTE)

Caulk, R. A., & Tomac, I. (2017). Reuse of abandoned oil and gas wells for geothermal energy production. Renewable energy, 112, 388-397.

Cohen, M., & Shivdasani, S. (2010). Spas and sustainability. In Understanding the Global Spa Industry (pp. 370-386). Routledge.

Colpan, C. O., Ezan, M. A., & Kizilkan, O. (Eds.). (2021). Thermodynamic Analysis and Optimization of Geothermal Power Plants. Elsevier.

COSO Energy (2024), https://cosoenergy.com/

Dickson, M., and Fanelli, M (2013). Geothermal energy-Utilization and technology, UNESCO, Paris, 2003, 224 p. Also, by: Routledge, Taylor and Francis Group, 2013.

Dincer, I., & Ezzat, M. F. (2018). 3.4 renewable energy production, Elsevier, Comprehensive Energy Systems, Vol. 3, pp. 126-207

Dincer, I., Ozcan, H. (2018). 1.17 Geothermal Energy, Elsevier, Comprehensive Energy Systems, Vol. 1, pp. 702-732

Dincer, I., Ozturk, M. (2021). Geothermal Energy Systems, Elsevier, pp 1-526

Eagle-Bluestone, J., Alamooti, M., Namie, S., Porlles, J., Ngobidi, N., Fry, N., ... & Gosnold Jr, W. (2022). Mandaree, North Dakota: A case study on oil and gas well conversion to geothermal district heating systems for rural communities. In Utilization of Thermal Potential of Abandoned Wells (pp. 341-371). Academic Press.

Erdlac Jr, R. J., Armour, L., Lee, R., Snyder, S., Sorensen, M., Matteucci, M., & Horton, J. (2007). Resource Assessment Status Report on Geothermal Energy within Deep Sedimentary Basins in Texas

European Geothermal Energy Council. (2023). EGEC Geothermal Market Report 2022. Retrieved from https://www.egec.org/media-publications/egec-geothermal-market-report-2022/

European Geothermal Energy Council. (2024). EGEC Geothermal Market Report 2023. Retrieved from https://www.egec.org/resource-type/geothermal-market-report/

Evans, K. (2010, September). Enhanced/engineered geothermal system: an introduction with overviews of deep systems built and circulated to date. In China geothermal development forum Beijing.

Farah, H. (2017). The Case of Geothermal Energy from Productive, Depleted and Abandoned Oil and Gas Wells. In Proceedings, 42nd Workshop on Geothermal Reservoir Engineering.

Franco, A. (2011). Power production from a moderate temperature geothermal resource with regenerative Organic Rankine Cycles, Energy for Sustainable Development 15 pp. 411–419

Franco, A., & Villani, M. (2009). Optimal design of binary cycle power plants for water-dominated, medium-temperature geothermal fields. Geothermics, 38(4), 379-391.

Franz, M. ; Barth, G.; Zimmermann, J.; Budach, I.; Nowak, K. & Wolfgramm, M. (2018): Geothermal resources of the North German Basin: exploration strategy, development examples and remaining opportunities in Mesozoic hydrothermal reservoirs, Special publications, 469(1) pp. 193-222. DOI: https://doi.org/10.1144/SP469.11

Glassley, W.E. (2015). Geothermal Energy: Renewable Energy and the Environment, Second Edition (2nd ed.). CRC Press. https://doi.org/10.1201/b17521

Global Wellness Institute. (2021). 2021 Wellness Tourism, Spas, Thermal/Mineral Springs | The Global Wellness Economy: Looking Beyond COVID. Retrieved from https://globalwellnessinstitute.org/wellness-tourism-spas-mineral-thermal-springs-the-global-wellness-economy-looking-beyond-covid-2021/

Gosnold, W., Abudureyimu, S., Tisiryapkina, I., Wang, D., & Ballesteros, M. (2019). The potential for binary geothermal power in the Williston basin. GRC Trans, 43, 114-126.

Gudmundsson, J. S. (1988). The elements of direct uses. Geothermics, 17(1), 119-136.

Gutiérrez-Negrín, Luis CA. "Evolution of worldwide geothermal power 2020–2023." Geothermal Energy 12.1 (2024): 1-60.

Habermehl, R., & Pestov, I. (2002). Geothermal resources of the great Artesian Basin, Australia. *GHC Bull.(20-26)*.

IEA Geothermal (2022) " 2021 Annual Report - Geothermal - December 2022", https://iea-gia.org/publications-2/annual-reports/

Kurnia, J. C., Shatri, M. S., Putra, Z. A., Zaini, J., Caesarendra, W., & Sasmito, A. P. (2022). Geothermal energy extraction using abandoned oil and gas wells: Techno-economic and policy review. International Journal of Energy Research, 46(1), 28-60.

Legmann, H. (2003). The Bad Blumau geothermal project: a low temperature, sustainable and environmentally benign power plant. Geothermics, 32(4-6), 497-503.

Liu, X., Falcone, G., & Alimonti, C. (2018). A systematic study of harnessing low-temperature geothermal energy from oil and gas reservoirs. Energy, 142, 346-355.

Lund, J. W., & Boyd, T. L. (2016). Direct utilization of geothermal energy 2015 worldwide review. Geothermics, 60, 66-93.

Lund, J. W., & Toth, A. N. (2021). Direct utilization of geothermal energy 2020 worldwide review. *Geothermics*, 90, 101915.

Manzella, A. (2017). Geothermal energy. In EPJ Web of Conferences (Vol. 148, p. 00012). EDP Sciences.

Monteson, P.A., Singer, J. (2004). Marketing a resort-based spa, J. of Vacation Marketing, Vol. 10, Issue 3., pp. 282-287

Moya, D., Akinsipe, O. C., & Kaparaju, P. (2021). Various cycle configurations for geothermal power plants. In Thermodynamic Analysis and Optimization of Geothermal Power Plants (pp. 3-15). Elsevier.

Nadkarni, K., Lefsrud, L. M., Schiffner, D., & Banks, J. (2022). Converting oil wells to geothermal resources: Roadmaps and roadblocks for energy transformation. Energy Policy, 161, 112705.

Nádor, A., Kujbus, A., & Tóth, A. (2019). Geothermal energy use, country update for Hungary. In Den Haag: European Geothermal Congress.

Naili, N., Hazami, M., Attar, I., & Farhat, A. (2016). Assessment of surface geothermal energy for air conditioning in northern Tunisia: Direct test and deployment of ground source heat pump system. Energy and Buildings, 111, 207-217.

Nardini, I. (2022). Geothermal power generation. In The palgrave handbook of international energy economics (pp. 183-194). Cham: Springer International Publishing.

Nordquist, J., & Johnson, L. (2012, September). Production of power from the co-produced water of oil wells, 3.5 years of operation. In Geothermal Resources Council Transactions, Geothermal Resources Council 2012 Annual Meeting (pp. 207-210).

O'Brien, G., Pearsall, N., O'Keefe, P. (2020), Renewable energy resources, in: The Future of Energy Use.

Pavlakovič, B., Demir, M. R., Pozvek, N., & Turnšek, M. (2021). Role of tourism in promoting geothermal energy: Public interest and motivation for geothermal energy tourism in Slovenia. Sustainability, 13(18), 10353.

Popovska, S. (2001). Geothermal energy direct application in industry in Europe. European Summer School on Geothermal Energy Applications.

Pujol, M., Ricard, L. P., & Bolton, G. (2015). 20 years of exploitation of the Yarragadee aquifer in the Perth Basin of Western Australia for direct-use of geothermal heat. Geothermics, 57, 39-55.

Rašković, P., Guzović, Z. Cvetković, S. (2013). Performance analysis of electricity generation by the medium temperature geothermal resources: Velika Ciglena case study, Energy, Vol. 54, pp. 11-31

Reyes, A. G. (2007). Abandoned oil and gas wells: a reconnaissance study of an unconventional geothermal resource. Lower Hutt, New Zealand: GNS Science.

Rubio-Maya, C., Díaz, V. A., Martínez, E. P., & Belman-Flores, J. M. (2015). Cascade utilization of low and medium enthalpy geothermal resources– A review. Renewable and Sustainable Energy Reviews, 52, 689-716.

S&P Global Platts (2016). "UDI World Electric Power Plants Data Base", https://www.platts.com/products/world-electric-power-plants-database

Sanyal, S.K. (2005) Classification of Geothermal Systems—A Possible Scheme. Proceedings of the 30th Workshop on Geothermal Reservoir Engineering, Stanford University, SGP-TR-176.

Sharmin, T., Khan, N. R., Akram, M. S., & Ehsan, M. M. (2023). A state-of-the-art review on geothermal energy extraction, utilization, and improvement strategies: conventional, hybridized, and enhanced geothermal systems. International Journal of Thermofluids, 18, 100323.

Shortall, R., Davidsdottir, B., & Axelsson, G. (2015). Development of a sustainability assessment framework for geothermal energy projects. Energy for sustainable development, 27, 28-45.

Spadacini, C., Xodo, L. G., & Quaia, M. (2017). Geothermal energy exploitation with Organic Rankine Cycle technologies. In Organic Rankine Cycle (ORC) Power Systems (pp. 473-525). Woodhead Publishing.

Szabó, Z., Kocsondi, J., & Lakner, Z. (2013). Role of thermal-tourism in regional development–a case study from Hungarian side of the Hungarian-Croatian border. Podravina: časopis za geografska i povijesna multidisciplinarna istraživanja, 12(23), 0-0.

Tabbachi, M. (2008). American and European spa. Understanding the global spa industry, 26-40.

Tartière, T., Astolfi, M.: A World Overview of the Organic Rankine Cycle Market, Energy Procedia 129 (2017) pp.2-9

Tomarov, G. V. , Nikol'skii, A. I. , Semenov, V. N., Shipkov, A. A., Geothermal Power Engineering: Reference Book, ed. by P. P. Bezrukikh (Interenergo-Izdat, Moscow, 2015) [in Russian].

Toth, A. N. (2020, April). Country update for Hungary. In Proceedings of the World Geothermal Congress (Vol. 1, pp. 1-10).

Toth, A. N., Nyikos, A., & Fenerty, D. K. (2019, June). Prospects for geothermal power projects in Hungary. In Proceedings of European geothermal congress, Den Haag, The Netherlands (pp. 11-14).

Toth, A. N., Szucs, P., Pap, J., Nyikos, A., & Fenerty, D. K. (2018, February). Converting abandoned Hungarian oil and gas wells into geothermal sources. In Proceedings, 43rd Workshop on Geothermal Reservoir Engineering (pp. 1-8).

USAID (2013). Geothermal Direct-Use Guidebook - A case study for Kenya. Washington g, The USA: US Agency for International Development (USAID), The volunteers for Economic Growth Alliance (VEGA), Powering African Agriculture Project (PAA) and Land O'Lakes Inc.

Valdimarsson P. (2015). Short course: Electricity Generation from Low Temperature Geothermal Resources, Melbourne, Australia vol. 5. Presented at 'WGC2015'.

Van der Vegt, J., & Vinci, L. (n.d.). Cyclolog user guide [User guide]. Cyclolog. Retrieved from https://cyclolog.com/

Van Erdeweghe, S., Van Bael, J., Laenen, B., & D'haeseleer, W. (2018). Feasibility study of a low-temperature geothermal power plant for multiple economic scenarios. Energy, 155, 1004-1012.

Wang, S., Yan, J., Li, F., Hu, J., Li, K. (2016). Exploitation and Utilization of Oilfield Geothermal Resources in China, Energies 2016, 9, 798; doi:10.3390/en9100798

Wang, K., Yuan, B., Ji, G., & Wu, X. (2018). A comprehensive review of geothermal energy extraction and utilization in oilfields. Journal of Petroleum Science and Engineering, 168, 465-477.

Weber, J., Born, H., Pester, S., Schifflechner, C., & Moeck, I. (2022). Geothermal energy use in germany, country update 2019-2021. In *Proceedings of the European Geothermal Congress 2022*.

Wight, N.M., Bennett, N.S., 2015. Geothermal energy from abandoned oil and gas wells using water in combination with a closed wellbore. Appl. Therm. Eng. 89, 908–915.

Xin, S., Liang, H., Hu, B., & Li, K. J. G. R. C. T. (2012). A 400 kW geothermal power generator using co-produced fluids from Huabei oilfield. Geothermal Resources Council Transactions, 36, 219-223.

Yang, Y., Huo, Y., Xia, W., Wang, X., Zhao, P., & Dai, Y. (2017). Construction and preliminary test of a geothermal ORC system using geothermal resource from abandoned oil wells in the Huabei oilfield of China. Energy, 140, 633-645.

Yuan, B. & Wood, D.A. (2018) A holistic review of geosystem damage during unconventional oil, gas and geothermal energy recovery, Fuel, Vol. 227, pp. 99-110.

F. Aquifer Thermal Energy Storage

F.1. Authors

Lingkan Finna Christi	GFZ	christi@gfz-potsdam.de	Germany
Yuxuan Liu	GFZ	yuxuan@gfz-potsdam.de	Germany
Hannes Hofmann	GFZ	hannes.hofmann@gfz-potsdam.de	Germany

Additional Input

Guido Blöcher	GFZ	guido.bloecher@gfz-potsdam.de	Germany
Elena Petrova	GFZ	elena.petrova@gfz-potsdam.de	Germany

F.2. Description of technology

In Aquifer Thermal Energy Storage (ATES) systems excess heat or chill is stored in the subsurface in a suitable aquifer via wellbores. The stored heat or chill is produced back when needed. This technology provides an environmentally friendly alternative to conventional greenhouse gas emitting fossil fuel supplied systems for building heating and cooling (Lerm et al., 2011) and is one of the few technologies to store large amounts of energy. ATES systems are considered as open systems where the naturally occurring groundwater is used as heat storage and transfer medium. The high (or low) temperature water is stored in a water-saturated confined aquifer that lays between two aquitards. This system typically has hot and cold wells that have both production and injection functions at each location, typically known as doublet systems. The energy stored in the aquifer and pumped back to the surface is then transferred through a heat exchanger at the surface to a secondary working fluid to allow direct use for both heating and cooling of a surface facility as shown in Figure F.2.1 (Lee, 2013).

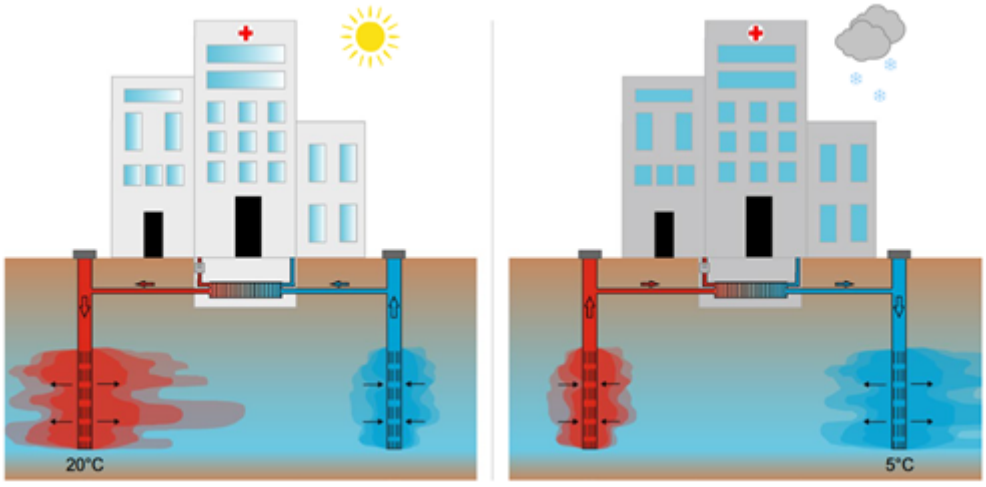

Figure F.2.1: Operational principle of an ATES system in summer (left) and winter (right) including the current temperature threshold for low temperature (LT) ATES in Germany (modified from Schüppler, 2019).

ATES works on a seasonal basis. In the summer, cold water is extracted from an aquifer through the cold well(s), for example to cool down buildings. This process heats up the fluid, which is then re-injected into the same or another aquifer through the warm well(s). In the winter, the process is reversed and warm water is withdrawn through the warm well(s) for heating, which cools down the fluid, which is then reinjected through the cold well (Duijff, 2021; Lu et al., 2019; Sommer, 2015). Thus, ATES requires drilling at least two wells into an aquifer to circulate water between storage areas, or reusing and modifying existing wells that access an aquifer. The wells are separated by a critical distance to ensure that the warm and cold storage remain separate and that thermal breakthrough does not occur within one season (Kun, 2010). Multi-well configurations have been employed where large volumes of water are required and in where individual well yields are too low to meet the demand. One of the largest ATES systems in Europe, located at Eindhoven University of Technology in the Netherlands, consists of more than 30 groundwater wells ranging in depth from 20 to 80 meter (Sommer, 2015). Single-well applications referred to as mono-well systems have also been employed using vertical separation of hot and cold groundwater where multiple aquifers exist. In this case, both hot and cold water are injected through the same well, but into different aquifers (Blöcher et al., 2024).

The uniqueness of an ATES project is that it must be designed to meet site-specific requirements, including geological and climatic conditions, heating/cooling demand, integrated facilities, and environmental and energy regulations. As later described in the ATES literature review of existing ATES projects worldwide, subsurface conditions and surface infrastructures need to be integrated to give the optimum performance of an ATES system. Thus, existing ATES systems have a wide range of operational and technical specifications. Fleuchaus et al. (2018) classified ATES into several categories including subsurface characteristics, system size, operational design, and Integrated facility characteristic to review the technical specification of ATES as follows.

F.2.1. Subsurface characteristic

Subsurface properties include geological and hydrogeological parameters such as potential storage formation, groundwater flow velocity, aquifer thickness and depth, porosity, permeability, groundwater temperature, fluid chemistry, and the composition of the gas contained in the aquifer.

Based on the range of the storage temperature, the depth of the aquifer and its purpose, ATES can be classified into three categories (Lee, 2013):

1) Low temperature (LT) ATES, which operates at temperatures below 30 ℃ and typical depths below 100 m. LT ATES is suitable for building or district heating and cooling applications.
2) Medium Temperature (MT) ATES refers to storage temperatures between 30 ℃ and 50 ℃ in deeper aquifers. The depth of MT ATES depends on the temperature gradient of the area. This type of ATES is suitable for building and district heating.
3) High Temperature (HT) ATES refers to aquifers with temperature higher than 50 ℃. This type of ATES is typically using aquifers between 400 m and 1000 m depth or deeper. Therefore, HT ATES is suitable for larger district heating networks.

The aquifers can be divided based on their subsurface characteristics into fracture dominated/carstic reservoirs and porous reservoirs. An additional separation is made between confined and unconfined aquifers.

F.2.2. System size

The system size is based on the number of wells used to supply an ATES system. A small system consists of 1 or 2 wells with a pumping rate of less than 40 m^3/hour and can generate less than 0.3 MW of thermal power. A medium size system consists of 2 to 6 wells with a pumping rate of 40 to 150 m^3/hour and generates

0.3 to 5 MW of thermal power. A large system consists of >6 wells with a flow rate of more than 150 m^3/hour and a capacity of 5 to 30 MW.

F.2.3. Operational Design

The operational design is divided into three classifications: mode of operation, purpose and well layout. Most of the ATES systems are operated in cyclic mode on a seasonal basis. The water is heated and injected back into the aquifer in the warm well, where it is stored until the next winter. The process is reversed in winter, when hot water is taken from the hot well and used for heating, in combination with a heat pump to achieve the required temperature. The water is cooled in the process and returned to the aquifer from the cold well, completing the 1-year cycle. The purpose of the system is integrated with the demand of surface infrastructure, it can be purposely made for district cooling, direct and indirect heating, direct and indirect cooling and heating or hybrid systems. The well layout depends on the number of the wells in one ATES system and the distance between wells to classify ATES into mono-well, doublet, and multi-well systems.

F.2.4. Building Characteristic

In general, building characteristics are divided into two main classifications, energy source and direct consumer of energy for heating and cooling. The energy source can be a heating or a cooling source.

The heat source for the hot well can be an industrial waste heat plant, a combined heat and power plant (CHP), or a renewable energy heating or power plant based on geothermal energy, solar thermal energy or biomass. Systems with this type of heat source are considered external heat source plants. Some ATES projects such as Reichstag Berlin (Germany), Neubrandenburg (Germany), and Utrecht University (The Netherlands) have implemented this system with CHP integration. ATES systems can also utilise the surplus heat from buildings This type of heat sources are considered as internal heat sources. The source of the cold for the cold well can be a cooling tower, a dry cooler or surface water, which are considered as external cold sources. The cold source can also be the building's surplus cold, which would be an internal cold source.

Direct consumers of heat/cold include industry, such as data centres, agriculture, such as greenhouses, residential buildings, such as apartment blocks, commercial buildings, such as offices, shopping centres and hotels, and public buildings such as universities, hospitals, airports and government buildings.

F.3. Literature review

F.3.1. History of ATES development worldwide

ATES development began in 1965 (Figure F.3.1) in Shanghai, China, where excessive groundwater extraction for industrial cooling had caused significant land subsidence (Morofsky 1994; Kun 2010). Artificial Recharge (AR) was used to reduce subsidence due to long-term over-pumping of groundwater, and studies showed that the injected surface water maintained its temperature for several months, making it suitable for industrial cooling (Shi, 2016; Fleuchaus, 2018). Due to the high demand for industrial cooling, the number of ATES applications gradually increased in the following years. By 1984, some 492 cold storage wells with a total storage capacity of 1100 TJ were in use annually, providing cold thermal energy to industries for cooling their machinery (Kun 2010, Fleuchaus 2018). Utilization of early ATES reached its peak in the early 1980s, with more than 20 cities using ATES in China (Shen, 1988; Zhou X 2015). However, the number of ATES systems continuously decreased due to groundwater resource problems and changes in government policies (Sommer, 2015). In addition, the technical problems of clogging of wells or heat exchangers due to

the hydrochemical properties of the aquifer fluid and inappropriate well configuration forced many ATES systems to cease operation (Fleuchaus, 2018).

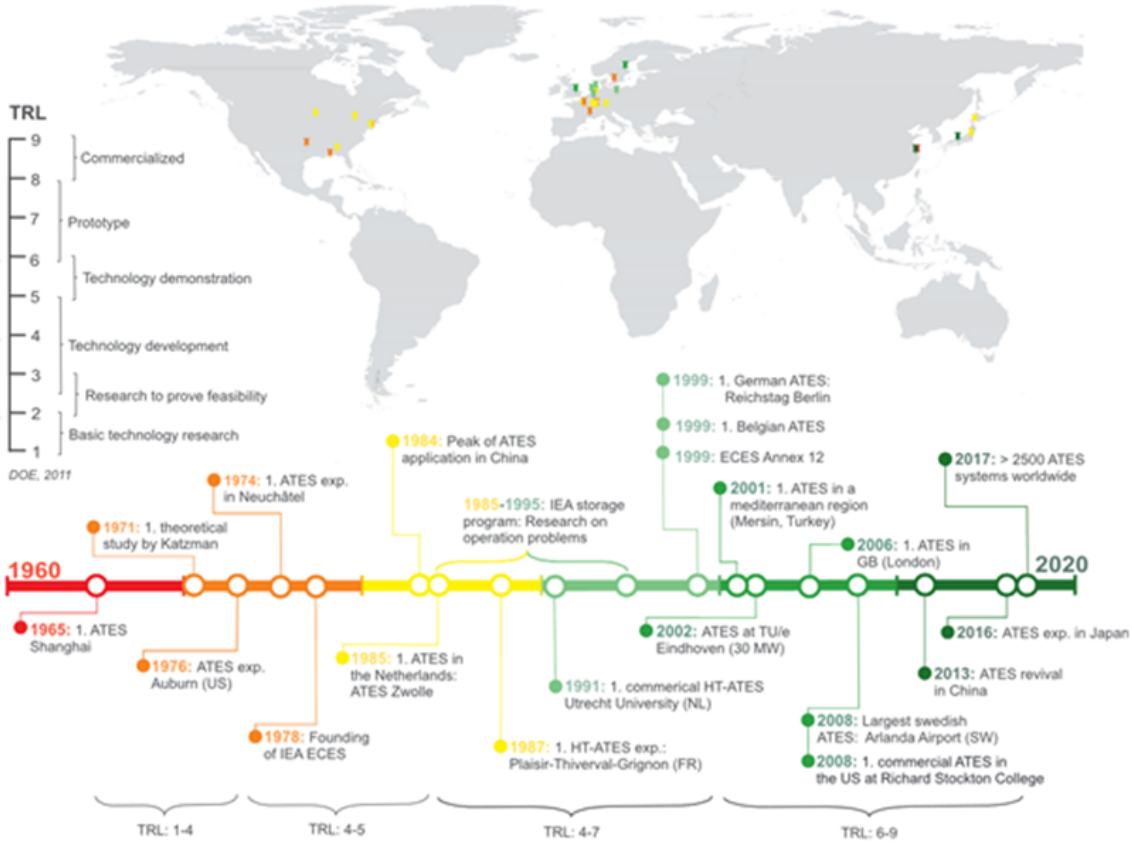

Figure F.3.1: Locations by country of ATES application worldwide in the frame of the historical development of the technology readiness level (TRL) (Fleuchaus et al., 2018).

In the mid-1970s, due to the oil crisis, research and development into energy storage intensified, and the idea of storing thermal energy in aquifers began to take off in North America and Europe (Anderson 1993; Anderson 2011). The early development of ATES in Europe and North America focused on the independent storage of cold and heat energy (Kun 2010; Sommer 2015). Several HT and LT ATES projects were developed in the U.S., such as Auburn University in 1976 and Texas A&M University in 1978 (Papadopulous 1978, Tsang 1978; Molsz 1978; Molsz 1979; Molsz 1981; Tsang,1981; Kanberg, 1981). In 1985, The first application of a combined heating and cooling ATES for a new building in Canada was the Government of Canada's Scarborough Centre building (Morofsky, 1993; Chant VG, 1991; Arthurs, 1988; Mirza, 1993; Wong, 2006; Cruickshanks,1995).

In the 1970s France, Switzerland, the USA and Japan led the field experiments and feasibility studies of thermal energy storage in aquifers (Tsang, 1980). Research focused primarily on the behaviour and recoverability of heat stored in the subsurface. Later, research expanded to include subsidence, water chemistry, and economic aspects (Meurs, 1985). In 1978, the International Energy Agency (IEA) established the Energy Storage Implementation Agreement (ECES) (Chant V, 1993; Snijders,1994). The aim of ECES was to support research and development of energy storage systems (IEA, 2016). Regular stock conferences were established to share experiences with TES, starting in 1981 in Versailles (Nordell, 2009).

Nine years later, in further coordination of various ATES-related studies, the International Energy Agency (IEA) initiated a research program in 1987 entitled: "Environmental and chemical aspects of thermal energy storage in aquifers and development of water treatment methods" (Brons, 1992). The program was focussed

on environmental and chemical aspects of ATES such as bacterial growth and biogeochemical precipitation reactions and effects on groundwater quality (Brons, 1992).

Since then, ATES technology has been utilised for various applications (Table F.3.1) such as governmental building heating system in Germany (Kranz and Frick, 2013), heating and cooling systems of buildings in The Netherlands (Rosen, 2016), hospitals in Belgium (Desmedt, 2007; Hoes, 2006), universities in Japan and USA (Tomigashi, 2011), airports in Norway and Denmark (Eggen, 2005; Midttømme, 2009; Birhanu, 2015; Larsen, 2015), IKEA stores in The Netherlands and Sweden (Snijders, 2008; Hellström, 2012), and air conditioning of a supermarket in Turkey (Paskoy, 2004). Most of the applications are directly integrated in local district heating and cooling systems. To date, 85 % of the more than 2800 ATES systems in operation are located in the Netherlands followed by Sweden (220), Belgium (30), and Denmark (55) (Fleuchaus et al., 2020). As shown in Table F.3.2, the depth of typical ATES systems is less than 400 m and their flow rates and capacities lie between 20 m^3/hr and 3000 m^3/hr and 0.2 - 20 MW. The majority of ATES systems are shallow LT systems.

Country	Locations	Year	Temperature (LT<40°C, HT>40°C)
USA	Auburn University	1976	HT
	ST. Paul	1982	HT
	Tuscaloosa, Alabama	1982	LT
	Stony Brook	1982	LT/HT
	Melville	1985	LT
	Texas A&M Univeristy	1978	LT
Switzerland	Colombier	1974	HT
	Lusanne - Dorigny	1982	HT
France	Aulnay - Sous - bois	1983	LT
	Plaisir	1987	HT
	Trappes	-	HT
	Bonnaud	1976	LT
	Campuget	1977	LT
	Montreuil	-	LT
Canada	Scarborough	1985	HT
	Carleton University	1990	LT
Japan	Yamagata Yonezawa	1977	LT
	Hokkaido, Sapporo	1982	HT
Sweden	Lomma	1991	LT
Germany	University of Stuttgart	1985	LT/HT
	Krefeld	1974	LT/HT
Netherlands	Gronigen	-	
	Bunnik	1985	LT
	Utrecht	1991	HT
Denmark	Horsholm	1983	HT

Table F.3.1: Summary of early ATES projects worldwide (Fleuchaus, 2018).

Country	City	Integrated Facility	Year	Well Depth (m)	Well Number	Flow Rate (m3/h)	Capacity (MW)
The Netherlands	Amersfoort	IKEA Store		-	2	200	1.4
	Utrecht	University	-	260	2	100	2.6
	Amersfoort	Office Building	1996	240	2	-	2
	Zwammerdam	Hospital	1998	150	2	20	7
	Amsterdam	District heating	2000	130	4	1100	8.3
	Eindhoven	University	2002	28 - 80	36	3000	20
Norway	Oslo	Airport	1998	20	18	200	7
Belgium	Brasschaat	Hospital	2000	65	2	100	1.2
	Malle ETAP	Office Building	2003	67	2	90	0.6
Sweden	Malmö	Expo Building	2001	75	10	120	1.3
	Malmö	IKEA Store	2009	90	11	180	1.3
	Arlanda	Airport	2009	20	11	720	10
Turkey	Mersin	Supermarket	2001	100	2	-	-
Denmark	Copenhagen	Hotel	2009	-	2	-	2.4
	Copenhagen	Office Building	2010	100	10	250	2.8
	Copenhagen	Airport	2015	110	10	-	5
UK	Greenwich	Museum Quarter	2011	60	2	45	0.33
	London	Apartments	2013	70	8	400	2.9
Shinshu	Japan	University	2011	50	5	-	-
Agassiz	Canada	Research Center	2002	60	5	40	0.22
US	New Jersey	University	2008	60	6	272	2

Table F.3.2: Worldwide application of ATES (Fleuchaus et al., 2018).

F.3.2. ATES systems in Central Europe

Stemmle et al. (2022) produced a series of maps of the spatial technical potential of shallow low-temperature ATES systems in Germany. In their study, they analysed the important criteria for efficient ATES operation, which include suitable hydrogeological conditions, such as aquifer productivity and groundwater flow velocity, and balanced space heating and cooling demand, which is based on the ratio of heating and cooling days, which is included as a time-dependent criterion to also evaluate the impact of climate change on the ATES potential. According to their investigations about 54% of the investigated German area is very good or good suitable for ATES applications for the coming decades, mainly concentrated on three regions, the North German Basin, the Upper Rhine Graben and the South German Molasse Basin (Figure F.3.2). By excluding the existing water protection zones, this share of very good and well-suited areas was reduced by about 11%. Nevertheless, the new assessment shows a huge potential for shallow low-temperature ATES systems in Germany.

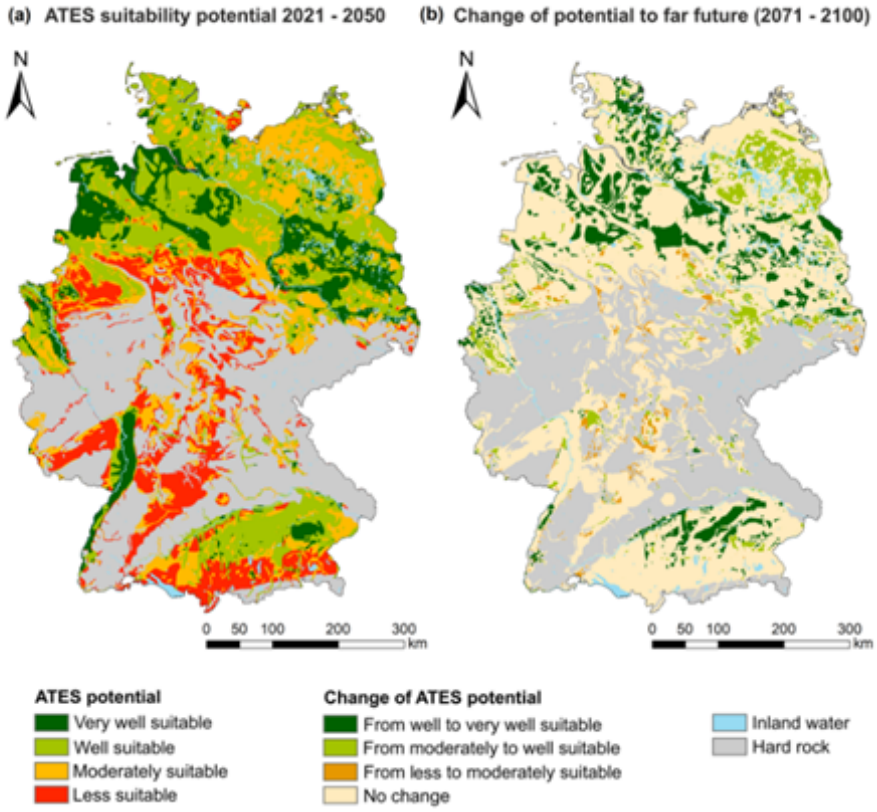

Figure F.3.2: ATES suitability potential in Germany (Stemmle, 2022).

Eight ATES projects were reviewed in Germany as shown in Table F.3.3, where three of the projects have been implemented (Neubrandenburg, Reichtstag, Rostock) and one is still in operation (Rostock). Four other projects are the testing site for research projects (Berlin Fasanenstrasse, Berlin Spandau, Lüneburg, Dingoflingen). One project (Adleshorf) is in the development stage under the project of GeoSpeicher Berlin.

No	Field	Start of Project	Type of ATES	Regional Basin	Targeted Reservoir	Reservoir Depth (m)	Origin of well	Number of well
North German Basin								
1	Berlin Reichstag	1999	HT- & NT-ATES	**North German Basin**	Quaternary Aquifer, Lower Jurassic sediments (Hettangian and Lower Sinemurian)	60 (cold)/ 300(warm)	Wells were designed purposely for ATES project	10 (5 for cooling, 5 for heating)
	Reference: Fleuchaus et al.,2021; Sanner et al. 2005; Kranz und Frick, 2013; Holstenkamp et al., 2017; Kabus and Seibt, 2000							
2	Berlin Fasanenstrasse	2020	TS-ATES	**North German Basin**	sandy sediments Triassic Exter Formation	235	Exploration well of ATES (Testing project)	1 (Gt BChb 1/2015)
	Reference: Saadat et al. 2016; Holstenkamp et al.,2017; Blöcher et al.,2024							
3	Berlin Spandau	2020	(not specified)	**North German Basin**	Triassic Muschelkalk Formation, Lower Muschelkalk (Schaumkalk)	585 - 620	Gas storage field	19 holes (3 wells were tested, BH3, BH2, B14)
	Reference: Blöcher et al., 2024							
4	Neubrandenburg	2005	HT-ATES	**North German Basin**	Upper Postera sandstone Rhaetian	1228 - 1268	Abandoned Geothermal Wells	2 (doublet)
	Reference: Holstenkamp et al., 2017; Würdemann et al., 2014							
5	Rostock	1999	NT/HT-ATES	**North German Basin**	Quaternary Aquifer	(15 - 30) & (13 - 27)	-	2 (doublet)
	Reference: Fleuchaus et al., 2021; Schmidt et al., 2004; Seibt und Kabus, 2006; Holstenkamp et al., 2017							

No	Field	Start of Project	Type of ATES	Regional Basin	Targeted Reservoir	Reservoir Depth (m)	Origin of well	Number of well
6	Lüneburg (Campus Leuphana)	2011	HT-ATES	**North German Basin**	Tertiary: Oligocene-Eozän (sandstone) Hauterive "Wealden" (sandstone) Jurassic Aalen (sandstone) & Hettang - Untersinemur (sandstone) Cretaceous Rhät (sandstone)	326 - 564.5	Natural gas well	11
	Reference: Fleuchaus et al., 2021; Holstenkamp et al., 2017; Kabus et al., 2012							
7	BMW (Dingoflingen)	-	HT-ATES	**Molasse Basin**	Jurrasic Limestone Aquifer (Malm Formation)	500 - 700	Research Borehole	1
	Reference: Holstenkamp et al., 2017; Ueckert and Baumann, 2019							
Molasse Basin								
8	BMW (Dingoflingen)	-	HT-ATES	**Molasse Basin**	Jurrasic Limestone Aquifer (Malm Formation)	500 - 700	Research Borehole	1
	Reference: Holstenkamp et al., 2017; Ueckert and Baumann, 2019							

Table F.3.3: Summary of ATES projects in Central Europe.

F. 3.2.1. ATES in the North German Basin

The North German Basin has been filled with sediments since the Permian period around 300 million years ago. Sandstones and mudstones, but also carbonates and evaporites (salt and anhydrite rocks) were deposited. The thickness of the sedimentary cover increases from the margin to 8 km in the basin interior (north of Berlin) (GTN, 2012). As summarised by Frick et al. (2023) in their study, identified five widespread Mesozoic reservoirs in the North German Basin with high ATES potential were identified (Table F.3.4 and Figure F.3.3).

Formation	Heat in place HIP (maximum) (GJ/m^2)	Heat Storage Potential HSP (maximum) (GJ/m^2)	Related existing ATES projects reservoir target
Lower Cretaceous Thickness: 1973 m Area: 1.20 × 10^3 km^2	69,170.9	11,079.1	-
Middle Jurassic Thickness: 1621.0 m Area: 4.78 × 10^4 km^2	3.914	6057.3	Lüneburg
Lower Jurassic Thickness: 1827.2 m Area: 9.17 × 10^4 km^2	3.949	12,951.1	Berlin Reichstag, Lüneburg
Upper Keuper/ Upper Triassic Thickness: 820.8 m Area: 9.93 × 10^4 km^2	3.688	6878.7	Berlin Fasanenstrasse, Neubrandenburg
Lower Triassic (Middle Buntsandstein) Thickness: 3111.6 m Area: 1.48 × 10^5 km^2	3.970	4878.1	Berlin-Spandau

Table F.3.4: Heat in place (HIP) and Heat storage potential of formation with high ATES Potential in the North German Basin (Frick et al., 2023).

F.3.2.2. ATES in the South German Molasse Basin

The South German Molasse Basin (SGMB) is a “foreland basin play type” (Moeck et al., 2020). The karstified Upper Jurassic carbonate aquifer called Malm in the SGMB is one of the most important low to medium enthalpy hydrothermal water resources in Europe (Goldscheider et al., 2010; Stober, 2014). The aquifer is also extensively used for drinking water and industrial purposes in the shallower parts at the northern and western margins and, therefore, represents an altogether important water reservoir for southern Germany (Florian, 2021). The only ATES project in the South German Molasse Basin that is a part of the Central European Region is the BMW Dingoflingen project (Ueckert and Baumann, 2019). The study on upper Jurassic as a large-scale ATES potency has been carried out by Ueckert and Baumann (2019) as one of the very few international projects in the Molasse Basin. This research project was funded by the Bavarian Ministry of Economic Affairs and the BMW Group. The concept involves the storage of intermittent excess energy in the Jurassic limestone aquifer Malm at about 500 m depth. The project combines field data with modelling and is supported by laboratory experiments. The water that is recovered from a production well is heated via a heat exchanger to up to 130°C and is subsequently fed back into the Malm aquifer via an injection well. The

test was run in a single well setting with five injection and production cycles, flow rates of 15 L/s and temperatures from 65 to 110 °C.

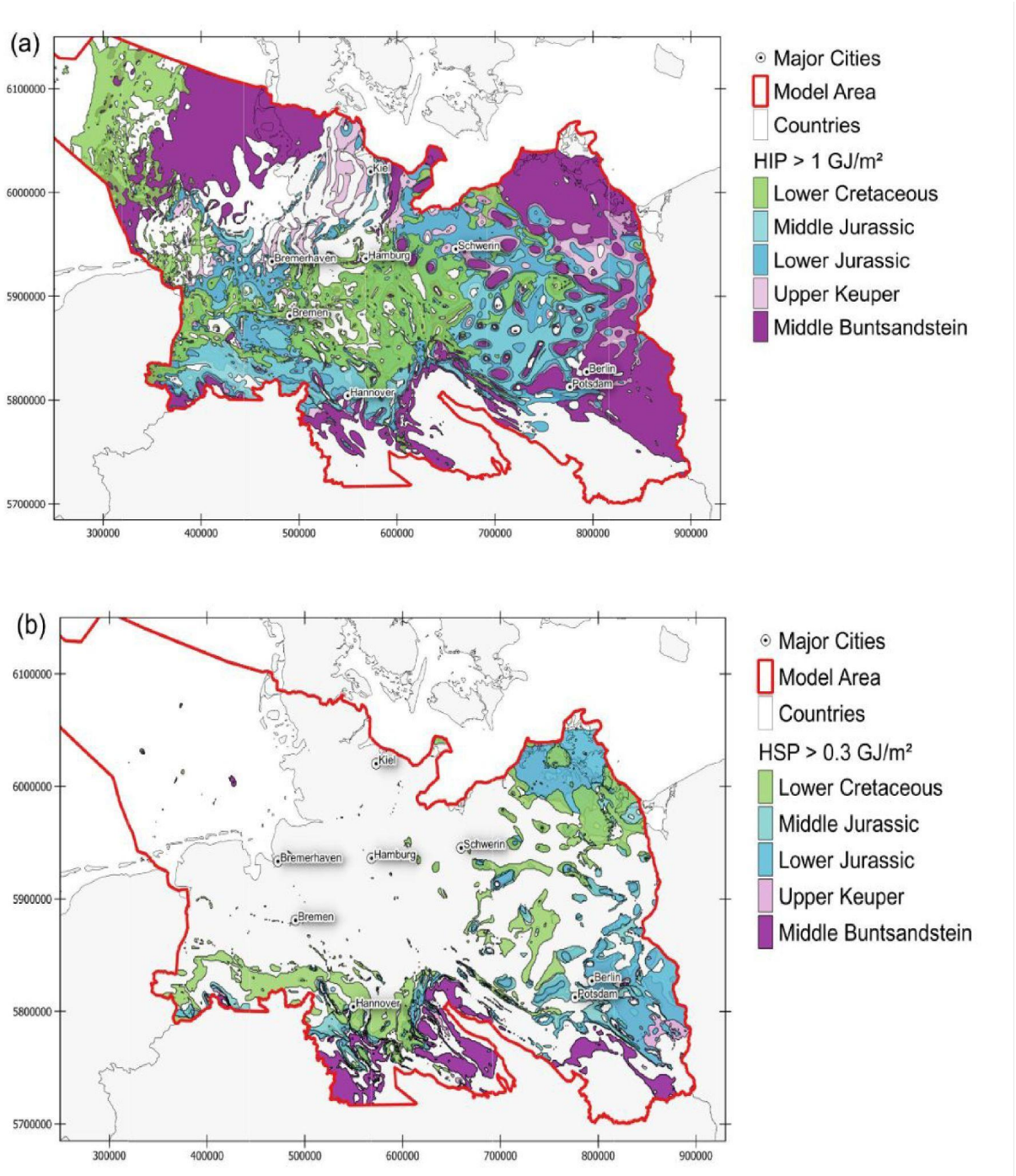

Figure F.3.3. Areas in the North German Basin with the heat in place (HIP) (a) > 1 GJ/m² and the heat storage potential (HSP) (b) > 0.3 GJ/m2 for each of the studied stratigraphic units (Frick et al., 2023).

F.3.3. Review of ATES well reuse projects in Central Europe

Only two projects in Central Europe can be classified as exemplifying well-reuse cases. These are the ATES feasibility study and planning project in Lüneburg (Campus Leuphana) and the Berlin-Spandau project, which was used as a reference site for model calibration in the TRANSGEO project. However, both of these projects were still in the feasibility study phase and have not yet been realised.

F.3.3.1. Lüneburg project

The feasibility study of the Lüneburg project primarily draws upon the research conducted by Wolfgramm et al. (2014). The site of the planned Lüneburg geothermal storage facility is located about two kilometres south of the Lüneburg salt dome. While the Cenozoic and Mesozoic strata dip steeply in the immediate vicinity of the salt dome, the depositional conditions at the proposed site can be characterised as a typical salt dome depression, where the strata dip is not so steep. The lower Quaternary contains Miocene sands, clays and silts, followed by the Oligocene. The middle Oligocene (Rupeltonian) is particularly prominent, with the clay layers separating the freshwater complex in the hanging wall (above) from the saltwater complex in the lying wall (below). The Upper Eocene begins partly clayey or fine sandy. Beneath this is the Neuengammer Gassand. The Upper Eocene begins partly clayey or fine sandy. The thickness varies between a few decimeters and up to 12 m. However, a 25-50 m thick layer of fine sand or fine sandstone is mainly present in the Upper Eocene. These sediments were encountered in all 11 boreholes (between 424 and 4946 m deep) that were investigated to assess the heat storage feasibility of different formations in the area. It is a very calcareous fine sandstone or calcareous fine sandstone. All relevant investigation results (profile survey, borehole measurements) of the oil and gas wells available for thermal utilisation were evaluated and interpreted in a complex manner. As part of the oil and gas exploration process, several reflection seismic surveys have been carried out in the study area. These data were used to map deeper subsurface structures such as geological strata and faults. The Following is a geological profile derived from seismic surveys and borehole data described in Table F.3.5.

Depth	Stratigraphy		Lithology
0-70	Quaternary		sand, boulder, clay
	Teriary		
90		Miocene	clay, sandy
250		Miocene	sand, lignite
300		Miocene	clay, silt
390		Upper and Middle Oligocene	clay, marl
405		Neuengrammer Gassand	sand
450		Upper Eocene	tone, mergling
485		Upper Eocene	fine, medium, sand
500		Lower Eocene	sand

Table F.3.5: Geological profile interpreted from seismic surveys and boreholes data (Wolfgramm et al. 2014).

Temperature measurements from various wells in the north-western part of the North German Basin, particularly in eastern Lower Saxony, were used to determine the geothermal gradient. These preliminary

investigations obtained from the old borehole and seismic data provide the following parameters for the ATES feasibility study in the Lüneburg area:

- Depth of target horizon (m below sea level): 450 – 485
- Stratigraphy: Upper Eocene
- Lithology: Fine, medium sand, calcareous
- Effective thickness (m): 30 m
- Porosity (%): 30
- Permeability (mD): 500 (estimated)
- Productivity index ($m^3/h/MPa$): 50
- Water temperature (°C): 25
- Salinity (g/l): 76,3

F.3.3.2. Berlin-Spandau project

Berlin-Spandau feasibility study was carried out under the geothermal utilisation of carbonate rocks in the North German Basin (ATES iQ) project (Blöcher, 2023). The Berlin natural gas storage facility to the west of Berlin was planned during the Cold War in the 1980s by the Allied Control Council to supply West Berlin as a self-sufficient strategic reserve and became operational in 1993. The storage facility consists of 21 wells to a depth of 1,000 m and has a working gas volume of 150 million Nm^3. The storage formation consists of massive porous sandstone without large cavities, from which the formation water was displaced by the stored gas, which was stored at up to 120 bar.

Berliner Erdgasspeicher GmbH (BES) is a GASAG Group company. BES has been marketing and operating the natural gas storage facility since 1993. Due to the poor economic situation, the GASAG Executive Board has decided to shut down the natural gas storage facility in December 2016. The decommissioning is currently in the approval and technical planning phase. The project is expected to be completed in 2023. The filling of the existing wells would preclude any further use of the wells. For this reason, reuse of the existing infrastructure has been considered in parallel with decommissioning. The use of geothermal energy as a hydrothermal energy source or as a thermal aquifer reservoir has already been demonstrated by BES internal feasibility studies. Apart from the existing wells, the most important prerequisites for the energetic use of the hydrothermal potential are suitable temperatures and sufficiently high flow rates. In the ATES iQ project, in which GFZ-Potsdam and BES are partners, three hydrocarbon wells were investigated for possible re-use of the three wells BH2, BH3 and B14.

Berliner Erdgasspeicher GmbH (BES) stores natural gas in the layers of the Buntsandstein formation. Above the Buntsandstein and the gas-tight layers of the Rötsalinar are the Muschelkalk layers at a depth of around 500 m (TVD). These are accessed by the BH1 to BH3 wells and the B14 well. The Muschelkalk was used in the past to inject reservoir water and to monitor gas tightness. Formation water from the Muschelkalk was sampled from the B14 well and analysed to validate the previous monitoring results. The well was drilled into the sandstone and is now partially filled up to the Muschelkalk. A production test was carried out to investigate and analyse not only water from the immediate vicinity of the well but also water from further away. Due to the strong cementation in the Muschelkalk area, it was not possible to gain good access to the Muschelkalk during the test. As a result, it was not possible to produce water from the reservoir. Further tests were carried out on BH2 and BH3. Both wells were evaluated for reservoir performance using a slug withdrawal test. BH3, which has the best access to the reservoir, was then subjected to further hydraulic testing, followed by analysis of the hydraulic tests and geochemical analysis of the produced water. After analysis, the produced water was injected back into the production horizon through the same well. Wells

BH2 and BH3 were drilled into the Muschelkalk. The wells are cased to surface and gas and fluid are sealed by cementation between the casing and the formation.

As a part of the TRANSGEO project, the Berlin-Spandau site is one of the reference sites for model validation and the ATES engineering workflow example of hydrocarbon well reuse. The advantage of subsequent use of the Berlin gas storage facility lies in the use of existing wells and the extensive wells and the extensive data on the geological formations that has been acquired over the years of storage operation. The extensive knowledge of the subsurface reduces the exploration risk. The detailed description of the sites, geological setting, borehole investigation, and numerical simulation are explained in the next section.

F.4 Numerical simulation

F.4.1. Method

The numerical simulation of ATES involves model validation with history matching of well tests from the former gas storage site Berlin Spandau, the simulation of a base case scenario and a sensitivity analysis of well and reservoir parameters.

We used CMG as the numerical simulation suite. CMG is a commercial software toolbox for hydrocarbon reservoir simulation. CMG Builder was used for pre-processing including grid creation and reservoir model building. The finite-difference thermal and advanced processes simulator CMG STARS was used to simulate the coupled thermal and hydraulic processes in the reservoir and wellbore based on mass conservation, energy conservation, Darcy's law and temperature-dependent fluid property correlations. CMG Results was used for post-processing of the simulation results including visualization and data analysis. CMG CMOST (Intelligent optimization and analysis tool) was used for history matching and sensitivity analysis. Flexwell was used to simulate fluid flow, pressure losses and heat transfer along the well paths.

For the model validation part, the data from 16-hour slug withdrawal tests performed on wellbore BH3 are used. With history matching in CMOST, the permeability of the reservoir model is calibrated to reproduce the historical production and injection data from these tests. The calibrated model was used to simulate a base case scenario with two wells for cold and heat storage to study the feasibility of an ATES system operating in the Muschelkalk formation in Berlin Spandau for 20 years. The well events are created following a pattern of seasonal operation. Finally, a sensitivity analysis of the most important well and reservoir parameters was carried out using CMOST to inform the criteria to determine the suitability of a well for reuse as an ATES well.

F.4.2. Model Validation of the reference site Berlin-Spandau

F.4.2.1. Site description

The former gas storage site Berlin Spandau is located in the southeastern part of the North German Basin (Figure F.4.1). In the past, Berliner Erdgasspeicher GmbH (BES) stored natural gas in the layers of the Buntsandstein. Above the Buntsandstein and the gas-tight layers of the Röt-Formation are the layers of the Muschelkalk at a depth of around 500 m, which are accessed via the auxiliary wells BH2 and BH3 and an access via the B14. In the past, the Muschelkalk formation was used as an injection horizon for

reservoir water and as a monitoring horizon to verify gas tightness. In this research, the numerical model covers the Muschelkalk formation and upper Buntsandstein formation.

The Muschelkalk formation in the study area is found at a depth roughly ranging from 400m to 700m. It is subdivided into the Lower Muschelkalk, the Middle Muschelkalk and the Upper Muschelkalk. The Lower Muschelkalk comprises two facies: Schaumkalk and Wellenkalk. The Schaumkalk (foam-limestone) is named for the bubble-like appearance of the ooids. The bio-genic/peloidal limestones alternating with marly peloidal/micritic limestones is called "Wellenkalk". The Middle Muschelkalk is composed of an alternating sequence of evaporites, marls and carbonates, while the Upper Muschelkalk consists mainly of micritic carbonates (Noak & Schröder, 2003).

For the Rüdersdorfer Schaumkalk in Berlin and Brandenburg, the Schaumkalk can be divided into 5 units as presented:

- Upper low permeable reservoir matrix (alternating layers of partly clayey micritic limestones with occasional layers of Schaumkalk);
- Upper porous layer (foam limestone layers with a few rather thin intermediate layers of clayey and/or micritic limestones);
- Low permeable interlayer (alternating clayey-micritic limestones with a few foam limestone layers);
- Lower porous layer (foam limestone layers with intermediate layers of clayey and/or micritic limestones);
- Lower low permeable reservoir matrix (alternating layers of partly clayey micritic lime with a few layers of foam limestone).

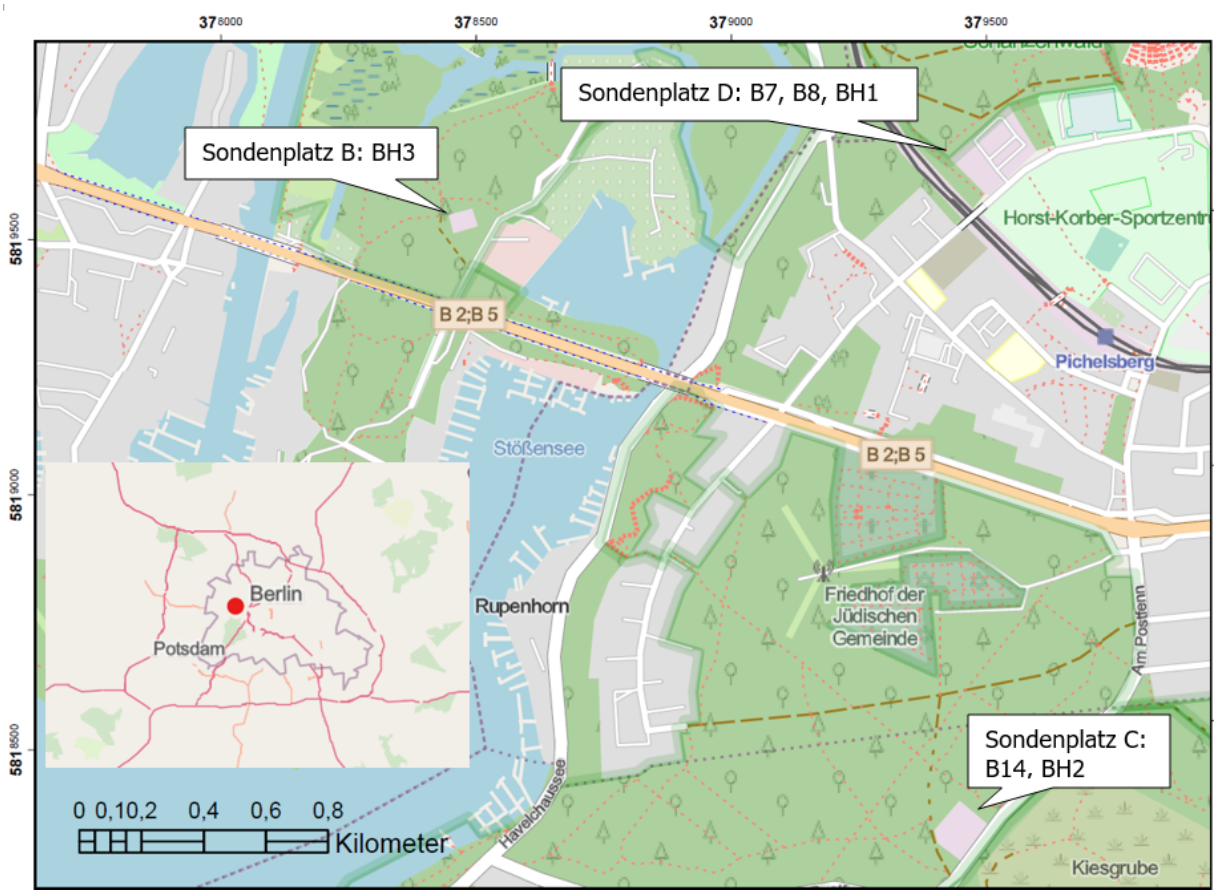

Figure F.4.1: Location of the well BH2, BH3, and B14 at Berlin-Spandau reference site.

F.4.2.2. Well BH2 information

Well BH2 was drilled in 1989 and used as an injection well until 2015. Here, reservoir water that was produced during gas extraction from the Detfurth Formation was injected into the Muschelkalk Formation. It was perforated in the upper porous Muschelkalk layer over approx. 7 m from depth 514-521m. For the pumping test, the well was reperforated in the area of the shell limestone. The work was completed with the start of the pumping test. The water level in the borehole depends on the density of the water column. With fresh water, the water level is above ground level, with salt water the level is below the surface. The brine of well BH2 contains 100 to 9,000 µg/L methane dissolved in water and 108.6 g/L sodium chloride. The pressure measured in well BH2 is approximately 51 bar at a perforation depth of 515 m MD or 495 m TVD, which is the initial pressure of the target reservoir horizon. Detailed well information on BH2 is described in Table F.4.1 and the wellbore configuration of BH2 is presented in Figure F.4.2.

Borehole Name	BH 2
Coordinate	4583176,98 R 5819415,36 H 53.00 m above sea level
Location	Sondenplatz , Am Postfenn ww, 13595 Berlin
Purpose of the borehole	Storage well durig the construction and exclusively observation well
Target horizon	Shell limestone Rüdersdofer Schaumkalk
Final depth	620 m, KET 600 m
Borehole volume	1-373 m* 4.54 l/m 373-600 m* 24.83 l/m 7331 l = 7.33 m^3

Table F.4.1: Well BH2 information (Blöcher, 2023).

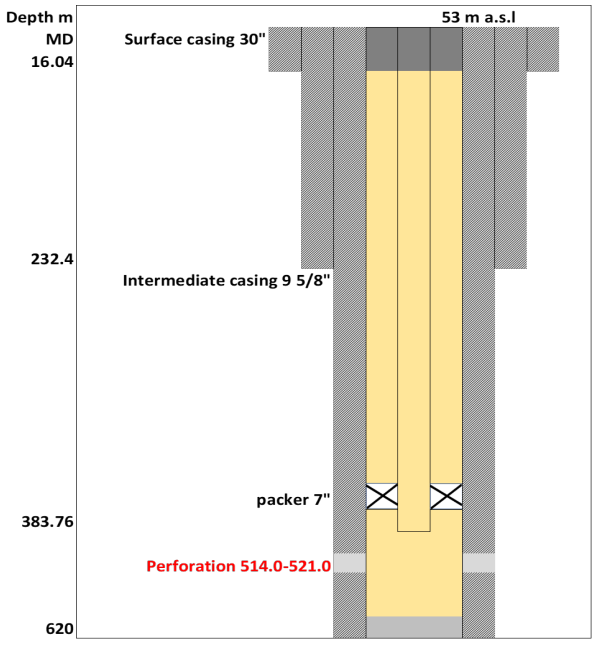

Figure F.4.2: Wellbore configuration of well BH2 including casing diameters and perforation depth (Modified from Blöcher et al., 2023).

F.4.2.3. Well BH3 information

The BH3 well was drilled in 1991 and used as an injection well until 2015. Here, reservoir water that was produced during gas extraction from the Detfurth Formation at well site B was injected into the Muschelkalk Formation. It has access to the Muschelkalk in the area of the lower porous layer over approx. 17 m. The water level in the well depends on the density of the water column. With fresh water, the water level is above ground level, with salt water the level is below GOK. The brine from the BH3 well contains 220 µg/l methane dissolved in water and 108.6 g/L sodium chloride. Details of well BH3 information are described in Table F.4.2 and the wellbore configuration is presented in Figure F.4.3.

Borehole Name	BH3
Coordinate	4582186,45 R 5820594,92 H 36.00 m above sea level
Location	Wellsite B, Pichelsweder
Purpose of the borehole	Monitoring well
Target horizon	Shell limestone (Rüdersdorfer Schaumkalk)
Final depth	585 m, KET 596 m
Borehole volume	1-487 m * 4.54 l/m 487 - 585 m *24.83 l/m 4648 l = 4.65 m^3
Borehole inclination	38.0°

Table F.4.2: Well BH3 information (Blöcher, 2023).

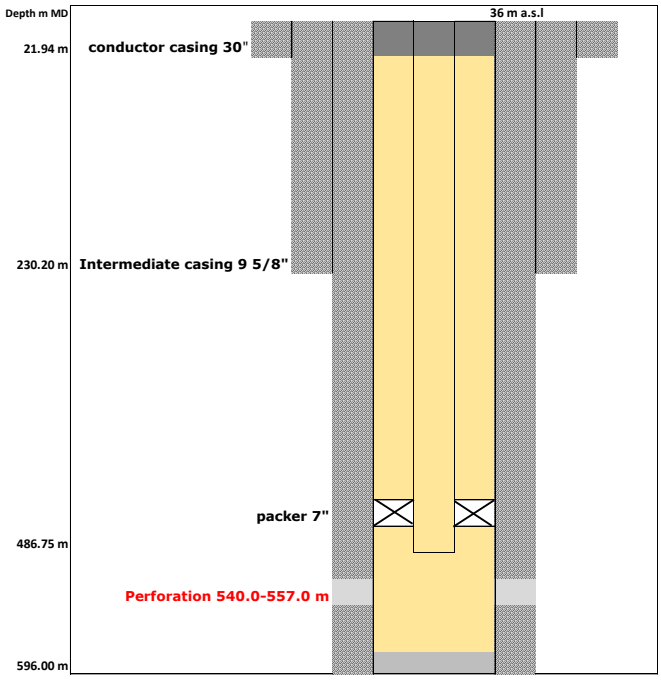

Figure F.4.3: Wellbore configuration of well BH3 including casing diameters and perforation depth (Modified from Blöcher et al., 2023).

F.4.2.4. Well B14 information

Well B14 was drilled in 1990 and has been used as a gas storage and observation well since then until 2018. The well was drilled into the Detfurth Formation, a geological sequence at a depth of approx. 1,000 meter. In order to safely separate the Detfurth layers previously used as underground storage from the shell limestone layers intended for geothermal use, the borehole was partially backfilled with cement approx. 10 - 15 m below the lower porous layer in 2018.Details of well B14 are presented in Table F.4.4 and Figure F.4.4.

Borehole Name	B14
District	Charlottenburg-Wilmersdorf, Grunewald Forest
Coordinate	45 83171.46 R 58 19408.04 H Well head position: 53.00 m above sea level
Final depth	603,0 m
Location	Wellsite B, Pichelsweder
Purpose of the borehole	Monitoring well
Target horizon	Shell limestone (Rüdersdorfer Schaumkalk)
Final depth	585 m, KET 596 m
Borehole volume	1-487 m * 4.54 l/m 487 - 585 m *24.83 l/m 4648 l = 4.65 m^3
Borehole inclination	38.0°

Table F.4.4: Well B14 location and information (Blöcher et al., 2023).

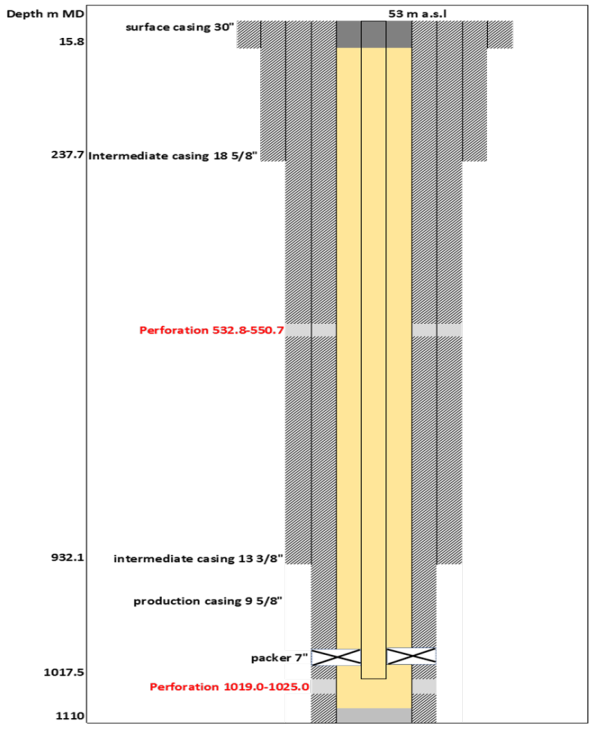

Figure F.4.4: Wellbore configuration of well B14 including casing diameters and perforation depth (Modified from Blöcher et al., 2023).

F.4.2.5. Workover and hydraulic tests carried out in well BH2 and BH3

Hydraulic tests were carried out in wells BH2 and BH3 to assess the hydraulic access of the boreholes to the shell limestone and to determine the suitability of the Muschelkalk for ATES operations. The following type and sequence of tests were performed:

- Two slug withdrawal tests (SWT) in BH2
- Three slug withdrawal tests (SWT) in BH3
- 5-stage performance test in BH3
- 16-hour production test in BH3 with a production rate of 1.75 m^3/h
- Depth pump on the BH3
- Injection test in BH3 with injection rates of up to 4.5 m^3/h

The test work was accompanied by a hydrochemical, physico-chemical and microbial monitoring program. The hydraulic test work was divided into two phases. In the first phase the perforated borehole B14 was investigated and hydraulically tested. In the second phase (Table 1.13), the BH2 and BH3 wells drilled into the Muschelkalk were tested. Slug withdrawal tests (15.04.2021 to 16.04.2021) were carried out on both wells to estimate hydraulic performance. Based on the results, BH3 was selected for further testing and a production and injection test (05.07.2021 to 08.07.2021) was conducted on BH3. Depth Water sampling was also carried out before and after the tests. The extracted brine was stored in a stilling vessel in a sealed storage tank after stilling. A total of 38.9 m^3 of water brine was extracted. Of this, 37.6 m^3 was injected into borehole BH3 and the remaining 1.3 m^3 was disposed of properly. The injection pressure was technically limited to a maximum of 1 bar above formation pressure due to the corridor spacing. The results of slug withdrawal tests are shown in Table F.4.5.

Parameters		BH2	BH3
Well head condition	(m above sea level)	53	36
Water level	(m below sea level)	22	10
Installation depth for pressure measurement instrument	(m below ground level)	380	550
Reservoir pressure	(bar)	36.4	54.41
Density of the column	(kg/m^3)	1036	1027
Thickness of the lower plus upper porous layer	(m)	23.6	19
Estimation of permeability from build-up pressure	(mD)	700	550 - 750
Estimation of productivity index from the build-up pressure	(l/s/bar)	0.5 - 1.1	0.4 - 1.2

Table F.4.5: Result of Slug withdrawal test conducted in BH2 and BH3 (Blöcher et al., 2023). The estimated productivity index from these tests was used for model validation.

F.4.2.6. Workover and hydraulic tests carried out in B14

For the workover operation, borehole B14 was partially backfilled, then it was perforated in the area of the shell limestone. Jet perforation was used as the appropriate method: extremely high pressures are generated by means of explosive charges, which perforate the pipe walls and the cementation. The tool is called a perforation cannon because it consists of several small bowls filled with dynamite. Precise holes can be made in the boreholes through the design of the gun and the layout of the explosive. The quality of the hydraulic access to the formation could be problematic with this form of perforation. Therefore, this well is excluded from the numerical modelling.
A series of hydraulic tests were performed following the workover operation. The aim of the hydraulic tests was to confirm the gas tightness of the overburden by measuring gas concentrations in the formation water of the Muschelkalk. On the other hand, hydraulic access of the boreholes to the shell limestone was to be established and the hydraulic, thermal, chemical and microbiological properties were to be determined by testing and monitoring the borehole and the deep water. The following sequence of tests were performed in well B14:

- A nitrogen lift test (NLT) with subsequent shut-in to determine the transmissibility and skin factor of the well, with distributed temperature sensing (DTS) and chemical and microbiological monitoring program
- Downhole fluid sampling to determine the gas concentration
- Two pneumatically SWT tests
- An injection test (IT) of the previously extracted thermal water to determine the injectivity

A hydrochemical, physicochemical and microbial monitoring programme was carried out during the tests. In addition, a temporary DTS cable was inserted into the borehole to provide information on the temporal and spatial temperature distribution during the tests. After settling, the extracted water (brine) was stored in a settling tank in a sealed storage container. A total of 53.2 m^3 of water (brine) was pumped. Of this, 28.8 m^3 was injected into borehole B14 and the remaining 24.4 m^3 was properly disposed of. The injection pressure was technically limited by the pump to a maximum of 4.8 bar.

F.4.2.7. Model setup

We used a single porosity model for simplification. The grid system is Cartesian. The geological data is imported using source from GFZ data services (Frick, M. et al). This data package has grid files that consists of 20 sedimentary units, it covers a rectangular area around the political boundaries of Berlin collectively. Take the starting point of the well trajectories as a reference point and use this point as the midpoint of the square with length of 1km, and the four sides of this square are the boundaries of the model. The coordinates of wellbore trajectories of BH2 are available, and the coordinates of four points of this square can be calculated. Extract the target sedimentary layers with these four coordinates to form the model. And the model contains two geological formations: Muschelkalk and Upper Buntsandstein.

(i) Reservoir geometry

The 3D model was built with I; J dimensions of 1000 m x 1000 m and K has thickness of around 300m. The thickness and depth of the geological layers are extracted from the geological model (Frick, M. et al). The thickness and depth of two porous layers are from Blöcher et al (2023). The entire reservoir 3D model consists of 170,000 grid cells, with 100 grid blocks in both the I and J-directions, and 17 blocks in the K-direction. The length of each block along the I and J-direction is 10m. Each small block in the K-direction has a different height, calculated by dividing the total thickness of each geological layer by the number of blocks within that layer. As shown in Figure F.4.5, there are a total of 17 layers, with the upper porous layers (UPL) and

lower porous layers (LPL) each consisting of 4 layers. The reservoir properties used in the model are detailed in Table F.4.6.

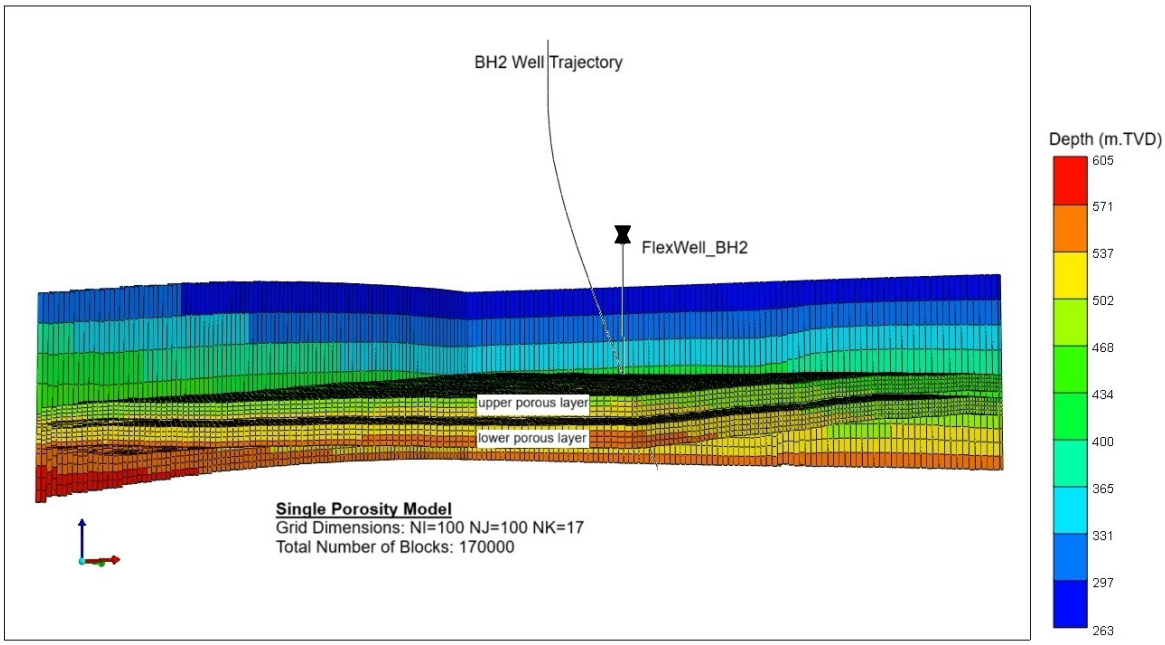

Figure F.4.5: 3D view of wellbore BH2 (for history matching) in 3D reservoir model.

Property of Reservoir		Unit	UPL	LPL	Upper Matrix	Lower Matrix	Interlayer
Layer			5-8	10-13	1-4	14-17	9
Porosity	φ	-	0.25	0.2	0.03	0.03	0.03
Permeability	k(i=j=k)	mD	500	500	0.5	0.5	0.5
Thermal Conductivity (bulk rock)	λ_s	J/(m•day•°C)	2.95E5	2.95E5	2.95E5	2.95E5	2.95E5
Volumetric Heat capacity (bulk rock)	c_s	J/(m³•°C)	2.4E6	2.4E6	2.4E6	2.4E6	2.4E6

Table F.4.6: Reservoir properties of the base case scenario. UPL = upper porous layer, LPL = lower porous layer. (Fuchs et al. 2015 and Noack et al. 2003).

(i) Wellbore model

We use Flex-Well model for both history matching and base case. In the history matching part, the wellbore model of BH2 consists of a tubing string and an annulus. The tubing is for producing events and the annulus is for injecting events. The wall ID of the tubing is 0.076m and the wall OD is 0.089m. The wall ID of the annulus is 0.164m and the wall OD is 0.178m. Due to the lack of experimental data, the

skin factor is set to zero in the simulation. The radius of the tubing is 0.0445m and the radius of the annulus is 0.0889m. The wellbore BH2 was perforated in the all-porous layers from layer 5 to 8 and layer 10 to 13.

A new deviated well named NewDrill is set up in the base case for simulating cold storage well. The well BH2 works as hot storage well in the base case. Same settings were applied for both wells: same tubing with annulus configuration and same well completion. The only difference is the wellbore trajectories. Wellbore NewDrill is more horizontal than well BH2 which makes the NewDrill has longer perforation length than BH2. And the new well path is the opposite direction to the well BH2.

For well operation, the tubing is open and the annulus is shut-in in history matching since only the productivity index is to be validated. In the base case, the tubing and annulus are open and shut-in in a circulated way for simulating seasonal storage, more details are described in next chapter.

The model from layer 5 to 15 was refined (Figure F.4.5). And the well in these layers was therefore discretized. The refinement was made by mainly considering the thermal front during circulated injection and production. The area enveloped by thermal breakthrough curves was covered in this refinement. This refinement aims to better observe the bubble-like thermal field of cold and warm storage during operation in the visualized results, ensuring that the thermal breakthrough curves of two storage do not intersect. Because this will affect the heat recovery factor of the hot storage well.

F.4.2.8. Model Parameterization

(i) Reservoir Properties

The reservoir is divided into five sections, from top to bottom: the upper matrix, upper porous layers, interlayer, lower porous layers, and lower matrix (Table E.3.5). The porosity values are based on rock core test results from Noak and Schröder (2003). The permeability values are assigned based on the results from the history matching. They are the same in I, J and K direction. The thermal properties of the reservoir are based on Fuchs et al. (2015). Details of reservoir properties are described in Table F.4.6.

Additional well constraints:

For the history matching: In order to get the intrinsic productivity index of the reservoir, there is no minimum and maximum well bottom hole pressure applied. The surface water rate is 1200 m^3/day and 2400 m^3/day.

For the base case: No well bottom-hole pressure constraints applied. The circulation rate is 600 m^3/day.

(ii) Ground water properties

The groundwater properties were analyzed through hydrochemical monitoring and in situ water sampling during production testing. For our modelling case, the values of the groundwater properties used for simulation are listed in Table F.4.7 based on the internal report by Blöcher et al. (2023).

Property - Groundwater	Symbol	Unit	Value
Total dissolved solids	TDS	$kg \cdot kg^{-1}$	0,11803
Density	ρ_f^*	$kg \cdot m^{-3}$	1081,8
Thermal Conductivity	λ_f^*	J/(m*day*°C)	5.2E4

Table F.4.7: Groundwater properties.

Equation 1 was used to simulate the temperature and TDS dependent water viscosity (Batzle & Wang, 1992) with salt content of 0.118 kg*kg-1:

$$\mu = 0.1+0.333s+(1.65+91.9TDS^3) \cdot exp(-[0.42(TDS^{0.8}-0.17)^2+0.045]\ T^{0.8}) \quad \text{(Equation 1)}$$

where

μ = water viscosity (cP);

TDS = total dissolved solids (kg*kg-1)

T = temperature (°C)

(iii) Initial and boundary conditions

The formula input into CMG STARS describe initial temperature changes over depth:

$$T = (x0 + x1) * 11 / 1200 + 21 \quad \text{(Equation 2)}$$

x0 = grid top (m)

x1 = grid bottom (m)

The temperature of the whole reservoir model covers a range from 27.8 to 32.6°C. This temperature range was determined from distributed temperature sensing in the reservoir according to the DTS monitoring graph from the internal report by Blöcher et al. (2023).

The pressure measured in borehole BH02 is around 51 bar at perforation depth [515 m(MD) or 495 m(TVD)] and thus corresponds to the initial pressure. Therefore, the initial pressure at reference depth is input as 5100kPa, the reference depth is true vertical depth 495m. The depth-average capillary-gravity method was applied with adding a phase pressure correction.

F.4.2.9. Results of history matching

The estimated productivity index from slug-withdrawal tests conducted on wellbore BH3 and BH2 were used for model validation (Table F.4.5). From the results as shown in Figure F.4.6, the hydraulic performance of two wells is very similar. From the well plan profile, the BH2 and BH3 were both penetrated through the same geological layers with approximative thickness. In the matching process, BH2 was validated. The validation was processed by CMG STARS considering the permeability of both upper and lower porous layers and surface water rate as variables. The permeability of the porous layers' ranges from 250mD to 700mD. The surface water rate ranges from 1200m^3/day to 2400m^3/day. For the purpose of validating the model, three production tests with permeability of 250mD, 500mD and 700mD for a period time of one month at a constant surface water rate 1200 m^3/day and 2400 m^3/day were simulated. The simulation result of three scenarios is shown in the following figure:

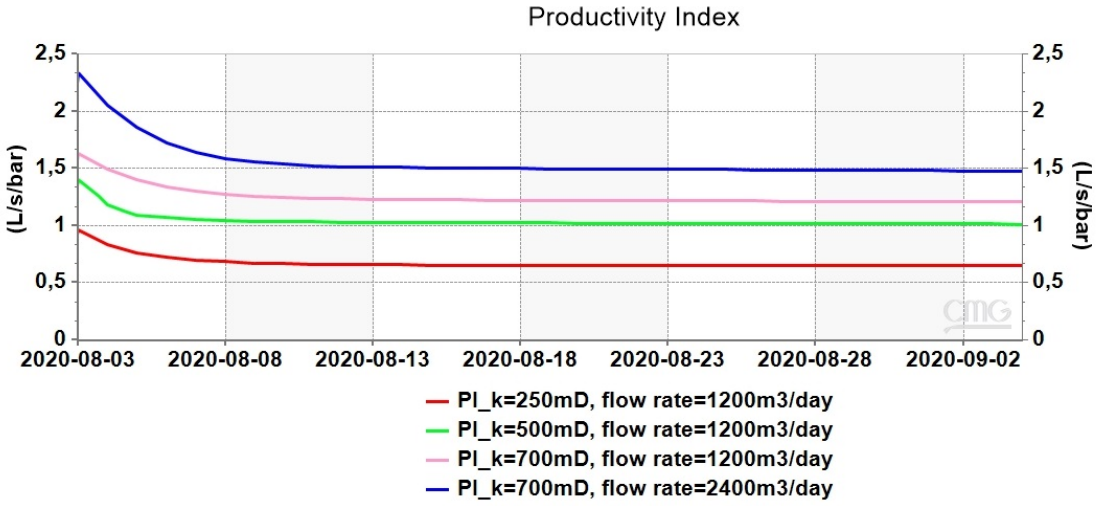

Figure F.4.6: Productivity Index matching results of BH2 with simulated permeabilities for porous layers.

From the simulated result: When k = 250mD for upper and lower porous layers, the simulated productivity index is higher than the estimated low boundary of the productivity index from the hydraulic tests. When k = 700mD, there is also a raised productivity index in comparison with the value estimated from the hydraulic tests. When k = 500mD, the curve shows a good predicted value of the productivity index lying in the range estimated from hydraulic tests (0.5-1.1 L/s/bar) in Table F.4.5.

F.4.3. Proof-of-concept (base case)

For the base case an additional deviated Flex-Well named NewDrill is introduced to the model for cold storage. The old well BH2 was simulated as hot well. As described in the wellbore model chapter, both Flex-Well models are applied with tubing and annulus configuration. The tubing string runs down the center of the well and is used for production. The annular space (between the tubing and casing) is used as an additional flow path, allowing for flexible seasonal changes between injection. This well was created by inputting horizontal trajectory data. The well path of two wellbore is shown in Figure F.4.7 with the distribution of permeability.

In the base case, we set the distance of the main perforation of these two wells as approximately over 200m, for this distance should prevent the thermal breakthrough. The simulation time is 20 years with seasonal well events. The setting of the time period starts on 01/08/2020 and ends on 01/08/2040. The heating period starts from 01/October each year and ends on 01/April in the next year. The cooling period starts on 01/April and ends on 01/October in the same year. The circulation rate is set as 600 m^3/day primarily considering the hydraulic properties of the reservoir and the thermal storage efficiency for this ATES system. The hydraulic properties set an upper limit on the flow rate to avoid excessive pressure drops or formation damage. For the thermal storage efficiency aspect, the circulation rate must be balanced to ensure water has enough residence time in the aquifer to retain or lose heat effectively and prevent thermal breakthrough. In order to determine a more realistic circulation rate, further studies need to be made for practical operation with aspects of heat/cooling demand, well capacity according to design and environmental and regulatory constraints. The injection temperature of water is set as 16°C for cold storage and 60°C for warm storage in the base case.

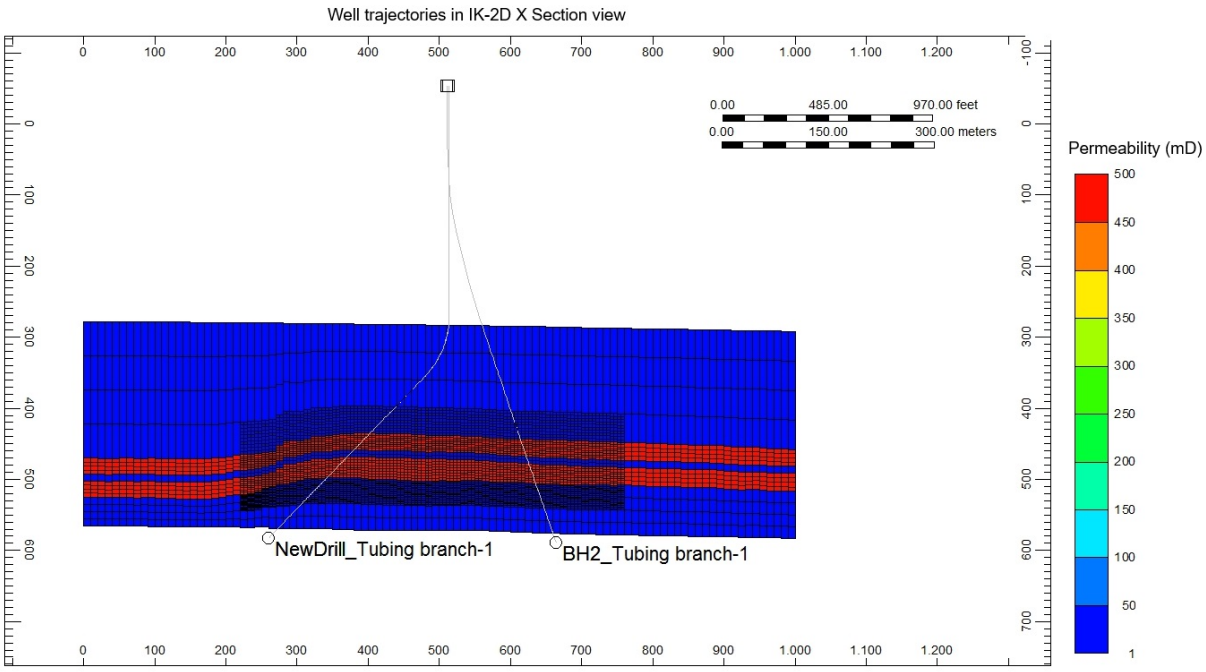

Figure F.4.7: Well trajectories of Flex-Well model of NewDrill and BH2 well.

The simulation results include the injectivity index (II) and productivity index (PI) for both cold and hot well storage, as well as the heat recovery factor for the hot well. The PI and II are used for evaluating the well performance. The heat recovery factor is for assessing how effectively the system recovers the stored energy. The heat recovery factor is defined as follows after Kranz, S. et al. (2015):

$$HRF = \frac{heat\ produced}{heat\ injected} = \frac{\int_{t0}^{t} \rho_w \cdot c_w \cdot Q_{pro}(t) \cdot [T_{pro}(t) - T_{reservoir}(t)]dt}{\int_{t0}^{t} \rho_w \cdot c_w \cdot Q_{inj}(t) \cdot [T_{inj}(t) - T_{reservoir}(t)]dt} \quad \text{(Equation 3)}$$

where

t0 = initial time (s)

t = time (s)

ρ_w = the density of the water ($kg \cdot m^{-3}$)

c_w = the volumetric heat capacity of water ($J \cdot m^{-3} \cdot K^{-1}$)

Q_{pro} = flow rate at production ($m3 \cdot s^{-1}$)

Q_{inj} = flow rate at injection ($m3 \cdot s^{-1}$)

T_{pro} = the temperature of produced water (°C)

T_{inj} = the temperature of injected water (°C)

$T_{reservoir}$ = the initial temperature of the reservoir (°C)

In the results of the base case simulation, the red dots and lines stand for hot well (BH2), and the blue ones represent cold well (NewDrill). The Figure F.4.8 shows that the productivity index of the hot well during the heating period is around 0.85 L/s/bar. The productivity index of the cold well during the cooling period is about 0.75 L/s/bar.

Even though the perforation length of the cold well NewDrill is longer than the perforation length of hot well BH2, both the productivity index and injectivity index of the hot well BH2 are higher than the cold well NewDrill. For practical considerations, pumping out hot water from hot well storage typically improves PI due to lower viscosity of the fluid.

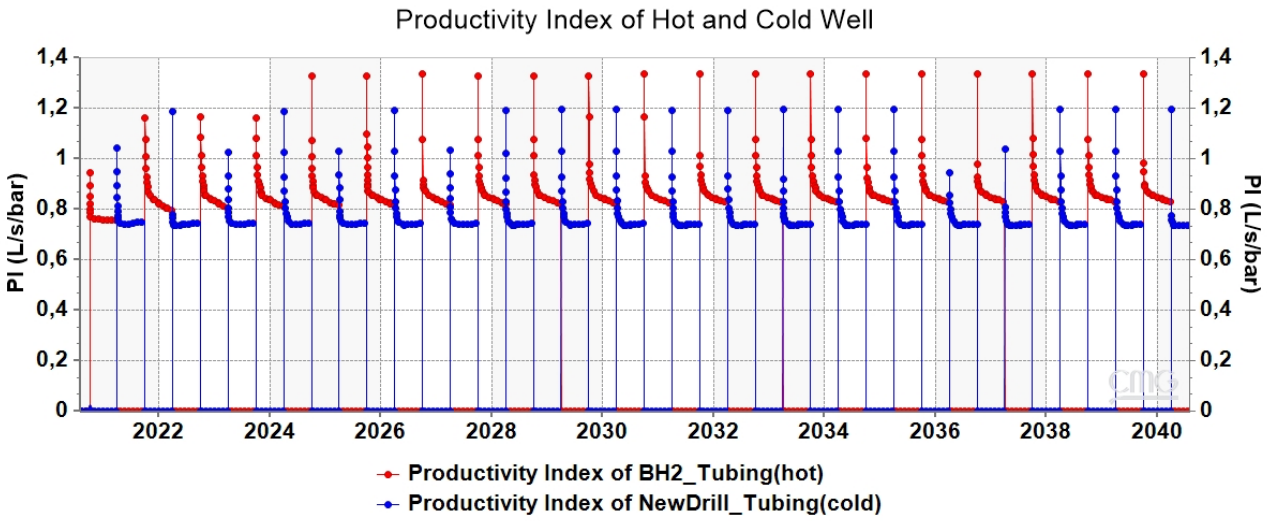

Figure F.4.8: Productivity index of cold and hot well.

From Figure F.4.9 the injectivity index of the hot well storage is 2.4 L/s/bar during the cooling period. Whereas the injectivity index of the cold well during the heating period is 2.2 L/s/bar.

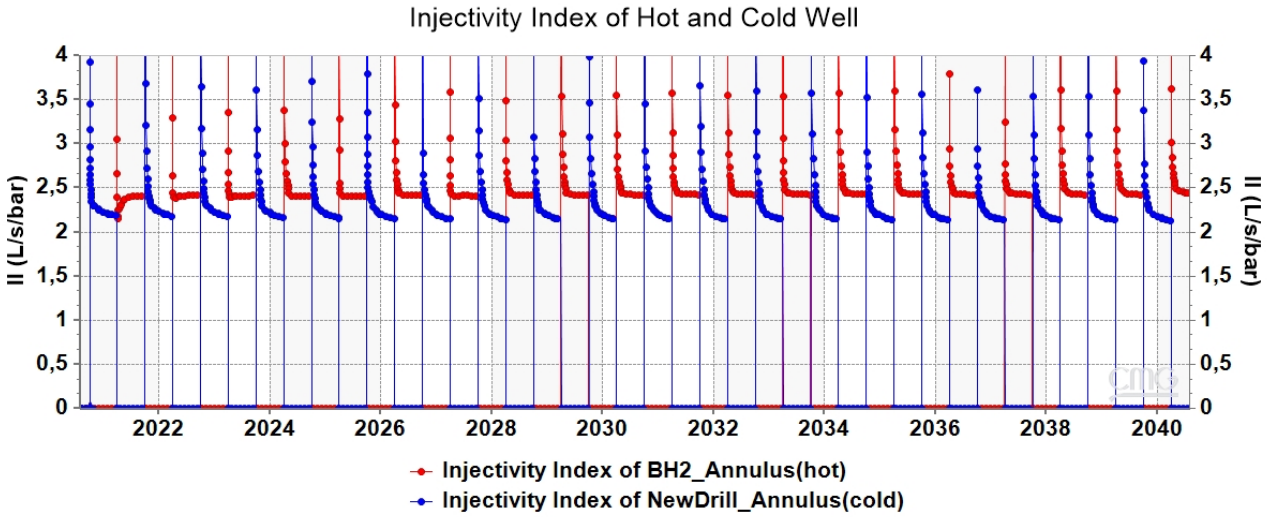

Figure F.4.9: Injectivity index of cold and hot well.

The heat recovery factor for hot well BH2 is projected to increase over the 20 years, reaching approximately 80% in the end (Figure F.4.10). The fluctuation in the heat recovery factor is due to cyclic injection and production. From equation 2, the heat recovery factor is calculated for every timestep. So, each declining phase represents a period of injection. Each increasing phase represents a production period.

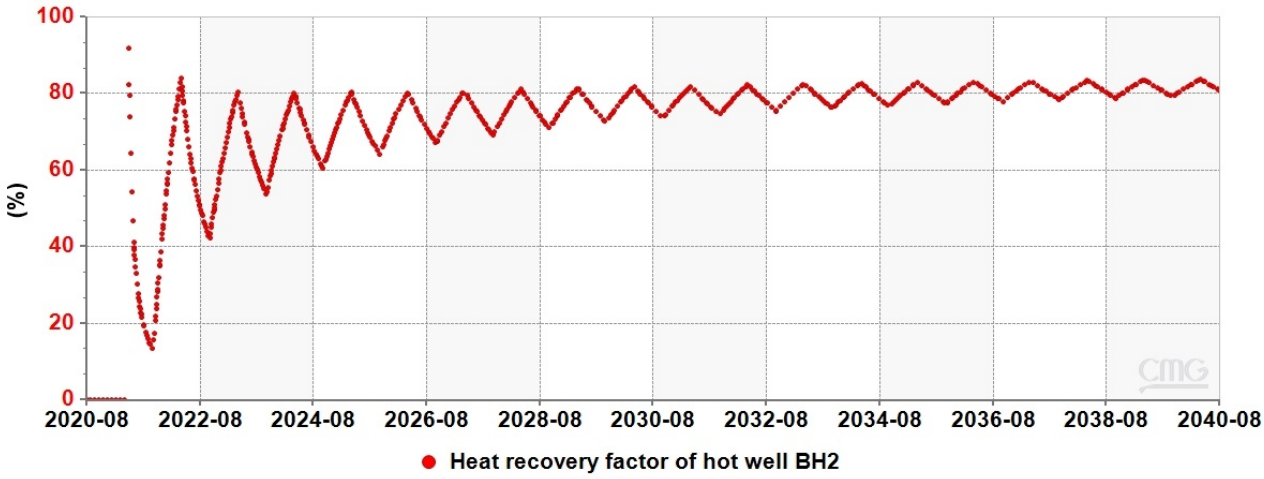

Figure F.4.10: Heat recovery factors of cold storage and warm storage wells in the base case scenario.

F.4.4. Sensitivity Analysis

In order to identify which parameter, have the most significant influence on model outputs of this ATES system, parameters of the reservoir of different ranges were modified according to references. The operating parameters such as injected water temperature are also included.

Thermal properties of reservoir and water, porosity and permeability of the reservoir, injecting temperature and formation compressibility are specified with different ranges in the parameterization part of CMOST as shown in Table F.4.8.

There are 67 experiments in total were simulated and analyzed by the CMOST. The results are illustrated in graphs by sobol analysis and Monte Carlo simulation.

Figure F.4.10 shows that the permeability of the perforated layers is the most influential parameter for the simulation result of the productivity index of the hot well during winter time. It accounts for almost 80% responsibility for the output of the PI from the hot well during winter.

However, the temperature of hot water injected into the hot well storage also has around 20% effect on influencing this output. As water temperature increases, its viscosity decreases, which reduces flow resistance. This can enhance the production rate for the same pressure drawdown, therefore, the PI increased.

There are 67 experiments in total were simulated and analyzed by the CMOST. The results are illustrated in graphs by sobol analysis and Monte Carlo simulation.

Parameters	Unit	Upper limit	Lower limit	Prior distribution	Number of Discrete Levels
Volumetric Heat Capacity of Rock	J(m/°C)	3.8E6	1.8E6	normal	11
Thermal Conductivity of Reservoir Rock	J(m·day·°C)	3.6E5	2.3E5	normal	11
Thermal Conductivity of Water Phase	J(m·day·°C)	6.048E4	4.752E4	normal	11
Temperature of water injected in cold well storage	°C	21	11	arithmetic sequence	6
Temperature of water injected in hot well storage	°C	85	35	arithmetic sequence	11
Permeability of Upper Matrix	mD	0.95	0.05	normal	11
Permeability of Upper Porous Layer	mD	700	250	normal	11
Permeability of Interlayer	mD	0.95	0.05	normal	11
Permeability of Lower Porous Layer	mD	700	250	normal	11
Permeability of Lower Matrix		0.95	0.05	normal	11
Porosity of Upper Matrix		0.090	0.001	normal	11
Porosity of Upper Porous Layer		0.34	0.10	normal	11
Porosity of Interlayer		0.090	0.001	normal	11
Porosity of Lower Porous Layer		0.34	0.10	normal	11
Porosity of Lower Matrix		0.090	0.001	normal	11
Formation Compressibility	kPa^{-1}	2E-5	2E-9	arithmetic sequence	10

Table F.4.8: Minimum and maximum values of different parameters input for the sensitivity analysis and their distribution.

Figure F.4.11 shows that the permeability of the perforated layers is the most influential parameter for the simulation result of the productivity index of the hot well during winter time. It accounts for almost 80% responsibility for the output of the PI from the hot well during winter. However, the temperature of hot water injected into the hot well storage also has around 20% effect on influencing this output. As water temperature increases, its viscosity decreases, which reduces flow resistance. This can enhance the production rate for the same pressure drawdown, therefore, the PI increased.

From Figure F.4.12, the productivity index of the cold well is mainly influenced by the permeability of the lower porous layers (58.3%) and the permeability of the upper porous layers (39.0%). Interestingly, the temperature of the injected water in the cold well has a minor effect of around 2.6% on the output of the PI from the cold well.

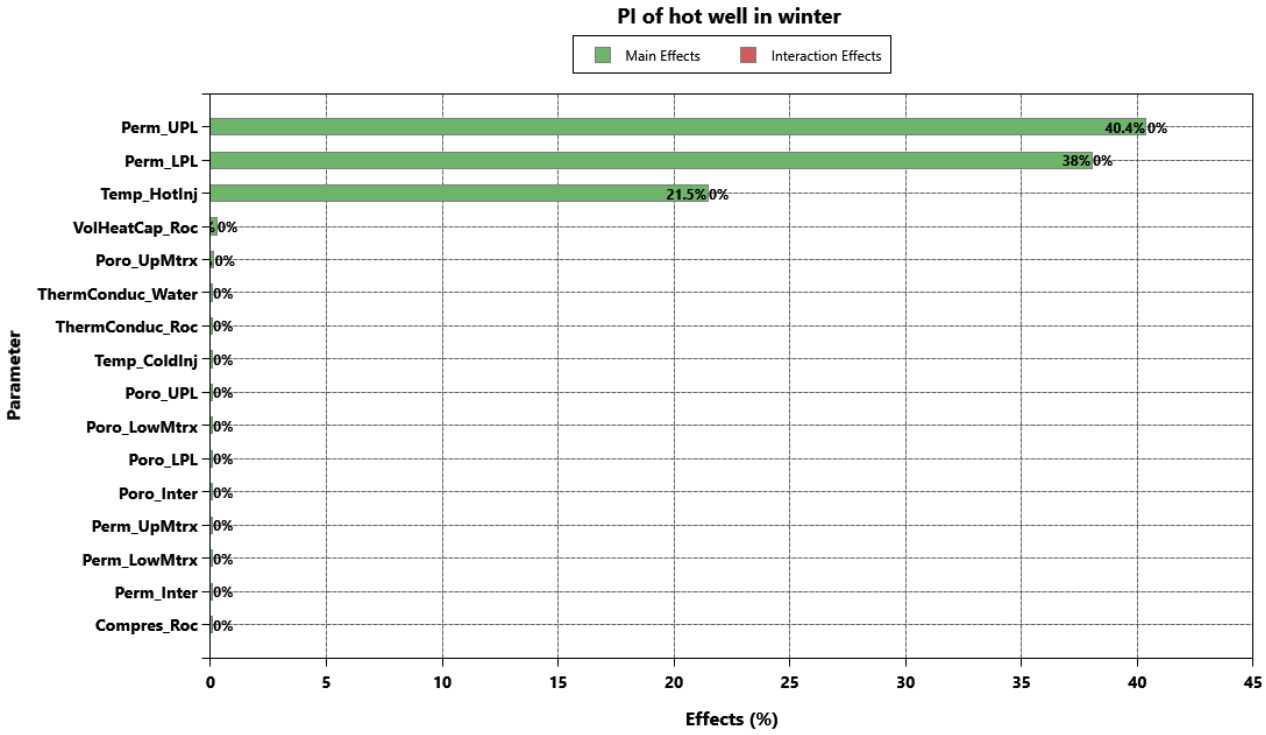

Figure F.4.11: Effect in % of parameters on the output of the productivity index of the hot well BH2.

Although the reason behind this result is the same due to the temperature influence on the viscosity of the water, the effect in percentage of the temperature of the injected water into the cold well on the output is not as significant as it on the output from the hot well. The possible reason is that the temperature difference between injected water into reservoir. For the hot storage, the biggest temperature difference is around 30 °C. Whereas for the cold well storage, the biggest temperature difference is only about 10°C.

Figure F.4.13 shows the same pattern with the results of the PI from hot well during winter. The effect in percentage of each parameter is 39.7% for permeability of the upper porous layers, 37.2% for permeability of the lower porous layers and 22.8% for the temperature of the injected water.

From figure F.4.14, the sobol analysis of the injectivity index from the cold well during winter also shows the similar results with the Figure 4.12. Same interpretation on the influence from these parameters can apply here.

Figure F.4.15 shows that the temperature of hot water injected in hot well storage is the most influential factor on the simulated results of the heat recovery factor. The interpretation behind this result is easy to draw as the formula of the heat recovery factor shows that, the influential part of its equation is the temperature difference between injected water and reservoir. However, the effect of the thermal conductivity of the bulk rock cannot be neglected, it influences around 5% of the output of the HRF. For this study site, the thermal energy exchange between the reservoir and the injected water is minor in the hot well storage. Even though high permeability ensures efficient fluid flow and porosity determines the effective storage volume of the reservoir, the permeability and porosity have little influence on the heat recovery factor for this study site. Besides that, the thermal process within aquifer is the dominant role, another possible reason is that the varying range of the permeability and porosity is not significant enough to affect the output of the HRF.

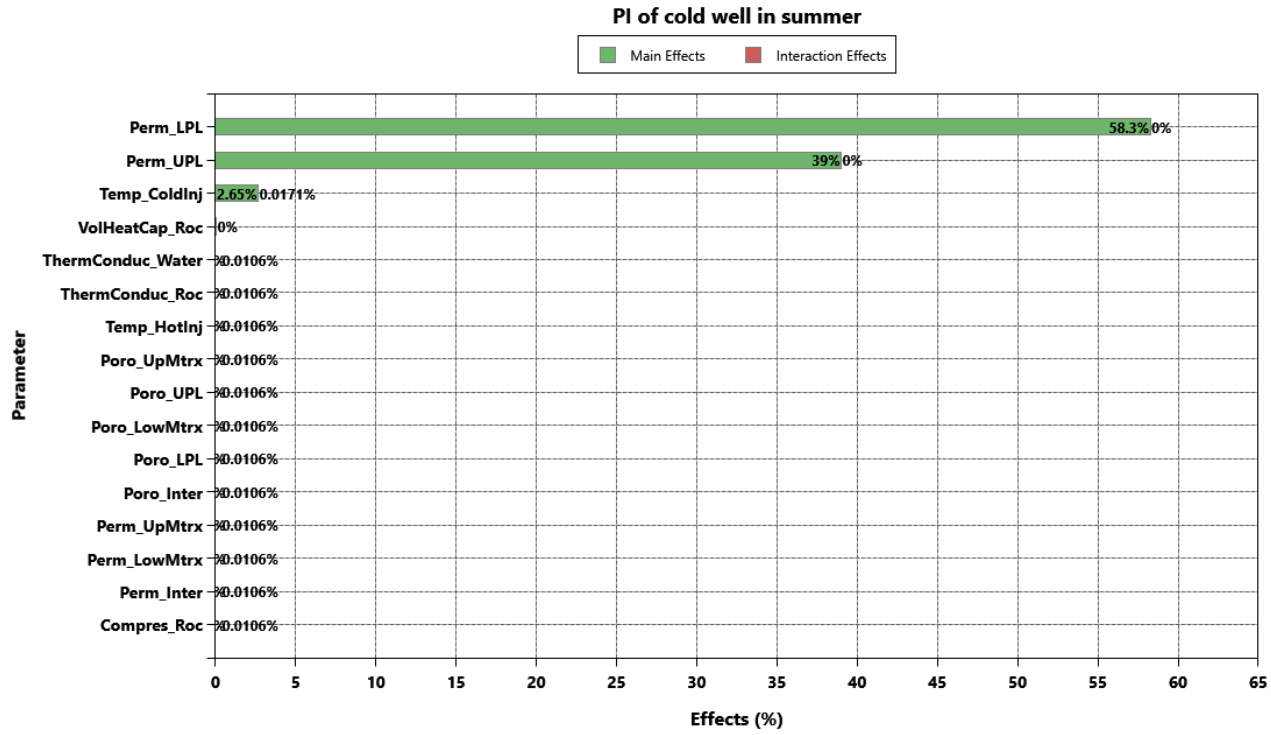

Figure F.4.12: Effect in % of parameters on the output of the productivity index of the cold well NewDrill.

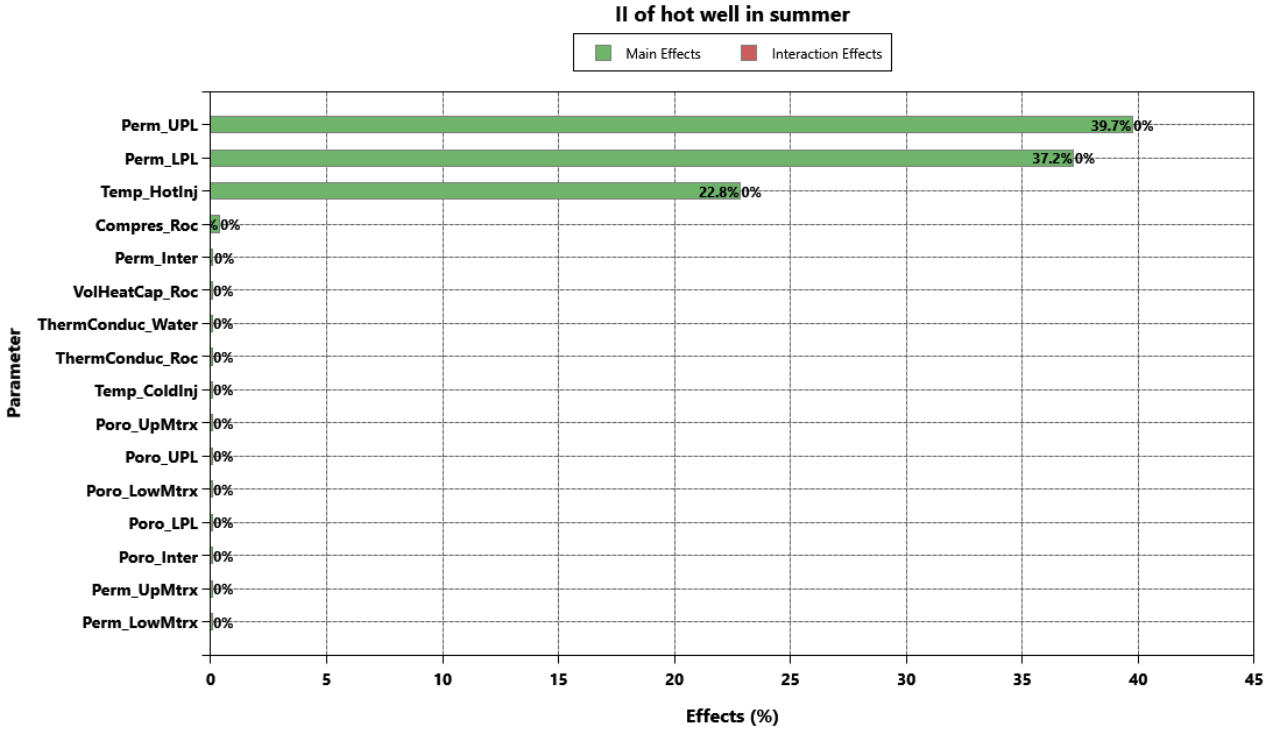

Figure F.4.13: Effect in % of parameters on the output of the injectivity index of the hot well BH2.

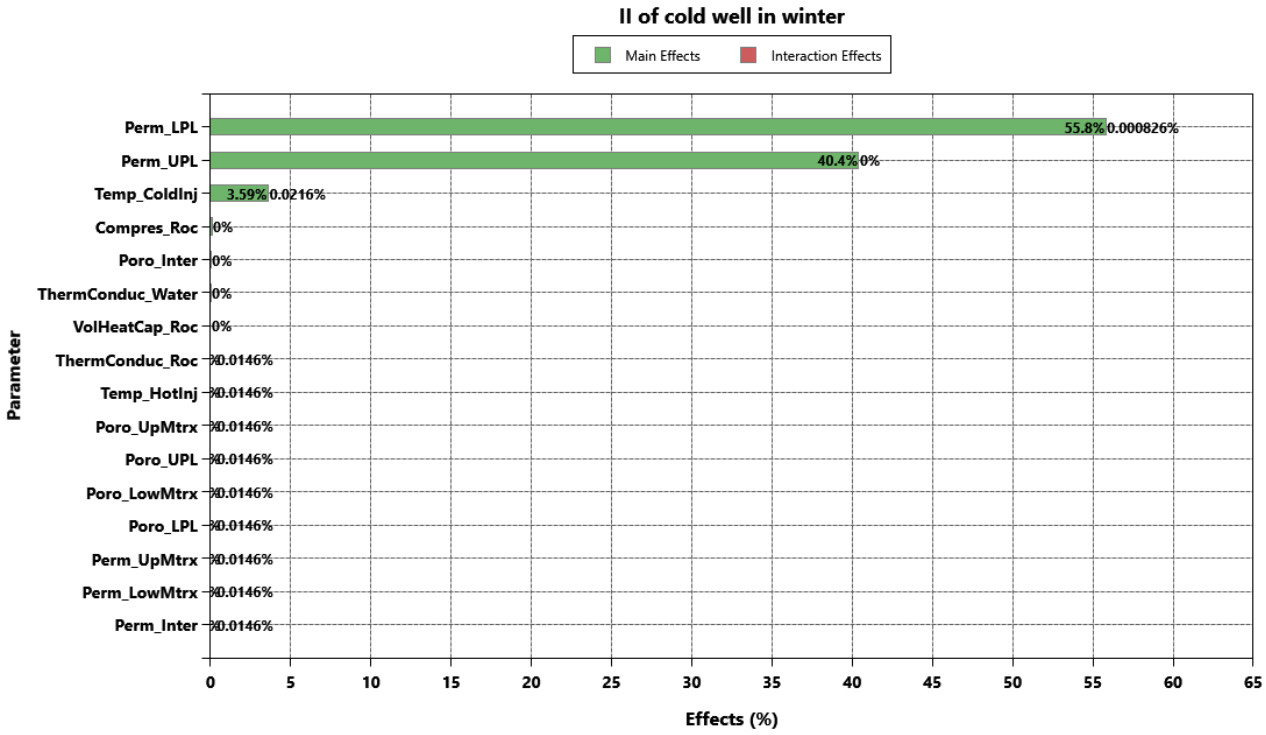

Figure F.4.14: Effect in % of parameters on the output of the injectivity index of the cold well NewDrill.

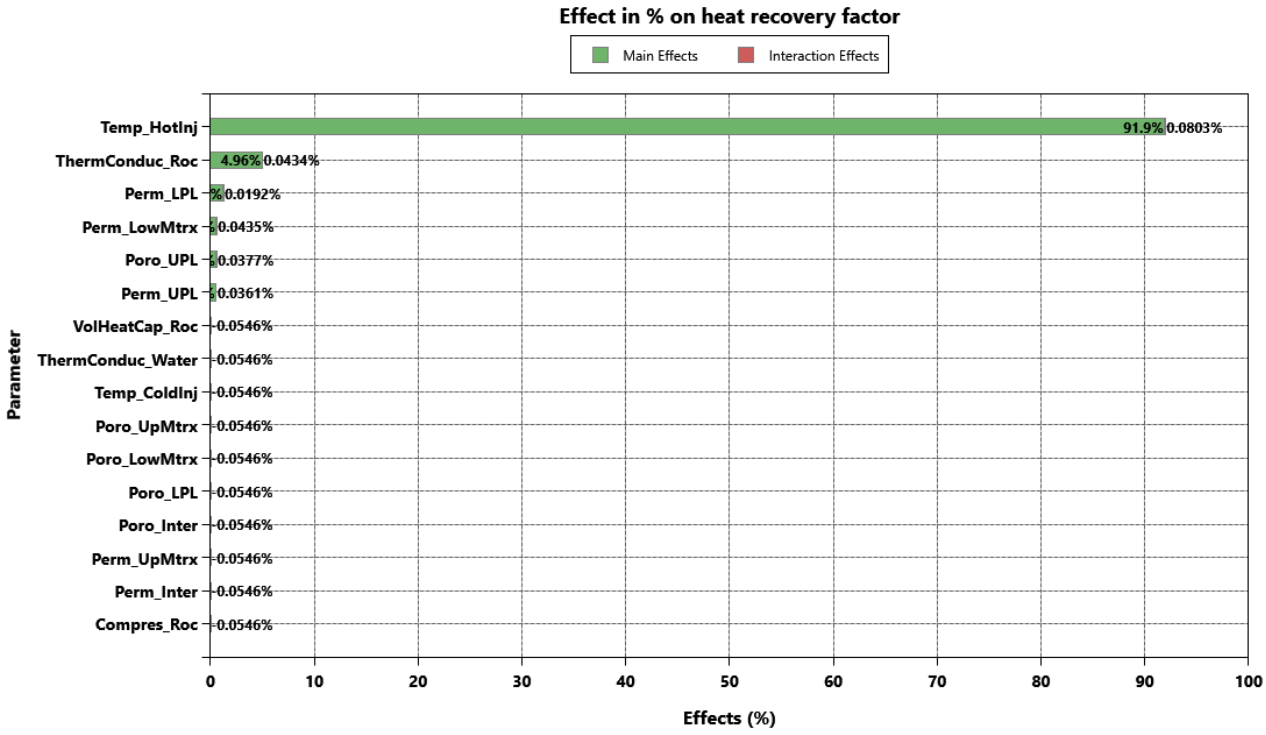

Figure F.4.15: Influential parameters and their effects in% on the heat recovery factor of hot well storage.

Figure F.4.16 shows the probability distribution of the PI and II from hot and cold wells using Monte Carlo simulation. The majority of the productivity index of the hot well lied between 0.7395 to 0.8843 L/s/bar, the median value is 0.8125 L/s/bar. This range is from 0.6722 to 0.7741 L/s/bar for the cold well, and the median value is 0.7235 L/s/bar. As for the injectivity index, the majority of them from the hot well ranged from 1.815 to 2.869 L/s/bar, it has a median value of 2.341 L/s/bar. For the cold well, the injectivity index ranged from 1.721 to 2.557 L/s/bar, the median value is 2.136 L/s/bar.

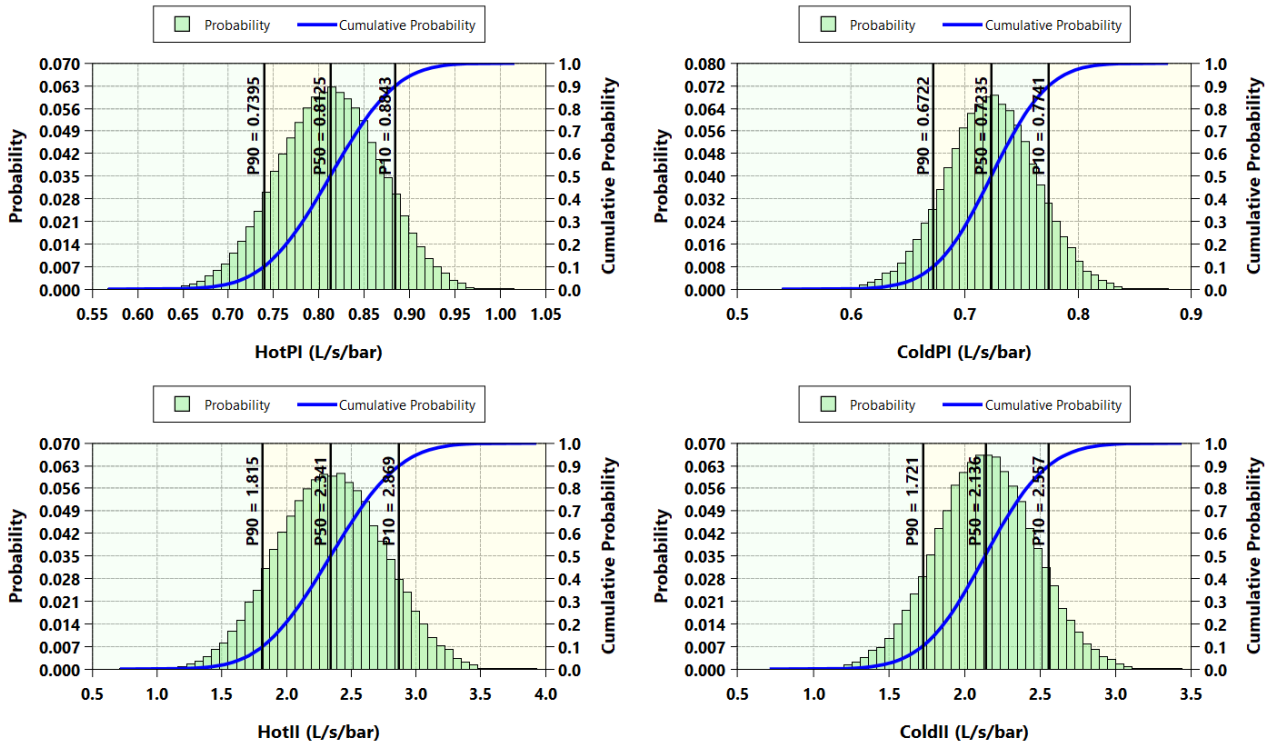

Figure F.4.16: Monte Carlo simulation results of PI and II of both hot and cold well.

The Monte Carlo simulation of the heat recovery factor at the end of whole operation shown in Figure F.4.17: indicates that the most part of the results lied between 80.27% to 81.40%.

In conclusion, many parameters can influence the outcome of the productivity index and injectivity index. From the aspect of aquifer properties, high-permeability with sufficient layer thickness support higher PI and II values. In well design point of view, proper well completion, for example longer perforation length enhances performance. Thermal properties of the rock and fluid also play role in well performance, because the viscosity differences between hot and cold water, which is influenced by the temperature, can impact flow resistance.

The thermal properties of reservoir rock and fluids play the most important part in the output of the heat recovery factor. Although the permeability can impact HRF by influencing the fluid flow and the porosity can determine the effective storage volume of the reservoir, very little effect was observed from the sensitivity analysis result. As the possible reason: The varying range for poro-perm parameters are presumably narrow and are same in all direction therefore lacking the heterogeneity.

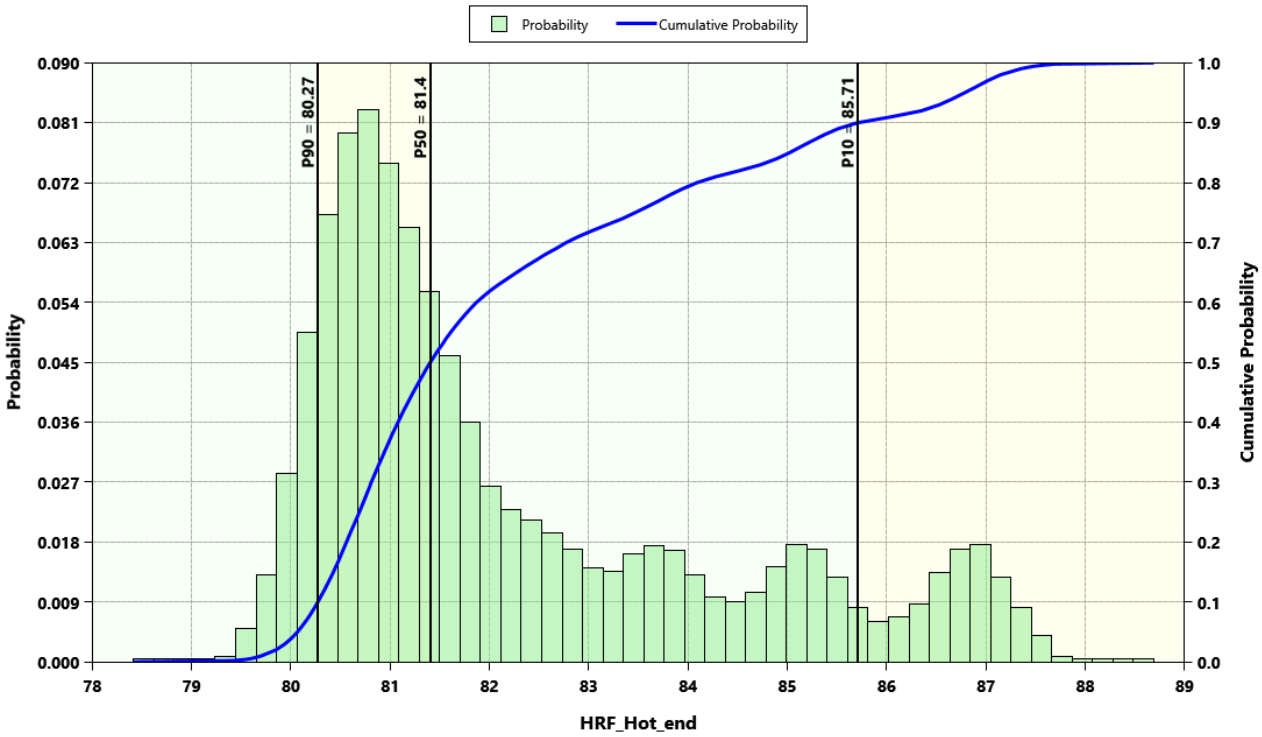

Figure F.4.17: Monte Carlo simulation results of heat recovery factor of hot well.

F.5. Requirements to reuse hydrocarbon wells for Aquifer Thermal Energy Storage

F.5.1. Reservoir and wellbore properties

Reservoir performance (productivity index PI or injectivity index II) depends mainly on the transmissivity (permeability * thickness) of a reservoir. Based on the literature review and modelling of the Berlin-Spandau reference site, a minimum transmissivity of 2e-12 m^3 or 200 m Dm is required for typical ATES systems. This is equivalent to a permeability of 1e-13 m^2 (100 mD) of a reservoir with a thickness of 20 m. In addition to permeability, porosity, volumetric heat capacity and thermal conductivity are the parameters that mostly affect the thermal recovery rate. This is related to the heat storage capacity in relation to the seasonal cycle of the ATES system. 90% of the recovery rate is expected from the reservoir for a balanced and sustainable production - injection of hot and cold wells for a cyclic system. Between cycles, the reservoir acts as a reservoir that must maintain a stable temperature for at least one cycle period or a 6 months interval period. A minimum porosity of 0.1 (10%) is required to develop a reservoir as an ATES system. Another point to consider is the groundwater velocity. High groundwater velocities would transfer the stored heat away from the storage well by natural convection. For example, in the Reichstag-Berlin project in Germany, a groundwater velocity of 3.65 m/year is required. Ideally, there would be no natural groundwater flow in an ATES, which is true for most deep reservoirs. The temperature requirements for ATES systems are highly case-specific as they depend on the required storage temperature. Most ATES systems are utilizing relatively shallow aquifers (in the range of 500 - 600 m depth). In the case of well reuse, the diameter of the bottom hole will have an impact on well productivity and injectivity indices, as studied dem. The larger the bottom hole diameter, the greater the impact on productivity and injectivity indices. The summary of requirements parameters for reservoir and wellbore properties are described in Table F.5.1.

F.5.2. Operating parameters

Based on the sensitivity analysis by varying the injection temperature as an operating parameter of the ATES system, the thermal recovery factor is strongly influenced by the injection temperature. Itt is highly dependent on the available heat source and the return injection temperature. The heat source could be industrial waste heat or excess heat from power generation that can be stored for seasonal heating/cooling demand by deploying an ATES system. A summary of the literature review of the operating parameters is described in Table F.5.2.

Parameters	Unit	Max	Median	Min	Reference Site	Required parameters to reuse hydrocarbon well for ATES
Reservoir Depth	m	1250	620	15	[Max] Neubrandenburg, Germany [Median] Spandau, Germany [Min] Rostock, Germany	< 1000
Max [Würdemann et al., 2014; Holstenkamp et al.,2017] Median [Blöcher et al., 2023] Min [Schmidt and Müller-Steinhagen, 2004]						
Reservoir Thickness	m	> 170	30	4	[Max] Reichstag-Berlin, Germany [Median] Spandau, Germany [Min] TU Berlin, Germany	> 5
Max [Kabus and Seibt, 2000; Sanner and Knoblich, 2004] Median [Blöcher et al., 2023] Min [Saadat et al., 2016]						
Natural Fluid Velocity	m/year	25	-	3.65	[Max] Minimum fluid velocity range in Netherlands [Min] Reichstag-Berlin, Germany	< 3.65
Max [Bloemendal, 2018] Min [Kranz und Frick, 2013]						
Reservoir Temperature	°C	140	54	13.2	[Max] Deepstore-KIT, Germany [Median] Neubrandenburg, Germany [Min] Adlershof-Berlin, Germany	< 100
Max [Deepstore description, 2020] Median [Würdemann et al.,2014] Min [Blöcher et al., 2018]						
Porosity	%	0.38	0.24	0.06	[Max] Reichstag-Berlin, Germany [Median] Spandau, Germany [Min] Adlershof, Germany	> 0.1
Max [Kabus et al.,2005] Median [Blöcher et al., 2023] Min [Blöcher et al., 2018]						
In-situ Permeability	m^2	1×10^{-10}	1×10^{-12}	1×10^{-13}	[Max, Min] Adlershof, Germany [Median] TU Berlin, Germany	$> 1 \times 10^{-13}$
Max, Min [Blöcher et al., 2023] Median [Saadat et al., 2016]						
Flow rate	L/s	135	60	5	[Max] Spandau, Germany [Median] Reichstag-Berlin, Germany [Min] TU Berlin	> 50
Max [Blöcher et al., 2023] Median [Kabus and Seibt, 2000] Min [Saadat et al., 2016]						
Bottom-hole diameter	inch	13 3/8	9 5/8	2	[Max, Median] Spandau, Germany [Min] Kieh University Project, Germany	> 7
Max, Median [Blöcher et al., 2023] Min [Heldt et al., 2021]						
Productivity Index/ Injectivity Index	L/s/MPa	24.86	15	5	[Max] Reichstag, Germany [Median] Spandau, Germany [Min] Spandau, Germany	> 10
Max [Kabus et al., 2005] Median, Min [Blöcher et al., 2023]						

Table F.5.1: Reservoir and wellbore parameters required for ATES Technology.

Parameters	Unit	Max	Median	Min	Reference Site
Recovery Rate	%	93	89	72	[Max] Reichstag-Berlin, Germany [Median] Westland, Neatherland [Min] Neubrandenburg
ATES Factsheet [Kleyböcker & Bloemendal., 2020]					
Temperature (in) Warm Borehole	Celcius	90	50	16	[Max] TU Berlin, Germany [Median] Rostock, Germany [Min] Adlershof, Germany
Max [Holstenkamp et al., 2017] Median [Schmidt et al., 2004] Min [Blöcher et al., 2018]					
Temperature (out) Warm Borehole	Celcius	90	50	25	[Max] Spandau, Germany [Median] Rostock, Germany [Min] Lüneburg, Germany
Max [Blöcher et al., 2023] Median [Schmidt et al.,2004] Min [Holstenkamp et al., 2017]					
Temperature (in) Chill Borehole	Celcius	130	85	5	[Max] BMW-Dingoflingen, Germany [Median] Lüneburg, Germany [Min] Reichstag-Berlin, Germany
Max [Ueckert et al. (2019), Holstenkamp et al., 2017] Median [Holstenkamp et al., 2017] Min [Kranz and Frick, 2013]					
Temperature (out) Chill Borehole	Celcius	25	10	5	[Max] Lüneburg, Germany [Median] Reichstag-Berlin, Germany [Min] Spandau, Germany
Max [Holstenkamp et al., 2017] Median [Kranz and Frick, 2013] Min [Blöcher et al., 2022]					

Table F.5.2: Summary of literature review of ATES operating parameters.

F.6. Workflow to reuse hydrocarbon wells for Aquifer Thermal Energy Storage

The workflow of ATES from the reuse case as described in this study is mainly adopted from the Spandau project (Blöcher et al., 2023) and best practice of ATES well development from the literature review. Considering the location of hydrocarbon wells are already within the radius of the district heating and potential geothermal gradient are known, the workflow is summarised as follows.

1. Well investigation

The objective is to provide optimum access to the depth of the target reservoir for storage. This includes the investigation of well integrity in relation to the condition of the casing. This hydraulic access as well as the hydrogeological characteristics of the target reservoir are then tested with appropriate hydraulics as part of the evaluation of the suitability of the reservoir for ATES implementation. The well investigation can also be carried out by performing the necessary logging such as pressure, temperature and calliper tests.

2. Well workover operation

Permits are required for any workover operation. As in the case of the Spandau project, permits are required to perforate at the interval depth of the target reservoir and to conduct hydraulic testing in the reservoir section. In the case of Germany, at least 4 permits are required for well completion and hydraulic testing:

- Special operating plan for the recompletion of wells BH2 and B14
- General operating plan and hydraulic test
- Application for a commercial geothermal exploration permit
- Water Law Permit to Conduct Hydraulic Tests

Perforation is particularly necessary if the potential reservoir is completely or partially backfilled with cement. This workover operation also includes the installation of downhole instruments such as DTS Downhole Temperature Sensing at the reservoir depth in preparation of the hydraulic tests. For this purpose, a fibre optic (FO) sensor cable is usually temporarily installed using a borehole winch. The temperature distribution along the borehole is then recorded using Distributed Temperature Sensing (DTS) technology. The sensor cable can also be used to insert a UGS depth gauge into the borehole to record pressure and temperature at the reservoir level. Distributed Acoustic Sensing (DAS) measurements were also taken using the sensor cable. The DTS and DAS measurements were taken continuously over a period of the nitrogen lift test.

3. Performing hydraulic test and downhole sampling

The following hydraulic tests are carried out to evaluate the reservoir and well parameters for each well. Prior to this test, depending on the availability of well data and the additional information required to conduct a feasibility study, it is recommended that the test be performed:

- **A nitrogen lift test (NLT) or short-term production test** with subsequent shut-in to determine the transmissibility and skin factor of the well, with DTS measurement and hydro-chemical and microbiological monitoring program. For this test, a surface facility as pump and surface tank were needed in the surface to accommodate the test and produced reservoir fluid. Simultaneously, temperature distribution along the borehole is then recorded using Distributed Temperature Sensing (DTS) technology. The sensor cable can also be used to insert a downhole gauge into the

borehole to record pressure and temperature trends. Distributed Acoustic Sensing (DAS) measurements are also taken using the sensor cable. The DTS and DAS measurements were taken continuously over a period of the nitrogen lift test and after the list test to observe the pressure recovery after conducting the nitrogen lift test.

- **Performing Step Rate Test (SRT)/ Slug Withdrawal test**. The purpose is to determine a reliable productivity index, steady state conditions. The transmissivity and storativity can be derived from the SRT tests. Both SRT and SWT can be used to determine the change in aquifer properties caused by hot water injection and change in storativity by conducting the same test procedure.
- **Push-Pull Tests (PPT) with tracers**. The purpose of this test is to analyse the longitudinal dispersion, natural groundwater velocity, and to obtain the attenuation factor caused by cross-flow. Injecting the tracers together with hot water and monitoring the temperature with **Distributed temperature sensing** (DTS) can improve the performance of Push-pull tests (PPT).
- **Injection test (IT)** of the previously extracted thermal water to determine the injectivity index. During the short-term production tests temperature and conductivity measurements on surrounding groundwater measurement points are recommended to be performed. As ATES is an open system, the monitoring is important to assess any impact of production-injection operation to the surrounding formation.
- **Downhole sampling** to determine gas concentration for gas wells or oil content for oil wells. Downhole sampling can be carried out after removing the downhole instruments used during short-term production testing and performing the necessary logging to obtain a fluid sample from the target reservoir. The fluid sample can be subjected to chemical and microbiological characterization and contaminant analysis.
- The short-term test is designed to evaluate the reservoir behavior over a given period of time. Long-term production tests or long historical production-injection data are therefore recommended to gain an understanding of reservoir properties such as permeability, which is the most important parameter for ATES feasibility assessment. The lesson learned from Spandau is that 16 hours of hydraulic testing is not enough to provide subsurface information. History matching is difficult to achieve in a short period of flow testing. A minimum of 2 weeks to 1 month of continuous production testing is required to justify the feasibility of reservoir performance.

4. Perform analytical and numerical modelling as a part of feasibility study

This step is important to evaluate the performance of the reservoir calibrated with the field measurement. The purpose is to evaluate an ideal operation parameter of the ATES system based on the given condition as observed during the short-term production test. This step will be followed by a feasibility study to plan the development of the ATES system. From this study, further well rehabilitation and modification can be designed to meet the required energy output expected from the reservoir by implementing the ATES technology.

5. Perform well modification and well completion or drilling a new ATES well as decided from the feasibility study

In ATES wells, depending on the size of the well, two strings can be installed in the same well to act as production and injection tubing. A single string can also be used in two different wells at different locations. ESP (downhole pump) for the production well, fibre optic/sensor cable for DTS and DAS measurement are the main elements for well completion. The completion of the ATES well, typically employ filters at the targeted reservoir depth interval. The bottom of the well, which is not exposed to the reservoir section, is usually filled with gravel or even cemented. The typical of ideal ATES design is shown in Figure F.6.1. This was an example from ATES Berlin Fasanenstrasse project (Blöcher et al., 2024).

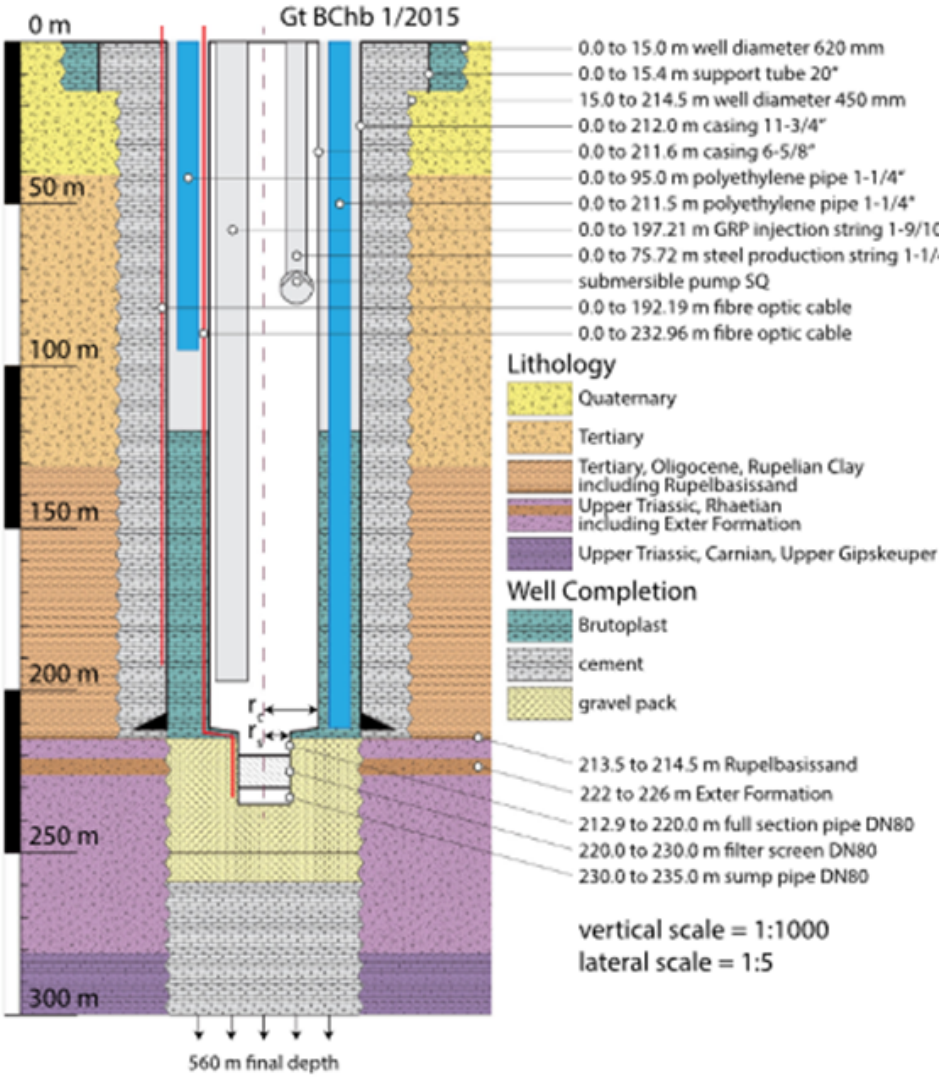

Figure F.6.1: Typical of ATES well completion design. Well completion and lithology of well Gt BChb 1/2015 (Blöcher et al., 2024).

F.7. References

Andersson, O., Sellberg, B. (1993) Swedish ATES Applications: Experiences after Ten Years of Development. In: Jenne EA, editor. Aquifer Thermal Energy (Heat and Chill) Storage: Proceedings of the 27th intersociety energy conversion engineering conference, San Diego, CA; 1993, p. 1–9.

Andersson, O., Hellström, G., Nordell, B. (2013) Heating and cooling with UTES in Sweden current situation and potential market development: Proceedings of the 9th international conference on thermal energy storage, Warsaw, Poland, Futurestock.

Benner, M., Bodmann, M., Mangold, D., NuÞbicker, J., Raab, S., Schmidt, T., Seiwald, H. (2003) Solar unterstützte Nahwärmeversorgung mit und ohne Langzeit-Wärmespeicher. Scientific Technical Report. ISBN-Nr. 3-9805274-2-5.

Beernink, S., Hartog, N., Bloemendal, M., Van der Meer, M. (2019) ATES systems performance in practice: analysis of operational data from ATES systems in the province of Utrecht, The Netherlands. In Proceedings of the European Geothermal Congress, Den Haag, The Netherlands.

Bloemendal, M., Van den Ven, Frans H.M., Slenders, H. L. A. (2016) Europe-wide Use of Sustainable Energy from aquifers. barrier assessment. Technical report.

Bloemendal, M., Hartog, N. (2018) Analysis of the impact of storage conditions on the thermal recovery efficiency of low-temperature ATES systems. Geothermics, 71, 306-319.

Bloemendal, M., Beernink, S., van Bel, N., Hockin, A., Schout, G. (2020) Transitie open bodemenergiesysteem Koppert-Cress naar verhoogde opslag temperatuur. KWR 2020.156.

Blöcher, G., Kranz, S., Saadat, A. (2018) Aquifer-Kälte-Speicher Campus Adlershof Geologische und energietechnische Bewertung. Scientific Technical Report.

Blöcher, G., Deon, F., Wenzlaff, C., Winterleiter, G., Regenspurg. S, Virchow, L. (2023) Abschlussbericht des Vorhabens Geothermische Nutzung der Karbonatgesteine im Norddeutschen Becken ATES iQ. Scientific Technical Report.

Blöcher, G., Regenspurg, S., Kranz, S., Lipus, M., Pei, L., Norden, B., Reinsch, T., Henninges, J., Siemon, R., Orenczuk, D., Zeilfelder, S., Scheytt, T., Saadat, A. (2024) Best practices for characterization of High Temperature-Aquifer Thermal Energy Storage (HT-ATES) potential using well tests in Berlin (Germany) as an example. Geothermics 116, 102830.

Bossennec C, Géraud Y, Böcker J, Klug B, Mattioni L, Bertrand L, Moretti I. Characterisation of fluid flow conditions and paths in the Buntsandstein Gp. sandstones reservoirs. Upper Rhine Graben BSGF. 2021;192:35. https:// doi. org/ 10.1051/ bsgf/ 20210 27.

Bär K. Assessment of the deep geothermal potentials of Hessen (Untersuchung der tiefengeothermischen Potenzialevon Hessen) [PhD thesis]: Technische Universität Darmstadt; 2012.

Chant V, Morofsky E. (1993) Overview of Projects with Seasonal Storage for Cooling from Four Countries. in: Jenne EA, editor. Aquifer Thermal Energy (Heat and Chill) Storage: Proceedings of the 27th intersociety energy conversion engineering conference, San Diego, CA p. 17–21.

CMG V2024.20. Calgary, Alberta, Canada: Computer Modelling Group Ltd.

Driesner, et al. (2021) Final report on tools and workflows for simulating subsurface dynamics of different types of High Temperature Underground Thermal Energy Storage. Heatstore-D2.1.

Drijver, B., Bakeman, G. Oerlemans, P. (2019) State of the art of HT-ATES in The Netherlands. European Geothermal Congress 2019 Den Haag, The Netherlands.

Duijff, R., Bloemendal, M., Bakker, M. Interaction effects between Aquifer Thermal Energy Storage Systems. https://doi.org/ 10.1111/gwat.13163.

Freeze, R., Cherry, J. (1979) Groundwater, Prentice-Hall, Engelwood Cliffs NJ.

Fleuchaus, P., Godschalk, B., Stober, I., Blum, P. (2018) Worldwide application of aquifer thermal energy storage – A review. Renewable and Sustainable Energy Reviews, 94, 861-876.

Fleuchaus, P., Schüppler, S., Godschalk, B., Bakema, G., Blum, P. (2020) a Performance analysis of Aquifer Thermal Energy Storage (ATES). Renewable Energy, 146, 1536e1548.

Fleuchaus, P. (2020) Global application, performance and risk analysis of Aquifer Thermal Energy Storage (ATES). Dissertation.

Fleuchaus, P., Schüppler, S., Bloemendal, M., Guglielmetti, L., Opel, O., Blum, P. (2020) Risk analysis of High-Temperature Aquifer Thermal Energy Storage (HT-ATES). Renewable and Sustainable Energy Reviews 133, 110153.

Fleuchaus, P., Schüppler, S., Stemmle, R., Menberg, K., Blum, P. (2021) Aquiferspeicher in Deutschland. Grundwasser - Zeitschrift der Fachsektion Hydrogeologie (2021) 26:123–134.

Frick, M.; Bott, J.; Scheck-Wenderoth, M.; Cacace, M.; Nasrin, H.; Schneider M. (2020): 3D geological model of Berlin - Germany. GFZ Data Services.

Frick, M., Kranz, S., Norden, B., Bruhn, D., Fuchs, S. (2022) Geothermal Resources and ATES Potential of Mesozoic Reservoirs in the North German Basin. Energies, 15, 1980.

Fuchs, S., Balling, N., & Förster, A. (2015). Calculation of thermal conductivity, thermal diffusivity and specific heat capacity of sedimentary rocks using petrophysical well logs. Geophysical Journal International, 203(3), 1977–2000. https://doi.org/10.1093/gji/ggv403

Goldscheider, N., M´adl-Sz˝onyi, J., Er˝oss, A., Schill, E., 2010. Review: Thermal water resources in carbonate rock aquifers. Hydrogeol. J. 18, 1303–1318.

Haffen S, Géraud Y, Diraison M, Dezayes C. (2012) Determining majors fluid-flow zones in a geothermal sandstone reservoir from thermal conductivity and temperature logs. In: EGU General Assembly; p. 9043.

Heine, F.N. (2021) Reservoir characterisation of the deep Upper Jurassic aquifer in the South German Molasse Basin using water chemical data and environmental isotopes [PhD thesis]: Technische Universität München.

Huenges, et al. (2005) Thermische Untergrundspeicher in Energiesystemen: Optimierung der Einbindung der Aquiferspeicher in die Wärme- und Kälteversorgung der Parlamentsbauten im Berliner Spreebogen (FKZ 0329809C).

Holstenkamp, L., Meisel, M., Neidig, P., Opel, O., Steffahn, J., Strodel, N., Lauer, J., Vogel, M., Degenhart, H., Michalzik, D., Schomerus, T., Schönebeck, J., Növig, T. (2017) Interdisciplinary review of medium-deep aquifer thermal energy storage in North Germany. Energy Procedia, 135, 327-336.

Holstenkamp, et al. (2017) Interdisciplinary Review of Medium-deep Aquifer Thermal Energy Storage in North Germany. Energy Procedia 135 (2017) 327–336.

IEA. (2016) Implementing Agreement for a programme of research and development on energy conservation through energy storage. Strategic Plan, 2016–21.

Kabus, F. and Seibt, P. (2000). Aquifer Thermal Energy Storage For the Berlin Reichstag building – new seat of the German Parliament. Proc. WGC 2000, 3611-3615.

Kabus, F., Seibt, P. (2000) Aquifer Thermal Energy Storage for the Berlin Reichstag Building-New Seat of The German Parliament. Proceedings World Geothermal Congress 2000, Kyushu - Tohoku, Japan, May 28 - June 10, 2000.

Kleyböcker, A., Bloemendal, M. (2020) Factsheet – Aquifer thermal energy storage (ATES).

Kranz, S., Frick, S., (2013) Efficient cooling energy supply with aquifer thermal energy storages, Applied *Energy*, 109 (2013) 321–327.

Kranz, S., Blöcher, G., Saadat, A. (2015) Improving Aquifer Thermal Energy Storage Efficiency. *Proceedings World Geothermal Congress*, Melbourne.

Lee, K.S. (2010) A Review on Concepts, Applications, and Models of Aquifer Thermal Energy Storage Systems. *Energies 3*, 1320-1334.

Lee, K.S. (2013). Underground Thermal Energy Storage. Springer London.

Lerm, S., Alawi, M., Miethling-Graff, R., Wolfgramm, M. (2011) Influence of microbial process on the operation of a cold store in shallow aquifer: impact on well injectivity and filter lifetime, *Grundwasser-Zeitschrift der Fachsektion Hydrogeologie*, 16:93–104. http://doi.org/10.1007/s00767-011-0165-x

Lerm, S. (2012) Mikroorganismen in geothermischen Aquiferen – Einfluss mikrobieller Prozesse auf den Anlagenbetrieb, Dissertation, Mathematisch-Naturwissenschaftliche Fakultät, Universität Potsdam.

Lu, H., Tian, P., He, Li. (2019) Evaluating the global potential of aquifer thermal energy storage and determining the potential worldwide hotspots driven by socio-economic, geo-hydrologic and climatic conditions. *Renewable and Sustainable Energy Reviews* 112 (2019) 788–796.

Meurs, A.M. (1985) Seasonal heat storage in the soil. Technische Hogeschool Delft: Pijnacker. Morofsky E. History of thermal energy storage. In: Paksoy HÖ., editor. Thermal Energy Storage for Sustainable Energy Consumption. Dordrecht: Springer Netherlands; 2007. p. 3–22.

Moeck, I.S., Dussel, M., Weber, J., Schintgen, T., Wolfgramm, M., 2020. Geothermal play typing in Germany, case study Molasse Basin: a modern concept to categorise geothermal resources related to crustal permeability. Netherlands J. Geosci. 98, 1–10.

Mraz, E., Wolfgramm, M., Moeck, I., Thuro, K. (2019). Detailed Fluid Inclusion and Stable Isotope Analysis on Deep Carbonates from the North Alpine Foreland Basin to Constrain Paleofluid Evolution. Geofluids vol. 2019, Article ID 8980794, 1–23. DOI: 10.1155/2019/8980794

Noack, V., Schroeder, J.H. Porosity development and distribution in the Rüdersdorfer Schaumkalk (Middle Triassic) of the Gas Store Berlin, Germany. Facies 48, 255–268 (2003). https://doi.org/10.1007/BF02667543

Noack, V., Scheck-Wenderoth, M., Cacace, M., Schneider, M. (2013) Influence of fluid flow on the regional thermal field: results from 3D numerical modelling for the area of Brandenburg (North German Basin). Environ Earth Sci (2013) 70:3523–3544. https//: doi.org/10.1007/s12665-013-2438-4

Nordell B, Gehlin S. (2009) 30 years of thermal energy storage – a review of the IEA ECES Stock conferences.

Paci, L., Pasquinelli, L., Fabricius L. (2016) Overview of high temperature aquifer thermal energy storage (HT-ATES): Challenges and strengths, Center for energy resources engineering and Technical University Denmark.

Regenspurg, S., Alawi, M., Blöcher, G., Börger, M., Kranz, S., Norden, B., Saadat, A., Scheytt, T., Virchow, L., Vieth-Hillebrand, A. (2018) Impact of drilling mud on chemistry and microbiology of an Upper Triassic groundwater after drilling and testing an exploration well for aquifer thermal energy storage in Berlin (Germany). Environ. Earth Sci. 77 (13), https://doi.org/10.1007/s12665-018-7696-8.

Regenspurg, S., Blöcher, G., Kranz, S., Saadat, A. (2019) Aluminium release by water-rock interaction during hydraulic tests in a siliciclastic aquifer in Berlin (Germany). E3S Web of Conferences 98, 07026.

Regenspurg, S., Alawi, M., Norden, B., Vieth-Hillebrand, A., Blöcher, G., Kranz, S., Scheytt, T., Horn, A., Burckhardt, O., Rach, O., Saadat, A. (2020) Effect of cold and hot water injection on the chemical and microbial composition of an aquifer and implication for its use as an aquifer thermal energy storage.*Geothermics,* 84, 101747.

Röhling, H., Lepper, J., Diehl, M., Dittrich, D., Freudenberger, W., Friedlein, V., Hug-Diegel, N., & Nitsch, E. (2018). Der Buntsandstein in der Stratigraphischen Tabelle von Deutschland 2016. Zeitschrift Der Deutschen Gesellschaft Für Geowissenschaften, 169(2), 151–180. https://doi.org/10.1127/zdgg/2018/0132

Saadat, A., et al. (2016) Effizienz und Betriebssicherheit von Energiesystemen mit saisonaler Energiespeicherung in Aguiferen für Stadtquartiere; FKZ 03ESP409A. Technical Scientific Report.

Sanner, B. (2005) Examples of GSHP and UTES Systems in Germany. Proceedings World Geothermal Congress 2005, Antalya, Turkey.

Sanner, B., Kabus, F., Seibt, P., Bartels, J. (2005) Underground thermal energy storage for the German parliament in Berlin, system concept and operational experiences. Proceedings World Geothermal Congress, Antalya, Turkey, 24.-29. April 2005.

Schmidt, T., Müller-Steinhagen, H. (2004). The Central Solar Heating Plant with Aquifer Thermal Energy Store in Rostock- Results after four years of operations. EuroSun 2004 – The 5th ISES Europe Solar Conference, 20-23 June 2004, Freiburg, Germany.

Schüppler, S., Fleuchaus, P., Blum, P. (2019) Techno-economic and environmental analysis of an Aquifer Thermal Energy Storage (ATES) in Germany. *Geothermal Energy (2019) 7:11.*

Seibt P, Kabus F. (2006) Aquifer thermal energy storage-projects implemented in Germany. In: Proceedings ECOSTOCK 2006; May 31 – June 2, Galloway, New Jersey, United States.

Shen, G.J. (1998) Research on energy storage in the underground water and its quality in Changzhou city. Jigastock. In: Proceedings of the international conference on energy storage for building heating and cooling, Versailles, France.

Snijders, A., L. (1994) Aquiferwärmespeicherung, ein Projekt der Internationalen Energieagentur (IEA) am Beispiel der Wärmespeicheranlage in Utrecht. Saisonale Wärmespeicher im Aquifer: Chancen und Risiken für die Umwelt. München: Oldenbourg; 1994.

Sommer, Wijbrand. (2015) Modelling and monitoring of Aquifer Thermal Energy Storage- Impacts of heterogeneity, thermal interference and bioremediation. Dissertation.

Stemmle, R., Hammer, V., Blum, P., Menberg, K. (2020) Potential of low-temperature aquifer thermal energy storage (LT-ATES) in Germany. *Geothermal Energy (2022) 10:24.*

Stober, I., Bucher, K. (2014) Geothermie, Lehrbuch. Springer Spektrum, Heidelberg. Todorov, O., Alanne, K., Virtanen, M., Kosonen, R. (2020) A method and analysis of aquifer thermal energy storage (ATES) system for direct heating and cooling: A case study in Finland. Sustainable Cities and Society, 53, 101977.

Tsang, C.F., Hopkins, D., Hellstrom, G. (1980). Aquifer thermal energy storage - a survey. Lawrence Berkeley Laboratory.

Ueckert, M.,Baumann, T. (2019) Hydrochemical aspects of high-temperature aquifer storage in carbonaceous aquifers: evaluation of a field study. *Geotherm Energy, 7:4.*

Winter, T., Aeschbach, W., Einsiedl, F. (2023) Reconstruction of the Pleistocene Paleoclimate From Deep Groundwater in Southern Germany From Noble Gas Temperatures Linked With Organic Radiocarbon Dating. *Water Resources Research* 10.1029/2023WR035644.

Wolfgramm, M., Lenz, G., Bartels, J., Diaz, S., Hoffmann, F., Kabus, F., ... & Kabus, B. (2014). Machbarkeitsstudie zur Bewertung der Möglichkeit der Speicherung von Abwärme einer Kraft-Wärme-Kopplung im Erdboden im Rahmen der klimaneutralen Campusentwicklung der Universität Lüneburg.

Würdemann, H., Westphal, A., Lerm, S., Kleyböcker, A., Teitz, S., Kasina, M., ... & Wolfgramm, M. (2014). Influence of microbial processes on the operational reliability in a geothermal heat store–Results of long-term monitoring at a full scale plant and first studies in a bypass system. *Energy Procedia*, *59*, 412-417.

Zhou, X., Gao, Q., Chen, X., Yan, Y., Spitler, J.D. (2015). Developmental status and challenges of GWHP and ATES in China. Renew Sustain Energy Rev 2015; 42:973–85.

G. Enhanced Geothermal Systems (EGS)

G.1. Authors

Lingkan Finna Christi	GFZ	christi@gfz-potsdam.de	Germany
Hannes Hofmann	GFZ	hannes.hofmann@gfz-potsdam.de	Germany

Additional Input

GFZ Internal

G.2. Description of technology

Enhanced Geothermal Systems (EGS) are defined as artificial or engineered reservoirs created to extract heat from low-permeability geothermal resources (Tester, 2006). Geothermal resources designated as EGS include those that are not currently in commercial production and require stimulation or enhancement. EGS excludes high-grade hydrothermal resources, but includes conduction-dominated or petrothermal systems, low-permeability resources in sedimentary and basement formations, and geopressured, magmatic, and low-grade unproductive hydrothermal resources. In the doublet system of production and injection wells, EGS concepts would recover thermal energy contained in subsurface rocks by accessing an open system of interconnected fractures through which water can be circulated down injection wells, heated by contact with the rock, and returned to the surface through production wells. In the U.S. Department of Energy's recent report, "Pathways to Commercial Liftoff: Next-Generation Geothermal Power" (Blankenship et al., 2024), EGS is defined as a subsurface circuit of multiple wells and fractures containing a fluid that is heated by the geothermal resource through direct contact with the resource. With respect to reused wells, Santos (2022) classifies EGS as an open-loop system in which the retrofitting of hydrocarbon wells for geothermal energy production has been explored as a technology option to extract heat, particularly from low-permeability reservoirs, at viable and economically potential temperatures. Unlike the conventional geothermal system (i.e., hydrothermal energy), which requires porous and naturally fractured reservoirs limiting the development of geothermal energy to certain geological and geographic locations, the EGS system is believed to enable the development of geothermal energy in the absence of porous and permeable reservoirs.

In many low permeability reservoirs, drilling will not necessarily open up a geothermal reservoir from which geothermal energy production is economically viable without further measures (Huenges, 2013). Well stimulation to increase the productivity and injectivity of geothermal wells then becomes the solution. To date, there are at least three types of stimulation technologies used in Enhanced Geothermal Systems (EGS) that have been adopted from the oil and gas industry. The three techniques are described as follows:

G.2.1. Hydraulic treatments

Hydraulic stimulation treatments may be divided into hydraulic shearing and hydraulic fracturing treatments. In both cases fluid is injected into a low permeability rock. In hydraulic shearing treatments the pressure is typically kept below the hydraulic fracturing pressure as the target is to induce a shear displacement of existing fractures/fracture networks to increase their permeability by self-propping of the rough displaced fracture surfaces. Hydraulic fracturing is a process through which one or multiple fractures

are created mechanically in the rock by fluid pressure increase. In hydrocarbon reservoirs this allows the natural gas or oil trapped in low permeability subsurface formations to move through those fractures to the wellbore from where it can then flow to the surface. Hydraulic fracturing can both increase production rates and increase the total amount of gas that can be recovered from a given volume of rock. First, a fluid is injected into the target formation by injection pumps until the formation breakdown pressure is reached and a fracture starts to grow from the well. Once the fracture is created the fracturing fluid carries proppant (e.g., well sorted sand or ceramics) into the hydraulic fracture to keep it open after fracture closure to allow the oil/gas/water to flow towards the well. While water and sand are the main components of hydraulic fracture fluid, chemical additives are often added in small concentrations to improve fracturing performance (Speight, 2019). Hydraulic fracturing treatments are performed as waterfracs, gel proppant fracs, or something in between called hybrid fracs (Sharma et al., 2004). The procedures are well known in the hydrocarbon industry (Shaoul et al., 2007a, b) and in EGS (Hettkamp et al., 2004; Baumgärtner et al., 2004; Schindler et al., 2008). The followings are the classification of hydraulic fracturing techniques:

- Waterfrac treatments

Waterfrac treatments are applied in the low permeable or impermeable rocks by injecting large volumes of water to create long fractures in the range of 100+ m with a small aperture (approximately 1 mm), and hence low conductivity. The success of the treatment depends on the self-propping of the rock and on the potential for shear displacement or on the capability to transport proppants with the injected water. High flow rates seem to be beneficial for the fracture performance, even if the intervals are limited in time. The proppants may be added in the fluid during the high rates to improve proppant transport (Zimmermann and Reinicke, 2010).

- Gel-proppant treatments

Gel proppant treatments are used to stimulate a little bit higher permeability reservoir with cross-linked gels (to reduce fluid leak-off and to transport proppants) in combination with proppants of a certain mesh size. The produced fractures have a shorter length of about 50 - 100 m, but a larger opening of up to 10 mm compared to water frac treatments. The extreme form of gel-prop proppant treatments are frac-and-pack treatments, which generate very short (~10 m) and very wide (~20 mm) fractures that are mainly used to avoid the wellbore skin in high permeability reservoirs. Gel-proppant treatments are typically more expensive compared to water frac treatments (Zimmermann and Reinicke, 2010). Gel-proppant treatments begin with a data FRAC (minifrac) to obtain information on the friction and tortuosity of the perforated interval. The main fracturing treatment, which follows the near-wellbore minifrac test, is performed by injecting gel and proppant into the fracture with a stepwise increase of the proppant concentration. The result of the treatment (propped fracture height, width and lengh) depends mainly on the injection rate, the proppant concentrations and their variation as a function of time (Huenges et al., 2013).

- Hybrid fracturing treatments

In hybrid fracturing treatments, slickwater is pumped first to generate a fracture. Then, a gel pad with cross linked gel is injected, followed by proppants or sand of a certain mesh size with a cross-linked gel to fill the fracture (Huenges, et al., 2013). The viscosity of the gel is between slickwater (used in waterfrac treatments) and cross-linked gel (used in gel-proppant fracturing treatments). This method can be applied to low-to-intermediate-permeable reservoirs. Fracture dimensions are typically in between gel-proppant and waterfrac treatments (Zimmermann et al., 2011).

- Multi-stage stimulation vs. massive open hole stimulation

The goal of multi-stage stimulation is to increase the surface area of the reservoir in contact with the wellbore. The idea of multi-stage stimulation is to create/stimulate multiple fractures in the target reservoir along the wellbore, as shown in Figure G.2.1. Multi-stage hydraulic fracturing with multiple perforated zones is most commonly demonstrated in cased wells. Open-hole multi-stage stimulations are possible, but more challenging due to potential crossflow around the packers through natural fracture networks (e.g., Hofmann et al., 2021). The growth of multi-stage fracturing has increased due to completion technology that can effectively place fractures at specific locations in the wellbore.

Prior to the development of the custom-designed system, the only options for completing an open-hole well were uncased holes or slotted or perforated liners. The development of a system that sets in the open hole provides mechanical diversion and allows multiple fractures to be performed along the entire open hole system with the benefit of cost and time savings. An open-hole mechanical packer system is capable of withstanding high differential pressures with fracturing ports located between the packers. Open Hole Multi-Stage Assembly (OHMSs) use hydraulically set mechanical packers to isolate sections of the wellbore.

Multi-stage hydraulic fracturing in cemented liners requires mechanical isolation in the liner by setting bridge plugs using pump-down wireline or coiled tubing (CT), followed by perforating and then fracturing the well to access the reservoir. This process is then repeated for the number of simulations desired for the production section of the well. After all stages are completed, CT is used to drill out the composite plugs and regain access to the bottom of the well. Compared to open hole stimulations production from this method can also be limited because cementing the well closes many of the natural fractures and fractures that would otherwise contribute to overall production. However, it is much more controllable than open hole packers.

Massive stimulation of a large stimulated reservoir volume (SRV) with significantly higher injection volumes and treatment times, as shown in Figure G.2.2, is typically performed in an uncased well. Typical examples are the Soultz-sous-Forets and Basel EGS.

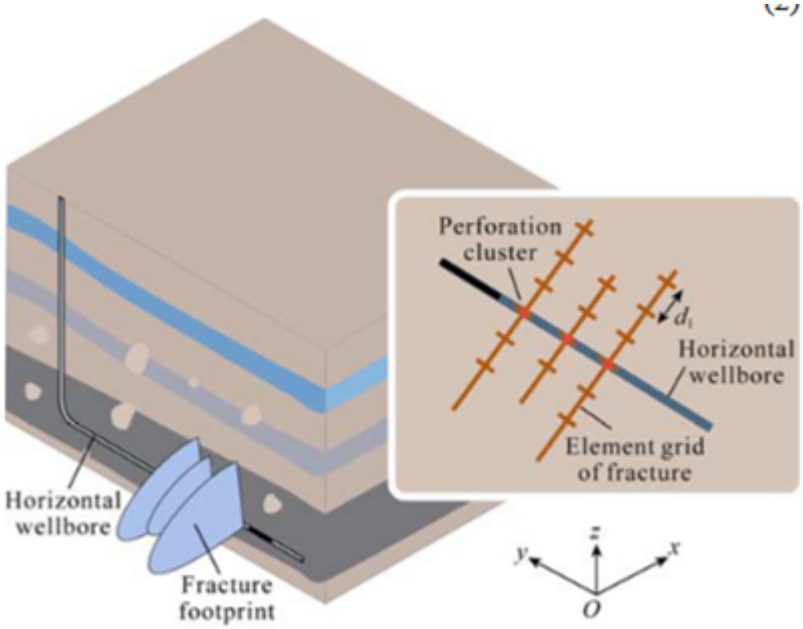

Figure G.2.1: Schematic diagram of multi-stage hydraulic fracturing (Jinzhou, 2017).

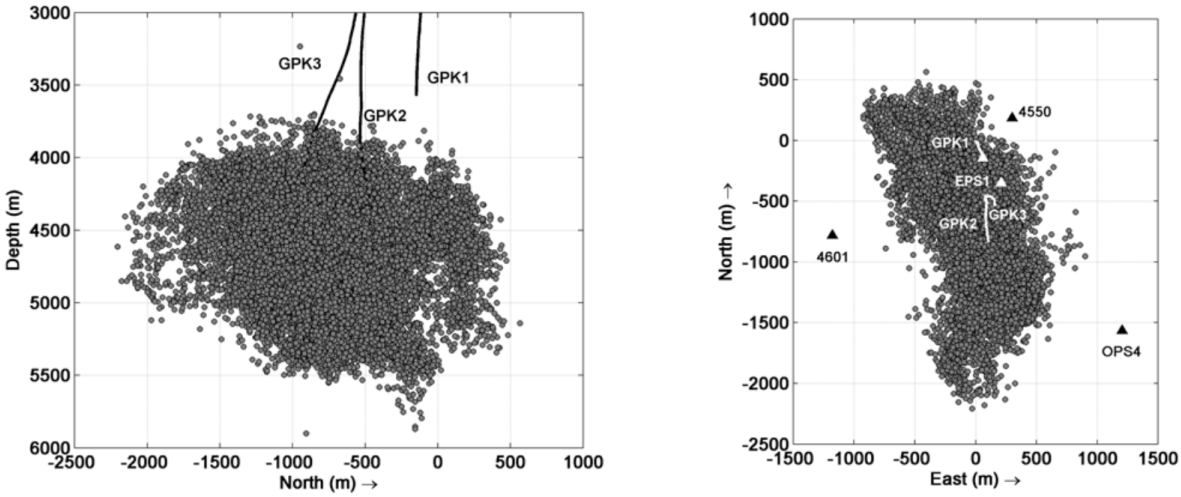

Figure G.2.2: Seismicity associated with the massive stimulation carried out at GPK-2 and GPK-3 of Soultz-sous-Fôrets in 2003. (a) Vertical view and (b) map view of the seismicity. The downhole seismic stations are represented by triangles on the map view. More than 21,000 events were located, and they are the starting point for the joint hypocenter determination and multiple analysis (Michelet et al., 2007).

G.2.2. Chemical treatments

Chemical stimulation techniques were originally developed more than a century ago to increase or restore oil and gas well production rates and have been applied to geothermal wells for the past 20 years (Portier, 2007). Acid stimulation jobs are designed to cleanse (pre-existing) fractures by dissolving fill materials (secondary minerals or drilling mud) and mobilising them for efficient removal by flow transport. By dissolving acid-soluble components in subsurface rock formations or removing material at the wellbore surface, the flow rate of oil or gas from production wells or the flow rate of oil displacement fluids into injection wells can be increased. The most common acids used in conventional acidizing treatment are Hydrochloric (HCL), Hydrofluoric (HF), Acetic (CH_3COOH), Formic (HCOOH), Sulfamic (H_2NSO_3H), and Chloroacetic ($ClCH_2COOH$). Acid washing is performed at low pressures. Depending on the purpose of the treatment and on the targeted formation, acidizing is divided into the following classifications:

- Matrix acidizing

This process targets the rock matrix. It is performed below fracturing pressure and is normally used for the removal of skin damage associated with drilling, work-over, well killing or injection fluids and to increase formation permeability in undamaged wells.

- Fracture acidizing

Fracture acidizing is performed above the fracturing pressure. Due to the reactive nature of the fluid, the addition of acid can dissolve and remove primary and secondary minerals (scale) that seal existing fractures or it can dissolve existing minerals at the fracture surface of new hydraulic fractures or existing natural fractures. The goal is to create flow paths that stay open also after fracture closure due to etching of the fracture surfaces.

G.2.3. Thermal treatments

Thermal stimulation treatments are used to increase the productivity or injectivity of a well by either increasing the permeability in the vicinity of the wellbore, which may have been reduced by the drilling operation itself (drill cuttings or mud clogging feed zones), or by opening hydraulic connections to naturally permeable zones that have not been intersected by the wellbore. This can occur either by reopening existing, possibly sealed fractures, or by creating new fractures through thermal or additional hydraulic stresses. This treatment type has been used in high temperature systems associated with volcanic activity. Stimulation typically begins with water circulation through the drill string, followed by pumping cold water into the wellbore. Injection may be interrupted by intervals of non-activity during which the well is allowed to heat up to its natural temperature. The injection of cold water leads to a cooling of the rock in the near wellbore environment, or adjacent to existing natural or induced fractures. The cooling of the rock matrix induces a tensile component of stress (thermo elastic stress) near the injection well or adjacent to the injection surface (fractures). The magnitude of this thermally induced tensile stress depends on the thermal and elastic rock properties, and the difference between the initial reservoir temperature and the temperature of the injected fluid (Zimmermann et al., 2011). In the end, a combination of thermally induced tensile stresses and pressure-induced tensile stresses can increase the permeability of existing fractures and create new ones (Huenges, 2013).

The workflow of the Enhanced Geothermal System technology is described in Figure G.2.3.

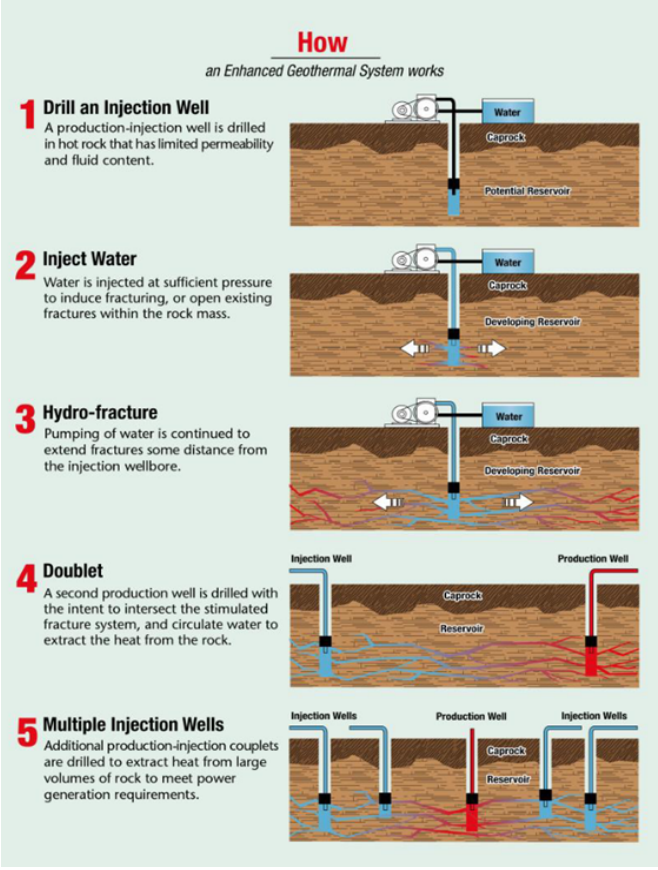

Figure G.2.3: The flow of developing EGS (https://www1.eere.energy.gov/geothermal/pdfs/egs.pdf).

G.3. Literature review

G.3.1. Enhanced Geothermal Systems worldwide and in Central Europe

Starting with the first EGS project in Fenton Hill, exploring hot dry rock in 1971, there have been around 70 EGS projects worldwide, including those designed for research purposes, to improve and maintain production of operating geothermal fields, and for petrothermal energy exploration targeting crystalline basement rocks and sedimentary rocks. Previous work on EGS has been extensively reviewed by Tester et al. (2006), Breede (2013), Pollack (2021), and Jia (2022). Each review has its own definition of EGS as the basis for comparing typical resources and methods of heat extraction that require EGS technology. Tester (2006) reviewed EGS based on the definition of EGS that was adapted to include all geothermal resources that are not currently in commercial production and require stimulation or enhancement, excluding high-grade hydrothermal but including co-produced hot water from oil and gas production as an unconventional EGS resource type. This assessment was then used by Breede (2013) to evaluate EGS technology on a project-by-project basis excluding geopressured and magma systems as proposed by European Geothermal Energy Council (EGEC) (2012) and GtV (2013). Pollack (2021) based his review on the definition of EGS by Williams et al. (2011), who proposed that EGS includes the portion of a geothermal resource for which a measurable increase in production over the natural state is or can be achieved by mechanical, thermal, and/or chemical stimulation of the reservoir rock. This definition has no restrictions on temperature, rock type, or existing geothermal use. This review here, the framework of the reuse of abandoned hydrocarbon wells for geothermal energy production, is based on Breede (2013) and Polack (2021) which consider all geothermal resources without restrictions on temperature and rock types. The review focuses on evaluating the technical parameters of the wells and geological parameters of the reservoir that led to the successful development of the EGS technology. Recently added EGS projects to the review of Breede (2013) and Polack (2021) are those developed between 2018 – 2023 including the demonstrations performed in the Horizon 2020 funded DESTRESS project in Mezőberény, Hungary (Brehme et al., 2024) and Geldinganes, Iceland (Hofmann et al., 2021), ongoing EGS projects in China including Qiabuqia (Lei et al., 2019) and Matouying (Feng et al., 2022), extensive EGS research currently being performed at Utah FORGE, USA (Hornby, 2023) and the recent milestone of a commercial EGS project in Blue Mountain, USA (Norbeck, 2023). The review by the number of projects in each country as well as their success rate is summarised in Figure G.3.1 and Table G.3.1 Detailed description of each project and reviewed parameters are provided below.

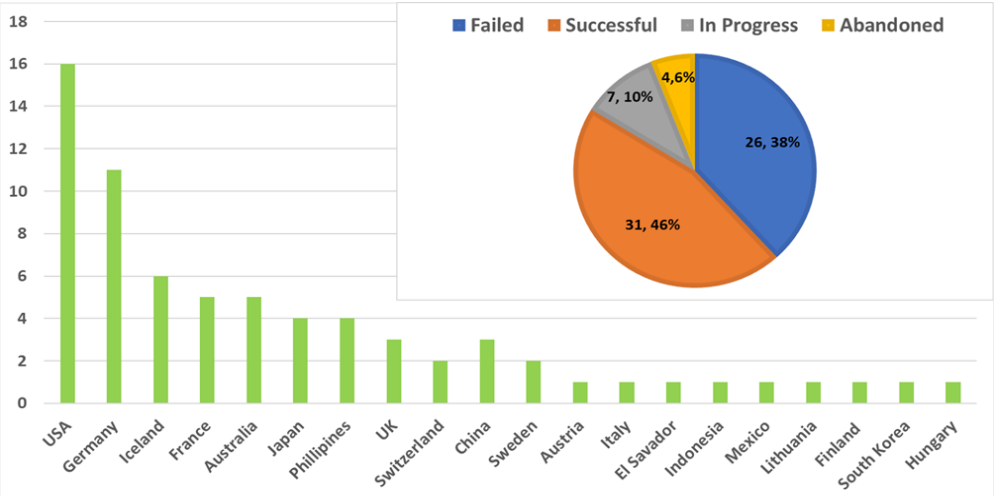

Failed = the stimulations were not successful; **Successful**= the stimulation was succesfully demonstrated;
In progress: still on going; **Abandoned**= the project was not proceeding due to non-technical reason.

Figure G.3.1: EGS projects worldwide and success rate.

Country	Project (start/end dates)
USA	[1]Newberry (2010/2015); [2]Coso (2002); [3]Dessert Peak (2002); [4]Blue Mountain (2012/2023); [5]East Mesa (1980); [6]Baca (1981); [7]Fenton Hill (1973/2000), [8]The Geysers Unocal (1981); [9]Northwest Geysers (2009/2012); [10]Southeast Geysers (2008/2009); [11]Bradys Hot Springs (2008); [12]New York Canyon (2008/2012); [13]Soda Lake (1991/2009); [14]Raft River (1979/2013); [15]Utah Forge (2016); [16]Dixie Valley (1983)
Germany	[17]Groß Schönebeck (2001/2013); [18]Horstbeg (2003/2007); [19]Hannover (2009); [20]Bruchsal (1983); [21]Landau (2003); [22]Insheim (2007); [23]Unteraching (2004); [24]Falkenberg (1977/1986); [25]Bad Urach (1977/1981); [26]KTB (1987/1995); [27]Geretsried (2021)
France	[28]Soultz-sous-Fôrets (1987/2016); [29]Le Meyet (1978); [30]Bouillante (1963/1996); [31]Rittershoffen (2005/2013); [32]Vendenheim (2019)
Iceland	[33]Mosfellssveit (1970); [34]Krafla (1980); [35]Seltjarnarnes (1994); [36]Hellisheidi (2003); [37]Reykjanes-IDDP-2 (2017); [38]Geldinganes (2019)
Australia	[39]Paralana (2005); [40]Cooper Basin-Habanero (2003/2013); [41]Cooper Basin-Jolokia (2022/2013); [42]Olympic Dam (2005); [43]Hunter Valley (1999/2015)
Japan	[44]Hijiori (1981/1986); [45]Ogachi (1989); [46]Hachimantai (1989); [47]Sumikawa (1989)
Philippines	[48]BacMan (1993); [49]Mindanau (1995); [50]Leyte (1996); [51]Tiwi (2000)
UK	[52]Rosemanowes (1977); [53]United Downs (2017); [54]Eden (2018)
Switzerland	[55]St. Gllen (2009); [56]Basel, Geneva (1996/2009)
China	[57]Qiabuqia (Gonghe); [58]Matouying (2020); [59]Xiongen (1982)
Sweden	[60]Lund (2001); [61]Fjälbacka (1984/1995)
Austria	[62]Altheim (1989)
Italy	[63]Lardarello – Super Hot EGS (1970 /2018)
El Savador	[64]Berlín (2001)
Indonesia	[65]Salak (2004/2008)
Mexico	[66]Los Azufres (2005)
Lithuania	[67]Klaipėda (2015)
Finland	[68]Otaniemi (2015)
South Korea	[69]Pohang (2010/2017)
Hungary	[70]Mezőberény (2011/2012)

Table G.3.1: List of EGS projects by country.

Most of the earlier EGS projects were pioneered by the U.S. Department of Energy, which sponsored 10 stimulation experiments in hydrothermal wells of the East Mesa, Raft River, Baca, The Geysers (California), and Beowawe (Nevada) geothermal fields. The Geothermal Reservoir Well Stimulation Program (GRWSP), from 1979 to 1984, included extensive literature reviews, laboratory work, field tests of hydraulic fracturing and acidizing treatments, explosive stimulation, and high-energy gas fracturing (Entingh, 2000). Since then, stimulation techniques from the oil and gas industry have been extended and adapted to geothermal wells with the goal of improving geothermal economics by developing stimulation with leveraged costs for the industry. Permeability hunting has been a bottleneck for geothermal resources to be exploited. The often-limited permeability is the cause of having a limited number of hydrothermal reservoirs that are viable to

be economically developed in the given area with productive wells. EGS brings a new solution to the geothermal industry to be able to extract heat regardless of the presence of permeability. It took decades to prove these technologies, but over time and numerous demonstration projects, now EGS could potentially be developed commercially as demonstrated by the Blue Mountain project in 2023.

In Central Europe, with Germany as the leading country, a total of 8 EGS projects have been demonstrated in 3 countries. The individual project, their locations and associated geological settings are listed in Table G. 3. 2. These projects are located in 3 of the 5 basins that have been investigated for geothermal energy production potential from hydrocarbon wells within the framework of the TRANSGEO project, namely the North German Basin, the Molasse Basin, and the Pannonian Basin.

In Central Europe, particularly in Germany and Austria, the Molasse Basin plays an important role for deep geothermal energy, targeting the calcareous limestones and dolomites of the Upper Jurassic (Malm) aquifer located between 4600 and 5200 m depth (Dorsch, 2021). With temperatures between 100°C and 155°C and high permeabilities (Bracke and Huenges, 2022), 29 deep geothermal projects have been realised (Flechtner, 2020) and 17 geothermal heating and/or power plants have been developed in the German Molasse Basin (Agemar et al., 2014) with production and injection rates ranging from 30 to 150 Ls^{-1} (Agemar et al., 2014). Most of them are located in the area around the city of Munich in Bavaria (Böhm et al., 2012). Based on the most recent review presented in Table G.3.2, there are 4 EGS projects in the Molasse Basin that targeted the Malm aquifer.

Country	Project name/ location	Basin
Germany	Groß Schönebeck	North German Basin
	Falkenberg	Crystalline Basement
	KTB	Crystalline Basement
	Bad Urach	Molasse Basin
	Unteraching	Molasse Basin
	Geretsried	Molasse Basin
Austria	Altheim	Molasse Basin
Hungary	Mezőberény	Pannonian Basin

Table G.3.2: List of EGS projects in Central Europe.

Another basin investigated in the TRANSGEO project is the North German Basin (NGB), as part of the Central European Basin System. With a temperature gradient of ~30℃/km and a depth of up to 7 km, the NGB has enormous geothermal resources of 2100 EJ (exajoules), consisting of 96% petrothermal systems (2016 EJ), 4% fault zones (84 EJ), and 1% hydrothermal systems (21 EJ) (Jung et al., 2002). The first deep prospective reservoir is located at a depth of 3800 – 4200 m b.s.l with temperatures ranging from 149 ℃ to 158 ℃ which is known to be the hydrocarbon bearing reservoir, Rotliegend. The second, which is shallower, is the Buntsandstein, located at a depth of 1500 - 2200 m b.s.l., which is the target of hydrothermal exploration with temperatures ranging from 80 ℃ to 100 ℃. (Norden, 2023; Tischner, 2010; Tischner,2013). For the development of EGS in the former hydrocarbon basins with hydrocarbon facilities, one EGS research project has been performed in the North German Basin.

The last one on the list of basins located in Central Europe is the Pannonian Basin which encompasses Hungary, Slovakia, Czech Republic, Romania, Serbia, Ukraine, and parts of Croatia. In Central Europe, Pannonian basin is well known for its rich geothermal resources. The CPBS has the greatest geothermal potential, as well as significant technological opportunities for the exploitation of geothermal energy in agriculture and the food industry (Malvi´c et al., 2021). The average geothermal temperature gradient in the CPBS is 0.049 °C/m (Tumara et al., 2019) while in the rest of Europe it is 0.03 °C/m (Lund et al., 2007).

Data on geothermal reservoirs were obtained from exploration wells that were primarily intended for locating oil and gas reservoirs. Great potential for the exploitation of geothermal energy is found in negative oil and gas wells, then in mature oil and gas reservoirs as well as in aquifers. Located in Central Europe, Hungary was ranked as the fifth country in Europe in 2017 for geothermal district heating and thermal-water heating cascade systems, with estimated amounts of 223.36 MW t installed capacity and 635.66 GW h production (EGEC, 2018). Individual space heating (mostly associated with spas) adds a further estimated installed capacity of about 77.2 MW t and 83.1 GW h annual production (2017), whilst the key player is still the agriculture sector, especially in southern Hungary, where heating of greenhouses and plastic tents accounts for about 358 MW t installed capacity (Nádor et al., 2019). Despite non-technical barriers (complex and time-consuming licensing processes, deficiency in capital investment), the geothermal sector in Hungary is developing fast, with an average of 10–20 new geothermal wells drilled each year. One of EGS projects, Mezőberény, has been successfully demonstrated in the hydrothermal geothermal system of Pannonian Basin in Hungary.

Several parameters have been summarised to characterise geothermal resources suitable for EGS development. In the in-situ state, reservoir depth, reservoir thickness, temperature, permeability and porosity are the main criteria to determine whether EGS can potentially be applied to extract heat from the reservoir. Over 70 projects, not all of which have published a complete set of data as required. From publicly available data, maximum and minimum ranges of parameters from these 70 EGS projects worldwide were summarised to provide an overview of reservoir and well characteristics that contribute to the development of a criteria catalogue for developing an EGS project under certain specific conditions of geothermal resource and well structure and configuration.

- **Reservoir Depth (meter)**

Most EGSs target crystalline basement reservoirs, mostly located in the deep part of the Earth's crust. This is a resource based on a conductive system. Other EGS target the reservoirs of conventional hydrothermal systems, which have relatively medium to shallow depths of less than 400 m. The deepest project where hydraulic stimulations were performed was the 9000 m deep (ultra-deep) KTB project (Germany). While some projects have depths greater than 5000 m, such as Soultz and United Downs. Mosfellssveit (Reykir), Fjälbacka, Falkenberg, Hachimantai have a shallow reservoir depth of around 100 - 750 m either due to high temperatures at shallow depth or due to their research character. The average depth of EGS reservoirs is about 3000 - 4000 m, which is based on the depth measured in Groß Schönebeck, Horstberg, St. Gallen, New Berry, Paralana, Boulliante, Lardarello, Fenton Hill, Northwest Geyser, Pohang, Reykjanes (IDDP 2), Unteraching, and Matouying projects. The depth of the reservoir is highly dependent on the interest and geological aspect to be exploited for a specific purpose. Based on the review of several EGS projects related to the reuse case and proven EGS commercial project example, the most ideal depth for EGS development considering its economic viability and proven depth is between 2500 m and 5000 m, which are the reservoir depth of Blue Mountain and Soultz projects. The reservoir depth overview from this review is shown in Figure G.3.2.

- **Reservoir Thickness (meter)**

The thickness of the reservoirs in the EGS projects varied over a fairly wide range. The maximum thickness was about 2000 to 4000 m. This range of thickness is found in the volcanic hydrothermal projects such as Boulliante, Lardarello, Geyser, Northwest Geyser projects. Medium range of thickness is around 200 – 1400 m found in Groß Schönebeck, Unterhaching, Qiabuqia. Projects that have medium thickness are representative of EGS projects in sedimentary environments and closely related to the hydrocarbon rich basins. Minimum range of thickness is around 10 to 100 m was measured in Horstberg, Ogachi, East Mesa, Seltjarnarnes, Klaipėda, Utah FORGE projects.

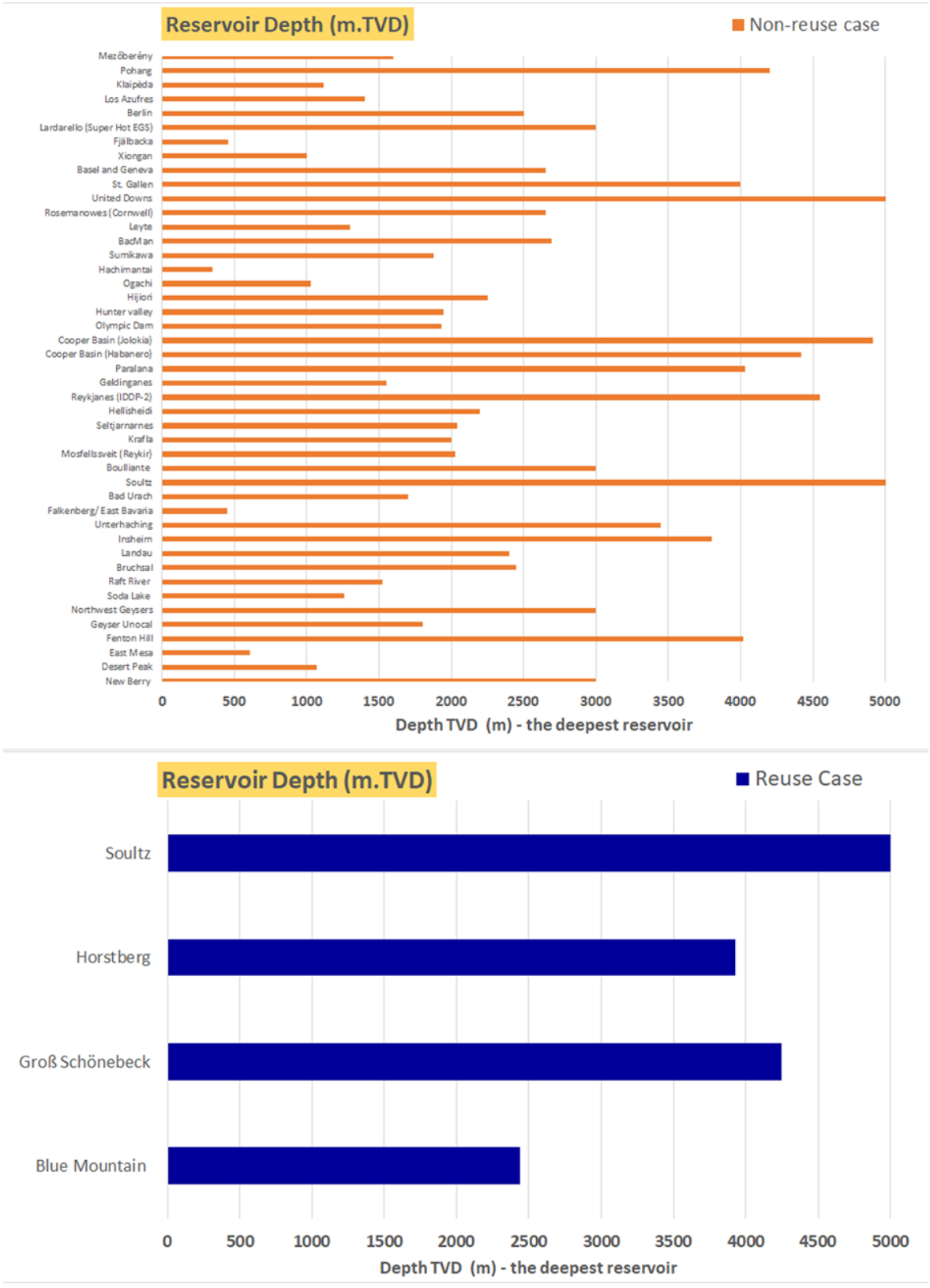

Figure G.3.2: Reservoir depth overview from the review of EGS projects worldwide.

- Temperature (℃)

Since the review is not limited to conventional and high-enthalpy geothermal systems, the temperature range in this review is wide. The maximum temperature could reach 400 ℃ measured in Northwest Geysers (USA) and Larderello (Italy) and the minimum temperature could reach 16 ℃ in the Fjälbacka project, Sweden. Any reservoir with a temperature above 224 ℃ is classified as a high-enthalpy geothermal system according to Hochstein (1990). These are reflected in the reviewed projects, such as Bacman, New Berry, Sumikawa, Salak, Northwest Geyser, which are operated commercially for electricity generation and the heat source is related to volcanic activity. The Cooper Basin project is an exception because the heat source is not related to the volcanic activity, but is located in the granitic basement with elevated radiogenic heat production (Hasterok and Webb, 2017). The medium temperature is around 100 ℃ to 150 ℃ achieved in GroÞ Schönebeck, Otaniemi (Helsinki Project), St. Gallen, Bruchsal, Unterhaching, Altheim, Mezőberény, Raft River, Seltjarnarnes, and Geldinganes. Most of the EGS projects having medium reservoir temperatures targeted a sedimentary rock and mostly a medium to low enthalpy geothermal system (Muffler and Cataldi, 1978; Haenel, Rybach and Stegena, 1988). The EGS project with the lowest temperature 16 ℃ is Fjälbacka, Sweden due to the shallow borehole depth of 500 m TVD, which was a pure research project (Wallroth et al., 1999). Temperature is an important parameter to develop an EGS project for heat extraction purposes. The overall achieved bottom hole temperatures from the reviewed EGS project are provided in Figure G.3.3.

- In-situ Permeability (m^2)

In the EGS project, permeability is the key parameter used to evaluate the potential for EGS. Recalling the definition of EGS, a man-made reservoir created where there is hot rock but insufficient or little natural permeability or fluid saturation (MIT, 2006), which is the opposite of a hydrothermal system that has natural permeability that allows fluid to be produced from the reservoir. Based on the review, the range of in-situ permeability is from 9.8 x 10^{-20} (Larderello; Feng et al., 2022) to 3.94769 x 10^{-12} m^2 (Klaipėda; Guinot, 2021). The average value of permeability is about 5.05 x 10^{-16} m^2 from the Groß Schönebeck (Huenges et al., 2002) and Salak (Stimac, 2008). The high permeability in Klaipeda is an example where reservoir stimulation methods are used to overcome near wellbore damage (skin) to access an otherwise permeable hydrothermal reservoir (Guinot, 2021).

- Porosity

In the review of 70 EGS projects, porosity ranges from a minimum of 0.01 (Lardarello; Feng et al., 2022) to a maximum of 0.41 (Tiwi; Stimac et al., 2004). The average porosity is 0.2, which is commonly found in sandstones or other well-sorted rocks that contain almost all grains of the same size. In the case of the Salak project, although the geothermal resource is related to the hydrothermal system, the reservoir of the Awibengkok area, as the reference of the average 20% porosity value of the EGS project, underlies the Mixed Volcanics-Sediments ("MVS") to form the basement of the reservoir (Golla, 2020). On the other hand, the Rotliegend formation in Groß Schönebeck site, which is one of the promising hydrocarbon-bearing reservoirs, is characterised by well-sorted sandstone with a porosity of 20%. These sediments can be tight as a result of compaction, which increases the need for EGS technologies. As for Groß Schönebeck, the porosity value was obtained from laboratory measurement of core sample and well logging data interpretation of well E GrSk 3/90 (Norden, 2023).

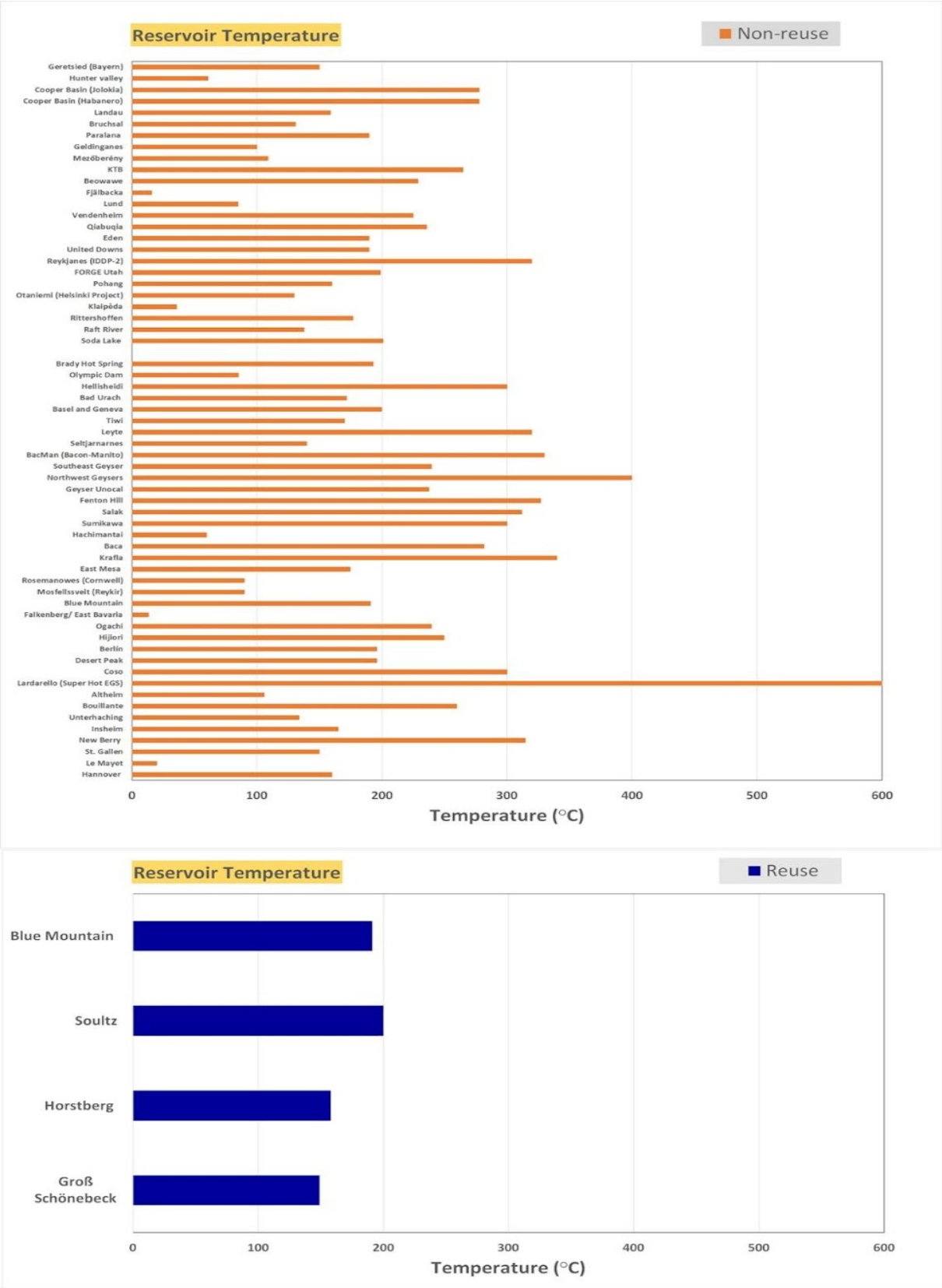

Figure G.3.3: Reservoir temperature overview from the review of EGS projects worldwide.

- **Flow Rate (Ls^{-1})**

The goal of EGS technology is to increase well productivity in the absence of reservoir permeability. Therefore, the flow rate is the important parameter to evaluate the success of the application of EGS technology. The maximum flow rate is 150 Ls^{-1}, which is obtained from the Unteraching and Boulliante sites. Both sites produce heat from a hydrothermal system where the Unteraching reservoir is located in the Malm Formation of the South Mollase Basin (Wolfgramm, 2007) and the Boulliante reservoir is volcanic lava in the Marie-Galante graben system (Bouchot, 2010). The median flow rate of approximately 75 Ls^{-1} is from the Soultz and Landau references. Soultz and Landau are EGS projects from petrothermal systems that require massive stimulations to be developed from research to commercial purposes. These after stimulation flow rates can be a standard for a commercial EGS project requirement in terms of flow rate. The lowest flow rate of less than 10 Ls^{-1} is obtained from the references of Horstberg, Le Mayet, Paralana, Hijiori, Falkenberg, Northwest Geyser, and Fjälbacka projects which are failed to move to the commercial development or were specifically designed as EGS research projects. Projects with a minimum or more than 50 Ls^{-1} flow rate will lead to a successful commercial development.

- **Initial Productivity Index and Injectivity index ($Ls^{-1}MPa^{-1}$)**

The initial productivity index ranges from 0.1 $Ls^{-1}MPa^{-1}$ as measured in GPK-1 Soultz (Vidal, 2018) and in SN-12 Seltjarnarnes (Tulinius, 1996) to 3.5 $Ls^{-1}MPa^{-1}$ as measured in GRT-2 Rittershoffen (Vidal et al., 2018). The injectivity index ranges from 0.2 $Ls^{-1}MPa^{-1}$ measured in GPK-3 Soultz (Vidal et al., 2018) to 21 $Ls^{-1}MPa^{-1}$ measured in the Mindanau project (Malate et al., 1995). From this review, the mean injectivity index is related to the Bacman field with an initial injectivity value of 9.7 $Ls^{-1}MPa^{-1}$. In the Rittershoffen project, the productivity is relatively high for the EGS project, which represents a hydrothermal system similar to both Mindanau and Bacman geothermal fields. However, in these fields, the reservoir productivity needs to be improved due to maintaining the stability of commercial heat production demand. Relatively low productivity index is the typical characteristic of a petrothermal system that needs EGS technology to create permeability in order to have the reservoir produced at the minimum rate, which is considerably not economically viable for heat or power production. We consider an initial productivity or injectivity index of <10 $Ls^{-1}MPa^{-1}$ as a rough estimate whether or not EGS technologies are required.

- **Borehole Depth/ Length (m)**

Well depth refers to True Vertical Depth (TVD) and well length refers to Measured Depth (MD), most commonly measured in metres or feet. Well depth and length are determined solely by the target reservoir/temperature. Therefore, the well depth is almost the same as the reservoir depth with the additional length to account for directional and horizontal drilling cases. In this review, the deepest demonstrated EGS well is 9010 m performed in the KTB scientific drilling site (Rabbel et al., 2004) and the shallowest well is set in Fjälbacka, Sweden to perform research on EGS at shallow depth with the plan to develop a heat pump greenhouse (Sundquist et al., 1988). The most common depths in many of EGS sites are around 3000 – 4000 m depth. The overall review of borehole length of the EGS project is provided in Figure G.3.4.

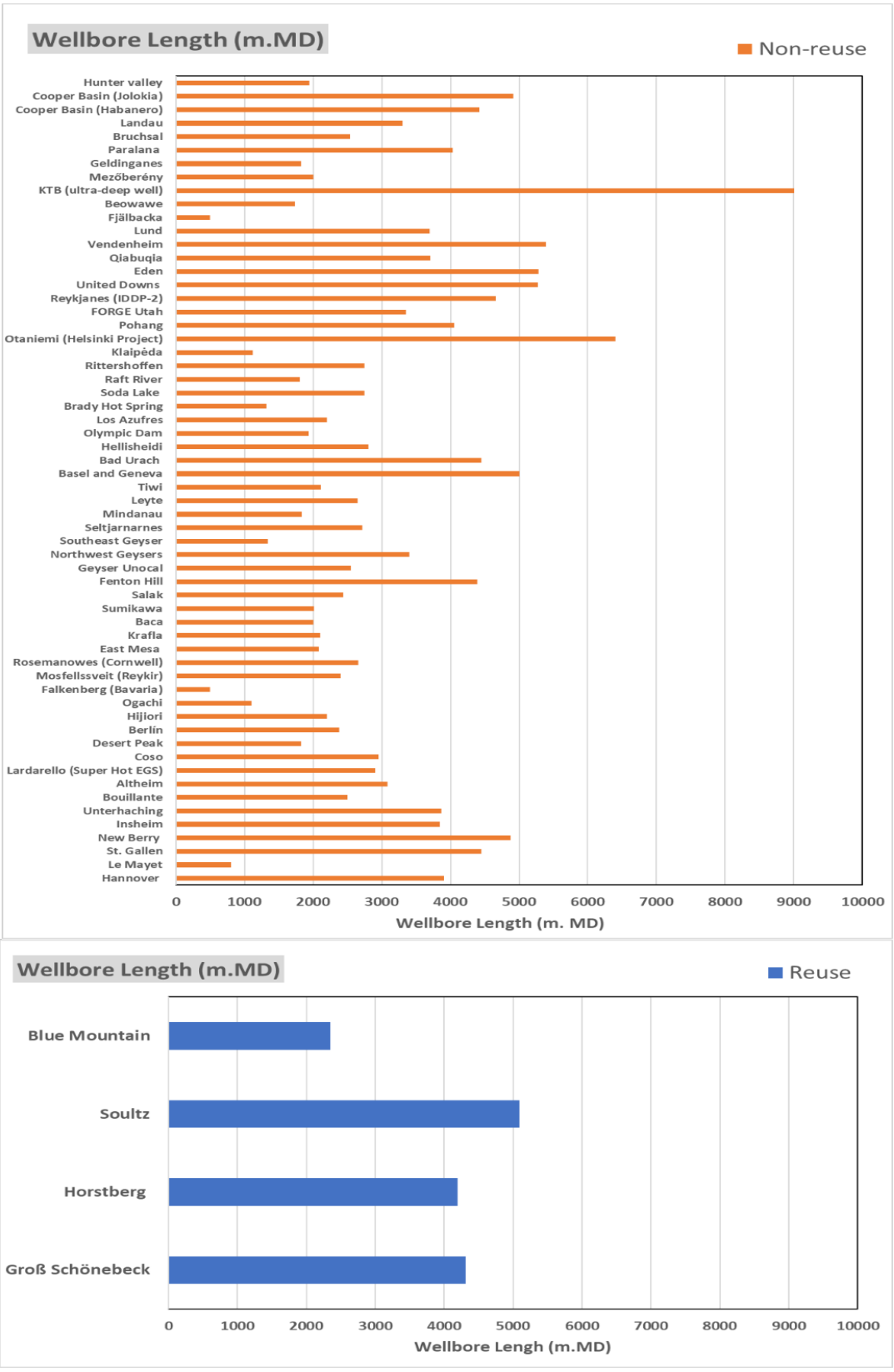

Figure G.3.4: Wellbore length overview of EGS project worldwide.

- Bottom Hole Diameter (inch)

For EGS development, the bottom hole part that is directly exposed to the reservoir is a critical parameter to optimise hydraulic fracturing performance and reservoir production. Wellbore design is based on the API standard worldwide Figure G.3.5. For every part in the world, the structure of the size should be the same depending on the surface casing size and the bottom hole diameter design.

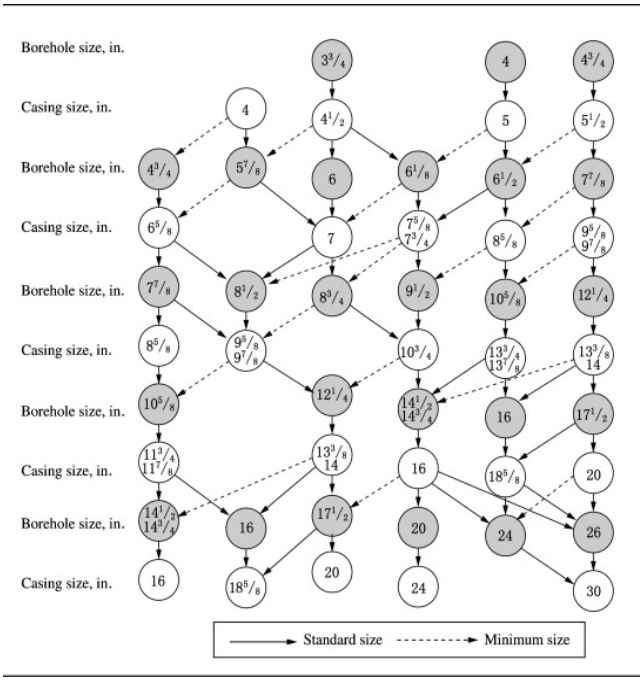

Figure G.3.5: API standard for casing and liner size configuration.

Figure G.3.6 shows the overview of the average bottom hole diameter reviewed in this project. The minimum size of borehole diameter is 2.9 inch in Salak project, Indonesia and the maximum bottom hole diameter is 10.75 inch from Ogachi project, Japan. The average size is 7 inch which are considered the minimum size of the bottom hole casing diameter to develop an EGS from an existing well. The effect of wellbore diameter and flow rate on the frictional pressure loss can be described by the following formula adopted from Austin (2012):

$$\Delta P = \frac{L\ rho^{0.8}\ Q^{1.8} \mu^{0.2}}{901.63\ D^{4.8}}$$

The output performance is highly dependent on the well bottom pressure, injection and production flow rate, and the size of well bottom diameter that can cause pressure loss due to the frictional pressure caused by inflow into the wellbore as presented in Figure G.3.7.

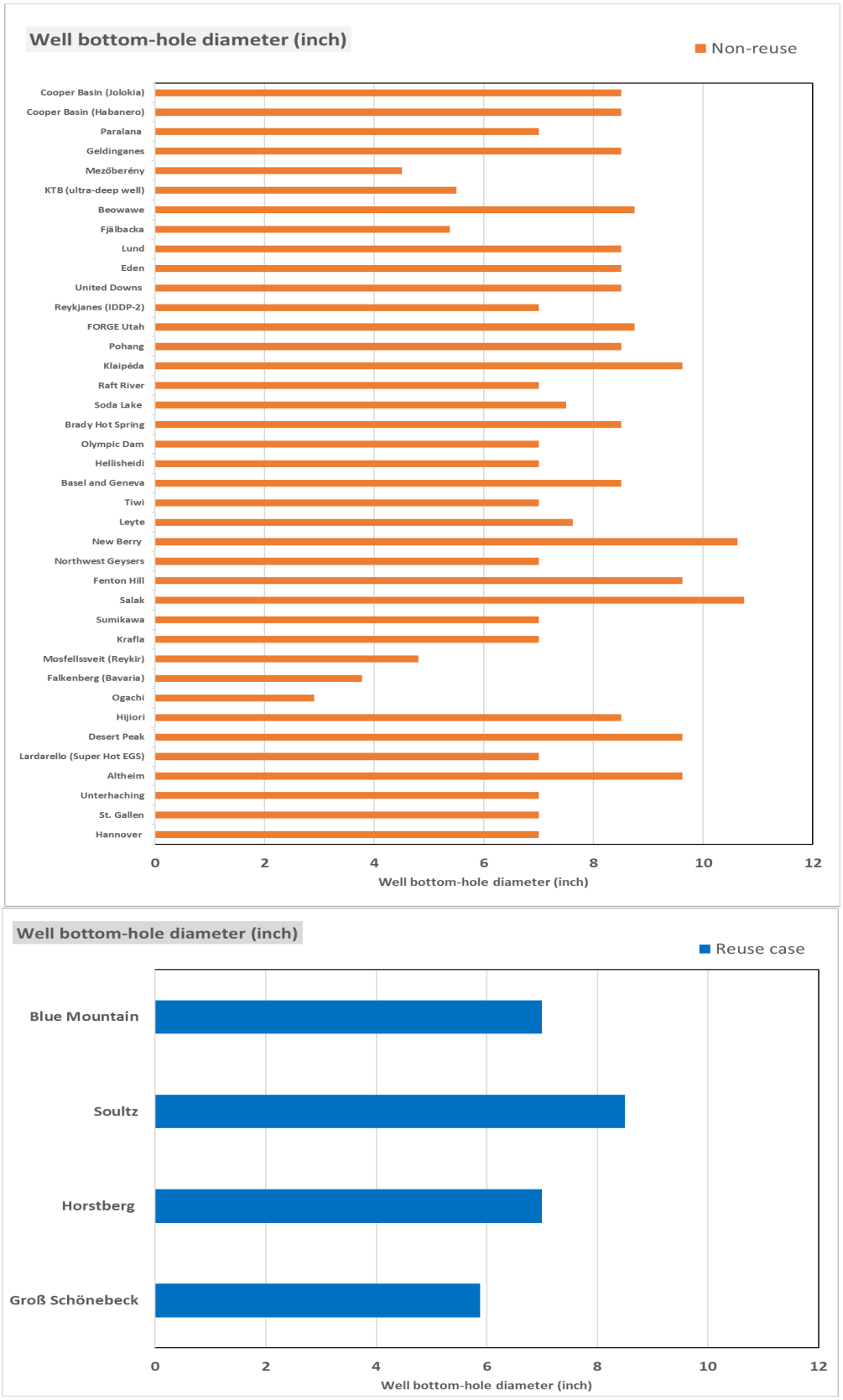

Figure G.3.6: Overview of bottom hole diameter of EGS project worldwide.

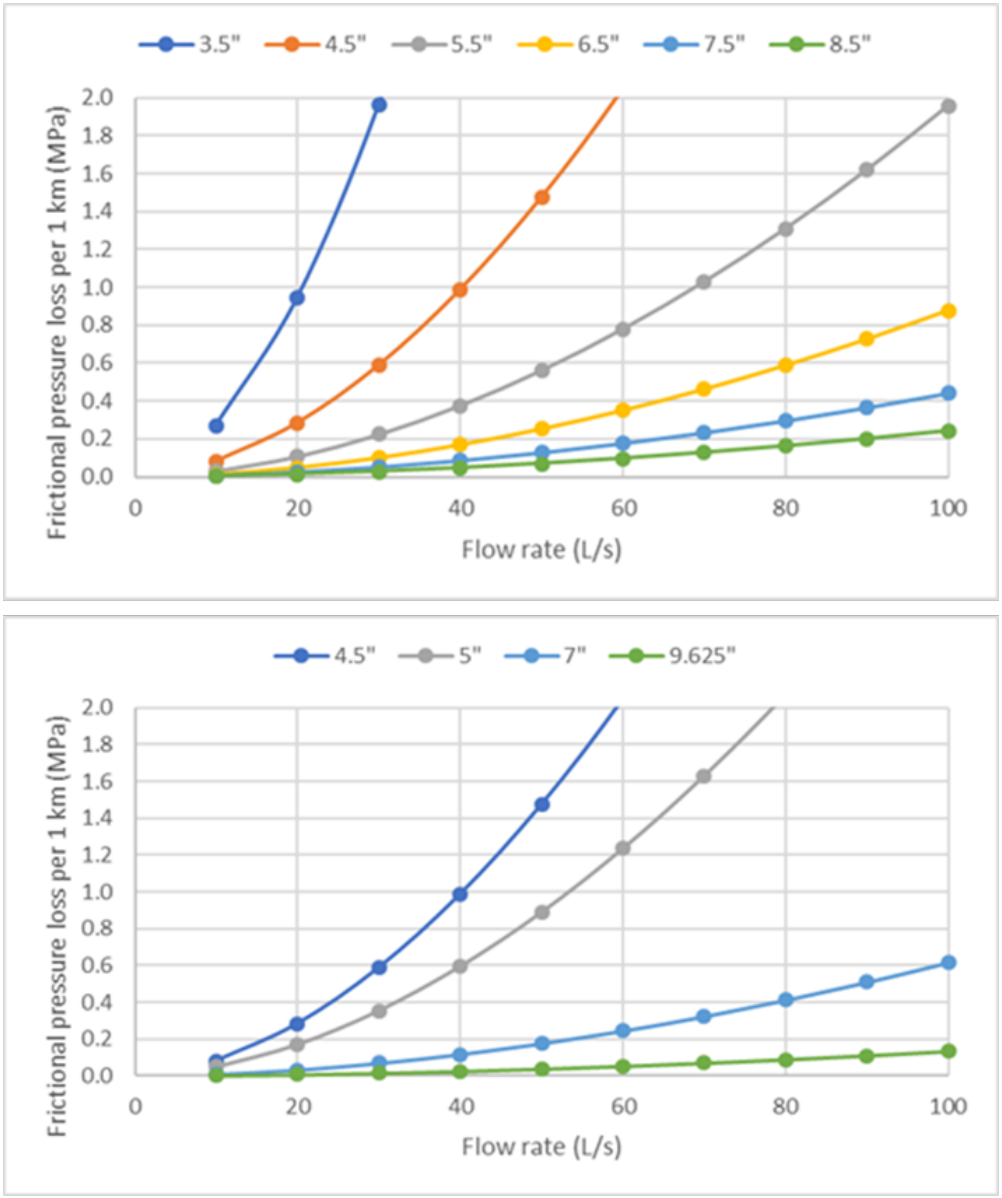

Figure G.3.7: The effect of wellbore diameter and flow rate on the frictional pressure.

G.3.2. Reuse of abandoned wells for EGS development worldwide and in Central Europe

Based on the review conducted within the TRANSGEO project, the most recent data on EGS project development worldwide shows a total of 4 EGS projects related to the reuse case. These projects are located in Germany, USA and France Table G.3.3.

Country	Project name/ location	Basin	Reservoir target	Origin of well	Project Status	Reference
Germany	Groß Schönebeck	North German Basin	Rotliegend Formation (tight sandstone)	Exploration well for hydrocarbon (gas)	Stimulation successful, but development failed	Legarth et al., 2003
	Horstberg	North German Basin	Middle Bundsandstein (sandstone)	Production well for hydrocarbon (gas)	Failed	Jung et al., 2005; BGR(https://www.bgr.bund.de/EN/Themen/Nutzung_tieferer_Untergrund_CO2Speicherung/Projekte/Geothermie/Abgeschlossen/Horstberg_Projekt.html?nn=1548118)
USA	Blue Mountain	Great Basin	Metasediment	Geothermal wells with image log data	1st successful commercial EGS project in the world	Norbeck et al., 2023
France	Soultz-sus-Forêts	Upper Rhine Graben	Basement (Granite)	Hydrocarbon well (oil)	Successful, commercial operation	Aichholzer et al., 2019

Table G.2.3: EGS project from well reuse.

As shown in Table G.3.3, there are 4 EGS projects worldwide that kicked-off with the discovery of high temperature gradients in the hydrocarbon wells or in the non-intended geothermal wells. The well reuse cases are located in Germany, USA, but the first research project aimed at exploring the basement of the hydrocarbon environment, which became the technology baseline for the subsequent EGS demonstration, is the Soultz project located in France. The Soultz project is also the first project that started the commercial development of EGS. The Soultz geothermal field was first known as an oil field by Pechelbronn in 1888 and was the first oil field where the first logging was carried out by Schlumberger in 1927 (Dezayes, 2005). Prior to the start of the European HDR geothermal project, a hydrothermal source was discovered in this field. Following the success of Soultz, Landau successfully started its commercial phase, but due to the impact of induced seismicity, the project was suspended in 2013. To date, in total, only 1 EGS project related to the reuse case in Central Europe. This project is Groß Schönebeck located in the North German Basin. This site is the reference site for EGS technology in the frame of TRANSGEO Project.

Based on the literature review of EGS parameters from published literature, several important parameters for finalising the decision to apply EGS technology are narrowed down to temperature, in-situ permeability, flow rate, and productivity & injectivity indices. In the case of reuse of hydrocarbon wells, the diameter of the bottom hole is a critical parameter.

In terms of temperature, the typical temperature for EGS from reuse is at least 100 °C, which is in the range of the intermediate enthalpy system. In Central Europe, geothermal energy is in most cases used for heating

rather than electricity generation. With a production temperature of at least 100°C, this is more than sufficient as a standard temperature for heating needs. Permeability can be as low as 0, which is why EGS needs to be carried out. The produced flow rate resulting from a given pressure drop in the reservoir, indicated by the production index, is also an important parameter for assessing the applicability of EGS. At Soultz, the initial productivity index was as low as 0.1 $Ls^{-1}MPa^{-1}$, and after stimulation it increased to 7 $Ls^{-1}MPa^{-1}$. The increase in the productivity index is a measure of the success of the implementation of EGS technology.

Considering the case of hydrocarbon reuse wells, the bottom hole diameter is an important parameter to evaluate the possibility of well modification and rehabilitation. A large wellbore diameter provides flexibility for workover activities such as deepening and side-tracking, as well as for well stimulation to be demonstrated. The performance of the well, in terms of flow rate and energy rate, is also highly dependent on the size of the bottom hole diameter. Based on the literature review, 7" is the minimum well bottom hole diameter for EGS technology to be implemented.

G.3.2.1. Best practice: Blue Mountain EGS

The Blue Mountain EGS project in Nevada, USA is the latest and most successful EGS development. It is a result of about 50 years of research and development and marks a new milestone for commercial EGS development worldwide. Two horizontal wells are connected by 16 hydraulic stimulation stages. The stimulations were performed as plug-and-perf stimulations from a perforated cemented liner. The stimulations were performed with sand as proppants and slickwater as injection fluid. The monitoring well was drilled first to be able to closely monitor induced seismic events during reservoir stimulation. After drilling and stimulating the first well, the second well was drilled into the stimulated reservoir volume. The second well intersected the fractures as shown by sand found in the cuttings. The lateral sections of the doublet were drilled with 9 ⅞" hole and completed with 7" casing. The maximum temperature is 191°C. A 37-day crossflow production test demonstrated flow rates of 227 m^3hr^{-1}, production temperatures of 169°C and a peak power production of 3.5 MWel. 4 existing wells with image log data adjacent to the EGS wells were reviewed to determine the local stress field, which is essential for the planning of EGS projects. This example shows how existing well data can be used for nearby EGS developments. The Blue Mountain EGS project is considered as the benchmark for new EGS drillings and reuse projects and the engineering procedure is what best represents the current state-of-the-art as shown in Figure G.3.8.

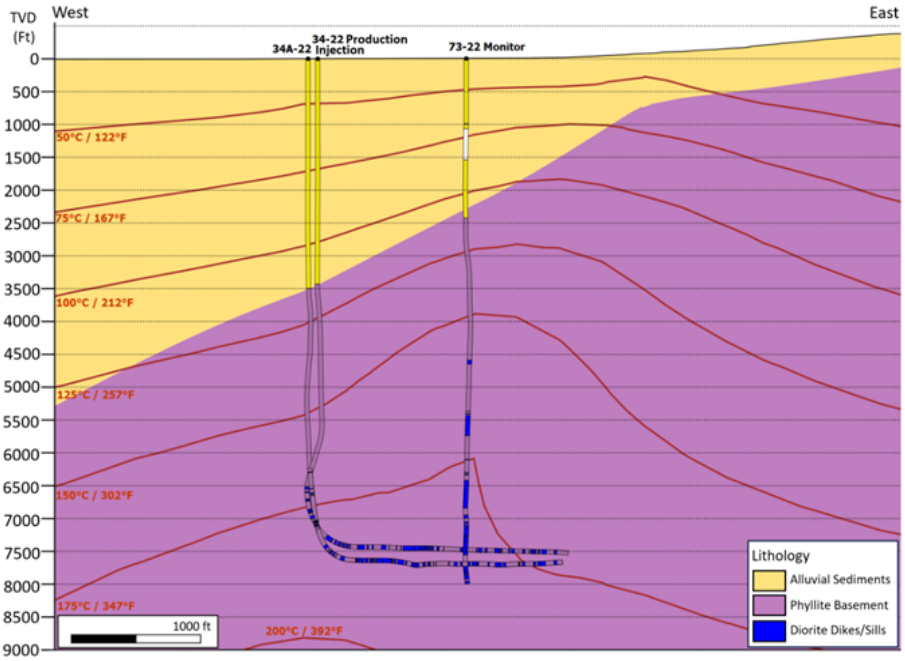

Figure G.3.8: Monitoring, production and injection well of the Blue Mountain EGS project (Norbeck et al., 2023).

G.3.2.2. Well reuse for seismic monitoring: Soultz-sous-Forêts EGS

At the Soultz-sous-Forets EGS site, four old oil wells (one of them EPS-1) were deepened to monitor micro-seismicity in 1989 and 1990 before stimulating and deepening GPK-1 and before stimulating GPK-2. After drilling of GPK-3 and GPK-4 in 2002 and 2003 and extensive production testing in 2003-2010, operation started in 2016 with an installed gross capacity of 1.7 MWel. GPK-1 and EPS-1 are currently used as monitoring wells. This example shows how existing wells can be used for monitoring purposes in new EGS developments as shown in Figure G.3.9.

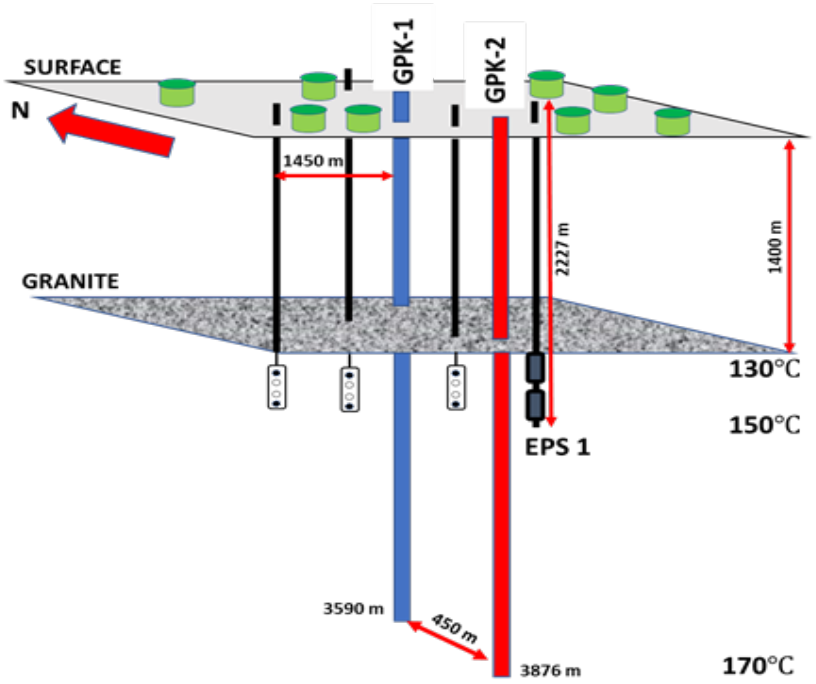

Figure G.3.9: Soultz-sous-Fôrets EGS project (modified from Baria et al., 1999) where old oil wells have been used for seismic monitoring during the development of the new EGS wells.

G.3.2.3. Well reuse example: Groß Schönebeck EGS

The description of the hydrocarbon well reuse example at Groß Schönebeck is largely based on Huenges et al. (2002). GFZ Potsdam was looking for a suitable site to demonstrate the Enhanced Geothermal System technology. The Rotliegend formation was chosen for this demonstration because it has a temperature above 120°C (formations deeper than 3000 m), a large regional extent, a variety of lithologies, and it is a well-investigated and extensively drilled gas reservoir. From more than 50 deep hydrocarbon exploration wells in northeast Germany the plugged and abandoned borehole E GrSk3/90 was chosen to be re-opened and to serve as an in-situ laboratory for Enhanced Geothermal System technologies.

GrSk 3/90 was drilled in 1990 to a depth of 4240 m. The well was cased until 3882 m (base of Zechstein formation) with the remainder (Rotliegend formation) left open. The Rotliegend includes 203 m siltstones and 146 m sandstones including 19 m of basal conglomerate and 9.5 m andesite.

Available data for planning well-repurposing operations were geophysical logs (caliper, gamma-ray, resistivity, induction, density, spectral-gamma, sonic and dipmeter), core measurements including 290 porosity measurements and 109 permeability measurements, a drilling report (EEG, 24.05.1991) and a plugging report (EEG, 22.01.1991).

The permitting procedure for the extraction of geothermal energy and brine (mineralised thermal water) required the following steps according to § 3 the Federal Mining Act (Bundes Berggesetz) from 13 August 1980 as these are non-mineable mineral resources ("bergfreie Bodenschätze"):

- **Application for right of way and drilling permit**

An application for drilling a well (i.e., re-opening) was submitted to the mining authorities. The following authorities were involved in the permitting process:

- forestry office Groß Schönebeck
- Brandenburg State Museum
- Military District Administration VII
- Mining Authority Rüdersdorf
- Uckermark-Barnim Regional Planning Office
- Cottbus Regional Finance Directorate
- State Environment Agency
- Joint State Planning Department
- District Administrator of the Barnim district
- Brandenburg State office for Geosciences and Natural Resources (LBGR)
- Schorfheide-Chorin Biosphere Reserve

The site was situated in a protected nature area. Therefore, noisy activities were only allowed in the period of mid-August to end of February. The area was covered with 7-year-old trees that had to be removed. Hence, an equivalent area had to be reforested elsewhere. The permit was granted on 26.10.2000 for the duration of 5 years with the requirement to restore and reforest the area after termination of the project.

- **Principal plan of operations**

The "main operating plan for the development of geothermal energy and brine in the well Groß Schönebeck 3/90" contained the following points after § 48 Abs. 2 and §§ 55, 56 Federal Mining Act ("Bundesberggesetz"):

- General information (exact location, land use, impact of the operations on the area)
- Goal of the drilling and related geological issues
- Description of the technical operations
- Installation of machinery and equipment on the site measurement and logging program
- Environmental impact
- Safety regulations (fire, gas)
- Estimated waste volume and disposal procedures
- Measures for warranty of public safety
- Ordnance survey, definition of boundaries
- Re-utilization or restoration of the site

The full details of the work were later included in the special plan of operations. The principal plan of operation was approved on 27 October 2000 and was valid until 31 December 2003.

- Special plan of operations

Following a call for tenders the drilling contractor UGS GmbH Mittenwalde was selected to perform the drilling activities. The company prepared the Special Plan of Operations including a chronogram of activities and information necessary to prove that all legal requirements are met.

- Permit for groundwater utilisation

The initial situation of the well is shown in Figure 1. Cellar and top of casing array were at 1 m depth and the well was secured with a concrete plate covered with earth and surrounded by trees. Cement plugs were set according to the reports at:

- 1-100 m (1 – 88 m measured),
- 2255 – 2430 m (2246.8 – 2348.0 m measured)
- 3818 – 3913 m (3801.0 – 3910.0 m measured)

The sections between the cement plugs were filled with old drilling mud. However, redrilling of the following sections was necessary, likely due to remains of cement, which were not put in the correct intervals according to the plan:

- 511 – 538 m (27 m, 9 5/8” casing)
- 1755.4 – 1758.6 m (3.2 m, 9 5/8” casing)
- 2348.0 – 2365.5 m (17.5 m, 7” liner)
- 2396.0 – 2500.0 m (104 m, 7” liner)

The old open hole section was redrilled with a 149.2 mm bit (3910-4240 m), which was slightly larger than the old diameter of 147.8 mm. This was done to remove the old filter cake and improve the near borehole area. To keep the costs and effort low the old drilling mud in the well was re-used. The mud was continuously monitored and partly exchanged when required. The borehole was then deepened from 4240 m to 4294 m to access the volcanic rocks for testing.

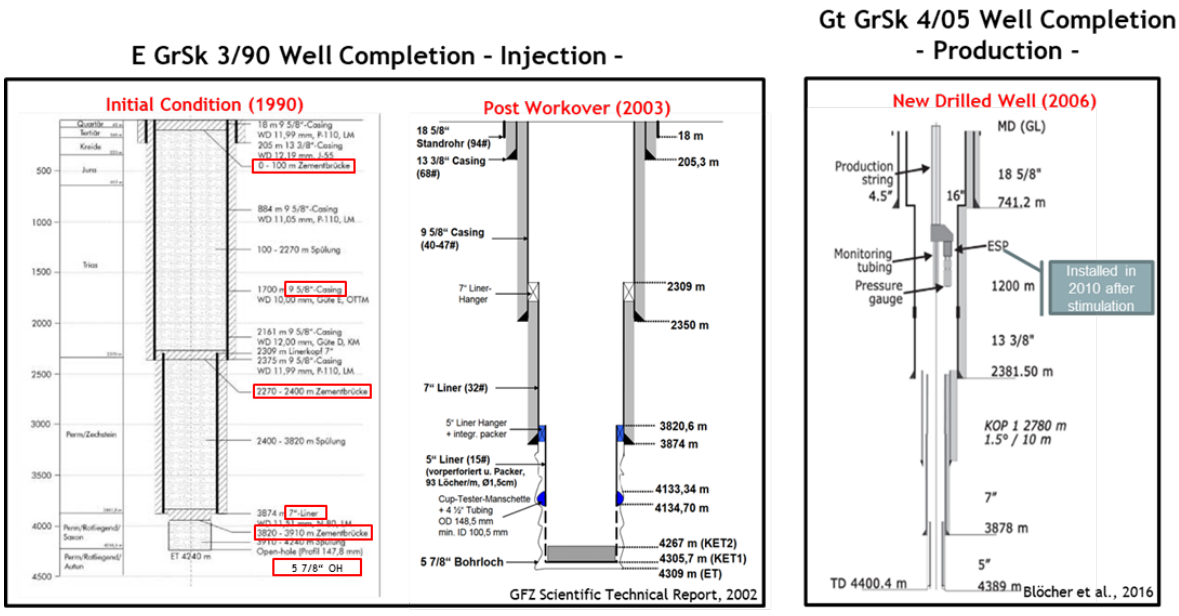

Figure G.3.10: Well completion of the repurposed injection well E GrSk 3/90 before and after workover and the newly drilled production well Gt GrSk 4/05 at the Groß Schnebeck EGS site.

The chronological operational sequence of repurposing well GrSk 3/90 as EGS in-situ laboratory was the following:

1. Preparation for drilling

2 Nov 2000	: Surveying and uncovering the borehole
3-14 Nov 2000	: Drill site construction exterior area and access road (Figure G.3.11, left)
15 Nov 2000	: Setting new drill cellar
20-23 Nov 2000	: Construction of construction site well including pump test
16-27 Nov 2000	: Drill site construction foundations for drill rig, core area, rig up (Figure G.3.11, right)
28 Nov 2000	: Acceptance of drill rig, installation of a new casing head housing on top of the 10 years old casing (Figure G.3.11, middle)

2. Workover of the well

29 Nov – 1 Dec 2000	: Assembly of borehole protection, Assembly of drill string with 8 ½" bit
1 Dec - 2 Dec 2000	**: Drilling first cement plug at 0 - 88 m**
2 Dec - 3 Dec 2000	**: Scraping 9 5/" casing, repeated drilling at 511.0 - 538.0 m & 1755.4 - 1758.6 m**
3 Dec 2000	**: Drilling second cement plug at 2246.8 - 2313.5 m**
4 Dec 2000	: Official site inauguration
5 Dec -6 Dec 2000	**: Change of drilling assembly to 5 7/8", drilling second cement plug at 2313.5 - 2348.0 m, repeated redrilling at 2348.0 - 2365.5 m & 2396.0 - 2500.0 m**
7 Dec 2000	: Assembling E-Manifold (gas protection)
8 Dec 2000	**: Drilling of third cement plug at 3801.0 - 3910.0 m**
9 Dec 2000	**: Redrilling open hole section at 3910.0 - 4167.6 m**
10-13 Dec 2000	: Stuck drill string
14 Dec 2000	: Drill string recovered
15 Dec 2000	: Change to spiral heavy pipes
16 Dec 2000	**: Redrilling open hole section 4167.6 - 4240.0 m**

3. Deepening of the well

17-19 Dec 2000	: Drilling 4240.0 – 4294.0 m, change of drilling mud to salt water in open hole area (8 m^3)
20 Dec 2000	: Well logging in open hole section, casing control (multi finger caliper log)
21 Dec 2000	: Scraping 7" casing
22 Dec 2000	: Change of drilling mud to salt water in 7" section (30 m^3), securing the well
23 Dec 2000 – 1 Jan 2001	: Holiday break, guarding the site

4. Test works

2 Jan 2001	: Commissioning the drill rig
3 Jan 2001	: Preparation of lift test
4-5 Jan 2001	: Installation of lift string to 1989.5 m, installation of measurement tools, lift test, failure online measurement tool, repair, lift test
6-7 Jan 2001	: Pressure build-up test
8 Jan 2001	: Removal of measurement tools, flowmeter measurement during new lift test
9 Jan 2001	: Collecting deep water sample
10 Jan 2001	: Cancellation of gas protection measures
10-21 Jan 2001	: Removal of lift string, rig-down, clearance of drill site, securing drill cellar
22 Jan 2001	: Acceptance of complete work

Figure G.3.11: Preparation of the drilling site (left), installation of a new casing head housing on top of the 10 years-old casing (middle), drilling rig (right).

In well E GrSk 3/90 the sandstone formations were completely plugged. This may be due to the drilling fluid and potential scaling, because this fluid was in the well between 1990 and the end of 2000.

G.4. Numerical simulation

G.4.1. Method

The Groß Schönebeck site was modelled by several authors as shown in Table G.4.1. with different simulators and purposes (Blöcher et al., 2010; Hofmann et al., 2022; Norden et al., 2023. In this study, the proof of concept by model calibration against field measurements is modelled using different simulators and incorporating the parameters reported by the previous authors.

Numerical simulation was carried out using finite differential simulator CMG STARS. This simulator is capable of modelling the coupled thermal and hydraulic processes in geothermal reservoir multi-phases and components used in the case of field-scale modelling (CMG, 2024). Additionally, the wellbore was modelled using FlexWells in CMG Builder module and the CMG module CMOST was used to facilitate the sensitivity analysis. The advantages of using these integrated modules are: 1) Its capacity for integrating wellbore and reservoir simulations, achieved by the inclusion of well completion and trajectory design; 2) The embedded CMOST module which facilitates the automated transfer parameters utilised in the simulation to the sensitivity analysis study.

Author/year	Simulator	Objective of modelling
Norden et al., 2023	PETREL (Commercial)	Petrophysically parameterized geological facies model to develop a new integrated site model using the recent 3D seismic data.
Hofmann et al., 2022	GOLEM (Open source)	Developing option of development to investigate the potential of resource extraction from the saline thermal fluid.
Blöcher et al., 2018	GOLEM (Open source)	Evaluating the spatial and temporal distribution of 26 micro-seismic events which were triggered by hydraulic stimulation
Blöcher et al., 2010	FEFLOW (Commercial)	Understanding the hydrothermal process occurring in an EGS during geothermal power production.

Table G.4.1: Previous modeller, software, and the objective of modelling

G.4.2. Model validation of the reference site Groß Schönebeck

G.4.2.1. Site description

The Groß Schönebeck deep geothermal research platform is located in the North German Basin (NGB), which is part of the Central European Basin System (CEBS) extending from Central England to Northern Germany, Poland and the Baltic States (Ziegler, 1990; Doornenbal and Stevenson, 2010), reflecting a low-enthalpy geothermal environment (Norden et al., 2023). Thermal relaxation, crustal extension and tectonic subsidence are the three main influences on basin evolution (van Wees et al. 2000), leading to the initial phase of rifting in the late Carboniferous to early Permian. These 307-277 Ma old volcanic rocks consist of rhyolites, ignimbrites, andesites and, to a lesser extent, basalts (Benek et al., 1996). This igneous event was followed by a long-lasting subsidence later than 250 Ma subsidence (Scheck et al., 1999) and sediment accumulation. A clastic sequence of early Permian Rotliegend of aeolian sandstones, fluvial fans as well as playa deposits covered the volcanic rocks. Subsequently, thick cyclic evaporites and carbonates up to 1.5 to 2.0 m thick were deposited in the late Permian Zechstein (Hoth et al., 1993; DEKORP-BASIN Research Group et al., 1999; Peryt et al., 2010; Huenges et al., 2002). The clastic Rotliegend sediments showing a considerable thickness were the target of hydrocarbon exploration (Burzewski et al., 2009; Maćkowski et al., 2017; Norden et al., 2023). In addition to the hydrocarbon potency, in the late Cretaceous to early Triassic, salt diapirism occurred, deforming the post-Zechstein succession and causing large lateral variations in salt thickness (Kossow et al. 2000; Huenges et al., 2002; Scheck-Wenderoth et al. 2008). Because the thermal conductivity of salt is two to three times higher than that of other sediments (Huenges et al., 2002), the salt structure strongly influences the subsurface temperature field.

The discovery of the well E GrSk 3/09 drilled into the geological setting shown in Figure G.4.1 marked the development of the Groß Schönebeck geothermal research platform. The well was originally intended to target a gas reservoir at a depth of more than 4 km in 1990. The well was drilled almost vertically and was cored in Rotliegend gas reservoir at the depth interval of 4040 – 4270 m measured depth (MD). Because of insufficient gas deposits, the well was closed immediately after drilling (Legarth et al., 2003). Later in 2000, the well was selected from 50 plugged and abandoned deep former oil and gas exploration wells in northeastern Germany as a candidate for reuse as geothermal research well. This is based on the observed bottom-hole temperature of 149°C at 4240 m MD and a large regional extent of the Rotliegend formation as a potential geothermal reservoir (Huenges et al., 2002). Since then, the well site was subsequently developed as an in-situ subsurface laboratory owned and operated by the GFZ, where extensive multidisciplinary subsurface research dedicated to geothermal development was carried out since 2002. The interpretation of lithology and stratigraphy around the well was carried out after the re-opening and deepening of well E GrSk 3/90 in 2000/2001. This was built upon an integration of drilling reports, geophysical logging data, seismic and DAS-VSP data interpretations and regional correlation based on the Brandenburg Geological Atlas. (König and Meyer, 1988; Hamann M and Schulz W, 1991; Hoth, 1993; Rockel

and Hurter, 2002; Lotz, 2004; Holl et al., 2005; Trautwein and Huenges, 2005; Stackebrandt et al., 2010; Krawczyk et al., 2019; Martuganova et al., 2022; Norden et al., 2022).

The initial well integrity condition of E GrSk 3/90 was investigated using a caliper log for casing inspection and the acoustic measurement using a full wave sonic tool to assess cement bond in the absence of cement bond log data. The result showed that there were no leaks and no serious cement losses. Below the casing shoe of the 7" liner, the well was left uncased. The result of the caliper run showed a 40% reduction in wall thickness at several points in the 7" liner section, but this does not affect the integrity of the whole casing configuration to withstand external pressures and changes in temperature.

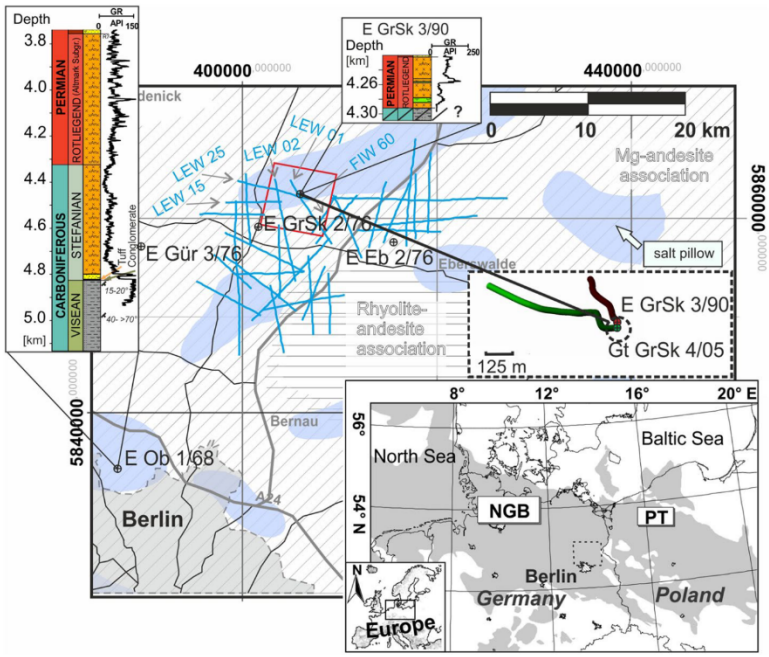

Figure G.4.1: Geological setting of Groß Schönebeck site (Norden et al., 2023).

As shown in Figure G.4.2, the initial appraisal test showed that the inflow measured by the downhole flowmeter came from the interval depth of 4220 to 4240 m MD, indicating the transition between the Havel subgroup and Volcanic formations, with a limited flow rate of 15.63 m^3h^{-1} (Wolfgramm et al., 2003). Based on the initial measurement, the expected reservoir target of the Rotliegend formation had insufficient permeability for hydrothermal energy production, however the permeability was considerably sufficient to pursue the development of matrix-dominated EGS. The well was stimulated to allow the fluid flow via the sandstone between the doublet wells. Following the development of E GrSk 3/90 and the hydraulic stimulation demonstration, a new geothermal well, the 4.4 km long Gt GrSk 4/05 (A2), was drilled in 2006 to serve as a production well (Huenges et al., 2007). The new directional well, with the subsurface distance approximately 472 m from the E GrSk 3/90 well in the Rotliegend and volcanic reservoir sections was then stimulated. The details of the hydraulic stimulations, including treatment parameters and generated fracture dimensions have been presented by Zimmermann et al., 2009; Zimmermann et al., 2010; Zimmermann and Reinicke, 2010; Blöcher et al., 2010; Zimmermann et al., 2011, and summarised by Blöcher et al. (2016).

G.4.2.2. Model Setup

The model setup and parameterisations were determined in comparison to the previous parameters deployed by previous modellers. The initial measurements and field data required for model calibration were sourced from the following publications: Huenges et al. (2002), Wolfgramm et al. (2003), Zimmermann et al. (2010), Reinsch et al. (2015), and Blocher et al. (2016). The data from aforementioned publications are presented in Table 4.2.

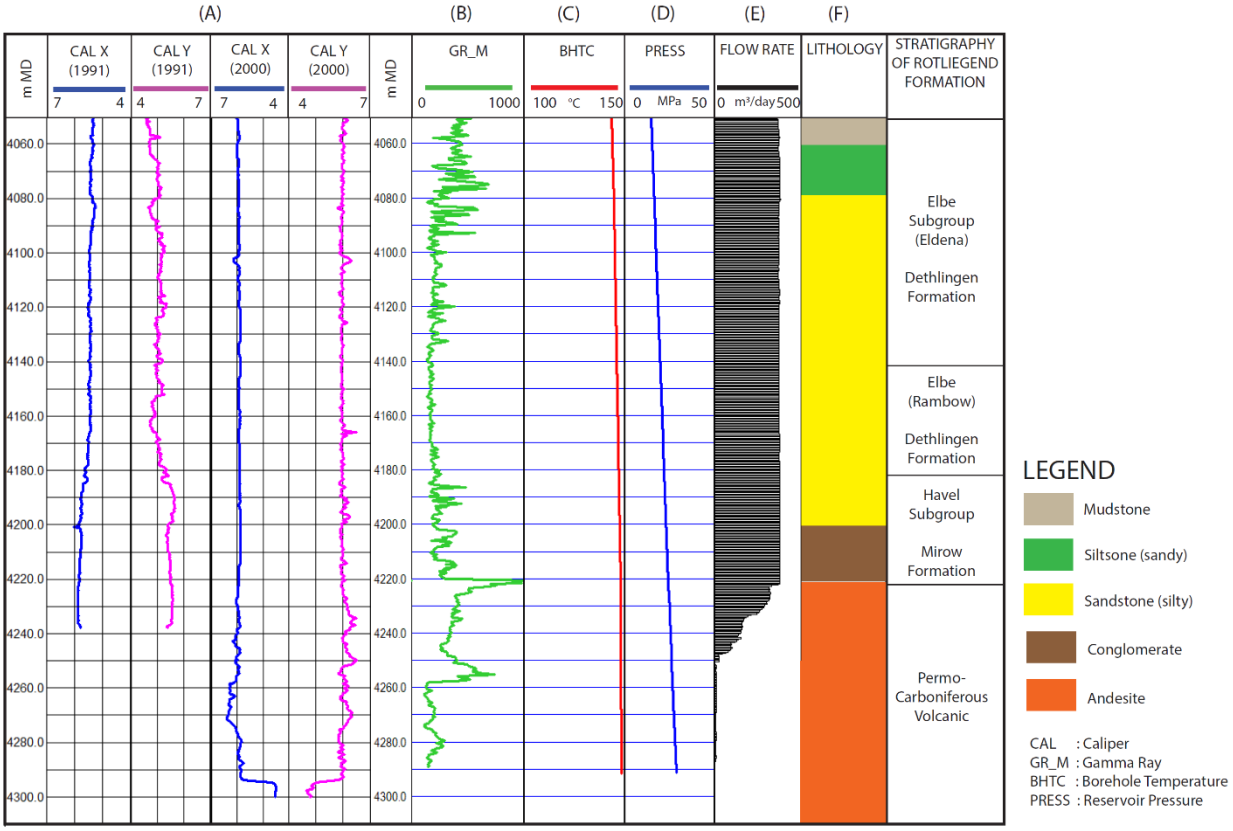

Figure G.4.2: Initial well testing result at E Grsk 3/90 after reopening and deepening the well in 2001 & Calliper test result. (A) Caliper measurement results in 1991 and 2000. (B) Gamma Ray (GR_M), (C) Temperature (BHTC), (D) Pressure (PRESS) measured in 2001. (E) Inflow measurement with down-hole flow meter after the re-opening of E GrSk 3/90 in January 2001. (F) Lithology and stratigraphy of well E GrSk 3/90 (modified from Huenges et al., 2002 and Norden et al., 2023).

The geometry of this reservoir model was defined on the basis of the 3D geological model derived from the most recent 3D seismic interpretation of the Gros Schonebeck site. This geometry was implemented for the first time in a reservoir dimension *(x,y,z)* of 1 km x 1.2 km x 4.3 km for calibration purposes. Each single grid cell has a dimension *(x,y,)* of 20 m x 20 m with vertical length varied according to the defined geological unit thickness. The geological units of the reservoir section as defined by Norden et al. (2023) were divided into five layers presented in Table G.4.3. The well completions presented in Table G.4.4 as described by Reinsch et al. (2015), were implemented for the wellbore model of well E GrSk 3/90 and well Gt GrSk 4/05 (A2).

Data	Reference
3D geological model	Norden et al. (2022), Norden et al. (2023)
Well trajectory	Norden et al. (2023)
Well completions	Reinsch et al. (2015)
Thermal and hydraulic properties	Huenges et al. (2002), Blocher et al. (2010), Hofmann et al. (2022), Norden et al. (2023)
Fracture properties	Zimmermann et al. (2010), Blocher et al. (2010), Blocher et al. (2016)
Fluid properties	Wolfgramm et al. (2003), Blocher et al. (2010)
Data from 139 hydraulic tests data (production - injection)	Reinsch et al. (2015), Blocher et al. (2016)

Table G.4.2: Data basis and sources for model setup and calibration.

Unit		Depth (m.TVD)	Thickness (m)	Number of layers
Hannover (Mellin - Peckensen)	I	3874 - 4084	209	10
Dethlingen (Eldena)	II	4084 - 4134	50	2
Dethlingen (Rambow)	III	4134 - 4185	51	2
Havel Formation	IV	4185 - 4222	37	2
Permo-Carboniferous Volcanic	V	4222 - 4292	70	7

Table G.4.3: Geological units as defined in Norden et al. (2023). The depth refers to True Vertical Depth (TVD) of well E GrSk 3/90.

Casing Type	Size - Outer Diameter (inch)		Depth/Top (m, MD)		Depth /Bottom (m. MD)		Grade	
Well	P	I	P	I	P	I	P	I
Conductor casing	25 63/64	13 3/8	0	0	41.6	18		
Surface casing	18 5/8	13 3/8	0	0	741.2	205	L80/X56	J55
Production casing	16	9 5/8	0	0	723	2375	N80/HCN 80	P110/DE/E
	13 3/8		723		1680		P110	
	13 5/8		1680		1803		Q125	
	13 3/8		1803		2381.5		P110	
Liner	7	7	2333	2309	3878	3874	L80	N80
Open hole section		5 7/8		3820		4305	L80	
Liner	5		3761		4355		HCI 10	L80

Perforated liner	5	5	4355	3820	4389		C95	
Production tubing with ESP pump installation	4 1/2		0		1163.3		13Cr/J55 (Isol. Joint)	
Injection tubing		4 1/2		0		305		J55

Table G.4.4: Doublet wellbore configuration. (P) Production well Gt GrSk 4/05 (A2); (I) Injection well E GrSk 3/90.

G.4.2.3. Model parameterisation

- **Initial and boundary conditions**

Initial and boundary conditions are based on the series of measurement of T-P-MRES-GR (Temperature, Pressure, Mud Resistivity, and Gamma Ray) performed at the well E GrSk 3/90 in 2001 immediately after the opening of the borehole (Huenges et al., 2002). The temperature of the reservoir model referred to the measured maximum temperature of 149 °C at the depth of 4230 m TVD with the average water level of 255 m TVD. Based on the linear regression of the initial temperature analysis at Groß Schönebeck, an average temperature gradient of 0.032 °C m-1 was applied in the *Eq. 1* to the reservoir section of the model. This reflected the temperature gradient of Rotliegend Formation from the depth interval of 3875 – 4300 m TVD. The surface temperature of 10 °C as the annual average temperature in the Northern Germany area was in the model (IEA, 2022).

$$T = 0.032\ ^{\circ}\mathrm{C}\ m^{-1} \times depth\ [m] + 10\ ^{\circ}\mathrm{C} \qquad \textit{Eq. 1}$$

The initial well bottom-hole pressure was calculated based on pore pressure (Pp) formula as shown in *Equation 2*:

$$Pp = \rho\ g\ z \qquad \textit{Eq. 2}$$

with reference reservoir fluid density () of 1150 kgm^{-3}, gravity acceleration (g) of 9.80 ms^{-2}, and height of the water column (z) of 4035 m at the depth of 4290 m TVD. Constant pressure and temperature boundary conditions are applied to the sides of the model by assuming an infinite reservoir, and infinite volume aquifer is assumed and is applied for the left, right, front, and back of the reservoir model.

- **Thermal and hydraulic properties**

Rock thermal conductivity and volumetric heat capacity were taken from Blocher et al. (2010). It is assumed that the properties of the solid fraction are similar to the bulk properties used by Blocher et al. (2010) due to the low porosity of the reservoir rock disclosed at the uncased hole and perforated liners applied in this study. Porosity and permeability parameters referred to the facies simulation parameterisation provided in Norden et al. (2023). Due to the low permeability, vertical and horizontal permeability were assumed to be equal in this study. However, in particular, for the Havel subgroup and Dethlingen (Rambow) Formation, permeabilities were defined based on the analysis of the first nitrogen lift test carried out in 2001 for 100 hours in E GrSk 3/90 (Huenges et al., 2002). The initial permeability of Havel subgroup and Dethlingen (Rambow) Formation was derived from transmissivity calculation by assuming a reservoir thickness of 20 m, the interval depth where inflow was detected during the initial inflow test, as shown in Figure G.4.2. The permeability was determined not higher than 5×10^{-15} m^2 based on well test analysis (Horne, 1995) and modelling of infinite homogeneous with nSIGHTS simulator (Pickens et al., 1987) assuming a radial flow into the wellbore. Thermal and hydraulic properties were implemented according to the geological units defined in this study as shown in Table G.4.5.

- Wellbore properties

The low permeability value of the Havel subgroup and the Dethlingen (Rambow) Formation is indicative of near wellbore formation damage. Accordingly, the initial condition of the reservoir was modelled using nitrogen lift test data and the skin factor was incorporated by applying the *Eq. 3*, which was developed by Horne (1995).

$$S = \left(\frac{k}{k_s} - 1\right) \ln \frac{r_s}{r_w} \qquad \textit{Eq. 3}$$

where S is the skin factor in the range of 1.8 to 2.9, k is the reservoir matrix permeability estimated to be 1.48×10^{-13} m^2 as obtained from logging data interpretation and core data measurement summarized by Norden et al. (2023), k_s is the reduced permeability zone obtained from the nitrogen lift test for the Havel subgroup and the Dethlingen Formation, estimated to be 4.4×10^{-15} m^2, r_s is skin zone estimated at a radius of 1 - 5 m from the wellbore to the surrounding formation, and r_w is the wellbore radius.

Geological unit	Φ (%)	k (m^2)	λ (Wm^{-1}K)	VHC (MJ m^{-3}K)
I. Hannover (Mellin Peckensen)	0.05	3.57 x 10^{-23}	1.90	2.40
II. Dethlingen (Eldena)	0.10	3.57 x 10^{-23}	1.90	2.40
III. Dethlingen (Rambow)	0.10	4.44 x 10^{-15}	2.80	2.40
IV. Havel subgroup	0.11	4.44 x 10^{-15}	3.00	2.60
V. Volcanic rock sequence (Permo -Carboniferous Volcanic)	0.11 - 0.13	1.77 x 10^{-21}	2.30	3.60

Table G.4.5: Thermal and hydraulic properties applied in the reservoir model. φ is porosity, λ is thermal conductivity, and VHC is volumetric heat capacity (Huenges et al., 2002; Blocher et al., 2010; Hofmann et al., 2022; Norden et al., 2023).

- Fluid properties

The composition of the formation fluid at Gros Schonebeck was established during the preliminary nitrogen lift test conducted in 2001. Chemical analyses were conducted on the water and gas phases of the fluid, and concurrently, temperature and pressure measurements were conducted. The brine had 265 gL^{-1} of Total Dissolved Solid (TDS) and pH 5.7 (Wolfgramm et al., 2003). As provided in Blocher et al. (2010), the dynamic viscosity of 0.72 mPa s and 0.3 mPa s at the temperature of 70 °C and 30 °C were applied at the injection and production wells respectively. The average reservoir fluid density of 1115 kg m^{-3} was applied to the simulation of the circulation tests. For the dynamic condition of the simultaneous injection and production tests, the viscosity and density were calculated as a function of salinity and temperature expressed in *Eq. 4* to *Eq. 6* (Batzle and Wang, 1992). Pressure and temperature data were based on a series of static and flowing Pressure and Temperature (P,T) measurements during the simultaneous injection and production test periods.

$$\rho_{fw} = 1 + 10^{-6}\left(-80T - 3.3T^2 + 0.00175T^3 + 489P - 2TP + 0.016T^2P - 1.3 \cdot 10^{-5}T^3P - 0.333p^2 - 0.002TP^2\right) \qquad \textit{Eq. 4}$$

$$\rho = \rho_{fw} + s\{0.668 + 0.44s + 10^{-6}[300P - 2400\,Ps + T(80 + 3T - 3300s - 13p + 47Ps)]\} \qquad \textit{Eq. 5}$$

$$\mu = 0.1 + 0.333s + (1.65 + 91.9s^3)exp\left(-[0.42\,(s^{0.8} - 0.17)^2 + 0.045]T^{0.8}\right) \qquad \textit{Eq. 6}$$

where ρ_{fw} is the density of freshwater, ρ is the dynamic viscosity of the reservoir fluid, and μ is the salinity of reservoir fluid. Temperature and salinity dependent viscosity used in this study is provided in Table G.4.6.

Temperature and salinity dependent viscosity																				
Temperature (°C)	10	20	30	40	50	60	70	80	90	100	110	120	130	140	150	160	170	180	190	200
Viscosity (mPa s)	1.55	1.38	1.22	1.08	0.96	0.85	0.76	0.67	0.60	0.53	0.47	0.42	0.37	0.33	0.29	0.26	0.23	0.21	0.18	0.16
Salinity (g L^{-1})	265	265	265	265	265	265	265	265	265	265	265	265	265	265	265	265	265	265	265	265

Table G.4.6: Temperature and salinity dependent viscosity.

- Fracture properties

In this study, fracture properties are defined as fracture height, fracture depth, half-length, and fracture width which were determined by Zimmermann et al. (2010) and Blocher et al. (2010). The centre of the fracture which was defined as the fracture origin was positioned in the respective perforated liner section of the specific depth interval in which the stimulations were carried out as illustrated in Figure G.4.3 (A). The fracture plane was applied as described in Figure G.4.3 (B) into the reservoir model. Fracture half-length, which was the half-length of a planar hydraulic fracture, was applied as the horizontal extent in the x direction. Fracture height and fracture depth were applied as the vertical extent of the fracture geometry above and below the centre of the fracture respectively. In this case, since the stimulation was intended to propagate the fracture perpendicular to the direction of the minimum horizontal stress (SH= 288◦), the grid was first rotated in the x-direction to the minimum horizontal direction, following the position of the wellbore, and then each of the fracture properties described in Table G.4.7 was assigned accordingly to the sequence of stimulations. The grid surrounding the fracture plane was refined in the x, y, and z directions, with a discretisation factor of 5(x), 5(y), and 3(z), respectively, for each geometry of fracture. Effective fracture permeability (k) applied as a matrix permeability was automatically calculated with the following *Eq. 7*.

$$k = \frac{w_f k_f}{fracture_{zone}} \qquad \textit{Eq. 7}$$

Where a $fracture_{zone}$ of 0.61 m is defined as a default smallest grid cell width of the inner most planes of fracture, w_f is the fracture width, and k_f is the intrinsic fracture permeability. The fracture permeabilities are assumed to be homogeneous in the entire fracture. Effective fracture permeability and intrinsic fracture permeability of each fracture was obtained from history matching of modelling flow back test at E GrSk 3/90 and initial communication experiment at Gt GrSk 4/05 (A2) as shown in Table G.4.8.

- History matching parameter

Parameters of model calibration expressed by Productivity Index (PI) and injectivity index (II) were calculated using *Eq. 8*, where q is the flow rate, ΔP is the pressure drawdown, P_{wf} is the pressure at the flowing condition and P_i is the initial reservoir pressure.

$$PI = II = \frac{q}{\Delta P} = \frac{q}{|P_i - P_{wf}|} \qquad \textit{Eq. 8}$$

Flow rates of both production and injection wells were applied in the surface, and the reservoir pressure calculation was obtained from the first perforated liner of the wells or in the top of open-hole sections. For calibration purposes, the following tests described in Table G.4.8 were modelled to obtain a historical matching of the model against field data.

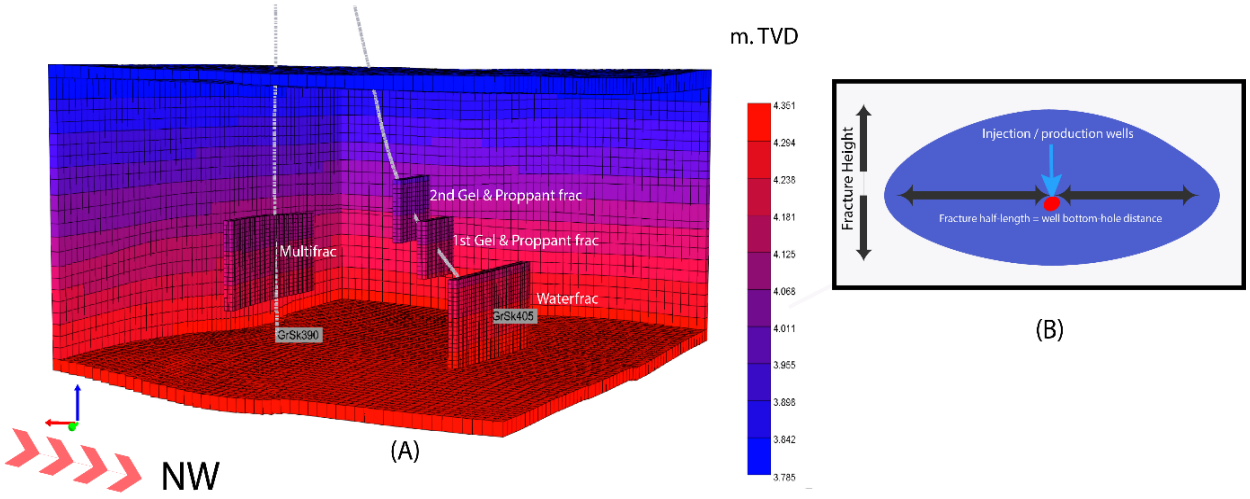

Figure G.4.3: (A) Fractures setup. (B) Hydraulic fracture schematic.

Well	Fracture	Stimulation type	Depth (m TVD)	Fracture height (m)	Fracture depth (m)	Half-length (m)	w_f (m)
E GrSk 3/90	1st Fracture	Multifrac	4076 - 4219	70	73	160	0.0192
Gt GrSk 4/05 (A2)	2nd Fracture	Waterfrac	4180 - 4325	73	72	190	0.0195
Gt GrSk 4/05 (A2)	3rd fracture	1st Gel and proppant	4082 - 4185	52	60	150	0.0195
Gt GrSk 4/05 (A2)	4th fracture	2nd Gel and proppant	4023 - 4118	48	60	140	0.0195

Table G.4.7: Fracture properties.

Well test	Final PI/II ($m^3h^{-1}MPa^{-1}$)
Gas lift test at E GrSk 3/90 in 2001	(II) 0.97
Flow back test at E GrSk 3/90, after first water frac in 2003	(II) 4.00
Initial communication experiment at Gt GrSk 4/05 (A2) in 2011	(PI) 5.8 - 8.9
Communication tests at GrSk 3/90 period 2011 - 2013	(II) 4.10

Table G.4.8: Calibration parameters of modelling existing matrix-dominated EGS concept.

G.4.2.4. Results of history matching

a. Initial condition

The initial state was determined through a gas lift test in 2001. It was mainly influenced by the dynamic state of the well, as the primary produced brine came from the post drilling fluid stored in the well. The simulation was therefore carried out using the Flexwell module which couples the reservoir to a full trajectory wellbore model. Based on the observation of the simulated pressure during the 100 hours of flow test, there is no significant pressure change in the reservoir near the wellbore. The initial condition result shows that the measured initial reservoir pressure of 44.45 MPa is captured from the reservoir block near the wellbore formation at a depth of 4107 m TVD. As the input parameter for the simulation, the simulated flow rate represents the measured flow rate at E GrSk 3/90 during the initial flow test. The output is the pressure response resulting in a productivity index range of 1 to 2 $m^3h^{-1}MPa^{-1}$ by applying a skin factor of 2 to express the damage at the near wellbore formation

b. Individual well testing

Individual well testing simulation was carried out as the transient test of a certain period that involved only one single well to test the productivity and injectivity of each well.

(i) Injection well E GrSk 3/90

The result of modelling the flow back test after water fracturing in 2003 is shown in Table G.4.9 (a) The reservoir model simulated the predefined induced fracture in the injection well. In this simulation, the flow rate was set constant at 59 m^3h^{-1}. The result shows that an injectivity index of 4.08 $m^3h^{-1}MPa^{-1}$ is achieved with a maximum flow rate of 59 m^3h^{-1} and a pressure drawdown (ΔP) of 13.4 MPa. Flow back was modelled by changing the injection well into the production well. The bottom hole pressure then was adjusted to mimic the highest bottom hole pressure after massive injection. The result shows a productivity index of 4.44 $m^3h^{-1}MPa^{-1}$ from the produced flow rate of 59 m^3h^{-1} with the ΔP of 13.3 MPa. The matched PI was obtained from model calibration with an effective fracture permeability of the multifrac induced fracture of 6.6E-13 m^2. The fitting parameters, intrinsic fracture permeability and effective fracture permeability and of the calibrated model, are adjusted to predict the initial and average injectivity indices during the communication test.

(ii) Production well Gt GrSk 4/05 (A2)

For the production well, the calibration parameters were based on the results of the communication experiment on Gt GrSk 4/05 (A2) carried out on June 2011. The aim was to calibrate the initial productivity index prior to the communication tests. The modelling was divided into two scenarios to evaluate the dependence of the productivity index on the fracture permeability at the production well. In the minimum scenario the minimum fracture permeability (k_2, k_3, k_4) of 1.42 x 10^{-12} m^2 was applied for the three induced fractures at the production well as shown in Figure G.4.3. For the maximum scenario, the maximum fracture permeability of 6.33 x 10^{-12} m^2 was applied at the waterfrac induced fracture, while the permeability of 1st and 2nd gel and proppant induced fractures remained the same as applied in the minimum scenario. The flow rate was set constant with several variations in order to encompass the minimum, average, and maximum flow rates that could be accommodated by ESP performed in the communication tests. These values were 30 m^3h^{-1}, 45.50 m^3h^{-1}, and 60 m^3h^{-1} respectively. Table G.4.9 (b) presented the results of calibration indicated by PI/II. The results demonstrated that the maximum PI of 8.10 $m^3h^{-1}MPa^{-1}$ was

achieved by applying the maximum flow rate of 60 m^3h^{-1} with a maximum pressure drawdown (ΔP) of 7.40 MPa.

	q ($m^3 h^{-1}$)	ΔP (MPa)	PI/II ($m^3 h^{-1} MPa^{-1}$)
(a) Injection well E GrSk 3/90			
Initial condition	13.5	14.00	0.97
Measured data	59.00	14.70	4.03
Simulated injection test	59.00	14.40	4.08
Simulated flow back test	59.00	13.40	4.44
(b) Production well Gt GrSk 4/05 (A2)			
Initial condition	31.60	13.30	2.4
Measured data	43.00 - 46.00	5.16 - 7.40	5.80 - 8.90
Minimum scenario	30.00	6.25	4.80
Maximum scenario		6.80	4.40
Minimum scenario	46.00	6.70	6.90
Maximum scneario		6.13	7.50
Minimum scenario	60.00	8.20	7.30
Maximum scenario		7.40	8.10

Table G.4.9: Result of history matching individual well performance. Minimum scenario was simulated by applying effective fracture permeability of 1.42e-12 m^2 for the three associated induced fractures at the production well. Maximum scenario was simulated by changing the effective permeability of the waterfrac induced fracture (2nd fracture) to 6.33 e-12 m^2.

c. Communication tests

From the first initial condition, where the induced fractures did not yet exist, the matrix permeability parameter (k) of the Havel subgroup and the Dethlingen Formation was determined by history matching the nitrogen lift test. In the next step, the individual well calibration, the associated effective fracture permeability of both injection and production wells was obtained from history matching of production-injection tests after a series of stimulations in each well. These parameters were then justified by history matching of doublet well communication tests based on the 139 hydraulic tests conducted between 2011 and 2013. The duration of each test ranged from 1 to 165 hours, the longest being the communication test at Groß Schönebeck. The simulation was carried out in two scenarios, as applied in the communication test experiments after calibration of individual wells. Figure G.4.4 shows the results of the calibration as indicated by PI for Gt GrSk 4/05 (A2) and II for E GrSk 3/90. The range of PI and II is described in Table G.4.10. The modelled and measured data for the production wells are off in late 2012 and 2023 due to a significant decline in the productivity index in the field, which was not considered in our model. Blöcher et al. (2016) outlined a number of possible explanations for this decline. Therefore, in this study, the history matching obtained in the E GrSk 3/90 well until the end of 2013 was used to justify the model calibration.

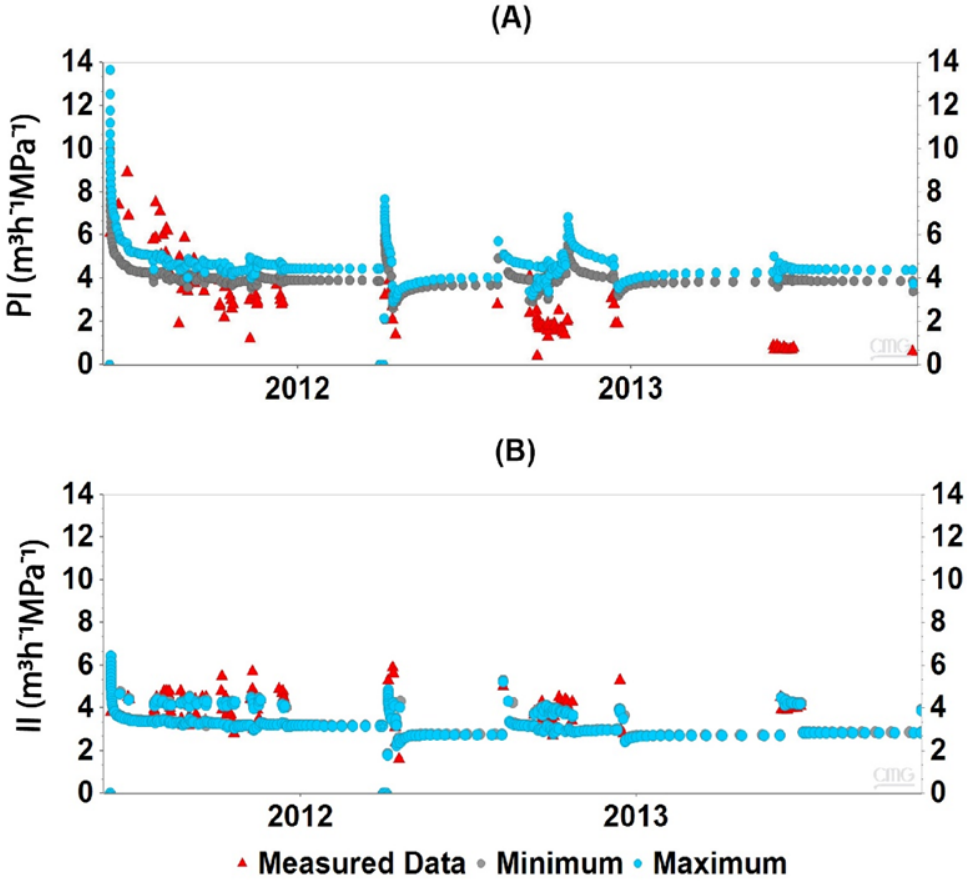

Figure G.4.4. Result of model calibration as shown by (A) Productivity index, PI, and (B) Injectivity index, II, fitting to the PI and II of the measured data. Minimum scenario was simulated by applying effective fracture permeability of 1.42 x 10^{-12} m^2 for the three associated induced fractures at the production well. Maximum scenario was simulated by changing the effective permeability of the waterfrac induced fracture (2^{nd} fracture) to 6.33 x 10^{-12} m^2.

	q ($m^3\,h^{-1}$)	P_i, maximum ΔP (MPa)	PI/II ($m^3\,h^{-1}\,MPa^{-1}$)
Minimum Scenario			
Injection well	5.90 - 49.84	P_i = 42.60, max ΔP = 14.30	1.80 - 6.80
Production well	5.90 - 49.84	P_i = 46.50, max ΔP = 14.00	2.10 - 10.00
Maximum Scenario			
Injection well	5.90 - 49.85	P_i = 42.60, max ΔP = 14.80	1.80 - 6.80
Production well	5.90 - 49.84	P_i = 46.50, max ΔP = 12.20	2.20 - 13.60
Measured data			
Injection well	5.90 - 49.84	P_i = 44.50, max ΔP = 12.23	1.6 - 5.9
production well	5.90 - 49.84	P_i = 46.00, max ΔP = 18.98	0.4 - 8.9

Table G.4.10: The range of PI and II of the calibrated models from the communication tests in comparison with the measurement data.

G.4.3. Proof-of-concept (base case)

The calibrated model was used to run a forward model of 20 years of doublet well performance in two scenarios and was generated from a calibrated model of 2.5 years of multiple well tests. The first scenario was set at a minimum flow rate of 30 m^3h^{-1} and the second scenario was set at a constant maximum flow rate of 60 m^3h^{-1}. The result shows a dominance of flow from the matrix dominated fracture zones as shown in Table G.4.11. Productivity and injectivity indices of each layer are presented in comparison with the total productivity and injectivity observed in the production and injection wells. In addition, the temperature distribution with the existing matrix dominated EGS concept is shown in Figure G.4.5. It indicates that the high permeability hydraulic fracture in the injection well distributes the cold water over the entire fracture surface area without thermal breakthrough for approximately 20 years. It could be concluded that the flow rate, as a key operational parameter, exerts a substantial influence on the ability to maintain temperature stability over the desired lifespan of the reservoir.

Well	Stimulation depth interval (m TVD)	Rock type	Stimulated fracture	PI/II		Flow Contribution (%)		measurement (*)
				30 $m^3 h^{-1} MPa^{-1}$	60 $m^3 h^{-1} MPa^{-1}$	30 $m^3 h^{-1}$	60 $m^3 h^{-1}$	
Production well	4057 - 4087	Sandstone	2nd gel and proppant induced fracture	0.9	1.0	23.40%	26.40%	20%
Gt GrSk 4/05 (A2)	4132 - 4148	Sandstone	1st gel and proppant induced fracture	1.8	2.1	36.8%	44.5	40 - 50%
	4239 - 4262	Conglomerate - Volcanic	water frac induced fracture	1.7	1.3	39.80%	29.10%	30-40%
			Well (PI)	4.2	3.40			
Injection well	4094 - 4117	Sandstone	multifrac induced fracture	0.27	0.30	8.45%	8.46%	
E GrSk 3/90	4117 - 4140	Sandstone		0.24	0.27	7.85%	7.84%	
	4140 - 4163	Sandstone		2.40	2.46	78.15%	78.16%	
	4163 - 4187	Conglomerate		0.16	0.17	5.55%	5.54%	
			Well (II)	3.07	3.20			

Table G.4.11: Results of forward modelling for 20 years of circulation. (*) Cumulative flow contribution from flowmeter measurement was sourced from Zimmermann and Reinicke (2010).

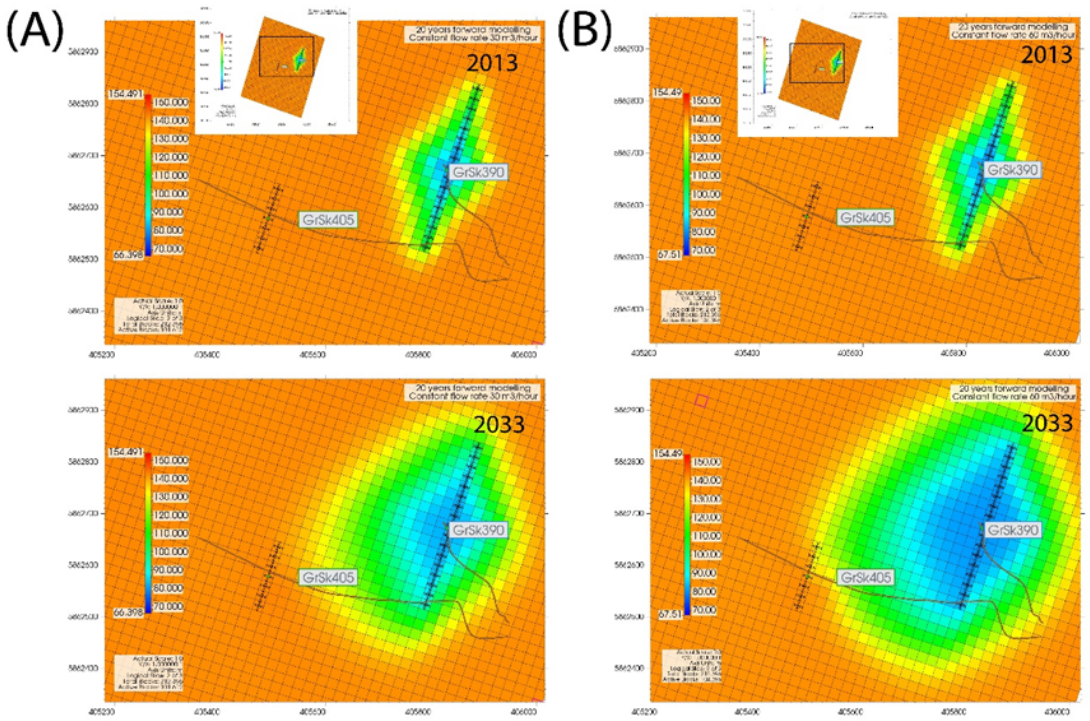

Figure G.4.5: Temperature distribution at a depth of 4150 m and at a constant flow rate of (A) 30 m^3h^{-1} (B) 60 m^3h^{-1}.

G.4.4. Sensitivity Analysis

G.4.4.1. Parameters and methodology of sensitivity analysis study

The objective of the sensitivity analysis is to evaluate model parameters summarised in Table G.4.12 with regard to the injectivity and productivity indices within the context of communication tests between doublet wells. The range of parameters is based on the most recent facies petrophysical model developed for the reservoir section of the Gros Schonebeck site (Norden et al., 2023). The sensitivity analysis was conducted using the global sensitivity analysis (Saltelli et al., 2008) with proxy modelling and Response Surface Methodology (RSM) provided in CMOST. In this method, which is equivalent to the all-at-once method, the output variation of parameters is induced by varying all the input factors simultaneously. Consequently, the sensitivity analysis considers both direct influence of each parameter and the joint influence due to interactions (Pianosi et al., 2016). The RSM employs polynomial regression to fit the simulation results, thereby ensuring relevance to the non-linear correlation between each input parameter and the objective function. This approach has been widely adopted in geothermal resource evaluation using numerical simulation (Pasikki et al., 2016; Quinao and Zarrouk, 2018; Ciriaco et al., 2020). The response surface method is coupled with the Design of Experiments (DoE) method, which allows the screening of parameters to determine the relationship between different variables (xs) affecting a process and the outputs of that process (ys) (CMOST, 2024). The DoE method is appropriate for the non-clustered parameter study, as applied in this study. Subsequently, the results were evaluated through the integration of Sobol (Sobo´l, 1993) and Morris (Morris, 1991) analyses, which were employed to assess the correlation between parameters and the objective function.

G.4.4.2. Result of sensitivity analysis study

For the sensitivity analysis, four studies were performed. For the first study, targeting constant flow rate of 30 m^3h^{-1} without variations in well size, 161 models were simulated. In the second study with the same constant flow rate, wellbore diameter was taken into account and 94 models were simulated to demonstrate the variation of parameters. The result of sensitivity study with a constant flow rate of 30 m^3h^{-1} is presented in Figure G.4.6. For the third study, targeting a constant flow rate of 60 m^3h^{-1} without variations in the wellbore bottom diameter size, 104 models were simulated. The fourth study, targeting constant for a flow rate of 60 m^3h^{-1} with variations in the wellbore bottom diameter size, 104 models were simulated. For the third and fourth studies, the results are shown in Figure G.4.7.

The results of the sensitivity study of the reservoir parameters indicated a similar conclusion across the four studies as presented in Figure G.4.8 to Figure G.4.11, which demonstrated the parameters with significant effect on PI and II as the performance indicators in the implementation of EGS technology. The matrix permeability of the reservoir rock, in this case the Havel subgroup, exerts the most significant influence on PI and II. In the context of pay zones, the transmissivity, which was directly influenced by the thickness of the reservoir interval, was considered to be of equal importance to the matrix permeability. Subsequently, fracture permeability represents the second most significant parameter, which is also influenced by fracture width or aperture in which the well intersects directly. In the context of EGS, the fracture permeability should be considered as the result of stimulation performed in the well to create a flow path within the reservoir. These two parameters, along with temperature as described in the forward modelling result, represent the primary reservoir parameters to be evaluated in the implementation of EGS technology.

In relation to the reuse case, the given wellbore geometry is the most important parameter to screen out the feasibility of reusing the old oil and gas wells. The two scenarios studied the effect of well bottom-hole diameter size on the productivity and injectivity indices show significant differences on the range of simulated injectivity and productivity indices. In the scenario without varying well diameter, the general

solutions model range is able to produce models with productivity index ranges from 0.6 to 5 $m^3h^{-1}MPa^{-1}$ and injectivity index from 0.5 to 7 $m^3h^{-1}MPa^{-1}$. Meanwhile, in the case where the bottom-hole diameter size was taken into account, the general solution models showed that the productivity index could range from 1 to 8.9 $m^3h^{-1}MPa^{-1}$, while the injectivity index is between 1.6 to 6.8 $m^3h^{-1}MPa^{-1}$. The results of 20 years-forward modelling of existing matrix-dominated EGS concept demonstrates that the productivity and injectivity indices of the well are inferior to those of the feed zones. This is due to the additional pressure lost in the wellbore. During the simulation run, high pressure friction due to small liner size was observed in production and injection wells with existing well configuration. In the case of Groß Schönebeck, the bottom hole diameter was exceptionally small for EGS development. This concludes the ideal well bottom-hole liner of at least 7" at the bottom-hole. The review of 70 EGS projects conducted within this study, not to count the reuse projects, 36 EGS projects deployed well bottom-hole diameter at minimum 7" to 10.75".

Parameter	Unit	Range of Parameter		
		Max	Base Case	Min
Permeablity of Havel Formation (a,b)	m^2	5.55E-15	4.44E-15	9.87E-16
Permeablity of Permo-carboniferous Volcanic (a,b)	m^2	9.87E-17	1.77E-21	1.77E-25
1st induced fracture permeability at E GrSk 3/90 (a,b)	m^2	9.30E-13	6.10E-13	3.17E-13
Fracture width (a,b)	m	0.02	0.0192	0.005
Intrinsic fracture permeability (a,b)	m^2	2.96E-11	2.11E-11	9.87E-12
2nd induced fracture permeability at Gt GrSk 4/05 A2 (a,b)	m^2	6.48E-12	6.31E-12	3.15E-13
Fracture width (a,b)	m	0.02	0.0195	0.005
Intrinsic fracture permeability (a,b)	m^2	1.97E-10	1.97E-10	9.86E-12
3rd induced fracture permeability at Gt GrSk 4/05 A2 (a,b)	m^2	1.94E-12	1.42E-12	3.17E-13
Fracture width (a,b)	m	0.02	0.0195	0.005
Intrinsic fracture permeability (a,b)	m^2	6.48E-12	6.31E-12	8.09E-14
4th induced fracture permeability at Gt GrSk 4/05 A2 (a,b)	m^2	1.94E-12	1.42E-12	9.47E-13
Fracture width (a,b)	m	0.02	0.0195	0.005
Intrinsic fracture permeability (a,b)	m^2	6.48E-12	6.30E-12	8.09E-14
Porosity of Havel Formation (a)	-	0.16	0.11	0.005
Porosity of Permo-carboniferous Volcanic (a)	-	0.11	0.013	0.0012
Volumetric Heat Capacity of Havel Formation (a)	MJ m^{-1} K^{-1}	3.4	2.6	1.9
Volumetric Heat Capacity of Permo-carboniferous Volcanic (a)	MJ m^{-1} K^{-1}	3.15	3.6	2.3
Thermal Conductivity of Havel Formation (a)	W m^{-1} K^{-1}	4	3	2.4
Thermal Conductivity of Permo-carboniferous Volcanic (a)	Wm^{-1} K^{-1}	2.1	2.3	1.4
Mass Density (b)	kg m^{-3}	1300	1115	1040
Wellbore diameter (Inner Diameter) - Injection well (b)	inch	8	5.875	4.4
Wellbore diameter (Inner Diameter) - Production well (b)	inch	8	4.2	3.6

Table G.4.12: Parameters for the sensitivity analysis study.

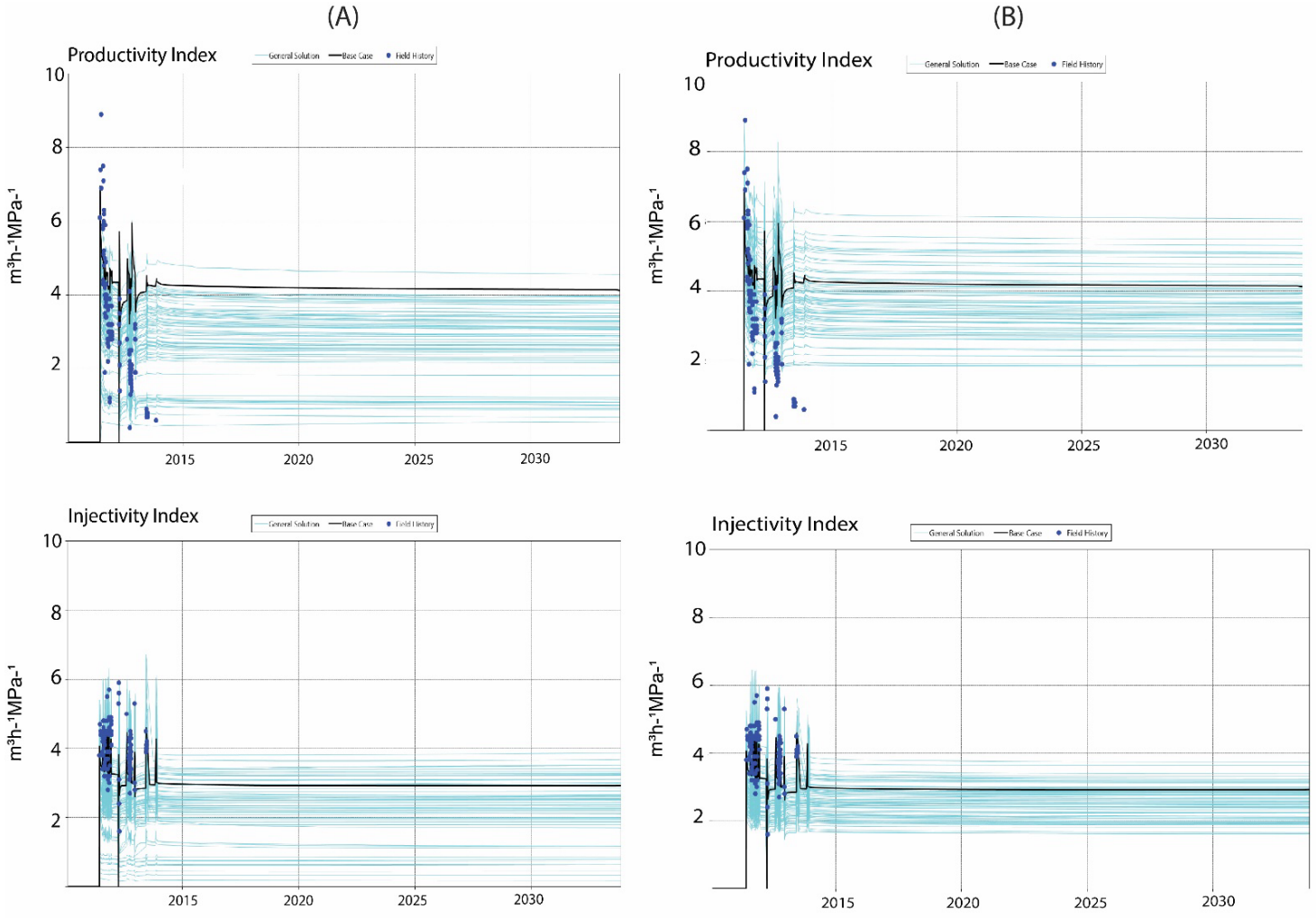

Figure G.4.6: Sensitivity analysis results showing productivity and injectivity indices as the objective function with a constant flow rate of 30 m^3h^{-1}. (A) without varying bottom-hole diameter; (B) by varying bottom-hole diameter.

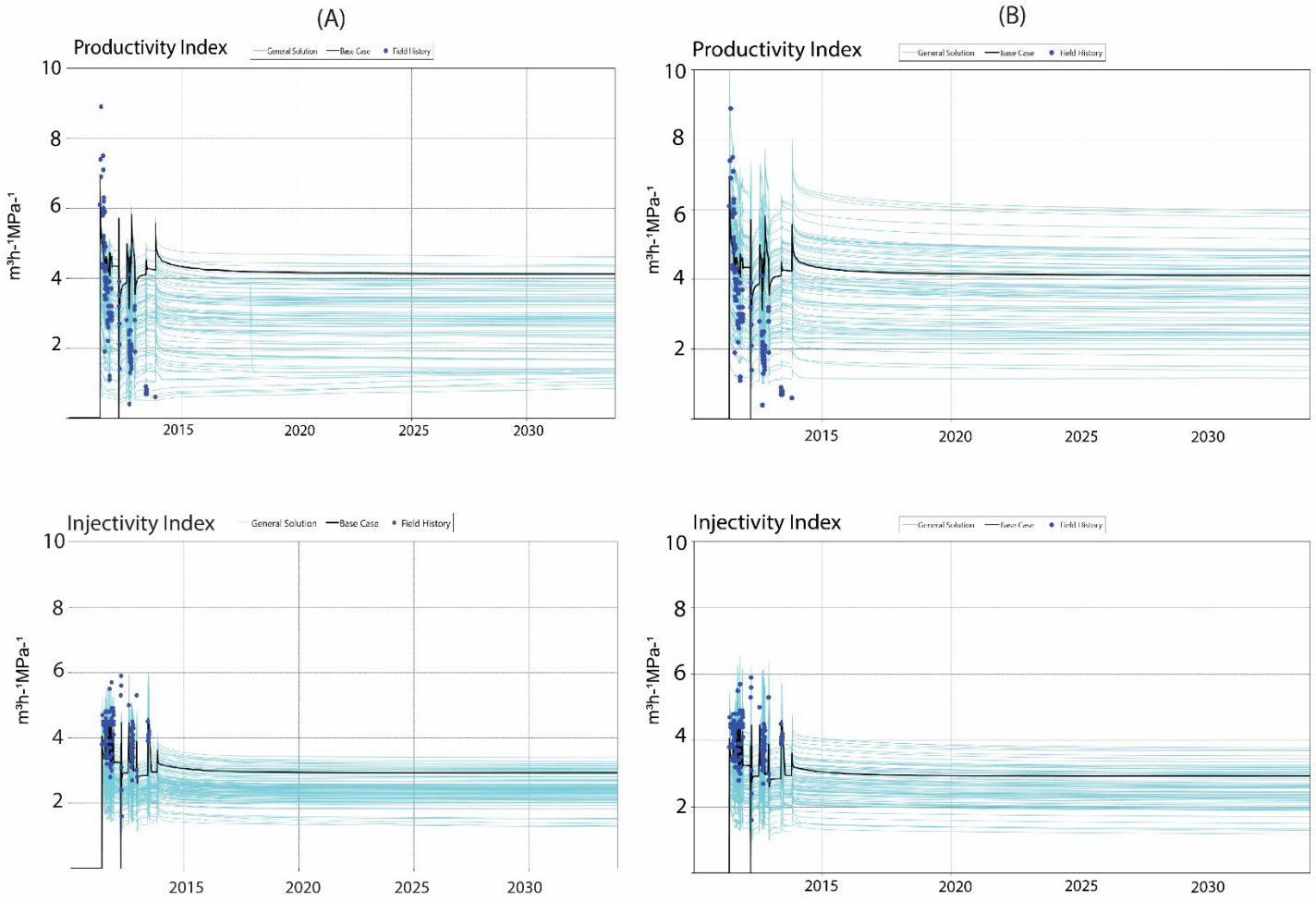

Figure G.4.7: Sensitivity analysis results showing productivity and injectivity indices as the objective function with a constant flow rate of 60 m^3h^{-1}. (A) without varying bottom-hole diameter; (B) by varying bottom-hole diameter.

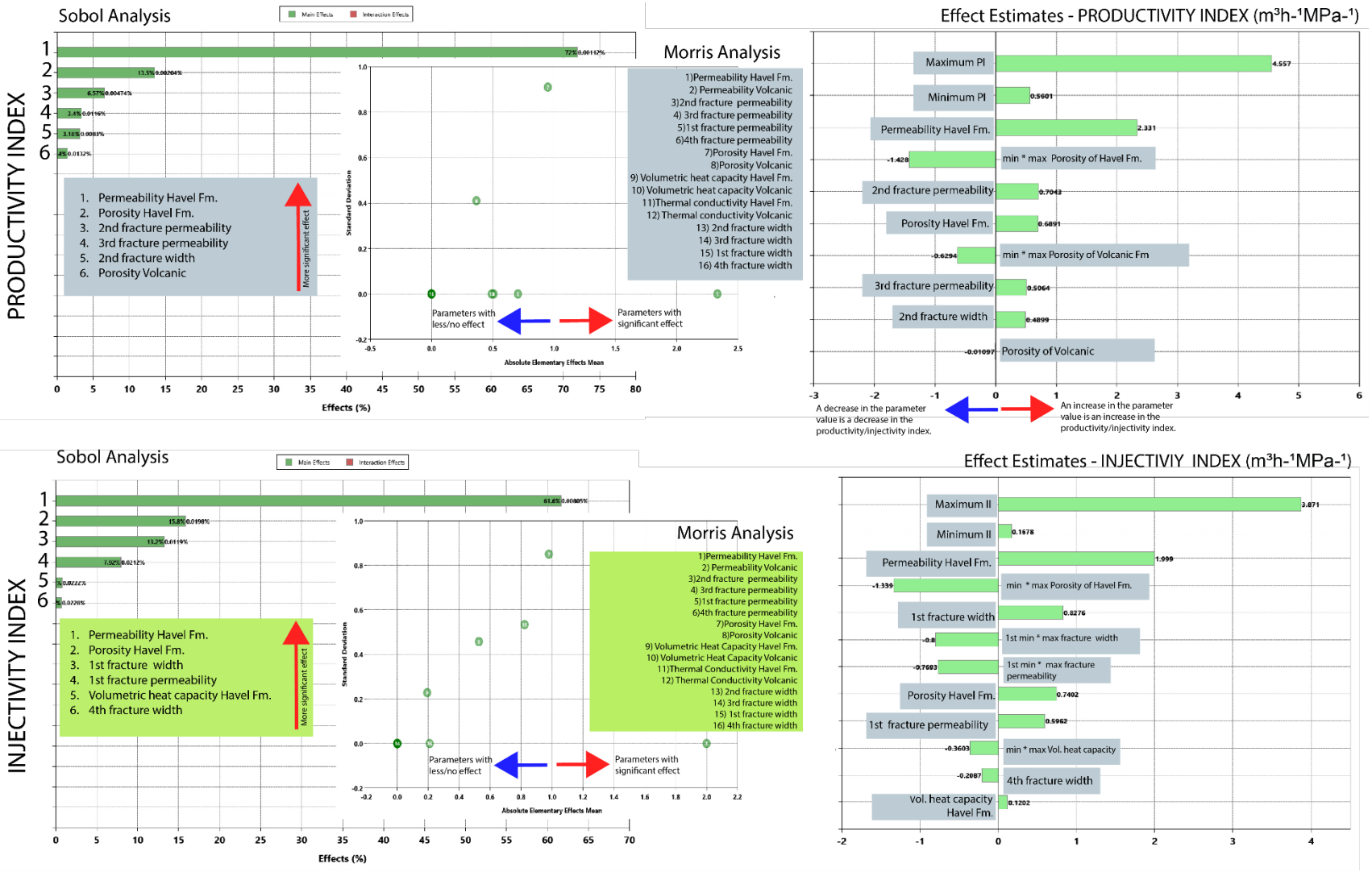

Figure G.4.8: Parameter correlation for scenarios without varying bottom-hole diameter size at constant rate 30 m^3h^{-1}.

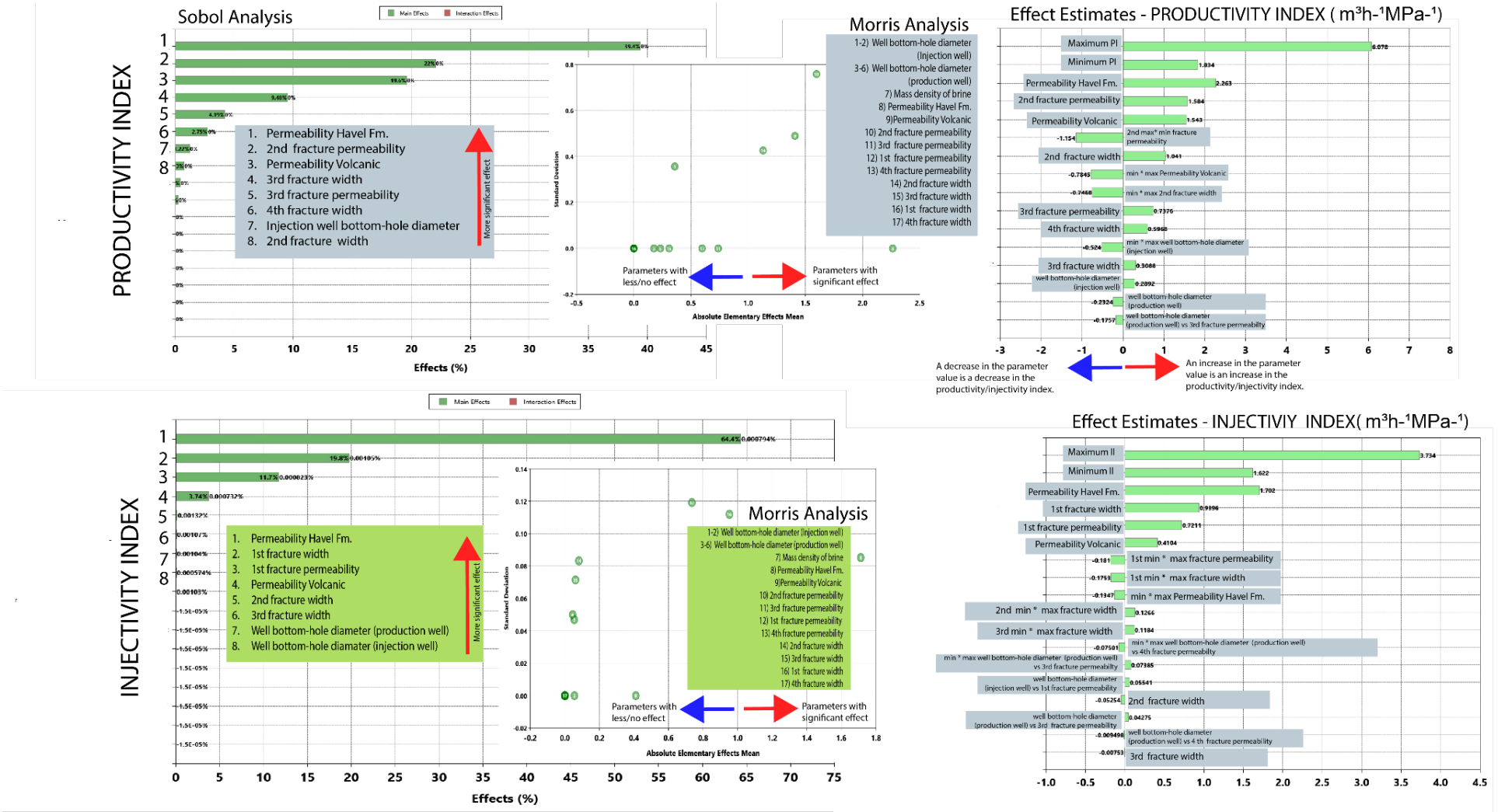

Figure G.4.9: Parameter correlation for scenarios by varying bottom hole diameter size at constant rate of 30 m^3h^{-1}.

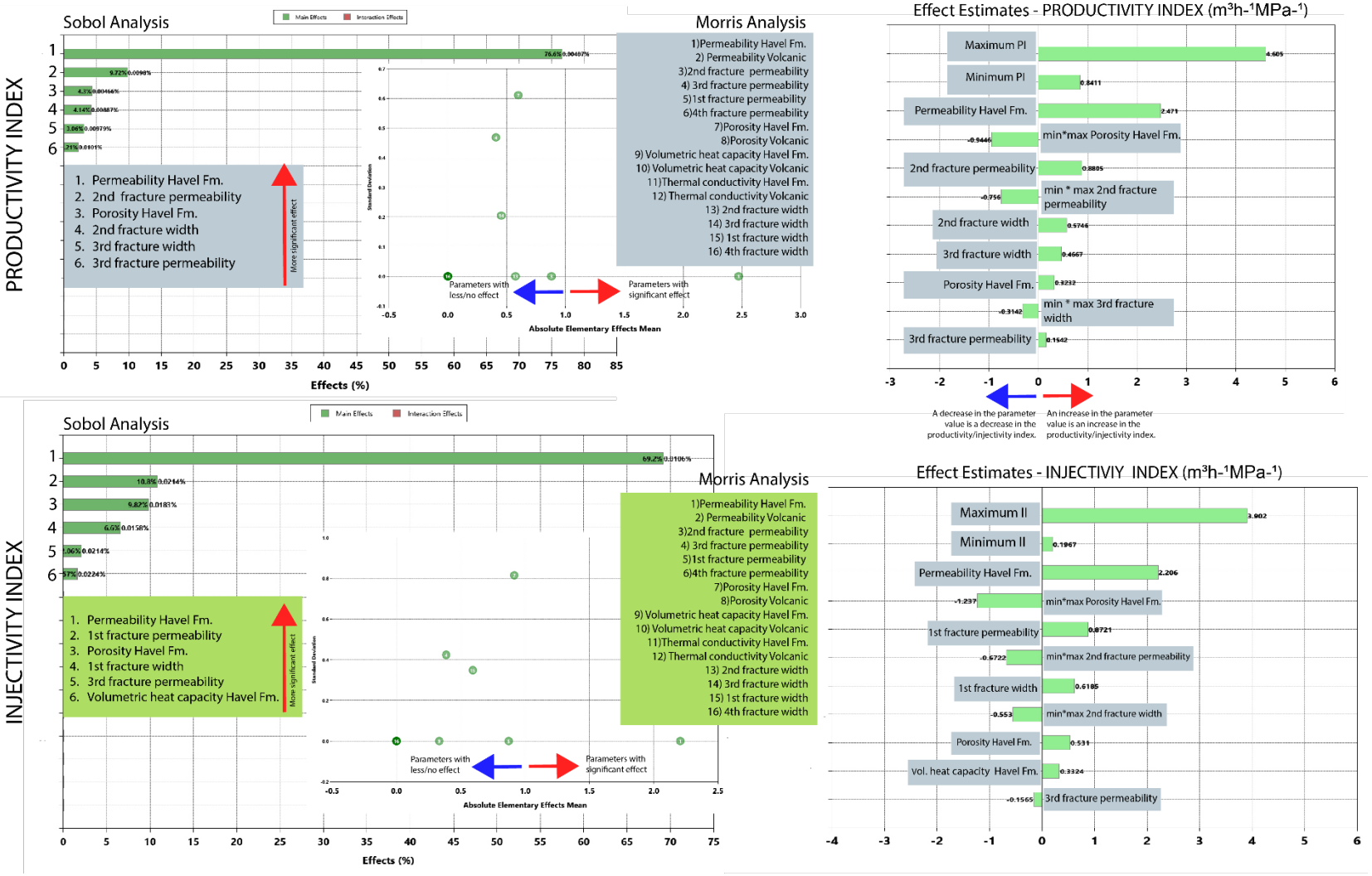

Figure G.4.10: Parameter correlation for scenarios without varying bottom-hole diameter size at constant rate 60 m^3h^{-1}.

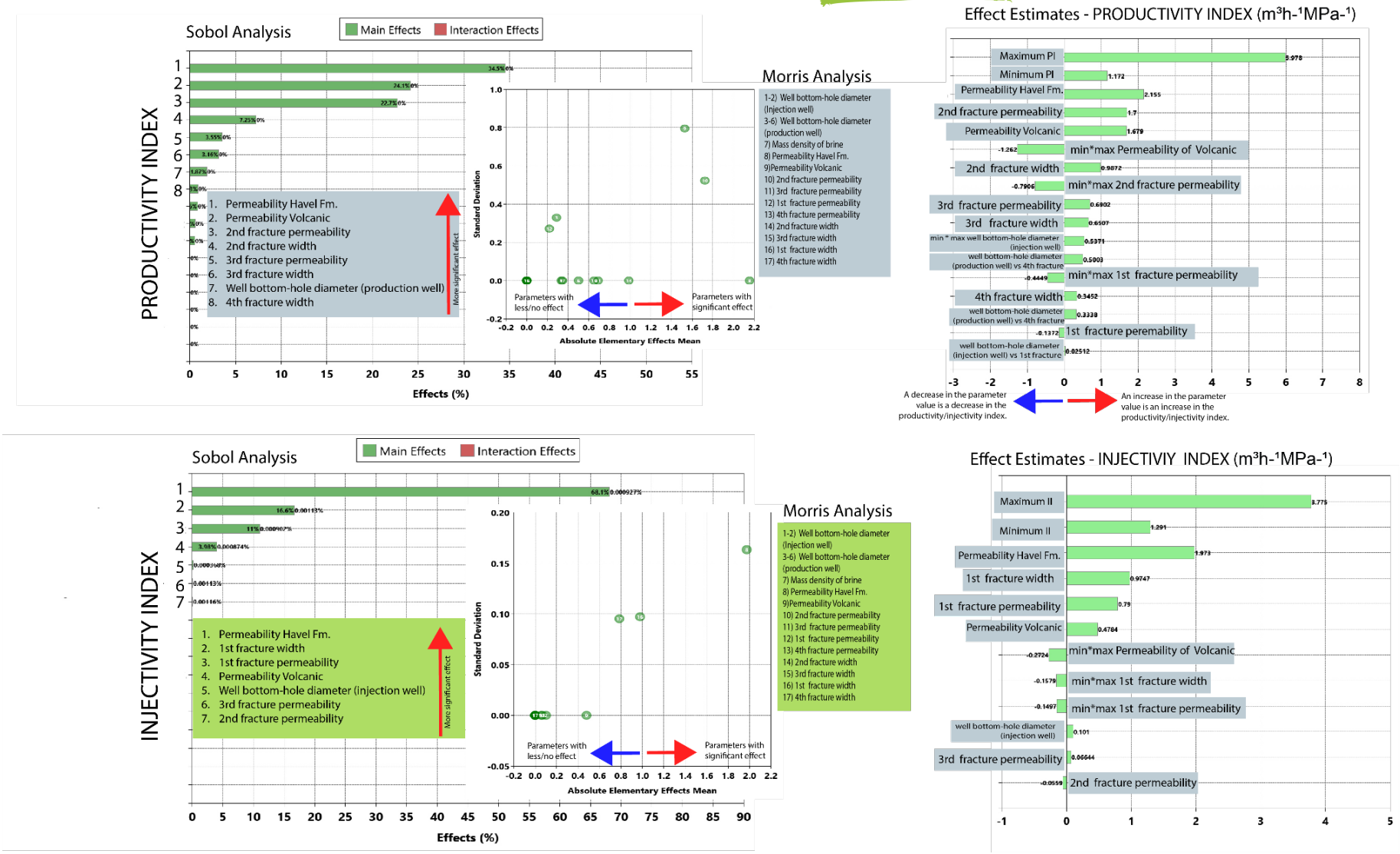

Figure G.4.11: Parameter correlation for scenarios by varying bottom-hole diameter size at constant rate 60 m^3h^{-1}

G.5. Requirements to reuse hydrocarbon wells as Enhanced Geothermal Systems

From the technical aspects, a review of the literature and sensitivity analysis study revealed that the screening criteria for potential geothermal resources in a hydrocarbon environment, which could be developed using EGS technology, are based on four main characteristics of the reservoir: temperature, in-situ permeability or transmissivity of the reservoir rock, flow rate, and Productivity (PI)/ Injectivity (II) indices. The initial permeability, flow rate, PI and II provide the basis for determining whether enhanced geothermal systems (EGS) are required and, if so, this is then followed by determining the stimulation techniques that should be employed in relation to the anticipated production rate. However, temperature is a fundamental parameter that plays a pivotal role in the deployment of EGS technology, particularly for applications such as power generation and heating. In the majority of instances where the reuse of hydrocarbon wells for geothermal energy production has been successfully demonstrated with EGS technology (Soultz-sous-Forêts and Blue Mountain), the temperature has exceeded 150 ℃, which is the typical threshold for electrical power generation of the medium enthalpy system (Muffler and Cataldi, 1978; Haenel et al., 1988). The temperature is a pivotal factor that encompasses the geology of the reservoir in terms of rock type. As previously stated in the description of technology, EGS allows for the unrestricted development of geothermal resources, irrespective of the rock types that comprise the reservoir. This is the main advantage of EGS. However, this presents a unique challenge in the application of stimulation methods, which vary significantly from one case to another.

In the context of the TRANSGEO project, which involves the participation of five countries, the temperature criteria are adapted in accordance with the demand of heating in each country. Accordingly, a minimum temperature of 100 ℃ has been established as the threshold for implementing EGS for heating purposes. The scale of the project is dependent upon the scale of the market that must cover the substantial upfront investment required for EGS, which is comparatively high when compared to other available technological options.

For the reuse cases, the diameter of the bottom hole represents a critical parameter in determining the possibility of reusing the old hydrocarbon well as an injection or monitoring wells for developing an EGS system, as described in the workflow of EGS technology. In addition to the significance of well integrity, the condition of the given well is of paramount importance. The impact of well bottom-hole diameter has been investigated through numerical simulation and sensitivity analysis in the present study. While the impact is not substantial in the context of reservoir performance, as indicated by its direct influence to PI and II, this decision should be made with consideration of the flexibility for well rehabilitation and modification. Consequently, a larger casing diameter will facilitate the installation of liners for side-tracking or deepening of existing wells, as well as the deployment of injection strings for stimulation purposes, downhole seismic geophones, or logging tools. The workover of abandoned and partially abandoned wells has been a crucial aspect in the workflow of EGS implementation. The cost of the workover activity will actually depend on the operation required to modify the well, and in this context the depth of the targeted reservoir and the length of the wellbore are the important parameters for estimating the cost. The review of reservoir properties and wellbore characteristics from 70 EGS projects worldwide and the required parameters to reuse hydrocarbon wells are summarised in Table G.5.1.

Parameters	Unit	Max	Median	Min	Requirement to reuse hydrocarbon wells with EGS technology
Reservoir Depth	m	5000 (Ultra deep case ~ 9000)	3000 - 4000	70 - 450	>1000
Reference	**[Max]** Soultz, United Downs, (Ultra deep case: KTB) **[Median]** GroÞ Schönebeck, Horstberg, St. Gallen, New Berry, Paralana, Boulliante, Lardarello, Fenton Hill, Northwest Geyser, Pohang, Reykjanes (IDDP 2), KTB, Unteraching, Matouying **[Min]** Mosfellssveit (Reykir), Fjälbacka, Falkenberg, Hachimantai				
Reservoir Temperature	°C	250 - 400	100 - 150	16	> 100
Reference	**[Max]** Bacman, New Berry, Cooper Basin (Habanero & Jolokia), Hijiori, Krafla, Baca, Sumikawa, Salak, Fenton Hill, Geyser, Northwest Geyser, Leyte, Hellisheidi, Reykjanes (IDDP-2), KTB **[Median]** GroÞ Schönebeck, Otaniemi (Helsinki Project), St. Gallen, Bruchsal, Unterhaching, Altheim, Seltjarnarnes, Raft River, Geldinganes, Mezőberény **[Min]** Fjälbacka				
In-situ Permeability	m^2	3.94769E-12	5.05E-16	9.8E-20	$<10^{-15}$
Reference	**[Max]** Klaipėda **[Median]** Groß Schönebeck, Salak **[Min]** Lardarello				
Flow Rate	Ls^{-1}	150	76	~10	<50
Reference	**[Max]** Unteraching, Boulliante (after stimulation) **[Median]** Soultz, Landau (after stimulation) **[Min]** Horstberg, Le Mayet, Paralana, Hijiori, Falkenberg, Northwest Geyser, Fjälbacka (before stimulation)				
Initial productivity Index	Ls^{-1}/MPa	35	-	~0.1	< 10
Reference	**[Max]** Rittershoffen **[Min]** Soultz, Seltjarnarnes				
Initial injectivity Index	Ls^{-1}/MPa	21	9.7	0.2	< 10
Reference	**[Max]** Mindanau **[Median]** Bacman **[Min]** Soultz				
Bottom Hole Diameter	inch	10.75	7	2.9	>=7
Reference	**[Max]** Salak **[Median]** Hannover, St. Gallen, Paralana, Unterhaching, Krafla, Sumikawa, Northwest Geyser, Tiwi, Hellisheidi, Olympic Dam, Raft River, Blue Mountain **[Min]** Ogachi				

Table G.5.1: Required parameters to reuse hydrocarbon wells with EGS technology based on literature review and sensitivity analysis study.

G.6. Workflow to reuse hydrocarbon wells as Enhanced Geothermal Systems

The workflow of EGS is presented in the following cases which reflect the choice of repurposing hydrocarbon wells as injection and monitoring wells.

Option 1 (reference site Groß Schönebeck): EGS with single stimulation in deepened well

1. Site preparation (5-10 days, depending on location)
2. Mobilisation and rig up (10 days)
3. Exchange wellhead (christmas tree) with blow out preventer (BOP) (2 days)
4. Run in hole and replace borehole fluid (2 days)
5. Drill out cement (1 day, for each additional cement plug add another 2+ days)
6. Deepen hole (50 - 250 m/day, depending on geology)
7. Logging (cement bond log, casing wall thickness, full logging suite of open hole [2 days])
8. Complete newly drilled section (slotted liner [2 days/km] or open hole or cemented liner to improve well integrity)
9. Hydraulic tests before stimulation (4 days)
10. Stimulation with injection string and packers and seismic monitoring (2 days)
11. Hydraulic tests after stimulation (4 days)
12. Drill new well into seismic cloud

Option 2 (reference site Blue Mountain): EGS with horizontal side-track and multi-stage stimulation

1. Site preparation (5 days)
2. Mobilisation and rig up (10 days)
3. Exchange wellhead (christmas tree) with blow out preventer (BOP) (2 days)
4. Run in hole and replace borehole fluid (2 days)
5. Drill out cement (1 day, for each additional cement plug add another 2+ days)
6. Set whipstock in 9 ⅝” (13 ⅜”) casing and mill out window with 8 ½” (12 ¼”) bit (5hr/km whipstock in and set + 5hr/km string out, 5hr/km in with mill bit, 24hr milling, 5hr/km out with mill bit) for a 7” production casing (or 8 ½” intermediate casing + 7” production liner)
7. Run in hole and deviated drilling to target formation with directional bottom hole assembly (RIH 5hr/km + 50-250 m/day depending on geology)
8. Logging (cement bond log, casing wall thickness, full logging suite of open hole [2 days])
9. Run and cement intermediate casing (2 days/km casing)
10. Run in hole and drill horizontal section with directional bottom hole assembly (RIH 5hr/km + 50-250 m/day depending on geology)
11. Logging (cement bond log, casing wall thickness, full logging suite of open hole [2 days])
12. Run and cement production casing/liner (2 days/km casing)
13. Plug and perf stimulation with seismic monitoring (200 m/hr RIH, 1 day stimulation, pull out of hole 200 m/hr)
14. Hydraulic tests after stimulation (4 days)
15. Drill new well into seismic cloud

Option 3 (reference site Soultz-sous-Forêts): Seismic monitoring well

1. Borehole investigation to confirm the depth and accessibility of the depth interval where the borehole geophone is to be positioned. This includes the necessary logging, such as a dummy tool or calliper test, to ensure that there is no obstruction to the tool during RIH.
2. Pressure and temperature measurement to confirm the downhole temperature and water level measurement. This is to confirm the downhole condition with the borehole geophone specification.
3. Run in hole and installation of borehole geophone.

G.7. References

Agemar, T., Weber, J., & Schulz, R. (2014). Deep geothermal energy production in Germany. *Energies*, *7*(7), 4397-4416.

Agemar, T., Alten, J., Ganz, B., Kuder, J., Kühne, K., Schummacher, S. & Schuly, R. (2014): The Geothermal Information System for Germany - GeotIS - ZDGG Volume 165 Issue 2, 129-144.

Aichholzer, C., Duringer, P., & Genter, A. (2019). Detailed descriptions of the lower-middle Triassic and Permian formations using cores and gamma-rays from the EPS-1 exploration geothermal borehole (Soultz-sous-Forêts, Upper Rhine Graben, France). *Geothermal Energy*, *7*(1), 34.

Austin, E. H. (2012). *Drilling engineering handbook*. Springer Science & Business Media.

Baria, R., Baumgärtner, J., Rummel, F., Pine, R. J., & Sato, Y. (1999). HDR/HWR reservoirs: concepts, understanding and creation. *Geothermics*, *28*(4-5), 533-552.

Baumgärtner, J., Jung, R., Hettkamp, T., and Teza, D. (2004) The status of the hot dry rock scientific power plant at *Soultz-sous-Forêts*. *Zeitsschrift für Angewandte Geologie*, 2, 12-16.

Benek, R., Kramer, W., McCann, T., Scheck, M., Negendank, J. F., Korich, D., ... & Bayer, U. (1996). Permo-carboniferous magmatism of the Northeast German Basin. *Tectonophysics*, *266*(1-4), 379-404.

Blankenship, D., Gertler, C., Kamaludeen, M., O'Connor, M., Porse, S. (2024). Pathways to Commercial Liftoff: Next-Generation Geothermal Power. U.S. Departement of Energy.

Bouchot, V., Traineau, H., Guillou-Frottier, L., Thinon, I., Baltassat, J. M., Fabriol, H., ... & Lasne, E. (2010, April). Assessment of the Bouillante geothermal field (Guadeloupe, French West Indies): toward a conceptual model of the high temperature geothermal system. In *World Geothermal Congress 2010* (pp. 8-p).

Bracke, R., Huenges, E., Acksel, D., Amann, F., Bremer, J., Bruhn, D., ... & Will, H. (2022). Roadmap for Deep Geothermal Energy for Germany: Recommended Actions for Policymakers, Industry and Science for a Successful Heat Transition.

Breede, K., Dzebisashvili, K., Liu, X., & Falcone, G. (2013). A systematic review of enhanced (or engineered) geothermal systems: past, present and future. *Geothermal Energy*, *1*, 1-27.

Brehme, M., Markó, Á., Osvald, M., Zimmermann, G., Weinzierl, W., Aldaz, S., ... & Huenges, E. (2024). Demonstration of a successful soft chemical stimulation in a geothermal sandstone reservoir in Mezőberény (Hungary). *Geothermics*, *120*, 102980.

Böhm F, Savvatis A, Steiner U, Schneider M, Koch R. (2013). Lithofazielle Reservoircharakterisierung zur geothermischen Nutzung des Malm im Großraum München. Grundwasser. 18:3–13.

Blöcher, G., Reinsch, T., Henninges, J., Milsch, H., Regenspurg, S., Kummerow, J., Francke, H., Kranz, S., Saadat, A., Zimmermann, G., Huenges, E. (2016): Hydraulic history and current state of the deep geothermal reservoir Groß Schönebeck. - *Geothermic*s, 63, pp. 27-43.

Blöcher, M. G., Zimmermann, G., Moeck, I., Brandt, W., Hassanzadegan, A., & Magri, F. (2010). 3D numerical modeling of hydrothermal processes during the lifetime of a deep geothermal reservoir. *Geofluids*, *10*(3), 406-421.

Ciriaco, A. E., Zarrouk, S. J., Zakeri, G., & Mannington, W. I. (2020). Refined experimental design and response surface methodology workflow using proxy numerical models for probabilistic geothermal resource assessment. *Geothermics*, *88*, 101911.

CMG. 2020. CMG CMOST Training Module. Calgary, Alberta, Canada: Computer Modelling Group Ltd.

CMG. 2024. CMG STARS Users's Guide. Calgary, Alberta, Canada: Computer Modelling Group Ltd.

DEKORP-BASINResearch Group. (1999). Deep crustal structure of the Northeast German basin: New DEKORP-BASIN'96 deep-profiling results. *Geology*, *27*(1), 55-58.

Doornenbal, H., & Stevenson, A. (2010). *Petroleum geological atlas of the Southern Permian Basin area*. EAGE.

Dezayes Ch., Gentier S., Genter A. (2005) – Deep Geothermal energy in western Europe: the Soultz project. BRGM/RP-54227-FR, 48 p., 7 fig.

Dorsch, K., Lentsch, D., Niederseer, C., & Götz, A. (2020). The deep hydrogeothermal project in Holzkirchen, Molasse Basin, Germany. In *World Geothermal Congress* (Vol. 1).

Duggal, R., Rayudu, R., Hinkley, J., Burnell, J., Wieland, C., & Keim, M. (2022). A comprehensive review of energy extraction from low-temperature geothermal resources in hydrocarbon fields. *Renewable and Sustainable Energy Reviews*, *154*, 111865.

EGEC (European Geothermal Energy Council) (2012) Geothermal market report, 2nd edition. European Geothermal Energy Council, Brussels, December 2012.

Entingh, D. J. (2000, May). Geothermal well stimulation experiments in the United States. In *Proceedings* (pp. 3689-3694).

Feng, C., Gao, G., Zhang, S., Sun, D., Zhu, S., Tan, C., & Ma, X. (2022). Fault slip potential induced by fluid injection in the Matouying enhanced geothermal system (EGS) field, Tangshan seismic region, North China. *Natural Hazards and Earth System Sciences*, *22*(7), 2257-2287.

Flechtner, F., Loewer, M., & Keim, M. (2020). Updated stock take of the deep geothermal projects in Bavaria, Germany (2019). In *Proceedings World Geothermal Congress* (p. 1).

Golla, G. U., Julinawati, T., Putri, R. P., Nordquist, G. A., Libert, F. T., & Suminar, A. R. (2020). The Salak Field, Indonesia: On to the next 20 years of production. *Geothermics*, *83*, 101715.

GtV (Bundesverband Geothermie) (2013) Liste der tiefen Geothermieprojekte in Deutschland. Liste der tiefen Geothermieprojekte in Deutschland, Liste der tiefen Geothermieprojekte in Deutschland, http://www.geothermie.de/wissenswelt/geothermie/in-deutschland.html. Accessed 20 Aug 2013.

Guinot, F., & Marnat, S. (2021, February). Death by Injection: Reopening the Klaipėda Geothermal Cold Case. In *Proceedings of the 46th Workshop on Geothermal Reservoir Engineering; Stanford University: Stanford, CA, USA* (pp. 15-17).

Haenel, R., Rybach, L., & Stegena, L. (1988). Fundamentals of geothermics. In *Handbook of Terrestrial Heat-Flow Density Determination: With Guidelines and Recommendations of the International Heat-Flow Commission* (pp. 9-57). Dordrecht: Springer Netherlands.

Hamann M, Kuhlee, Schulz W, Priebe. (1991). Geologisch-technisch-oekonomischer Abschlussbericht der Bohrung E Gross Schönebeck 3/90, Erdoel-Erdgas Grimmen GmbH, Hauptabteilung Geologie, Grimmen, 24.5.1991, 66 pages and 11 enclosures. (In German).

Hasterok, D., & Webb, J. (2017). On the radiogenic heat production of igneous rocks. *Geoscience Frontiers*, *8*(5), 919-940.

Hettkamp, T., Baumgärtner, J., Baria, R., Gerard, A., Gandy, T., Michelet, S., & Teza, D. (2004). Electricity production from hot rocks. In *Proceedings, 29th Workshop on Geothermal Reservoir Engineering, Stanford University, Standford, California, USA*.

Hochstein, M., 1990. Classification and assessment of geothermal resources. In: Dickson, M.H., Fanelli, M. (Eds.), Small Geothermal Resources: A Guide to Development and Utilization. UNITAR, New York, pp. 31–57.

Hofmann, H., van Rooijen, W., Blöcher, G., Zimmermann, G., Regenspurg, S., & Huenges, E. (2022). Development opportunities for deep geothermal energy in the North German Basin using the example of the Enhanced Geothermal System (EGS) research site Groß Schönebeck. In *European Geothermal Congress 2022*.

Hofmann, H., Zimmermann, G., Zang, A., Aldaz Cifuentes, S. R., Cesca, S., Heimann, S., ... & Mignan, A. (2021). Hydraulic Stimulation Design for Well RV-43 on Geldinganes, Iceland. In *World Geothermal Congress 2020+ 1*.

Holl, H. G., Moeck, I., & Schandelmeier, H. (2005, April). Characterisation of the Tectono-Sedimentary Evolution of a Geothermal Reservoir–Implications for Exploitation (Southern Permian Basin, NE Germany). In Proceedings World Geothermal Congress (pp. 1-5).

Hoth, K. (1993). *Die tiefen Bohrungen im Zentralabschnitt der Mitteleuropäischen Senke: Dokumentation für den Zeitabschnitt 1962-1990; mit 2 Tabellen*. Verlag der Gesellschaft für Geologische Wissenschaften.

Huenges et al. (2002): In-situ Geothermielabor Groß Schönebeck 2000/2001. Scientific Technical Report. ISSN 1610-0956.

Huenges, E., Moeck, I., Saadat, A., Brandt, W., Schulz, A., Holl, H., Bruhn, D., Zimmermann, G., Blöcher, G., Wohlgemuth, L. (2007): Directional drilling and stimulation of a deep sedimentary geothermal reservoir. - Scientific drilling: reports on deep earth sampling and monitoring, 5, pp. 47-49.

Huenges, E., Kohl, T., Kolditz, O., Bremer, J., Scheck-Wenderoth, M., & Vienken, T. (2013). Geothermal energy systems: research perspective for domestic energy provision. *Environmental Earth Sciences*, *70*, 3927-3933.

Hornby, Brian. *Utah FORGE: Hydraulic Fracture Width Determination Using Stoneley Wave Pressure Testing and Electrical Borehole Scans*. United States. https://gdr.openei.org/submissions/1557

IEA (2022). Temperature in Germany, 2000-2020. Accessed: 2024-08-16.

Jia, Y., Tsang, C. F., Hammar, A., & Niemi, A. (2022). Hydraulic stimulation strategies in enhanced geothermal systems (EGS): a review. *Geomechanics and Geophysics for Geo-Energy and Geo-Resources*, *8*(6), 211.

Jinzhou, Z. H. A. O., Xiyu, C. H. E. N., Yongming, L. I., Bin, F. U., & Wenjun, X. U. (2017). Numerical simulation of multi-stage fracturing and optimization of perforation in a horizontal well. *Petroleum Exploration and Development*, *44*(1), 119-126.

J.L. Renner. The Navy I geothermal power plant near Coso Hot Springs, California. https://www1.eere.energy.gov/geothermal/pdfs/egs.pdf) (last accessed April 2024

Jung, R., Orzol, J., Kehrer, P. Jatho, R. (2005): Verbundprojekt: GeneSys, Vorstudie – Erprobung der Wasserfractechnik und des Einsonden-Zweischichtverfahrens für die Direktwärmenutzung aus gering permeablen Sedimentgesteinen. Abschlussbericht.

Kossow, D., Krawczyk, C., McCann, T., Strecker, M., & Negendank, J. F. (2000). Style and evolution of salt pillows and related structures in the northern part of the Northeast German Basin. *International Journal of earth sciences*, *89*, 652-664.

König H, Meyer W. (1988). *Ergebnisbericht Finow 2.1/Liebenwalde 2.1, VEB Kombinat Erdöl-Erdgas Gommern*, 15.11, p.35. (In German).

Krawczyk CM, Stiller M, Bauer K, Norden B, Henninges J, Ivanova A, Huenges E. (2019). 3-D seismic exploration across the deep geothermal research platform Groß Schönebeck north of Berlin/Germany. *Geothermal Energy*.

Legarth, B. A., Tischner, T., Huenges, E. (2003): Stimulation experiments in sedimentary, low-enthalpy reservoirs for geothermal power generation, Germany. *Geothermics*, 32, 4, pp. 487-495. https://doi.org/10.1016/j.geothermics.2003.07.007.

Lei, Z., Zhang, Y., Yu, Z., Hu, Z., Li, L., Zhang, S., ... & Xie, Y. (2019). Exploratory research into the enhanced geothermal system power generation project: The Qiabuqia geothermal field, Northwest China. *Renewable Energy*, *139*, 52-70.

Lund, H. (2007). Renewable energy strategies for sustainable development. *Energy*, *32*, 912–919.

Lotz B. (2004). Neubewertung des rezenten Wärmestroms im Nordostdeutschen Becken. Potsdam: Scientific Technical Report 04/04.

Maćkowski, T., Kwolek, K., & Górecki, W. (2017). The potential for locating hydrocarbon traps in the Rotliegend formation, based on the results of experimental seismic surveys. *Geology, Geophysics and Environment*, *43*(3), 191-199.

Malate, R. C. M., Buñing, B. C., Molina, P. O., Yglopaz, D. M., & Lacanilao, A. M. (2000). SK-2D: A Case History on Geothermal Wellbore Enhancement, Mindanao-1 Geothermal Production Field, Philippines. In *Proc. World Geothermal Congress 2000*.

Malvić, T., Barudžija, U., Pašić, B., & Ivšinović, J. (2021). Small unconventional hydrocarbon gas reservoirs as challenging energy sources, case study from Northern Croatia. *Energies*, *14*(12), 3503.

Martuganova E, Stiller M, Norden B, Henninges J, Krawczyk CM (2022). 3D deep geothermal reservoir imaging with wireline distributed acoustic sensing in two boreholes. *Solid Earth*.

Michelet, S., & Toksöz, M. N. (2007). Fracture mapping in the Soultz-sous-Forêts geothermal field using microearthquake locations. *Journal of Geophysical Research: Solid Earth*, *112*(B7).

Morris,M. D. (1991). Factorial sampling plans for preliminary computational experiments. Technometrics, 33(2):161–174.

Muffler, P., & Cataldi, R. (1978). Methods for regional assessment of geothermal resources. *Geothermics*, *7*(2-4), 53-89.

Nádor, A., & Lenkey, L. (2025). Geothermal resources of Hungary: a play-based review. *Geological Society, London, Special Publications*, *555*(1), SP555-2024.

Norbeck, J., Latimer, T., Gradl, C., Agarwal, S., Dadi, S., Eddy, E., ... & Woitt, M. (2023, February). A review of drilling, completion, and stimulation of a horizontal geothermal well system in North-Central Nevada. In *Proceedings of the 48th Workshop on Geothermal Reservoir Engineering* (pp. 6-8).

Norden, B., Bauer, K., & Krawczyk, C. M. (2023). From pilot knowledge via integrated reservoir characterization to utilization perspectives of deep geothermal reservoirs: the 3D model of Groß Schönebeck (North German Basin). *Geothermal Energy*, *11*(1), 1.

Pasikki, R. G., Cita, F., & Hernawan,A. (2016). Application of experimental design (ED) in geothermal greenfield size assessment. In *Proceedings the 4th Indonesia international geothermal convention & exhibition,* Jakarta, Indonesia.

Peryt, T. M., Raczyn´ski, P., Peryt, D., and Chłodek, K. (2012). Upper permian reef complex in the basinal facies of the zechstein limestone (ca1), western poland. Geological Journal, 47(5):537–552.

Pianosi, F., Beven, K., Freer, J., Hall, J. W., Rougier, J., Stephenson, D. B., & Wagener, T. (2016). Sensitivity analysis of environmental models: A systematic review with practical workflow. *Environmental Modelling & Software*, *79*, 214-232.

Portier, S., André, L., & Vuataz, F. D. (2007). Review on chemical stimulation techniques in oil industry and applications to geothermal systems. *Engine, work package*, *4*, 32.

Pollack, A., Horne, R., & Mukerji, T. (2020, April). What are the challenges in developing enhanced geothermal systems (EGS)? Observations from 64 EGS sites. In *Proceedings of the World Geothermal Congress* (Vol. 1).

Quinao, J. J. D., & Zarrouk, S. J. (2018). Geothermal resource assessment using experimental design and response surface methods: The Ngatamariki geothermal field, New Zealand. *Renewable Energy*, *116*, 324-334.

Rabbel, W., Beilecke, T., Bohlen, T., Fischer, D., Frank, A., Hasenclever, J., ... & Smithson, S. (2004). Superdeep vertical seismic profiling at the KTB deep drill hole (Germany): seismic close-up view of a major thrust zone down to 8.5 km depth. *Journal of Geophysical Research: Solid Earth*, *109*(B9).

Reinsch, T., Blöcher, G., Kranz, S. (2015): Data from the Groß Schönebeck Research Platform 2011-06-01 - 2013-12-31 (Report), (Scientific Technical Report - Data; 15), Deutsches GeoForschungsZentrum GFZ: Potsdam, 71 p.

Rockel W, Hurter S. Tiefe Altbohrungen als Beitrag zur Nutzbarmachung klüftig-poröser Speichergesteine (geologische Grundlagen): Groß Schönbeck. Scientific Technical Report STR00/23. 2000. p. 29–50 (In German).

Santos, L., Taleghani, A. Dhani, Elsworth, D. (2002): Repurposing abandoned wells for geothermal energy: current status and future prospect. Renewable Energy 194, 1288 – 1302.

Saltelli, A., Ratto, M., Andres, T., Campolongo, F., Cariboni, J., Gatelli, D., Saisana, M., and Tarantola, S. (2008). *Global Sensitivity Analysis: The Primer*, *John Wiley and Sons*, 2008.

Schindler, M., Nami, P., Schellschmidt, R., Teza, D., & Tischner, T. (2008). Summary of hydraulic stimulation operations in the 5 km deep crystalline HDR/EGS reservoir at Soultz-sous-Forêts. In *Proceedings, 33rd Workshop on Geothermal Reservoir Engineering*.

Scheck, M., & Bayer, U. (1999). Evolution of the Northeast German Basin—inferences from a 3D structural model and subsidence analysis. *Tectonophysics*, *313*(1-2), 145-169.

Scheck-Wenderoth, M., Maystrenko, Y., Hübscher, C., Hansen, M., & Mazur, S. (2008). Dynamics of salt basins. *Dynamics of complex intracontinental basins, the Central European Basin System*, 17-34.

Sharma, M. M., Gadde, P. B., Sullivan, R., Sigal, R., Fielder, R., Copeland, D., ... & Weijers, L. (2004, September). Slick water and hybrid fracs in the Bossier: Some lessons learnt. In *SPE Annual Technical Conference and Exhibition?* (pp. SPE-89876). SPE.

Shaoul, J., Ross, M., Spitzer, W., Wheaton, S., Mayland, P., & Singh, A. P. (2007, May). Massive hydraulic fracturing unlocks deep tight gas reserves in India. In *SPE European Formation Damage Conference and Exhibition* (pp. SPE-107337). SPE.

Speight, J. G. (2019). *Shale oil and gas production processes*. Gulf Professional Publishing.

Stackebrandt W, Manhenke V. (2010). Atlas zur Geologie von Brandenburg. Cottbus: Landesamt für Bergbau, Geologie und Rohstoffe.

Stimac, J., Nordquist, G., Suminar, A., & Sirad-Azwar, L. (2008). An overview of the Awibengkok geothermal system, Indonesia. *Geothermics*, *37*(3), 300-331.

Stimac, J. A., Powell, T. S., & Golla, G. U. (2004). Porosity and permeability of the Tiwi geothermal field, Philippines, based on continuous and spot core measurements. *Geothermics*, *33*(1-2), 87-107.

Sobol, I. (1993). *Sensitivity Estimates for Nonlinear Mathematical Models*, Matematicheskoe Modelirovanie 2, 112-118.

Sundquist, U., Wallroth, T., & Eliasson, T. (1988). The Fjällbacka HDR Geothermal Energy project: reservoir characterisation and injection well stimulation. *Chalmers University of Technology, Report Number Fj-9, Gothenburg, Sweden*.

Tester, J.W. (2006) The Future of Geothermal Energy, Impact of Enhanced Geothermal System (EGS) on the United State in the 21st Century: An Assessment by an MIT-Led Interdisciplinary Panel. Idaho National Laboratory, Report ISBN 0-615-13438-6, Idaho Falls.

Tischner, T., Thorenz, C., Jung, R., Kessels, W. (2002): Ergebnisse des Primärtests: Hydraulik. STR02/14, Geothermie Report 02-1. Pages 107 – 130.

Tischner, T., Evers, H., Hauswirth, H., Jatho, R., Kosinowski, M., & Sulzbacher, H. (2010, April). New concepts for extracting geothermal energy from one well: the GeneSys-Project. In *Proceedings of the world geothermal congress, Bali* (Vol. 2530).

Tischner, T., Krug, S., Pechan, E., Hesshaus, A., Jatho, R., Bischoff, M., & Wonik, T. (2013). Massive hydraulic fracturing in low permeable sedimentary rock in the GeneSys project. In *Proceedings of the Thirty-Eighth Workshop on Geothermal Reservoir Engineering, SGP-TR-198, Stanford University, Stanford, CA, USA* (pp. 11-13).

Trautwein, U., & Huenges, E. (2005). Poroelastic behaviour of physical properties in Rotliegend sandstones under uniaxial strain. *International Journal of Rock Mechanics and Mining Sciences*, *42*(7-8), 924-932.

Tumara, D., & Pavlović, D. (2019). Geotermalna energija i njezin potencijal u vremenu energetske diversifikacije i tranzicije republike hrvatske. *Nafta i plin*, *39*(161.-162.), 53-62.

Vidal, J., Genter, A., Glaas, C., Hehn, R., Cuenot, N., & Baujard, C. (2018). Temperature signature of permeable fracture zones in geothermal wells of Soultz-sous-Forêts in the Upper Rhine Graben. *GRC Transactions, Reno, Nevada, USA*.

Wallroth, T., Eliasson, T., & Sundquist, U. (1999). Hot dry rock research experiments at Fjällbacka, Sweden. *Geothermics*, *28*(4-5), 617-625.

Wolfgramm, M., Seibt, A., Hurter, S., Zimmermann, G. (2003): Origin of geothermal fluids of Permo-Carboniferous rocks in the NE German Basin (NE Germany). *Journal of Geochemical Exploration*, 78-79, p. 127-131.

Williams CF, Reed MJ, Anderson AF (2011) Updating the classification of geothermal resources. In: Proceedings of the thirty-sixth workshop on geothermal reservoir engineering. Stanford University, Stanford, 31 Jan–2 Feb 2011.

Ziegler, P. A. (1990). *Geological atlas of western and central Europe* (Vol. 52). The Hague: Shell Internationale Petroleum Maatschappij BV.

Zimmermann, G., Moeck, I., Blöcher, G. (2010): Cyclic waterfrac stimulation to develop an enhanced geothermal system (EGS): Conceptual design and experimental results. *Geothermics*, 39, 1, pp. 59-69.

Zimmermann, G., Blöcher, G., Reinicke, A., & Brandt, W. (2011). Rock specific hydraulic fracturing and matrix acidizing to enhance a geothermal system—concepts and field results. *Tectonophysics*, *503*(1-2), 146-154.

Zimmermann, G., & Reinicke, A. (2010). Hydraulic stimulation of a deep sandstone reservoir to develop an Enhanced Geothermal System: Laboratory and field experiments. *Geothermics*, *39*(1), 70-77.

Zimmermann, G., Tischner, T., Legarth, B., Huenges, E. (2009): Pressure dependent production efficiency of an Enhanced Geothermal System (EGS): Stimulation results and implications for hydraulic fracture treatments. *Pure and Applied Geophysics*, 166, 5, pp. 1089-1106.